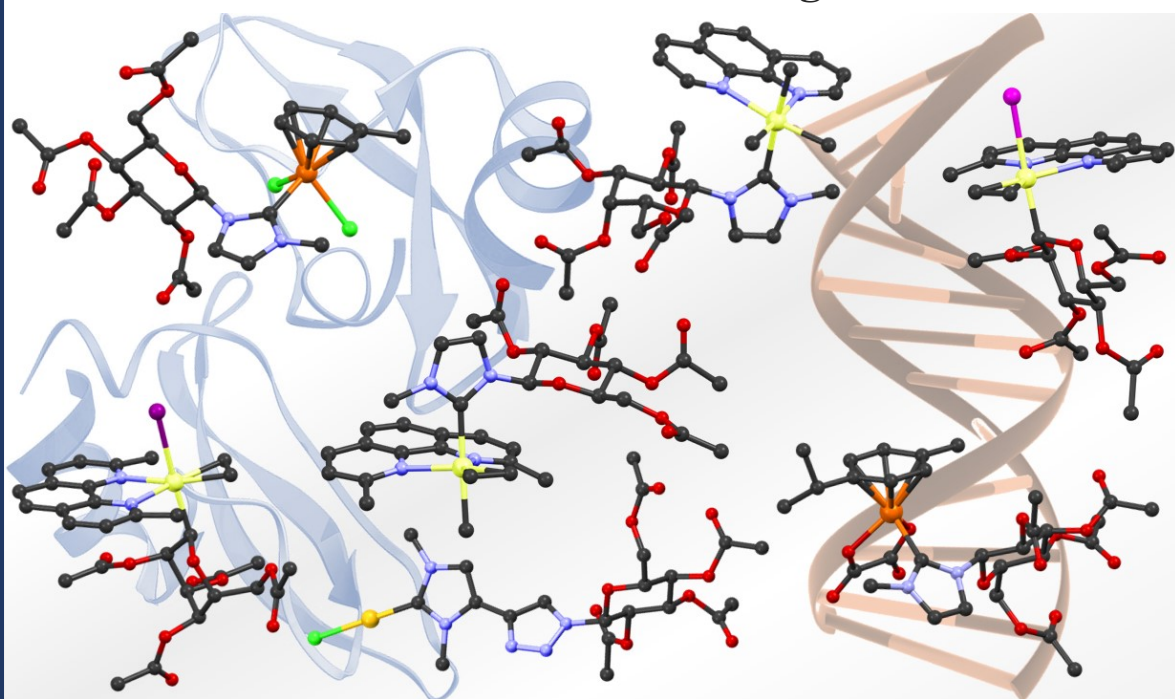


University of Naples Federico II  
Polytechnic and Basic Sciences School  
Department of Chemical Sciences



Ph.D. in Chemical Sciences

**Design, Synthesis and Study of Novel  
Glycoconjugate Organometallic Complexes as  
Potential Anticancer Agents**



**Alfonso Annunziata**

***Advisors:***

***Prof. Francesco Ruffo***

***Dr. Maria Elena Cucciolito***

***Examiner:***

***Prof. Daniela Montesarchio***

XXXIV Cycle 2018 – 2021  
Coordinator: Prof. Angelina Lombardi

*“To understand your direction,  
you must know both your roots and your reach.”*

Ana Johns, *The Woman in the White Kimono*

*“Per capire quale direzione prendere,  
devi conoscere sia le tue radici sia le tue potenzialità.”*

Ana Johns, *La donna dal Kimono Bianco*

# TABLE OF CONTENTS

<b>TABLE OF CONTENTS</b>	<b>i</b>
<b>Abstract</b>	<b>viii</b>
<b>1 Introduction</b>	<b>1</b>
<b>1.1 Metal Compounds in Medicinal Chemistry: An Overview</b>	<b>1</b>
<b>1.2 Platinum-Based anticancer drugs</b>	<b>4</b>
1.2.1 Cisplatin and its derivatives	4
1.2.2 Side Effects of Platinum-based chemotherapies	11
1.2.3 Organoplatinum(II) complexes	12
1.2.4 Platinum(IV) “pro-drugs”	18
<b>1.3 Alternatives to Platinum anticancer drugs</b>	<b>31</b>
1.3.1 The “Ruthenium Era” in anticancer treatment	31
1.3.2 Gold-based anticancer compounds	37
<b>1.4 Targeting groups in anticancer metal complexes</b>	<b>40</b>
1.4.1 Glycoconjugation for Selective Delivery of Metal Drugs	40
<b>1.5 Aim of the Work</b>	<b>47</b>
<b>2 Square planar vs. trigonal bipyramidal geometry in Pt(II) complexes with glucoconjugate N-based ligands</b>	<b>51</b>
<b>2.1 General Overview</b>	<b>51</b>
<b>2.2 Results and Discussion</b>	<b>54</b>
2.2.1 Synthesis of the glucoconjugate ligands	54
2.2.2 Synthesis and characterization of complexes <b>4-6</b>	55
2.2.3 In-solution reactivity	58
2.2.4 Biological studies	64

2.2.5	Reactivity with model biomolecules	67
2.2.5.1	Interaction with model DNA	67
2.2.5.2	Reactivity with S-donor molecules	70
<b>2.3</b>	<b>Experimental Part</b>	<b>74</b>
2.3.1	General	74
2.3.2	Synthesis and characterization	74
2.3.2.1	Synthesis of the ligands	74
2.3.2.2	Synthesis of compounds <b>4-5</b>	76
2.3.2.3	Synthesis of <b>6</b>	77
2.3.3	<sup>1</sup> H NMR and ESI-MS in-solution studies	78
2.3.4	Evaluation of the biological activity	78
2.3.4.1	Cytotoxicity Experiments	79
2.3.4.2	LDH release	79
2.3.4.3	Western blot analyses	80
2.3.4.4	Analysis of mitochondrial membrane potential	80
2.3.5	Ethidium bromide displacement fluorescence assay	81
<b>3</b>	<b>Pt(0) olefin complex with a glucoconjugated iminopyridine ligand</b>	<b>82</b>
<b>3.1</b>	<b>General Overview</b>	<b>82</b>
<b>3.2</b>	<b>Results and Discussion</b>	<b>85</b>
3.2.1	Synthesis of complex <b>7</b>	85
3.2.2	In-solution stability	90
3.2.3	Cytotoxic activity of <b>7</b>	91
<b>3.3</b>	<b>Experimental Part</b>	<b>93</b>



3.3.1	General	93
3.3.2	Synthesis and characterization of <b>7</b>	93
3.3.3	Evaluation of the biological activity	94
<b>4</b>	<b>C-glycoconjugate <i>thp</i> Pt(II) complexes</b>	<b>96</b>
<b>4.1</b>	<b>General Overview</b>	<b>96</b>
<b>4.2</b>	<b>Results and Discussion</b>	<b>99</b>
4.2.1	Synthesis and Experimental Mechanistic Study	99
4.2.2	Preliminary computational investigation	107
4.2.3	X-ray crystallographic structures of <b>8<sup>α</sup>-I</b> and <b>8<sup>β</sup>-I</b>	109
4.2.4	Biological studies	111
<b>4.3</b>	<b>Experimental Part</b>	<b>113</b>
4.3.1	General	113
4.3.2	Oxidative addition of <b>Glu<sub>1</sub>-X</b> and <b>Gal<sub>1</sub>-X</b> (X = <b>Br</b> , <b>I</b> ) to [Pt(dmphen)ethene]	113
4.3.3	Oxidative additions of <b>2-glu-Br</b> or <b>2-gal-Br</b> to [Pt(dmphen)(ethene)] with TEMPO	115
4.3.4	X-ray crystallography	115
4.3.5	DFT-Calculations.	116
4.3.6	Evaluation of the biological activity	117
4.3.6.1	Cytotoxicity Experiments	117
4.3.6.2	Analysis of the mechanism of action.	118
<b>5</b>	<b>Pt(II) versus Pt(IV) in NHC glycoconjugates complexes</b>	<b>119</b>
<b>5.1</b>	<b>General overview</b>	<b>119</b>
<b>5.2</b>	<b>Results and Discussion</b>	<b>124</b>
5.2.1	Synthesis and Structural Characterization of the Complexes	124

5.2.1.1	Synthesis of the pro-carbene ligands	124
5.2.1.2	Synthesis of the Ag-NHC intermediates	125
5.2.1.3	Synthesis of Pt(II) complexes <b>12-16</b>	127
5.2.1.4	Synthesis of Pt(IV) complexes <b>17-20</b>	128
5.2.1.5	Structural characterization of Pt(II) and Pt(IV) complexes	129
5.2.2	In-solution reactivity	137
5.2.2.1	Stability in aqueous media and coordinating solvents	137
5.2.2.2	Reactivity in presence of reducing agents	142
5.2.3	Biological studies	144
5.2.3.1	Cytotoxicity and Cellular Uptake	144
5.2.3.2	Study of the mechanism of Cell Death induced by <b>12</b>	147
5.2.4	Interaction with model biomolecules	148
5.2.4.1	Reactivity with model DNA	148
5.2.4.2	Reactivity with model proteins	155
<b>5.3</b>	<b>Experimental Part</b>	<b>157</b>
5.3.1	General	157
5.3.2	Synthesis and Characterization	158
5.3.2.1	Synthesis of the pro-carbene ligands <b>1-R</b>	158
5.3.2.2	Synthesis of the Ag(I) NHC precursors <b>2-R</b>	159
5.3.2.3	Synthesis of the Pt(II) precursor ( <b>b</b> )	160
5.3.2.4	Synthesis of Pt(II) NHC complexes <b>12-14-16</b>	160
5.3.2.5	Synthesis of the deprotected Pt(II) NHC complexes <b>13-15</b>	162
5.3.2.6	Synthesis of the Pt(IV) precursor ( <b>e</b> )	163
5.3.2.7	Synthesis of the Pt(IV) NHC complexes <b>17 and 19</b>	163

5.3.2.8	Synthesis of the deprotected Pt(IV) NHC complexes <b>18</b> and <b>20</b>	165
5.3.3	X-ray crystallography	166
5.3.4	NMR studies	167
5.3.4.1	In-solution reactivity	167
5.3.4.2	Studies of reduction of <b>17</b>	167
5.3.5	Electrochemical Studies	168
5.3.6	Evaluation of the biological activity	168
5.3.6.1	Cytotoxicity Experiments	168
5.3.6.2	Uptake Experiments	169
5.3.6.3	Analysis of cell death mechanism	169
5.3.7	Reactivity with model biomolecules	170
5.3.7.1	UV-vis measurements	171
5.3.7.2	Fluorescence experiments	171
5.3.7.3	Circular Dichroism experiments	171
5.3.7.4	NMR experiments	172
5.3.7.5	ESI-MS experiments	172
<b>6</b>	<b>Glucosylated NHC Ru(II)-Arene complexes</b>	<b>174</b>
<b>6.1</b>	<b>General Overview</b>	<b>174</b>
<b>6.2</b>	<b>Results and Discussion</b>	<b>176</b>
6.2.1	Synthesis and Spectroscopic Characterization of the complexes	176
6.2.2	Hydrolytic behaviour	185
6.2.3	Interaction with biological molecules	192
6.2.3.1	Reactivity with model nucleophiles	192
6.2.3.2	Reactivity with model proteins	194

6.2.3.3	Reactivity with model DNA	199
6.2.4	Evaluation of the Cytotoxic Activity	202
<b>6.3</b>	<b>Experimental Part</b>	<b>205</b>
6.3.1	General	205
6.3.2	Synthesis and Characterization	206
6.3.2.1	Synthesis of the arene precursor ( <b>e'</b> )	206
6.3.2.2	Synthesis of the Ru(II) arene dimer <b>e</b>	207
6.3.2.3	Synthesis of Complexes <b>22-27</b>	207
6.3.2.4	Synthesis of Complex <b>28</b>	210
6.3.2.5	Synthesis of Complexes <b>29-30</b>	211
6.3.3	X-ray crystallography of the complexes	213
6.3.4	Reactivity in aqueous media	214
6.3.4.1	NMR Experiments	214
6.3.4.2	UV-vis measurements	214
6.3.5	Reactivity with model biomolecules	214
6.3.5.1	ESI-MS experiments with model nucleophiles	215
6.3.5.2	ESI-MS experiments with Ubiquitin	215
6.3.5.3	Fluorescence experiments with proteins and DNA	216
6.3.5.4	Crystallographic studies	217
6.3.5.5	Circular Dicroism Experiments	217
6.3.6	Evaluation of the biological activity	218
<b>7</b>	<b>Glycoconjugate Au(I) NHC complexes</b>	<b>220</b>
<b>7.1</b>	<b>General overview</b>	<b>220</b>
<b>7.2</b>	<b>Results and Discussion</b>	<b>223</b>

7.2.1	Synthesis and Characterization of the Pro-Carbene Ligand	223
7.2.2	Synthesis and Characterization of the Complexes	226
7.2.3	In-solution stability	231
7.2.4	Cytotoxic activity of <b>31-37</b>	236
<b>7.3</b>	<b>Experimental Part</b>	<b>239</b>
7.3.1	General	239
7.3.2	Synthesis and Characterization	240
7.3.2.1	Synthesis of the pro-carbene ligand <b>L-im-Me</b>	240
7.3.2.2	Synthesis of complex <b>35</b>	240
7.3.2.3	Synthesis of complex <b>36</b>	241
7.3.2.4	Synthesis of complex <b>37</b>	241
7.3.3	In-solution experiments	242
7.3.4	Evaluation of the biological activity	242
<b>8</b>	<b>Concluding Remarks and Future Perspectives</b>	<b>244</b>
	<b>Appendix</b>	<b>248</b>
	<b>List of publications related to this work</b>	<b>255</b>
	<b>Bibliography</b>	<b>257</b>

## Abstract

An important application of coordination chemistry consists in the design of metal complexes with anti-tumor activity. The advantage of this methodology lies in the control of the properties of the compounds, through the wide choice of the metal, its oxidation state, the number of coordination and the relative geometry.

Within this frame, the present PhD thesis proposed the design of new organometallic complexes containing carbohydrate-derived ligands. The presence of a sugar fragment can have several beneficial effects on the resulting species, by enhancing the biocompatibility, water solubility and selectivity (Warburg Effect).

Platinum anticancer drugs are regularly used in clinical therapy, despite the serious issues related to their administration. Therefore, in recent years several efforts were performed for searching valid alternative metallodrugs. In the first part of the PhD, organometallic platinum complexes were studied, by exploring different oxidation states, molecular geometries, and type of glycoconjugate ligands. Particular attention was given to coordinatively saturated Pt(II), by far less represented than square planar Pt(II), and octahedral Pt(IV) species. The synthesis, the structural characterization, and the study of the reactivity in miming-biological conditions were performed, followed by preliminary investigations of the *in vitro* cytotoxicity and of the mechanism of action. The results allowed to individuate key structural features that influenced the anticancer properties of the designed compounds. The last part of the PhD activity was carried out at the École Polytechnique Fédérale de Lausanne (EPFL, Switzerland) under the supervision of Prof. Paul Dyson. In this frame, glycoconjugation was extended to ruthenium and gold organometallic scaffolds, considered valid alternative to more represented platinum ones.

The results obtained during the PhD revealed that coordinatively saturated Pt(II) complexes displayed general high cytotoxicity and, in some cases, enhanced selectivity depending on the sugar fragment.

Among the studied species, a trigonal bipyramidal Pt(II) complex with a glucoconjugate N-Heterocyclic Carbene ligand emerged as the most promising candidate drug, displaying an activity 100-fold higher than cisplatin and being 180-fold more selective on the cell lines explored. Preliminary investigations of the *in vitro* mechanism of action were performed, laying the foundations for further studies on the application of this compound as anticancer drug.

# 1 Introduction

## 1.1 Metal Compounds in Medicinal Chemistry: An Overview

Metal-based compounds are an exceptional pool of opportunities in modern medicine. To date, numerous coordination and organometallic compounds are used in the treatment and in the diagnosis of several diseases, and as many are candidates in clinical trials.<sup>1</sup> Some representative examples are reported in **Figure 1.1**.

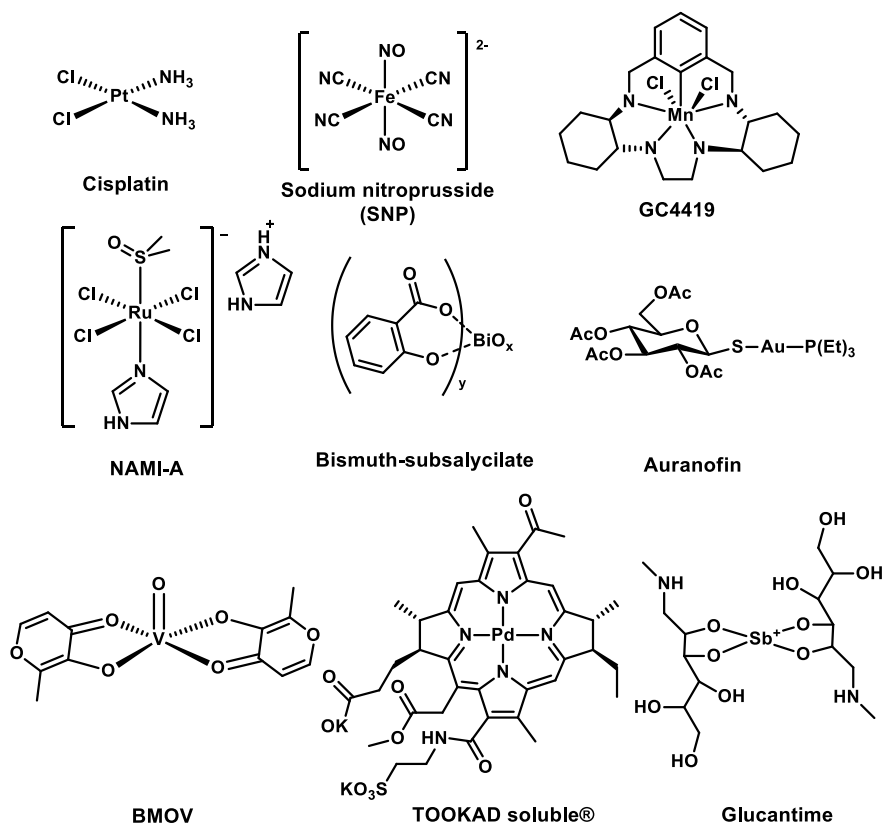


**Figure 1.1** Structures of some approved or candidate drugs that are in clinical trials



By the limited number of examples reported in **Figure 1.1**, it is clear that metal compounds offer huge possibilities in designing new drugs, with respect to organic molecules. Metal elements are a highly versatile platforms, since the variation of the metal ion, its oxidation state, coordination numbers and the consequent wider number of relative geometries, makes possible the access to uncountable different combinations. Moreover, modifications of the ligands allow to fine-tune physical-chemical properties, reactivity, thermodynamics, and kinetic stabilities of the resulting species.<sup>2,3</sup>

In this frame, antitumoral metal-compounds occupies a leading role, and a prominent part of efforts in searching new drugs is focused to discover new agents for fighting cancer. Cancer is a worldwide health problem and one of the principal causes of death in the world.<sup>4</sup> Proposing valid therapies to neutralize its devastating power is a strong social urgency which motivates and supports the research. Historically, modern medicinal inorganic chemistry was born in late '60, when Barnett Rosenberg and Loretta Van Camp serendipitously discovered that platinum compounds were able to inhibit cell growth.<sup>5</sup> Subsequent studies led to the approval and to the introduction in anticancer clinical treatments of the compound *cis*-dichlorodiamineplatinum(II), commonly known as cisplatin, by the U.S. Food and Drug Administration in 1978.<sup>6</sup> Several multidisciplinary contributions regarding its in-solution reactivity, binding to biomolecules, mechanism of action, pharmacodynamic, pharmacokinetic, and every aspect involved in its activity as antitumor drug have been published over years.<sup>7-12</sup> This outcome was a watershed in the field, stimulating several generations of chemists to explore and to design new metal complexes for the treatment of cancer. Following cisplatin, other Pt-based compounds have been proposed and approved for clinical use, making platinum the most represented metal within anticancer drugs.<sup>13</sup>

Although their efficacy in curing cancer, the use of Pt-based drugs involves severe drawbacks, which limit their administration over time. Several strategies have been pursued in recent years to find new alternatives able to overcome such drawbacks. The most interesting ones involve use of organometallic Pt(II) complexes, Pt(IV) “pro-drugs”, the use of different metals, the use of devices to target the therapy (conjugation to bio-derived fragments, nanocarriers, supramolecular assemblies), and treatments different by chemotherapy (PDT, PACT, thermotherapy). Behind all these strategies there is the awareness that the design of metal-drugs offers enormous chances, due to the high tunability of metal complexes, which often results in unpredictable as well as unexpected diversity in their biological activity, pharmacological properties, and mechanism of action.

## 1.2 Platinum-Based anticancer drugs

### 1.2.1 *Cisplatin and its derivatives*

Cisplatin (**Figure 1.2**) is the “progenitor” of Pt-based anticancer drugs, and several studies have been performed on its pharmacological properties. It is a neutral Pt(II) coordination complex, with two ammonia and two chlorido ligands disposed in *cis* arrangement. As common for  $d^8$  metal ions, it is a  $16 e^-$  square planar complex.

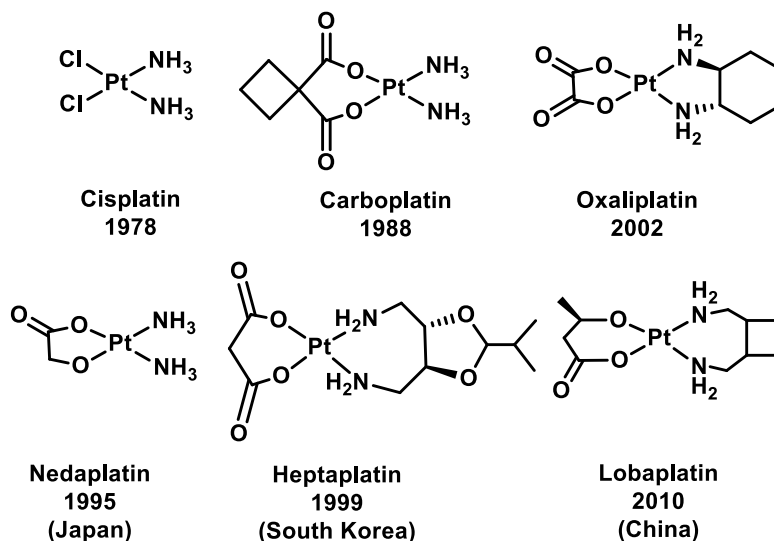


**Figure 1.2** Platinum-based anticancer drugs used in clinical treatments in the world or in single nation state, with the year of approval

The most accepted theories summarize the mechanism of action of cisplatin in four key steps,<sup>14</sup> depicted in **Figure 1.3**:

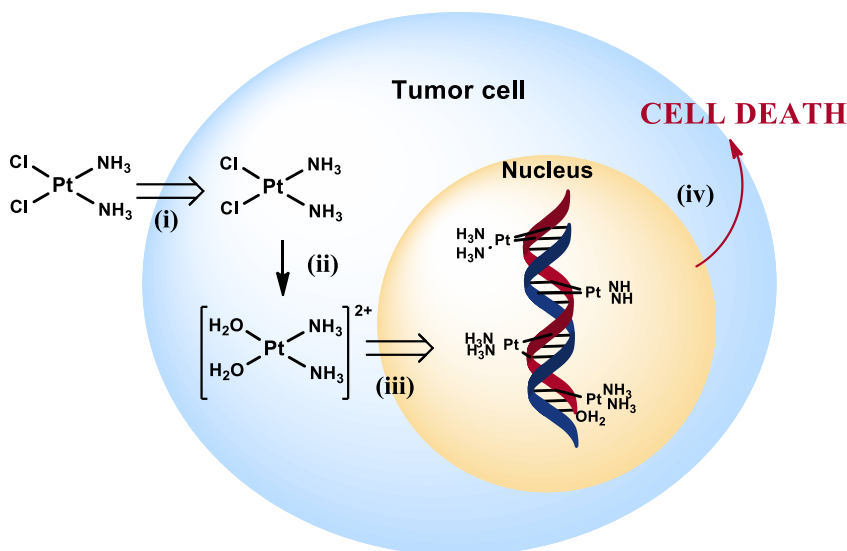


**Figure 1.3** Cellular and molecular events describing *cisplatin* mechanism of action

- (i) **Cellular uptake.** Cisplatin can be internalized in cells by passive diffusion through the cellular membrane, facilitated by the small size, the neutrality, and the planar geometry of the molecule.<sup>15,16</sup> Alternatively, membrane proteins, as copper transporters are invoked in the process of internalization.<sup>17,18</sup> To date, it is not clear which one is the predominant mechanism, but it is reasonable to affirm that both can occur simultaneously.
- (ii) **Activation by aquation.** Once into the cell, cisplatin undergoes to aquation of one or both chlorido ligands,<sup>19</sup> which *activate* it. Before entering the cell, the hydrolysis is suppressed or at least reduced, due to the high chloride concentration in plasma ( $\sim 100$  mM).<sup>20</sup> In cytosol, chloride concentration drops ( $\sim 4$  mM), and the hydrolysis of the chlorido

occurs, yielding a highly electrophilic aqua-species, reactive with nucleophiles.

- (iii) **DNA binding.** Aqueated cisplatin arrives at the nucleus and binds nuclear DNA, via coordination to the *N*-heterocyclic nucleobases. In particular, N7 atoms of purine residues (mostly guanine) are the preferential sites of coordination, since they are the most nucleophilic ones.<sup>21,22</sup> Such monofunctional adducts can evolve by the coordination of another guanine, forming *inter*- or *intra*-strand cross-links on the double helix (**Figure 1.4**).<sup>23</sup>

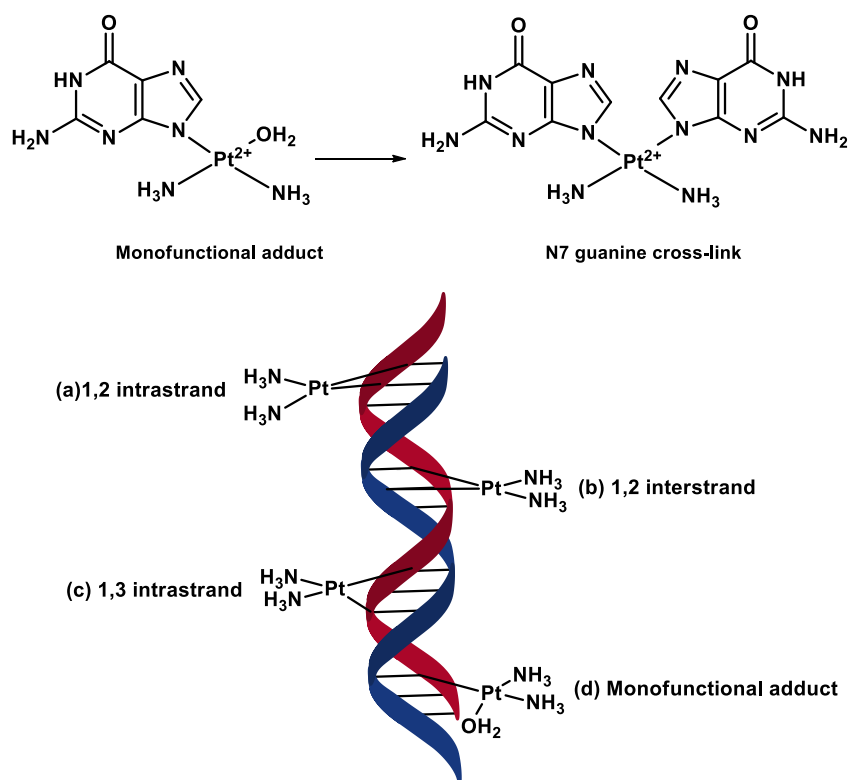


**Figure 1.4.** Possible adducts formed between *cisplatin* and DNA (N7) guanine

- (iv) **Cellular response to DNA binding.** Cisplatin-DNA adducts distort the structure of the double helix. Adducts with different Pt-based drugs, resolved by X-ray crystallography or NMR spectroscopy (**Figure 1.5**), evidenced bending and unwinding of the double helix.<sup>24</sup> The presence of coordinated Pt molecule interferes with the transcription process and with duplication of DNA during cell cycle replication, and if the cell is not able to repair the damage, there is the activation of pathways which leads to the programmed death of the cell.<sup>25</sup>

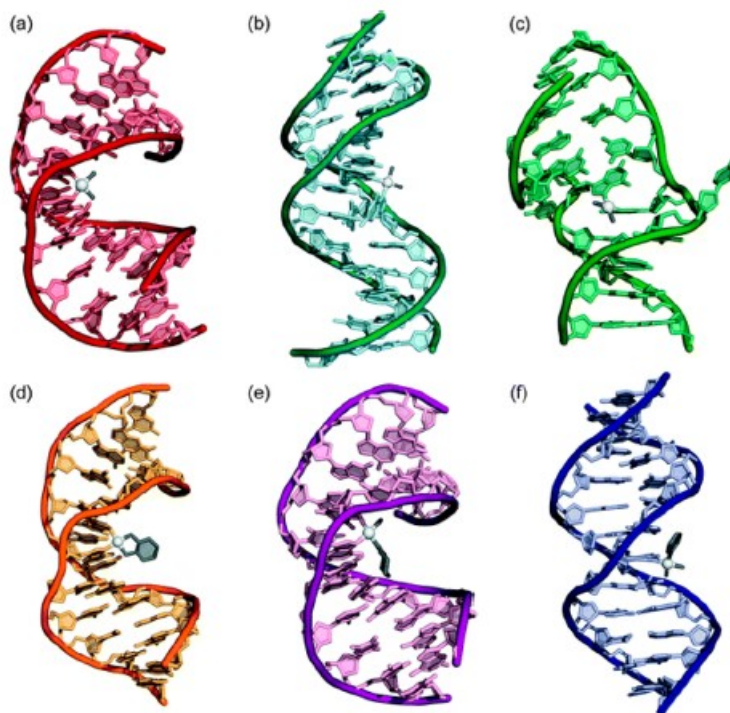


**Figure 1.5.** Structures of double-stranded DNA adducts of different platinum anticancer agents as determined by X-ray crystallography or NMR spectroscopy. (a) Cisplatin 1,2 intrastrand cross-link (PDB 1AIO). (b) Cisplatin 1,3 intrastrand cross-link (PDB 1DA4). (c) *Cisplatin* interstrand cross-link. (d) Oxaliplatin 1,2 intrastrand cross-link (PDB 1PG9). (e) Satraplatin 1,2-d intrastrand cross-link (PDB 1LU5). (f) cisplatin monofunctional adduct (PDB 3CO3). Figure Reproduced with permission from ref 24.

It should be noted that the events described represent the most desirable pathways following cisplatin administration. Indeed, binding to DNA does not ensure apoptosis, since cisplatin lesions can be removed by the nucleotide excision repair (NER) mechanism, that can ultimately lead to cells resistant to cisplatin treatment.<sup>26,27</sup> It is also worth to mention that coordination to DNA may not be the unique interaction which triggers cell death. In a recent review, Dyson and Sava support the hypothesis that binding to proteins and to RNA can be considered to play a role in the pathway ending with the programmed death of the cell.<sup>28</sup> Another hypothesis invokes the ability of platinum drugs to modulate the immune system, and a detailed account of such mechanism has been described.<sup>29</sup>

However, it is also known that a considerable amount of administrated cisplatin embraces different fates, not leading to cell death. Once in the bloodstream it can interact with other blood components, mainly the protein HSA (human serum albumin) which is rich of *soft* sulfur-donor residues, particularly available to coordinate platinum ions.<sup>30,31</sup> The sequestration of cisplatin by serum proteins inactivates the drug and dramatically reduces the amount of platinum which reaches the target. Moreover, even the part of drug that arrives in cell the target can be inactivated by metallothioneins and glutathione (GSH), involved in detoxification processes of the cell. Indeed, glutathione-cisplatin adducts are readily removed from the cytoplasm by dedicated export pumps, preventing cisplatin to perform its action.<sup>26</sup>

Along with studies on the biological mechanisms involved in anticancer activity of cisplatin, attempts to improve its pharmacological performances resulted in the introduction in clinical use of several derivatives. In carboplatin and nedaplatin (**Figure 1.2**) the chlorido ligands are replaced by chelating carboxylate ligands. Chelating ligands still act as leaving groups in the aquation process, but the chelating effect changes the kinetic of the process making the whole complex

more stable.<sup>32,33</sup> Moreover, glycolate in nedaplatin enhance water solubility with respect to cisplatin (10 mg/mL vs 2.5 mg/mL).<sup>14</sup> Following to these, chelating diamines were combined to chelating carboxylates, resulting in the discovery of other three drugs (**Figure 1.2**). Heptaplatin, developed and clinically approved in South Korea has a malonate and a chelating 2-(1-methylethyl)-1,3-dioxolane-(4,5-dimethanamine), which forms a seven-membered ring with the Pt center, giving the drug its name. Lobaplatin, regularly approved in China, also forms a seven-membered ring similarly to heptaplatin, with a stereogenic diaminocyclobutane ring, instead of the the dioxolane ring. Interestingly, the drug is formulated with a racemic mixture of diaminocyclobutane, containing both the *R,R* and *S,S* enantiomers. Since the leaving group is the chiral *S*-lactate, the drug is available as a mixture of diastereoisomers.<sup>34</sup> Finally, the most recent globally approved cisplatin derived is oxaliplatin characterized by a chelating *trans*-1,2-diaminocyclohexane (DACH) in the configuration the *R,R*, and an oxalate leaving group.<sup>35</sup> In this case, only one stereoisomer is used, and it has been proved that the enantiomeric *S,S* as well as the *cis-meso* form of DACH have a reduced anticancer activity. By crystallographic studies performed on adduct between oxaliplatin and a DNA dodecamer duplex, Lippard et al. observed that *R,R* ligand forms a hydrogen bond using a pseudo-equatorial N-H hydrogen atom with the O6 atom of a guanine residue that binds oxaliplatin. Such interaction is not possible with the *S,S* and the *meso* ligands.<sup>36,37</sup>

Compared to cisplatin, the described drugs present differences in the chemical structure which alter the pharmacological profile and the scope of application in clinical therapies. A summary with the main characteristics and target tumors which distinguish discussed drugs is reported in **Table 1.1**.



**Table 1.1.** Main characteristics of the clinically approved platinum drugs (table adapted with permission from ref 28)

Drug	Main Characteristics	Target tumours
<b>Cisplatin</b>	The most clinically used platinum drug; included in many combination regimens comprising biological/biotechnological drugs	Ovarian, testicular, bladder, colorectal, lung and head and neck cancers
<b>Carboplatin</b>	Same as cisplatin but less toxic and suitable for more aggressive high-dose chemotherapy	Same as cisplatin but with limited efficacy against testicular germcell cancers, squamous cell carcinoma of the head and neck and bladder cancer
<b>Nedaplatin</b>	Similar to carboplatin. Recommended therapeutic dose 80–100 mg/m <sup>2</sup> .	Non-small and small cell lung cancer, esophageal cancer, uterine cervical cancer, head and neck cancer, or urothelial cancer
<b>Heptaplatin</b>	Active in cisplatin resistant tumours	Gastric cancer
<b>Lobaplatin</b>	Structurally very similar to oxaliplatin; standard dose: 35 mg/m <sup>2</sup>	Chronic myeloid leukemia, small cell lung cancer, breast cancer
<b>Oxaliplatin</b>	Bulkiness and lipophilicity are believed responsible for differential processing of platinum-DNA adducts	Mainly colorectal cancers but under clinical trials for pancreatic, gastric, breast and non-small cell lung cancers

However, shared features are predominant. Indeed, cisplatin derivatives display a general mechanism of action very similar to their progenitor. One aspect of this mechanism should be underlined: *platinum drugs do not have any feature that allow them to distinguish between cancer cells and non-cancer cells*. This means that the events discussed in this section can occur indiscriminately in tumor and healthy tissues, with dramatic effects for patients. Indeed, the administration of platinum-drugs very often results in the insurgence of disabling side-effects that

along with phenomena of resistance to therapy, dramatically reduce their efficacy in clinical use.

### *1.2.2 Side Effects of Platinum-based chemotherapies*

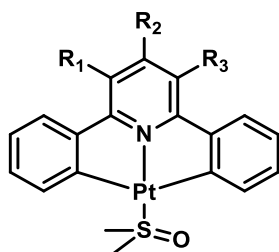
Side-effects related to Pt-based anticancer chemotherapies have been subject of study in medicine, biology, and biochemistry for years. The lack of selectivity for cancer cells leads to the accumulation of the drug in healthy organs and tissues. Fast-growing cancer cells uptake great amount of nutrients and platinum-based drugs are internalized thanks to this necessity. Similarly, also healthy fast-growing tissues uptake platinum-drugs and are particularly affected by chemotherapies, resulting in neurotoxicity, gastrointestinal toxicity, loss of hair, and reduced production of red and white blood cells. Kidney and liver are affected since the detoxification processes of the body involves the excretion in urine or attempts to metabolise the drug in the liver.<sup>38</sup> Platinum drugs side effects are also related to their high reactivity with serum proteins and targets involved in detoxification processes. The development of cisplatin derivatives was rationally based to reduce the uncontrolled reactivity of cisplatin. Indeed, substitution of chloridos with chelating ligands, which enhance the inertness of the complex toward aquation, led to reducing the level of toxicity of cisplatin. Such reactivity is also considered in the formulation and administration of platinum drugs. Cisplatin is formulated in NaCl solution to slow down the rate of aquation, while carboplatin and oxaliplatin are usually formulated in glucose solutions, since in presence of an excess of chlorides the carboxylate can be replaced giving rise to cisplatin analogues, losing the beneficial effect of chelating ligands.<sup>38</sup>

The close relationship between reactivity and drawbacks related to the administration of platinum-based drugs prompted chemists to explore different

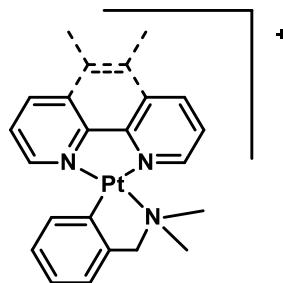
strategies to access new platforms and classes of metal compounds able to overcome these limitations and to improve the quality and the efficacy of metal drugs. Some of these strategies will be discussed in following sections, starting from the use Pt(II) organometallic agents.

### 1.2.3 *Organoplatinum(II) complexes*

Platinum organometallic complexes offer extensive opportunity in medicinal chemistry, and they can be considered valid alternatives to approved anticancer drugs. The presence of  $\sigma$  C-Pt bonds deeply modifies the overall properties of the resulting complexes. It can give access to different reactivities affecting the interactions with biological molecules and resulting in alternative modes of action. Moreover, the great variety of available organic fragments allows to finely tune the properties of organoplatinum compounds, much more than in their non-organometallic counterparts. Typically, organoplatinum(II) complexes are square planar (*sp*) 16  $e^-$  species and their versatile chemistry allows to choose ligands from a wide pool of possibilities involving alkyl or aryl groups, halides, amines, imines, sulphides, phosphines, and alkenes.<sup>39</sup> In this frame, cyclometalated organoplatinum(II) with aromatic scaffolds are a notable class, widely explored in anticancer theranostics.<sup>40,41</sup> Indeed, cyclometalated complexes can exhibit remarkable optical properties and they are tested as anticancer agents as well as to target biomolecules acting as luminescent probes.<sup>42</sup> Recently, a series of Pt-DMSO complexes with [C,N,C] functionalized ligands has been studied by Zhang et. al.<sup>43</sup> (**Figure 1.6** left).



Zhang, X.Tian,Y.Tian et al.  
2021



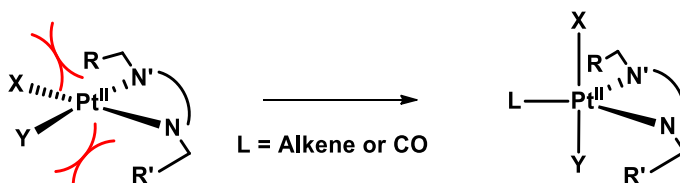
Zamora, Barone,Ruiz et al.  
2021

**Figure 1.6.** Cyclometalated Pt(II) complexes reported as anticancer theranostics agents

The compounds showed remarkable thermal and photostability and enhanced multi-photon absorption and emission properties. Their results showed a notable *in vitro* and *in vivo* cytotoxicity and a preferential localization of the complexes in lysosome was observed by confocal microscopy. Similarly, a series of [C,N] complexes with aromatic chelating diimine studied by Zamora et al.<sup>44</sup> (**Figure 1.6** right) was found to recognize and bind specific DNA sequences in distinct way, as stated from different changes in their light-emission properties. Moreover, the complexes were active in low micromolar concentrations ( $IC_{50}$ ) in 2D cell culture and 3D tumor spheroids.

However, platinum(II) organometallic chemistry spans over different molecular geometries and other structures are accessible whereas less represented. Five-coordinate  $18\ e^-$  organoplatinum(II) complexes are achievable through an opportune choice of the ligand environment.<sup>45</sup> Indeed, the coordination of a N,N' bidentate ligand with steric hindrance in the plane destabilizes *sp* geometry, by unfavourable steric interactions with the adjacent ligands. In presence of neutral  $\pi$ -acid ligands L, as alkenes and CO, the addition occurs resulting in the formation

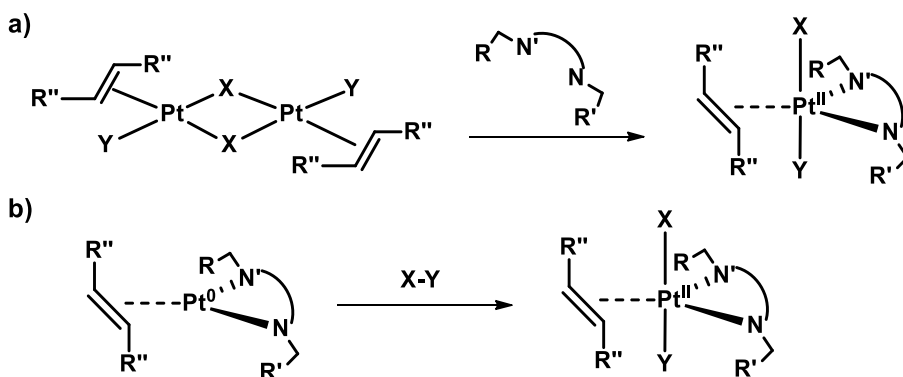
of a trigonal bipyramidal complex (*tbp*, **Scheme 1.1**) with the N,N'-bidentate and L in the equatorial plane and ligands X and Y in apical positions.<sup>46</sup>



**Scheme 1.1.** Addition of  $\pi$ -acid ligands and formation of *tbp* complexes

Olefin complexes have been intensively studied in last decades by A. Panunzi group and G. Natile group, as regards their synthesis, stereochemistry and reactivity. Such type of compounds has been studied in the present work, therefore some of their chemical characteristic will be now discussed.<sup>47</sup>

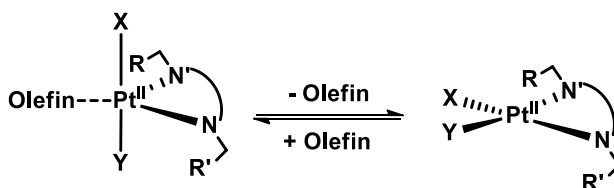
The addition path showed in **Scheme 1.1** is not the only method to access five-coordinate *tbp* complexes.<sup>48</sup> Other general strategies are reported in **Scheme 1.2**



**Scheme 1.2.** Alternative routes to access organoplatinum(II) *tbp* complexes

According to path a) in **Scheme 1.2** the reaction of the appropriate N,N'-ligand with Zeise's dimer results in the formation of stable five-coordinate Pt(II) olefin complex. Another strategy involves the oxidative addition to a suitable Pt(0) three-coordinate precursor. These synthetic strategies have been adapted to several

systems resulting in the synthesis and characterization of a plethora of *tbp* Pt(II) olefin complexes with many different olefins, N-N' ligands, and axial ligands. The nature of both the N,N'- and alkene ligands strongly affects the thermodynamic stability of the resulting complexes. Indeed, in many cases *tbp* complexes are in equilibrium with the analogue *sp* species following release/addition of the olefin (Scheme 1.3).<sup>48</sup>



**Scheme 1.3.** Reversible release/addition of olefin in *tbp* Pt(II) complexes

N,N' is usually a nitrogen bidentate ligand forming five-member ring upon coordination to Pt center. Planar  $sp^2$  hybridized N-N' ligands have been found to be the most suitable ligands to afford stable *tbp* complexes. The bulkiness in the equatorial plane of the *tbp* was found to be the crucial aspect governing the stability of the *tbp*. Indeed, by reducing the steric hindrance the resulting compounds become less stable. The impact of the N,N'-ligand on complexes stability is well explained considering a model complex [PtClMe(ethene)N-N] where N-N are phenanthroline derived ligands (**Figure 1.7**):

- in the 2,9-dimethyl-1,10-phenanthroline (*dmphen*) complex no release of ethene was observed even at high temperatures;
- the mono methyl 2-methyl-1,10-phenanthroline (*Me-phen*) analogue is isolable at ambient temperature, but reversible ethene release was observed and the equilibrium dissociation constant was determined;
- in the 1,10-phenanthroline (*phen*) complex there is an irreversible release of the ethene, and the compound not isolable.

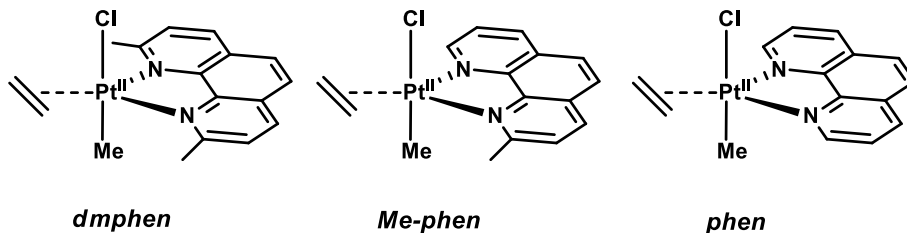


**Figure 1.7.** [PtClMe(ethene)N-N] complexes with different phenanthroline ligands

Consequently, *dmphen* emerged over years as privileged N,N' to get stable *tbp* olefin complexes, even considering its symmetry which reduces the number of possible stereoisomers in complexes with substituted alkenes. Strong electron-withdrawing olefins increase the stability of the corresponding *tbp* complexes due to the high metal-to-olefin  $\pi$ -back donation which result in a partial  $sp^2 \rightarrow sp^3$  rehybridization of alkene carbons, and the whole structure representable as a hybrid between two mesomeric forms, depicted in **Figure 1.8**.<sup>49</sup>

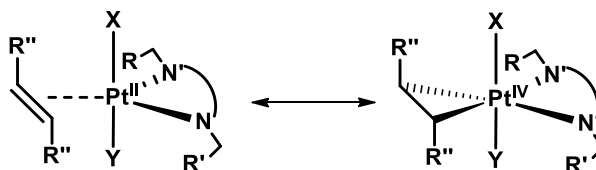


**Figure 1.8.** Mesomeric structures in olefin *tbp* organoplatinum(II)

The apical positions of the bipyramid are usually occupied by strong  $\sigma$ -donor groups which contribute to the overall stability of the *tbp*. The synthetic adaptability of this system resulted in the preparation over years of several compounds containing a variety of fragments as anionic alkyl, aryl,<sup>50</sup> halides,<sup>51</sup> chalcogenides,<sup>52,53</sup> hydrides,<sup>54</sup> or neutral nitrogen-<sup>55</sup> or sulfur-containing ligands,<sup>56</sup> as well as other organometallic fragments, e.g., Hg<sup>57</sup> and Pb<sup>58</sup> containing portions.

In some case, the anticancer properties of *tbp* organoplatinum(II) have been evaluated. The structure of some representative example is reported in **Figure 1.9**.

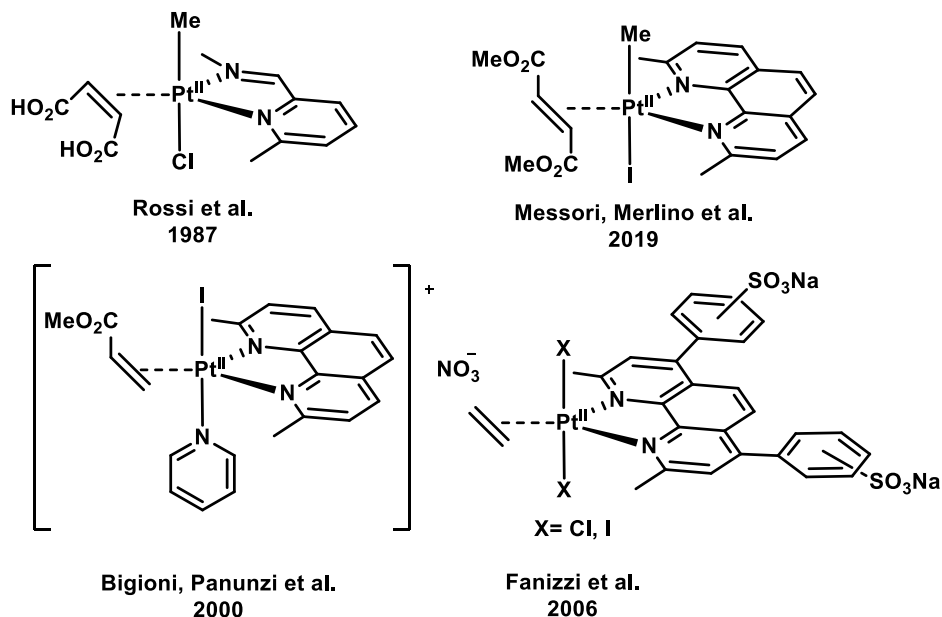


**Figure 1.9.** Structures of some *tbp* Pt(II) complexes tested as anticancer agents

One of the first reports dates to 1987, when Rossi et al. tested a *tbp* complex having an imino-pyridine chelating ligand, a chlorido and a methyl in apical positions, and maleic acid as olefin ligand.<sup>59</sup> The biological activity of the compound was found close to cisplatin in terms of cytotoxicity and cell growth inhibition. Interestingly, it was postulated that the presence of strong *trans* activating methyl ligand could promote the substitution of the chlorido in *trans* position, generating a coordination position to bind biomolecules with retention of the coordination number. Such hypothesis was recently verified by Messori, Merlino et al. by studying the reactivity of a dimethyl fumarate-*dmphen* complex with a methyl and a iodido ligand in apical positions, by X-ray crystallography.<sup>60</sup>



The complex forms an adduct with the model protein RNaseA by substituting the iodido ligand with an amino-acid residue and retention of the *thp* geometry. Another interesting example was reported by Bigioni, Panunzi et al. who reported a series of water-soluble cationic iodo-pyridine complexes with different N,N' and olefin ligands.<sup>61</sup> Among them, the derivative with *dmphen* and methyl acrylate was found to be the most cytotoxic showing an activity comparable or higher to cisplatin depending on the cell line. Finally, another class of *thp* organoplatinum(II) was reported by Fanizzi et al. in 2006. In this work authors used sulfonated 2,9-dimethyl-4,7-diphenyl-1,10-phenanthroline ligand as *dmphen* analogues, to increase water solubility in a series of di-halo (chloro and iodo) ethene complexes.<sup>62</sup> The compounds were soluble and stable in water, and they displayed a cytotoxicity close to cisplatin with even higher cellular uptake. Such data are consistent with the hypothesis that organoplatinum(II) complexes may be a valid alternative to approved Pt(II) drugs either in *sp* or in *thp* fashions. In both cases evidence of different reactivity and mechanisms of action with competitive cytotoxicity have been obtained.

#### 1.2.4 Platinum(IV) “pro-drugs”

Pt(IV) compounds have been thought to reduce side effects of Pt(II) drugs, by reducing the “intrinsic reactivity” of the complex. Pt(IV) compounds are generally defined “prodrugs”, referring to the their ability to transform in biological environment with the *in situ* formation of the active drug.<sup>63</sup> In last years, the promising efficacy of Pt(IV) prodrugs led to the entering in clinical trials of the four complexes reported in **Figure 1.10**, although none of them was found suitable to reach the clinical use.

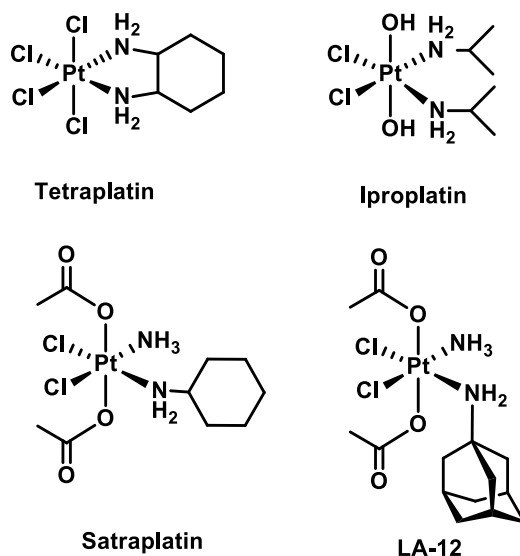


**Figure 1.10.** Pt(IV) drugs undergone to clinical trials

The general structure of a Pt(IV) prodrug is reported in **Figure 1.11**:

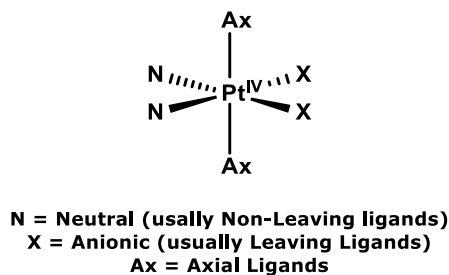
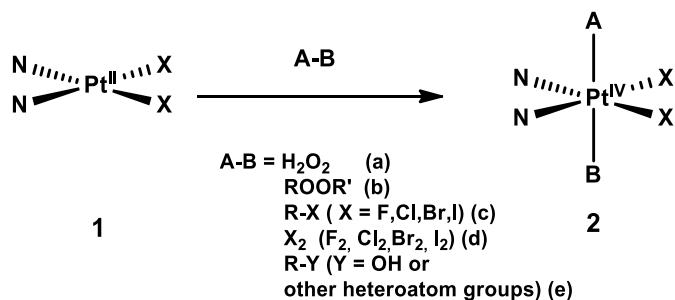


**Figure 1.11.** General structure of a Pt(IV) prodrug

The switch to the oxidation state +4 reduces unwanted interactions with proteins and relevant biomolecules in bloodstream.<sup>64</sup> Indeed, Pt(IV) is a  $d^6$  ion, that nearly always forms low-spin,  $18 e^-$  complexes in octahedral coordination environment. Such features make the complexes highly inert toward ligand substitution and

limit the reactivity toward nucleophiles with respect to tetracoordinate, 16 e<sup>-</sup> Pt(II) agents. Non-leaving ligands (N) are usually amines or N-based ligands in monodentate or chelating fashion. X ligands are usually anionic species as halides or chelating carboxylates, similarly to the leaving groups described for Pt(II) drugs.<sup>63</sup> In some cases, alkyl or aryl groups can be used as ligands, giving rise to organometallic species. As already mentioned for Pt(II) organometallic compounds, the presence of a  $\sigma$  C-Pt bond can dramatically change the properties of the complex, affecting the overall stability and providing the access to a different reactivity which can result in unpredictable mechanisms of actions.<sup>65</sup> Axial positions (Ax) are usually occupied by anionic ligands derived by carboxylic acids, *e.g.*, carboxylates, carbamates, or carbonates. The general synthetic approach to access Pt(IV) compounds is reported in **Scheme 1.4**.<sup>66,67</sup>

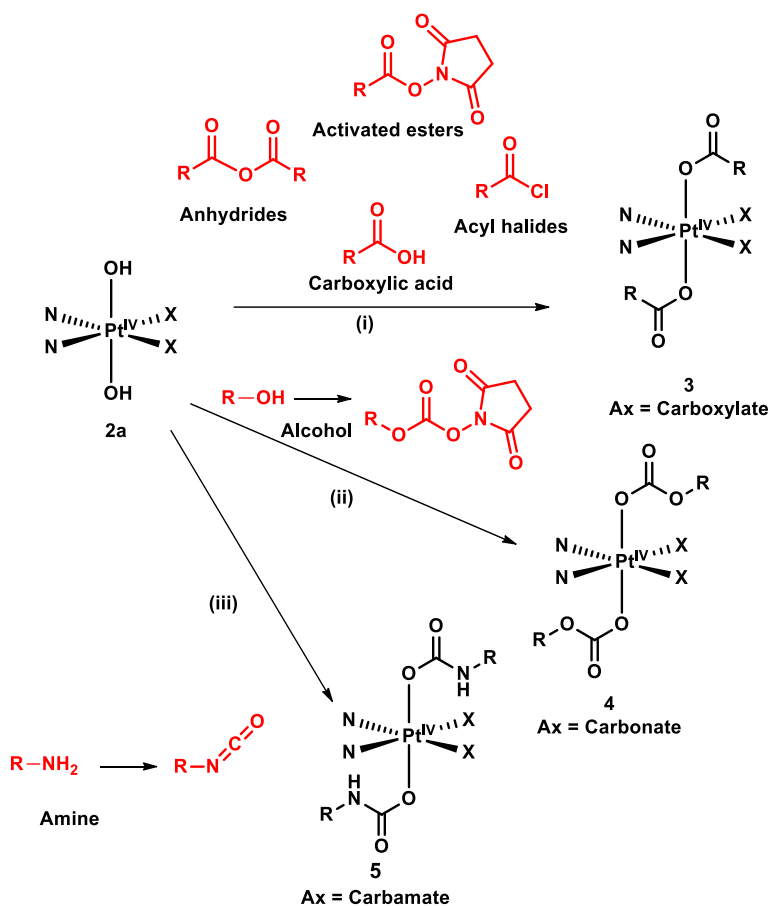


**Scheme 1.4.** Synthetic strategy to access Pt(IV) complexes

A selected Pt(II) complex (**1**) can be oxidized to the Pt(IV) species (**2**) by oxidative addition with the appropriate oxidant, most commonly H<sub>2</sub>O<sub>2</sub>, organic peroxides, alkyl or aryl halides or molecular halides. The hexacoordinate Pt(IV) product display a stereochemistry strictly dependent on the nature of the ligands and on the mechanism of reaction by which the oxidative addition occurs. With the

appropriate ligands on the Pt(II) reagent, an intramolecular oxidative addition can occur, resulting in the organometallic cyclometalated Pt(IV) product.<sup>68</sup>

However, as for Pt(II), organometallic species are a minority in current literature. The most common type of Pt(IV) prodrugs are obtained by oxidizing cisplatin, carboplatin or oxaliplatin cores with H<sub>2</sub>O<sub>2</sub>. Usually, the product has the four ligands of the starting Pt(II) core occupying the coordination position in the equatorial plane of the octahedron and two OH occupying axial positions.<sup>69</sup> The di-hydroxide Pt(IV) species (**2a** in **Scheme 1.5**) resulting from the oxidation by H<sub>2</sub>O<sub>2</sub> is a versatile intermediate which can be used for further functionalization in axial positions.<sup>70</sup> Most common synthetic strategies involve the use of carboxylic acid derivatives, to functionalize the apical positions. Some general examples are reported in **Scheme 1.5**.



**Scheme 1.5.** Common synthetic strategy to access to axial functionalization of dihydroxido Pt(IV) complexes

The OH ligands in **2a** (**Scheme 1.2**) are nucleophilic moieties, close in reactivity to organic hydroxyls. Indeed, the **2a** can be reacted with carboxylic acids (path (i) in **Scheme 1.2**) in typical organic condensation reactions using DCC, EDC, TBTU, or HBTU. Alternatively, it is possible to convert the acid to a more reactive derivative as acyl halides, anhydrides, and activated esters, to yield product of

type **3** in **Scheme 1.5**. It is also possible to access carbonates (**4**) or carbamates (**5**) derivatives, starting from alcohols or amines respectively.<sup>71–73</sup> In this case, the organic substrate is converted to a reactive carbonate or isocyanate, subsequently reacted with the di-hydroxide Pt(IV) compound. Indeed, the rational selection of the ligands allows to enhance the biological performances of the drug by tuning lipophilicity, enhancing tumour-targeting properties cells, and conjugating to bio-active fragments or to nanocarrier systems, able to lead the drug selectively in cancer tissues.

Such synthetic variety is reflected in the chemical and biological properties of the resulting prodrugs. **Ax** may also be a bio-active fragments, as an organic drug, able to exert an independent anticancer or synergistic pharmacological activity when released into the cell. It is generally accepted that Pt(IV) complexes are activated by reduction to the analogue Pt(II) species, in highly reducing cellular environment (**Figure 1.12**).<sup>70</sup>

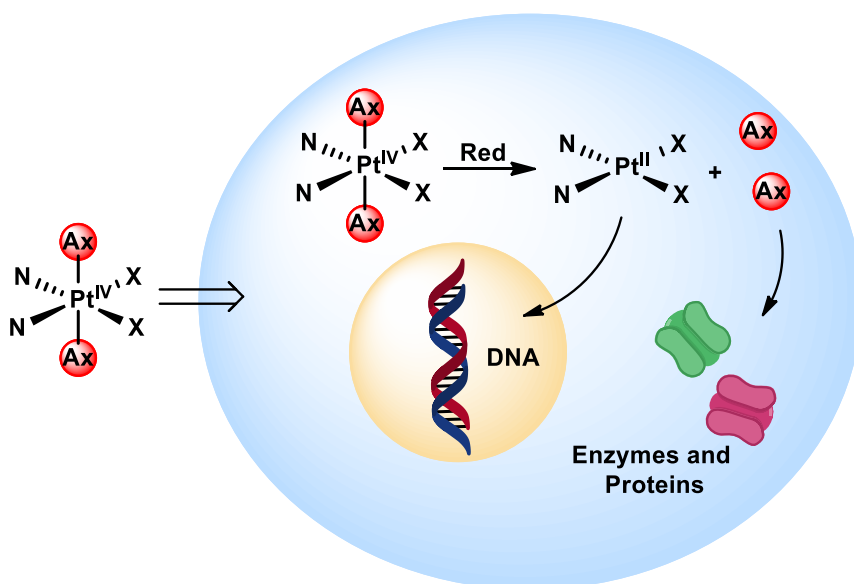


**Figure 1.12.** Schematic representation of the mechanism of action of Pt(IV) prodrugs

Glutathione, ascorbate, nicotinamide adenine dinucleotide (NADH) and cysteine-rich proteins are considered the most likely reducing agents for Pt(IV) complexes.<sup>74–76</sup> Arnesano et al. reported that also cytochrome c could be involved in the reduction of Pt(IV) to Pt(II), playing a catalytic role in the electron-transfer reaction.<sup>77</sup> It should be mentioned that the same process could occur either in cancer or non-cancer cells. However, the hypoxic environment in cancer cells favors the reduction process, while in normal oxygenated cells the drug is reduced but rapidly re-oxidized to the Pt(IV) inactive form. Indeed, it has been found that the coordination of Pt(IV) complex to DNA and proteins occurs slowly and it is not of clinical relevance.<sup>64</sup> The reduction process leads to the release of an active Pt(II) fragment, able to bind DNA, and of the two axial ligands.

If **Ax** is a rationally selected bio-active fragment, it will interact with enzymes or other specific cellular targets once released, giving rise to a dual-target anticancer effect. Promising studies on dual-action Pt(IV) platforms have been reported in recent years, attracting great interest toward this class of compounds. Some examples are reported in **Figure 1.13**

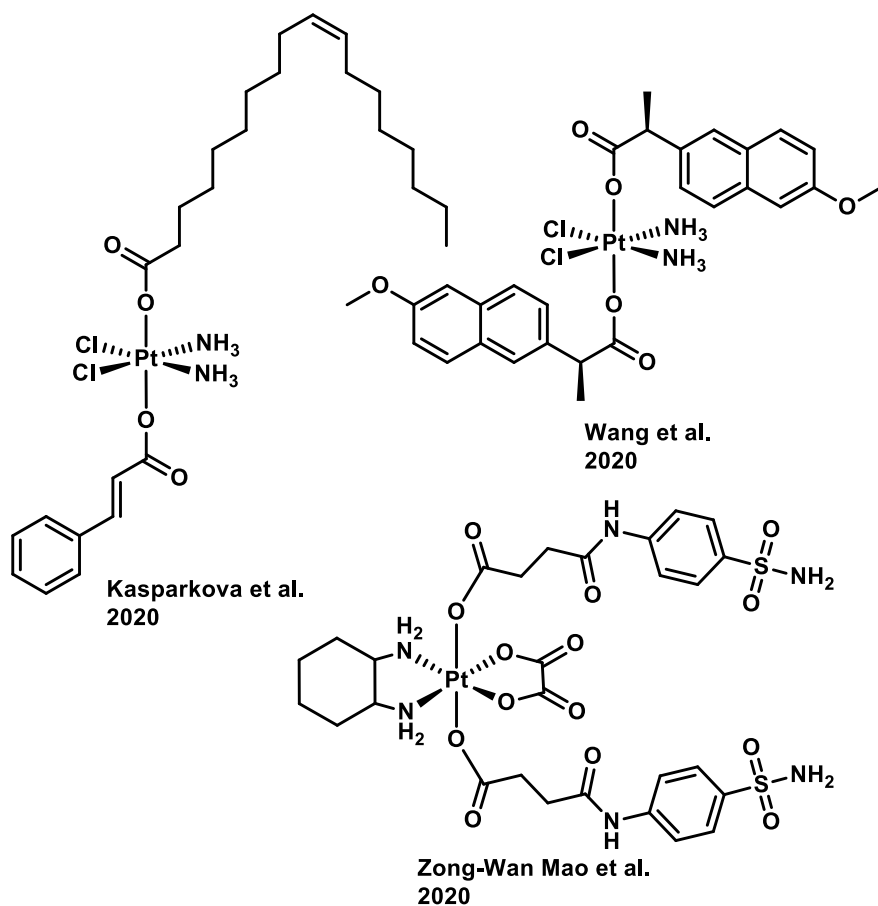


**Figure 1.13.** Structure of recently reported Pt(IV) dual-target platforms

Wang et al reported a Pt(IV) complex combining a cisplatin-like core with two units of the non-steroidal anti-inflammatory drug *Naproxen*, which showed promising activity toward breast cancer.<sup>78</sup> Indeed, *Naproxen* is an inhibitor of the enzyme cyclooxygenase COX-2, overexpressed in breast cancer and involved in several pathways related to inflammatory processes and proliferation of breast cancer. Their study showed the multi-specificity of the complex that kills cells



and reduces tumorigenesis by inhibiting the expression of COX-2, binds DNA, and inhibits pro-inflammatory cytokines.

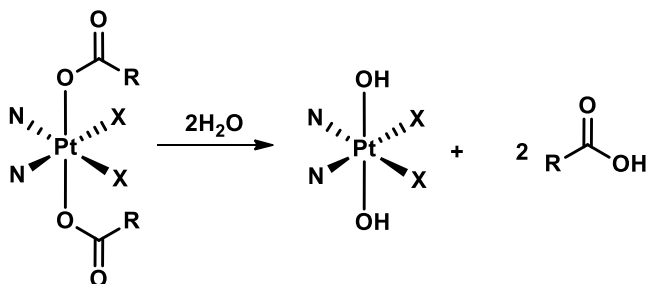
Zong-Wan Mao et al. targeted the transmembrane protein carbonic anhydrase IX (CAIX) by conjugating cisplatin and oxaliplatin cores to a CAIX inhibitor.<sup>79</sup> CAIX is overexpressed in cancer tissues, and it is responsible for the intra- and extra- cellular pH regulation, catalyzing CO<sub>2</sub> hydration. Their compounds were found to be fairly active and selective for cancer tissues, and to affect tumor microenvironment and metabolic pathways of the cell with reduced in-vivo side effects.

Finally, Kasparkova et al., designed a non-symmetric Pt(IV) cisplatin-based complex with oleic (OA) and *trans*-cinnamic acid (CA) as axial ligands.<sup>80</sup> OA was found to suppress HER2 in breast cancer, a growth factor receptor typical of some type of cancer that are poorly responsive to chemotherapeutic regimens. Similarly, CA was found to affect HER2, to sensitize cancer cells to cisplatin activity, and to protect at some extent normal cells from the toxic effects of cisplatin itself. The complex showed a high antiproliferative activity against breast cancer cell lines, and both OA and CA released after intracellular reduction can trigger processes leading to downregulation of HER2. Simultaneously, the cisplatin core can bind nuclear DNA, resulting in cell apoptosis. Such examples provide a general overview on the advantage of synergistic and simultaneous effects exerted by dual-target platinum(IV) platforms.

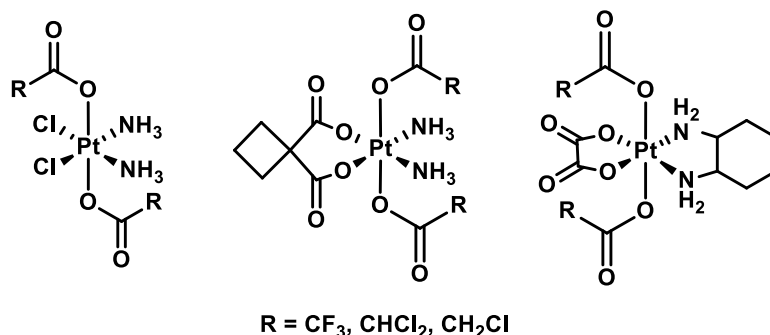
Beyond the biological effect of bio-active fragments, the choice of the axial ligands has an impact on the chemical properties of the resulting complexes, affecting the stability, the hydrolytic reactivity in aqueous media (**A** and **C** in **Figure 1.14**), and the redox potential. The second aspect is crucial to get the dual-target action of the axial ligands. The latter is fundamental in the light of the activation by reduction mechanism previously mentioned. Intense studies, aimed

to clarify the hydrolysis and the mechanism of reduction of Pt(IV) prodrugs, have been carried out, in recent years. Interestingly, the rate of hydrolysis was found to increase by increasing the electron-withdrawing ability of halogen substituents in a family of Pt(IV) halo-acetate complexes containing cisplatin, carboplatin and oxaliplatin cores (**B** in **Figure 1.14**). CF<sub>3</sub>- and CHCl<sub>2</sub>- substituted complexes were found to undergo fast hydrolysis, while CH<sub>2</sub>Cl- analogues were stable in aqueous solution.<sup>81</sup>

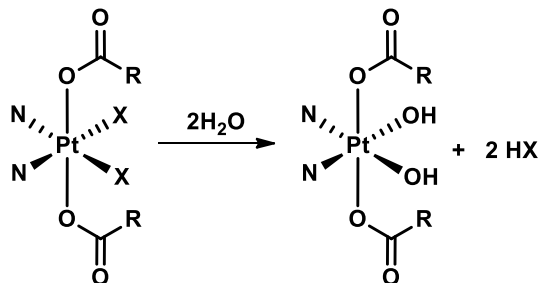
**A) Hydrolysis of Axial ligands in Pt(IV) prodrugs**



**B) Gibson et al. 2015**



**C) Hydrolysis of Equatorial ligands in Pt(IV) prodrugs**



**D) Kowol et al. 2019**

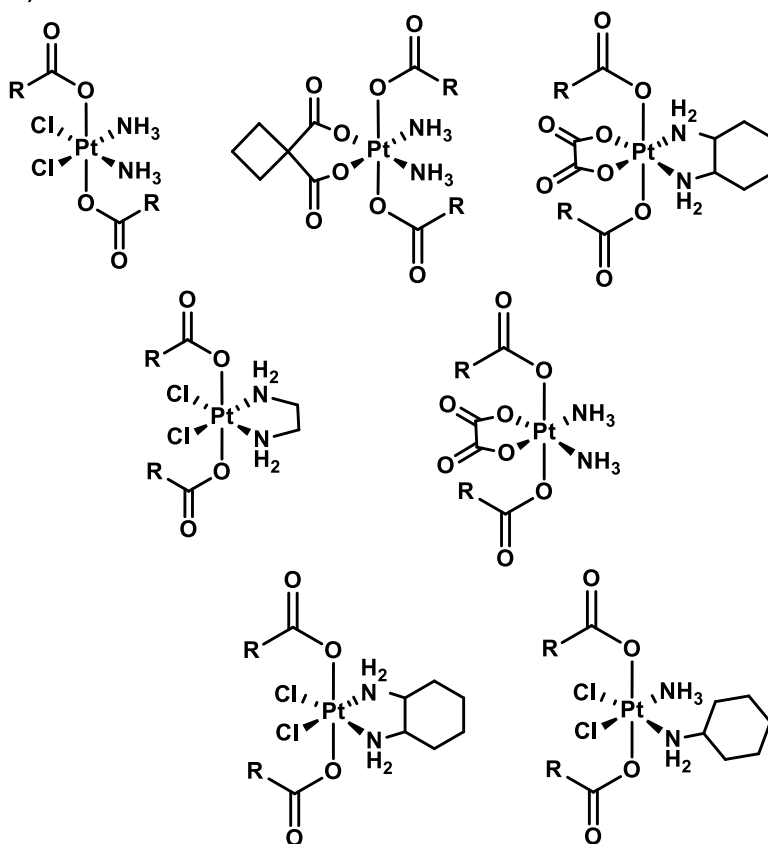
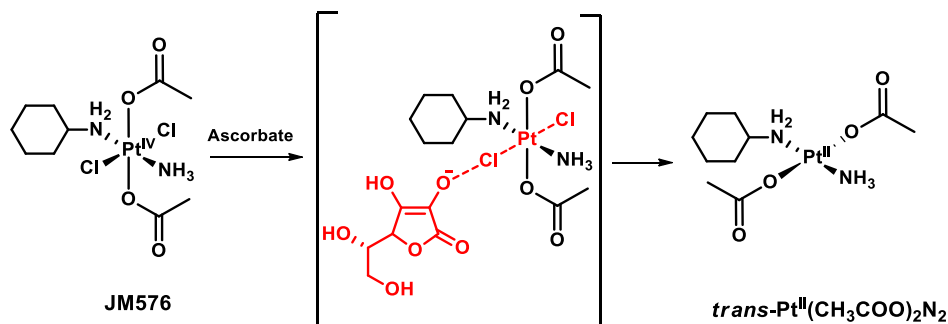


**Figure 1.14.** Hydrolysis of axial (A) and equatorial (C) ligands in Pt(IV) prodrugs and examples of compounds object of studies (B and D)

More recently, Kowol et al. definitively put in doubt the “dogma” of the high kinetic inertness of Pt(IV) prodrugs, with an extensive study on the hydrolysis of equatorial ligands in Pt(IV) prodrugs (**C** in **Figure 1.10**). They studied a group of Pt(IV) complexes (**D** in **Figure 1.10**) combining amines, chlorides and chelating carboxylates, and observed that the hydrolysis of the axial ligands deeply alters the biological performances and the reduction potential of the complexes.<sup>82</sup> Such result confirms that the accurate design and the proper selection of ligands have an enormous impact on the biological performances of the resulting drug.

Concerning the reduction of Pt(IV) prodrugs, it would be crucial to control features that govern the potential and the kinetic of reduction, to optimize its spatial-temporal action. Indeed, if the complex is easily reducible, it will probably react before reaching target cells. This means that the complex would act as a Pt(II) drug binding biomolecules in bloodstream, not benefiting of the effect given by the higher oxidation state. Conversely, if the compounds are inert toward reduction, it would be considered inactive, since the coordination of Pt(IV) to DNA is too slow to trigger cell death. The reduction of Pt(IV) complexes occurs either via inner-sphere or outer-sphere electron transfer, and the type of Pt(II) product formed, as well as the kinetic of reduction depend on the structure of the complex and on the nature of the reducing agents.<sup>75</sup> The presence of chlorido or hydroxido ligands favours the kinetic of reduction since they act as bridge in faster inner-sphere electron transfer from the reductant to the Pt centre. An explicative example on the reduction of prodrug Satraplatin (JM216) and of its trans isomer (JM576), is reported in **Figure 1.15** and it is helpful to clarify all aspects involved in reduction of Pt(IV) prodrugs.<sup>83</sup>

**A) Inner-sphere electron transfer**



**B) Outer-sphere electron transfer**

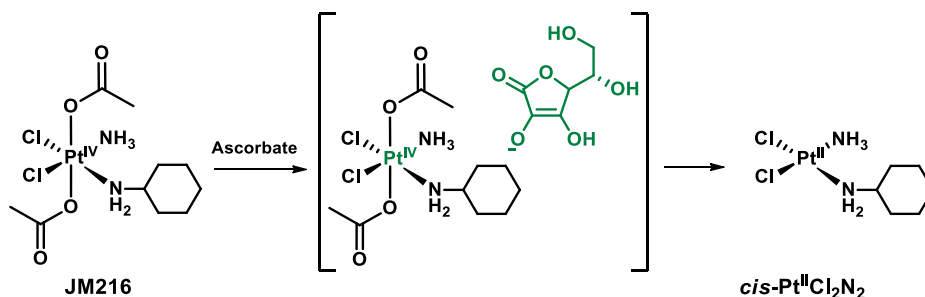


**Figure 1.15.** Reduction of two Pt(IV) prodrugs JM576 and JM216 by ascorbate through inner and outer sphere electron transfer mechanism

*Trans* chlorides in JM576 form a bridge involving **Asc-Cl-Pt<sup>IV</sup>-Cl** (Figure 1.11 A) that results in a fast inner-sphere electron transfer and formation of the Pt(II) product with the axial acetate ligands in *cis* configuration. In JM216 the *cis* arrangement of Cl<sup>-</sup> does not allow any bridging disposition and the reduction occurs through a slower outer-sphere mechanisms (kinetic constants were measured in the work), yielding a different Pt<sup>II</sup> product that retained chlorides. Finally, it is worth to mention that the activation of Pt(IV) prodrugs can be achieved by different strategies than chemical reduction. Indeed, in recent years several examples of photo-activated Pt(IV) prodrugs, usually reduced by

irradiation with visible light, have been proposed showing promising results for future clinical developments.<sup>84</sup>

### 1.3 Alternatives to Platinum anticancer drugs

The success of platinum compounds in anticancer therapy opened the way for finding other metal compounds with cytotoxic activity and reduced toxicity. Although it would be possible to find at least one example of compound tested as anticancer agent for almost every metal of the periodic table, ruthenium- and gold-based complexes have obtained the largest success.

#### 1.3.1 The “Ruthenium Era” in anticancer treatment

The beginning of the “*ruthenium era*” in the field of anticancer compounds started with the development of the series of KP- compounds proposed by Keppler’s research group<sup>85</sup> and with the analogue NAMI-A developed by Alessio research group (Figure 1.16).<sup>86</sup>

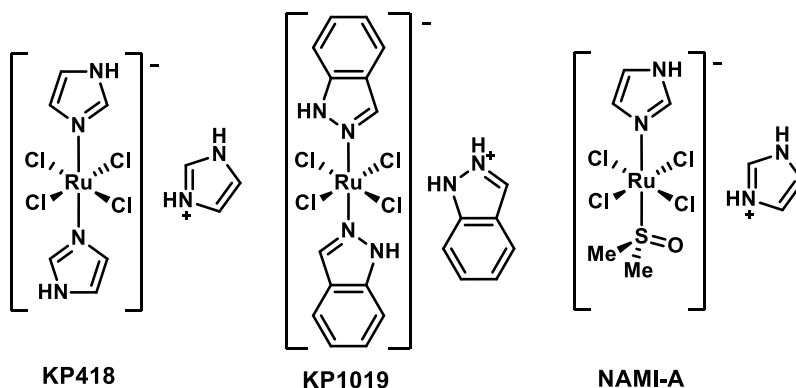


**Figure 1.16.** Structure of KP type and NAMI-A.

All these compounds underwent to clinical trials and KP1019 and NAMI-A successfully completed the Phase I. Intense efforts have been performed to clarify

the reactivity in biological media, the binding to biomolecules and the mechanism of action of Ru-based anticancer agents. It emerged that ruthenium has several features making it an appealing metal to develop drugs:

- Slow ligand exchange (comparable to Pt complexes) enhances the kinetic stability of the resulting complexes, a desirable feature in a highly and variegated reactive environment as physiological systems;
- Accessibility to several oxidation states (+2,+3,+4) in physiological conditions allows to differentiate the reactivity and the mechanism of action through the choice of the coordination environment;
- Similarity to iron makes ruthenium able to bind and to exploit iron-based biological systems. It is known that cancer cells need an increased amount of iron than healthy ones, and, through iron transport proteins, ruthenium can preferentially accumulate in cancer cells, reducing the systemic toxicity.<sup>87</sup>

Studies on the mechanism of action also revealed that probably in physiological conditions Ru(III) is reduced to Ru(II), which is considered the active species. Such hypothesis, so-called “activation by reduction” mechanism, inspired the research to explore Ru(II) complexes, avoiding the reduction step. The most important and considered Ru(II) classes of compounds are RAPTA-<sup>88</sup> and RAED-types,<sup>89</sup> whose structure is reported in **Figure 1.17**.

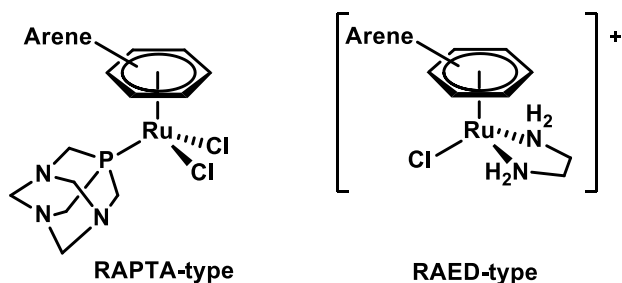


**Figure 1.17.** Structure of RAPTA and RAED complexes

Both the families are half-sandwich Ru(II) arene complexes, also known as piano–stool complexes. They are organometallic complexes in octahedral coordination environment and pseudo-tetrahedral molecular geometry. Indeed, the arene ligand occupies three coordination sites but it is often considered as a single ligand. The arene ligand enhances the inertness of the complex toward substitution reactions, and it stabilizes the ruthenium centre in different conditions of pH and redox potentials. Moreover, the arene is highly functionalizable, and it can be synthetically modified to confer to the resulting complexes specific properties. Its bulky hydrophobic surface can be helpful for the interaction of ruthenium centre with biomolecules. The other ligands are peculiar and determine substantial differences in the action of the two families of compounds. RAED-type complexes are cationic (usually hexafluorophosphate salts) and have one chlorido ligand and a chelating ethenediamine. Sadler group intensively studied this class over years achieving notable results in determining structure-activity relationships. They observed that the presence of apolar and hydrophobic substituents on the arene increase the cytotoxicity with respect to arenes with polar substituents. The best results were achieved with fused rings as tetrahydroanthracene (**Figure 1.18**). Moreover, it was demonstrated that di-alkyl diamine reduced the biological activity, suggesting that the presence of NH can have an important role in the interaction with biomolecules.<sup>90,91</sup>



Cytotoxicity

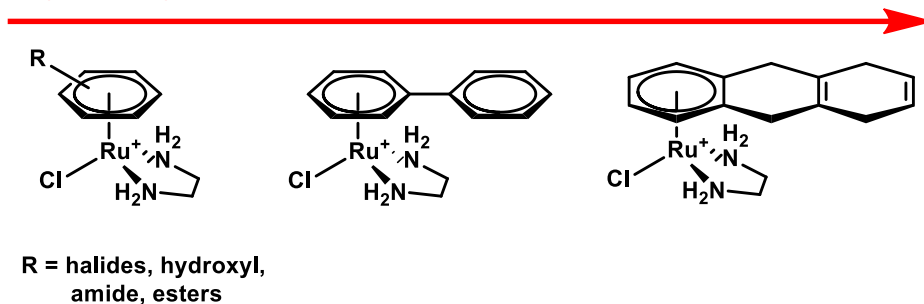


**Figure 1.18.** Cytotoxicity versus influence of the arene ligand in RAED complexes

The hypothesis of the importance of NH groups was confirmed by studying the reactivity with biomolecules. As for platinum compounds, DNA was individuated as the preferential target rather than proteins. In an exhaustive study performed on the reactivity between RAED complexes and model DNA nucleobases it was revealed that the compounds preferentially bind guanine residues rather than adenine in a highly selective way. The preferential recognition is due to the hydrogen bond established between NH groups and the exocyclic oxygen of guanine (**Figure 1.19 A**). Conversely, the NH group on ethenediamine repulses the exocyclic NH group on adenine residues as depicted in **Figure 1.19 B**.<sup>92,93</sup>

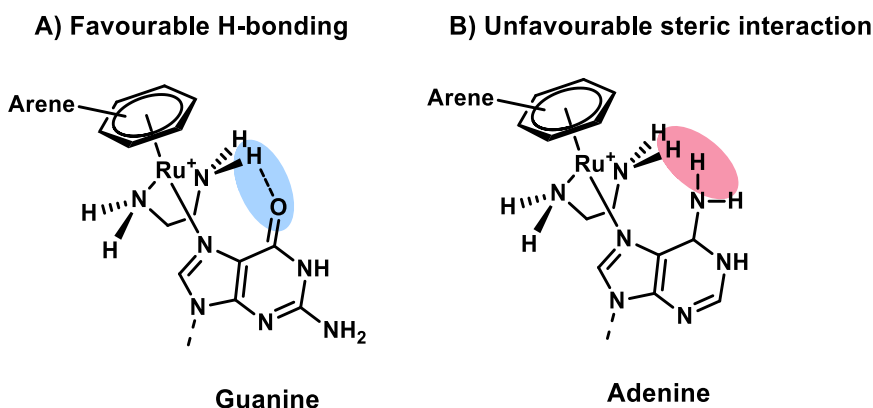
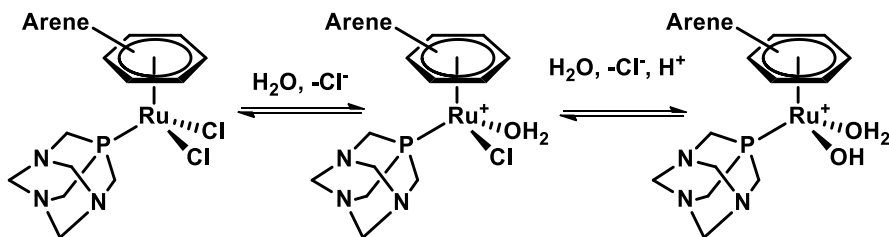


**Figure 1.19.** Representation of the interactions between RAED-type and nucleobases guanine and adenine

RAPTA-TYPE complexes have been developed by Dyson research group and are neutral compounds characterized by two chlorido ligands and a monodentate phosphine PTA, which notably enhance water solubility of the complexes. Chlorido ligands are labile, undergoing to aquation which activates the complex, when the chloride concentration is low (*e.g.*, 4 mM, miming intracellular Cl<sup>-</sup> concentration) and reduced at higher concentrations (100 mM in bloodstream).<sup>94,95</sup>

The aquation reaction is schematized in **Scheme 1.6**:



**Scheme 1.6.** Hydrolysis of RAPTA complexes

Such reactivity is similar to what observed for cisplatin. Indeed, the activation of RAPTA complexes leads to the formation of highly electrophilic species, reactive with nucleophilic residues of biomolecules. Conversely to cisplatin and RAED, proteins, particularly histones protein core, seem to be the main target for RAPTA complexes. Cell surface proteins and extracellular components have also been considered as possible targets. Regarding the anticancer activity, the most promising members of first generation of RAPTA family are the so-called RAPTA-C, RAPTA-T and RAPTA-B (**Figure 1.20**).<sup>96</sup>

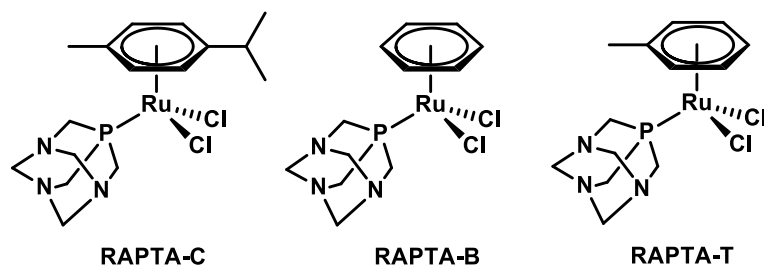


**Figure 1.20.** Members of the first generation of RAPTA complexes

Although the *in vitro* activity of RAPTA complexes was not particularly encouraging, RAPTA-T showed interesting antimetastatic properties which led to continue the study with *in vivo* evaluations. Both RAPTA-B and RAPTA-C were found to be effective in reducing metastases and reducing tumour growth. Subsequent studies revealed that RAPTA-C was able to bind histone in nucleosome core altering secondary and tertiary structure of DNA.<sup>97</sup> Pre-clinical studies confirmed its antimetastatic and anti-angiogenic activity,<sup>98</sup> and good results were obtained by combining RAPTA-C to other drugs in mixed regimens.<sup>99</sup> Although it has never entered in clinical trials, such encouraging results make it a valid candidate for further studies.

The success of RAPTA complexes encouraged the research to explore Ru(II) arene derivatives. The ruthenium-arene scaffold is a useful and versatile platform

which allows several variations on the theme.<sup>100</sup> Beyond the already mentioned arene functionalization, it is possible to coordinate a multiplicity of ligands to the ruthenium centre. Most interesting modifications regards substitution of chlorido ligands with bromido, iodido, and anionic chelating carboxylates, or 1,3-diketonato ligands.<sup>101</sup> The substitution of PTA ligand with different phosphines, phosphites and *N*-heterocyclic ligands resulted in a vastness of compounds whose biological properties have been evaluated over years.<sup>102–107</sup> Finally, the use of bioactive fragments adapted as ligands in mono- or bi-dentate fashions with mixed -N, -C, -O and -S coordinating atoms, has emerged, and an intense work have been carried out by C. Pettinari research group.<sup>108–112</sup> Some interesting compound by their works is reported in **Figure 1.21**.

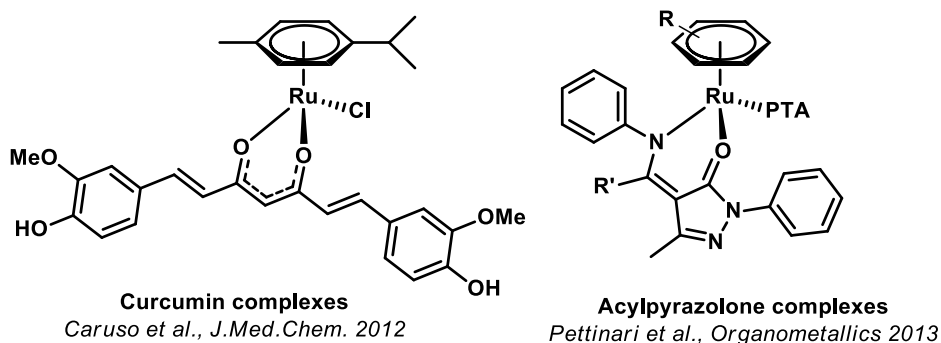


**Figure 1.21.** Complexes with bio-active ligands reported by C. Pettinari group

### 1.3.2 Gold-based anticancer compounds

Gold was used for medicinal application in Arabic and Chinese ancient cultures starting from thousands of years BC.<sup>113</sup> Several reports on the use of gold in medicine are available over centuries and following the outbreak of metal complexes in 20<sup>th</sup> century, it assumed a prominent role in the pool of metals whose compounds display notable biological activity.<sup>114</sup> Gold coordination chemistry

span between linear Au(I) and Au(III) compounds, the latter usually found in square planar geometry. The Au(III) similarity in the structure as well as in the electronic configuration to Pt(II) (both  $d^8$  ions) motivated studies on the anticancer properties of gold compounds.<sup>115</sup> One of the main task to handle in gold chemistry for biological applications is the marked tendency to reduce to Au(0), especially in reducing aqueous biological environment. For this reason, a comprehensive part of the scientific production concerning gold compounds with biological activity is based on organometallic compounds, aimed to stabilize Au(I)/(III) oxidation states through highly stable gold-carbon bonds.<sup>116</sup> Among the compounds studied in last years, Au(I) *N*-Heterocyclic carbene (NHC) and cyclometalated Au(III) complexes emerged. Relevant examples belonging to the former class are reported in **Figure 1.22**.

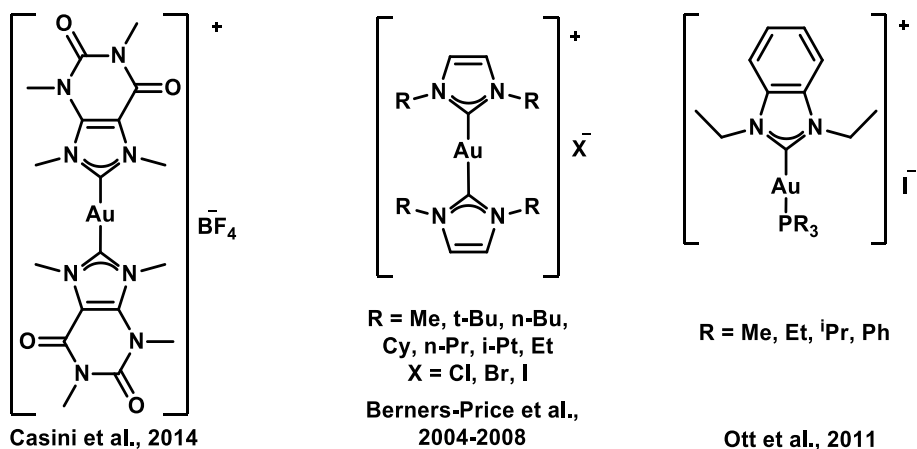


**Figure 1.22.** Au(I) NHC complexes reported

One of the first studies on Au-NHC complexes was in 2004, by Berners-Price et al.<sup>117–119</sup> They evaluated a series of cationic bis-NHC ligands with a wide range of substituents tuning the lipophilicity of the complexes. The compounds showed to target mitochondria, and in some case, they displayed a certain degree of

selectivity correlating with the lipophilicity. In subsequent years, more studies identified the thioredoxin system (TR) as one of the principal targets for gold-based compounds.<sup>120</sup> TR is a multiprotein system involved in oxidative stress and redox balance of the cell. In particular the inhibition of the enzyme thioredoxin reductase (TrxR) leads to an accumulation of hydrogen peroxide which react with different targets triggering cell death. The interaction between Au-complexes and TrxR is considered the most significant for the development of new gold-based anticancer drugs. Indeed, TrxR is able to coordinate gold complexes via thiol and selenol group of its amino acid residues, particularly congenial to gold. Ott et al. reported a series of Au(I)-NHC-phosphines complexes which showed to selectively inhibit TrxR, probably binding the protein through the substitution of the phosphine ligand.<sup>121–123</sup> More recently, A. Casini research group showed that Au(I) NHC complexes can also target DNA. A cationic bis-NHC gold compound having caffeine derived ligands, showed to be selective against human ovarian cancer cells and to target and stabilize DNA secondary structures, named G-quadruplexes.<sup>116</sup> The selective stabilization of G-quadruplexes is considered to have important effect on cellular mechanisms, and small molecules able to bind G4 are considered capable of damaging DNA.<sup>124</sup> The complex showed to be stable in aqueous media and to preferentially bind G4 rather than duplex DNA, probably through non-covalent interactions (mainly  $\pi$ – $\pi$  stacking). Whereas less explored than platinum and ruthenium, results achieved from gold compounds open new frontiers for the development of drugs with new targets and mechanism of action, representing a promising alternative in the fight to cancer diseases.<sup>125</sup>

## **1.4 Targeting groups in anticancer metal complexes**

The development of novel anticancer agents with improved pharmacological performances led to a plethora of scientific outcomes and a number of strategies have been employed to achieve the goal. It has been already said that one of the main drawbacks of platinum based anticancer therapy is the lack of selectivity for cancerous cells and tissues, which result in the insurgence of severe side effects for patients. The use of nano-carrier systems, including proteins formulations, liposomes, MOFs, organic polymers etc., to selectively accumulate the drug in cancer tissues has been pursued with very interesting results.<sup>14</sup> Alternatively, the introduction of targeting groups in the coordination sphere of the metal can be the option to monitor and to tune the physical-chemical properties of the drug on molecular scale.<sup>126</sup> A targeting group is usually a bio-derived molecular fragment able to confer to the resulting complex a specificity for malignant cells, reducing the general toxicity. A targeting group is generally chosen to target a receptor, a protein, or a biological entity which is overexpressed in cancer cells either on the cellular membrane or in specific cellular compartments. The overexpression of the target is crucial since it creates the “marker” that will be exploited by the drug to distinguish and to exert a different action on cancerous and non-cancerous cells, and/or tissues. Several bio-derived molecules have been used in recent years, involving steroids,<sup>127</sup> amino acids and small peptides,<sup>128–130</sup> nucleic acids, and carbohydrates. The latter ones are object of the present work and will be discussed in the next section.

### ***1.4.1 Glycoconjugation for Selective Delivery of Metal Drugs***

Carbohydrates are the main source of energy and essential nutrients for cells. Carbohydrates (mainly glucose) are internalized through transmembrane proteins,

called GLUTs.<sup>131</sup> Once inside, glucose undergoes an enzyme-catalyzed oxidative pathway, known as glycolysis which converts it into pyruvate. Pyruvate enters mitochondria where it is converted to acetyl-coenzyme A, the principal substrate of the Krebs cycle, which results in the production of NADH. This latter is indispensable to produce ATP in the oxidative phosphorylation process, which is the last stage of carbohydrate catabolism (path (i) in **Figure 1.23**).

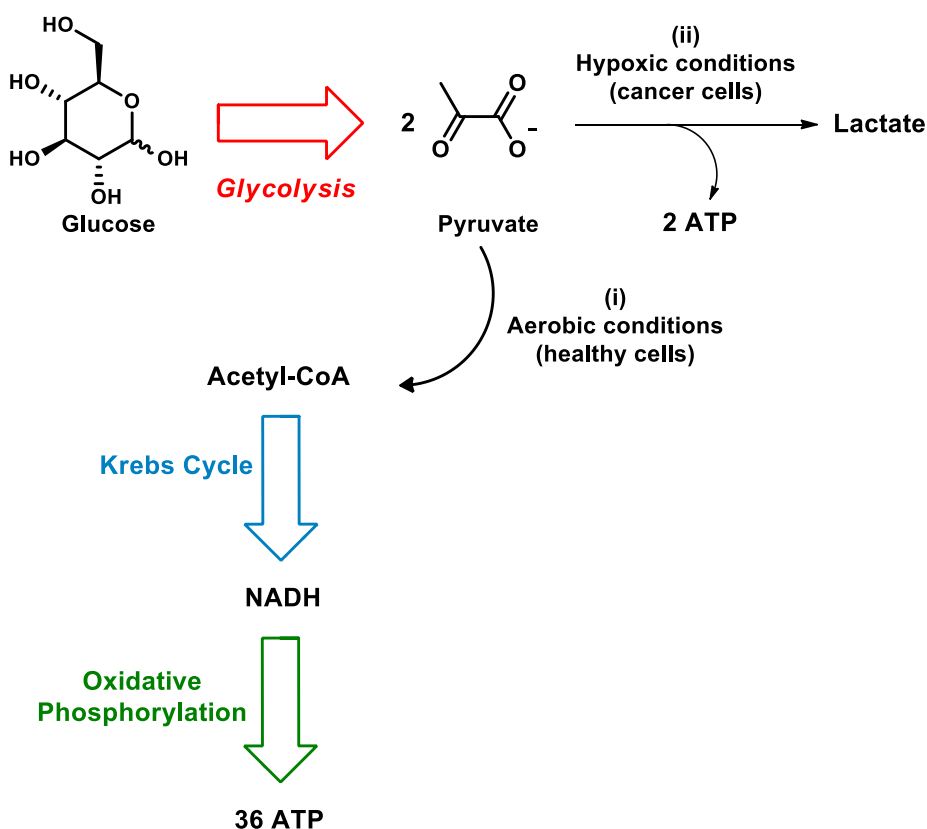


**Figure 1.23.** Schematic representation of the glycolytic pathway in normal and cancer cells

In normal cells the pathway glycolysis-oxidative phosphorylation results in the overall production of 36 molecules of ATP for every glucose molecule.



Cancer proliferation is characterized by several modifications in cellular homeostasis. The fast abnormal growing of cancer tissues involves reduced vascularization, and consequently reduced diffusion of oxygen.<sup>28</sup> The low oxygen concentration is called hypoxia, and severely affects normal biological mechanisms of the cell.<sup>132</sup> Carbohydrate metabolism is deeply altered in hypoxic conditions; indeed, pyruvate does not enter Krebs cycle, rather it is converted to lactate (path (ii) in **Figure 1.23**). This phenomenon derives the oxidative phosphorylation pathway of its “fuel”. The energetic balance of the cell is affected by such events, since only 2 molecules of ATP are produced by glycolysis with respect to 36 molecules produced when glycolysis is coupled to oxidative phosphorylation. Cancer cells proliferate at abnormal rate, much higher than healthy ones, and to respond to the metabolic reprogramming induced by hypoxia, increase the demand and consumption of carbohydrates. To ensure an appropriate amount of sugars, cancer cells overexpress carbohydrate receptors (GLUTs) with respect to healthy ones. Such phenomenon is known as *Warburg Effect* and it was firstly postulated by Otto Warburg in 1924.<sup>133</sup>

Warburg Effect stimulates the introduction of sugar fragments in anticancer metallodrugs. Indeed, a glycoconjugate metal complex is a molecule that can be preferentially recognized by GLUTs and internalized in the cell, acting as Trojan Horse (**Figure 1.24**).<sup>131</sup> The overexpression of GLUTs in cancer cells can lead to an enhanced accumulation of the drug, with resulting increasing of the selectivity of the drug. Moreover, the presence of a sugar residue can have favorable effects by enhancing the biocompatibility and providing enantiomeric purity to the resulting molecule. It can improve the water solubility, a desirable feature for metal-based drugs which are often very poorly soluble in aqueous media (**Figure 1.24**).

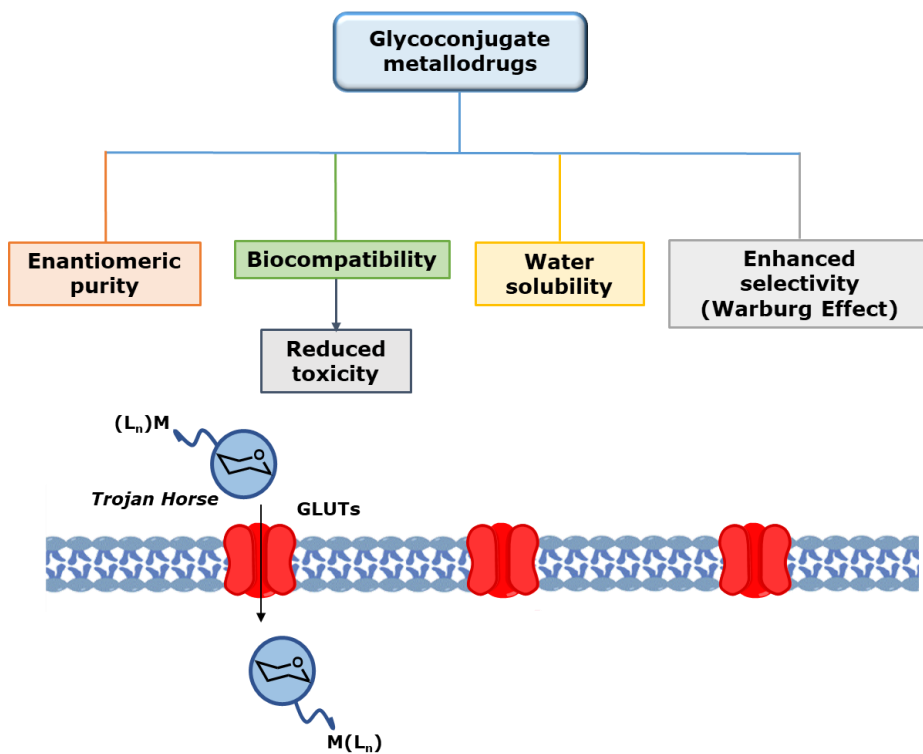


**Figure 1.24.** Beneficial properties of glycoconjugate metallodrugs and “Trojan Horse mechanism”

Glycoconjugation has been successfully exploited in recent years on different metal scaffolds. Most significant examples are reported in **Figure 1.25**.

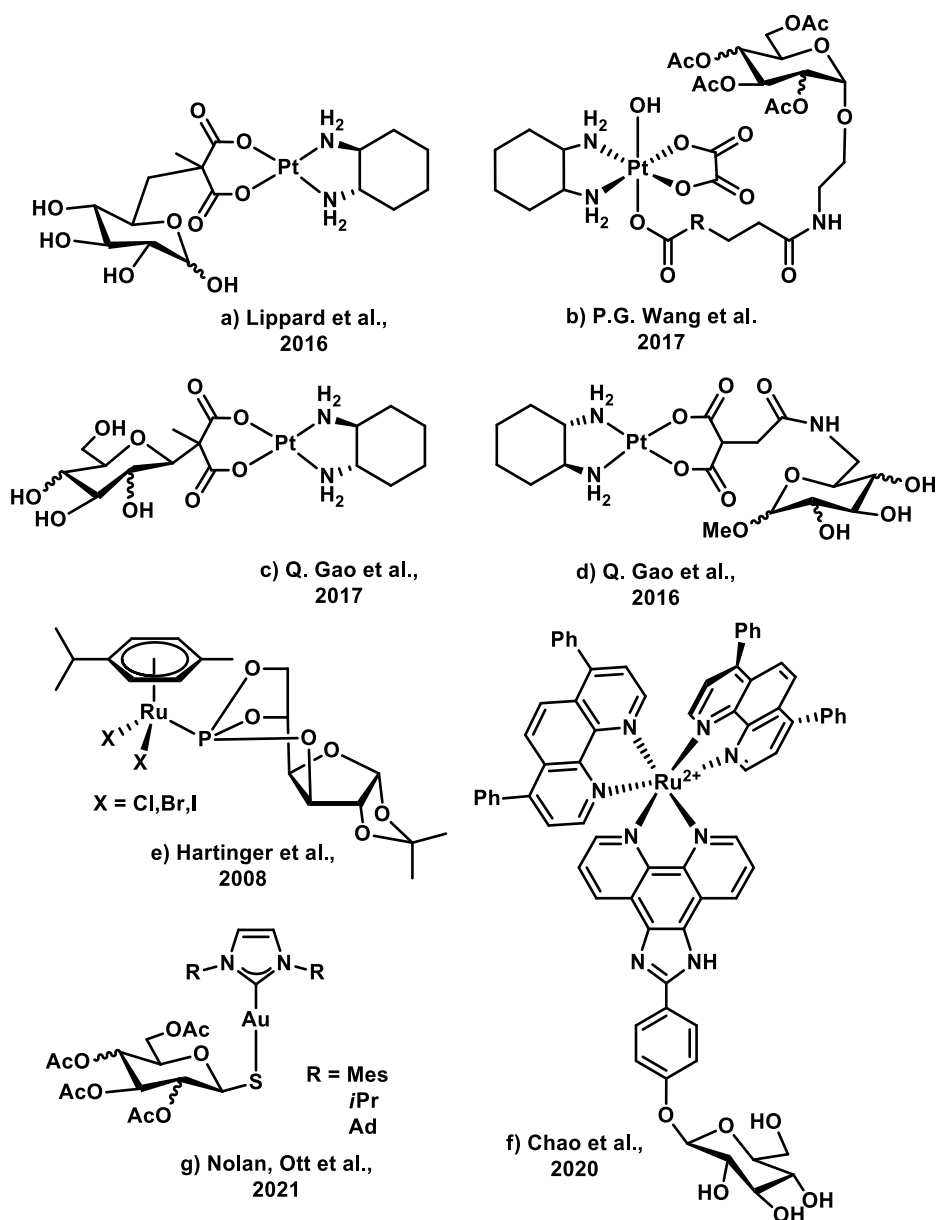


**Figure 1.25.** Selected examples of glycoconjugate metal complexes tested as anticancer drugs

In 2016 Lippard et al. reported three examples of oxaliplatin-like complexes in which the oxalate was replaced by a malonate linked to a glucose unit in position C6.<sup>134</sup> The design and the selection of this position to connect the sugar were guided by previous docking studies with a DFT optimized structure of the complex and the crystal structure of a bacterial carbohydrate transporter. Studies on the internalization of the complexes revealed that complex **a** in **Figure 1.25** was translocated into the cell through glucose transporters displaying excellent toxicity and selectivity for cancer cells.

In a subsequent work the same authors studied the effect of linking the sugar unit through every of the six accessible positions of the glucose scaffold, observing that the conjugation through C1 and C2 leads to the most efficient accumulation of the drug in cells.<sup>135</sup>

Q. Gao research group intensively studied glycoconjugation strategy in different fashions. A family of compounds (**c** in **Figure 1.25**) similar to those reported by Lippard were studied in 2017.<sup>136</sup> In this case the sugar unit is linked through the C1 to the malonate, and glucose, galactose and mannose were used as carbohydrate residues. They observed involvement of GLUTs in the uptake of the drugs, and interestingly the nature of the sugar dramatically affects water solubility which decreases in the order glucose > galactose > mannose. Similar outcomes were observed using 6-amino-6-deoxy-D-pyranoside (gluco-, galacto- and manno-) studied by the same authors in 2016 (**d** in **Figure 1.25**).<sup>137</sup>

Glycoconjugation has been successfully employed in Pt(IV) prodrugs. P.G. Wang et al. prepared a wide panel of monofunctional carboxylate compounds (**b** in **Figure 1.25**) with sugar fragments conjugate through an amide linker, combining different sugar scaffolds and alkyl spacers.<sup>138</sup> The panel of complexes showed to be promisingly active and selective both *in vitro* and *in vivo*.

Hartinger et al. prepared several RAPTA derivative replacing *pta* with a phosphite ligand derived by  $\alpha$ -D-glucofuranoside. They performed exhaustive studies by varying the halogen leaving ligands and substituents on the sugar fragment. Generally, the compounds displayed a certain degree of selectivity and despite extensive studies on their hydrolysis, and their reactivity with model biomolecules, no clear structure-relationship was obtained to clarify the role of the sugar in the biological activity of the complexes.<sup>139</sup>

Conversely, Chao et al., recently presented a glucoconjugate Ru(II) photosensitizer as candidate for anticancer photodynamic therapy (PDT), an alternative to classical chemotherapy which exploits the electronic properties of metal complexes to produce reactive oxygen species triggering cell death. Beyond the photophysical interesting properties of the complex, they disclosed the involvement of glucose transporters in the cellular uptake of the conjugate species, that preferentially accumulates in cancer cells.<sup>140</sup>

Finally, in a recent work Nolan and Ott reported a panel of NHC gold complexes with thio-sugar ligands and they studied the *in vitro* cytotoxic activity. The ligand 1-thio- $\beta$ -D-glucopyranose-2,3,4,6-tetraacetato-S is used in the Au(I) complex known as Auranofin, commercially available as anti-arthritis drug and widely studied for its anticancer activity. In this work glucose, galactose and mannose derivatives disclosed promising cytotoxicity toward different cell lines.<sup>141</sup>

Such promising data support the use of glycoconjugation as valid and versatile strategy to improve the biological performance of anticancer metal-based drugs.

## 1.5 Aim of the Work

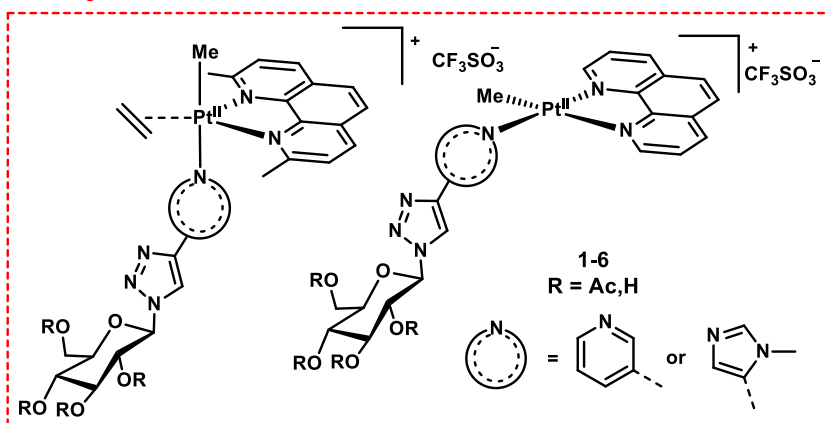
The aim of the present PhD thesis was to perform a systematic study on glycoconjugate organometallic complexes as potential anticancer agents. Such class of compounds is generally less represented in literature than coordination compounds, despite the peculiar properties provided by the presence of at least one metal-carbon bond. The first and most consistent part of the present PhD work involved the molecular design, the synthesis, the structural characterization, and the study of chemical properties and reactivity of glycoconjugate organometallic platinum complexes. The high versatility of platinum organometallic chemistry as well as the synthetic adaptability of carbohydrates allows to choose among several structural fashions to tune chemical-physical properties of the compounds. **Table 1.2** contains an overview of the features considered in the design of the complexes reported in this work.

**Table 1.2.** Features to be considered in the design of glycoconjugate Pt-organometallic complexes

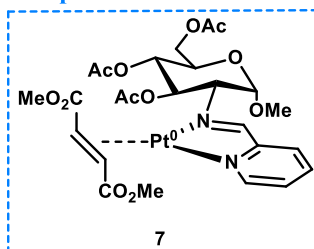
Feature	Scope
Oxidation State	Pt(0), Pt(II), Pt(IV)
Coordination Number	3,4,5,6
Molecular Geometry	<ul style="list-style-type: none"><li>- Trigonal planar</li><li>- Square planar</li><li>- Trigonal Bipyramidal</li><li>- Square Pyramidal</li><li>- (pseudo)Octahedral</li></ul>
Glycoconjugated ligand(s)	<ul style="list-style-type: none"><li>- N-,O-,S-,P- donor ligands</li><li>- Chelating ligands</li><li>- Direct C-Pt bond</li></ul>
Type of sugar fragment	<ul style="list-style-type: none"><li>- Nature of the sugar scaffold</li><li>- Choice of the protecting groups or functionalization of -OH</li></ul>
Other ligands	Alkyl groups, Olefins, Halides, Chelating ligands

Within this frame, several panels of Pt-complexes, whose general structures are reported in **Figure 1.26**, were prepared, and studied.

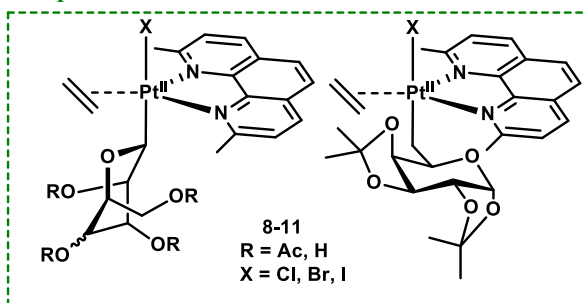
### Chapter 2



### Chapter 3



### Chapter 4



### Chapter 5

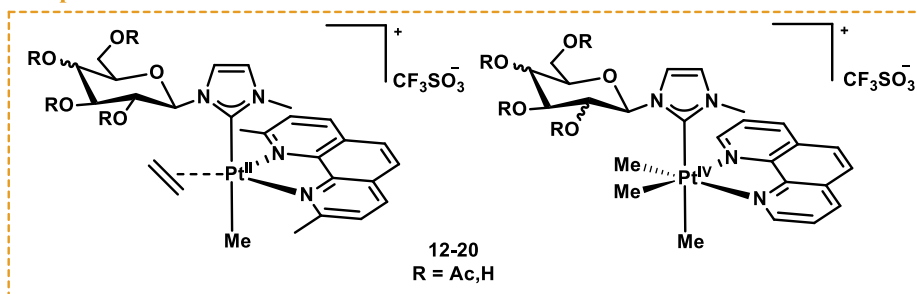


**Figure 1.26.** General structures of the families of Pt-complexes studied in this work. Selected glycoconjugate ligands were used in different Pt-scaffolds, to compare the effect of the metal oxidation state, the molecular geometry, and the sugar

portions on the biological properties of the complexes. The evaluation of the anticancer activity and preliminary studies of the mechanism of action were carried out. Furthermore, studies on the interaction with model macromolecules (DNA and proteins) were performed to get preliminary information on the biological targets of the complexes and the interactions responsible of the biological response.

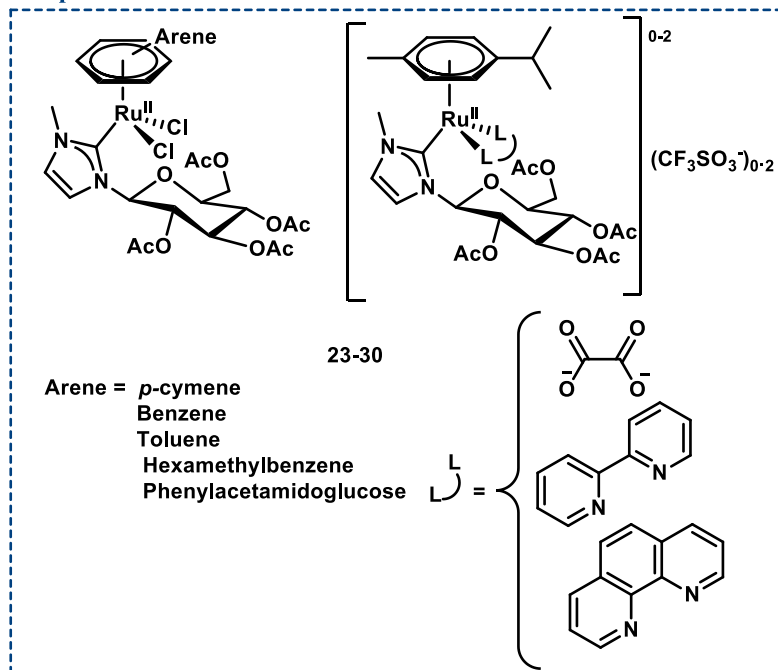
The goal of this projects was to explore different sugar-containing Pt-based molecular structures, and to identify the key-features that influence their chemical and biological properties.

The last part of the present PhD work was performed during a period of research at the École Polytechnique Fédérale de Lausanne (EPFL), under the supervision of Prof. Paul J. Dyson. In this frame, the beneficial effects of glycoconjugation were extended to different organometallic scaffolds. Ru(II) and Au(I) complexes (whose structure are reported in **Figure 1.27**) bearing sugar-based ligands were prepared, and their chemical and biological properties were studied.

The compounds presented in this thesis are divided according to the type of glycoconjugate ligands, and for every family of compounds a brief overview that explains its rational design will be given.



## Chapter 6



## Chapter 7

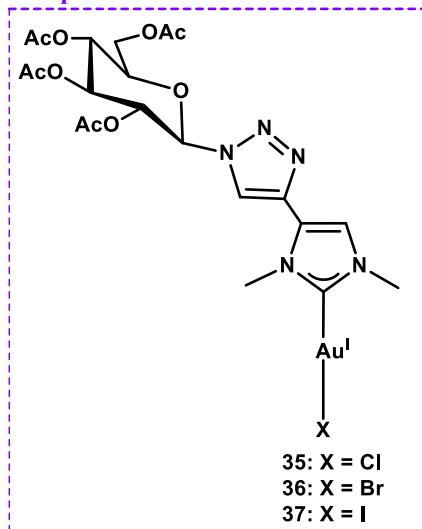


**Figure 1.27.** Structure of Ru and Au complexes studied in this thesis



Such class of compounds combined the active oxidation state Pt(II) with the coordinative saturation which can preserve the integrity of the complex to the target, reducing unwanted side reactions. The positive charge and the extended hydrophobic portions can balance hydrophilicity and lipophilicity enhancing both water solubility and the capability to interact with lipophilic systems (cellular membrane, proteins hydrophobic regions). The complexes were found to be by far more active than cisplatin although no selectivity for cancer cells was observed. On this basis, further studies have been developed. Aiming to evaluate the effect of the molecular geometry on the anticancer properties of this class organoplatinum(II) complexes with *N*-based ligands, a family of analogue square-planar compounds (**Figure 2.2**) was prepared within this study. This represented a rare case of homogeneous comparison between two families of Pt-based anticancer agents sharing the oxidation state and the type of the ligands in two different coordination geometries.<sup>62</sup>

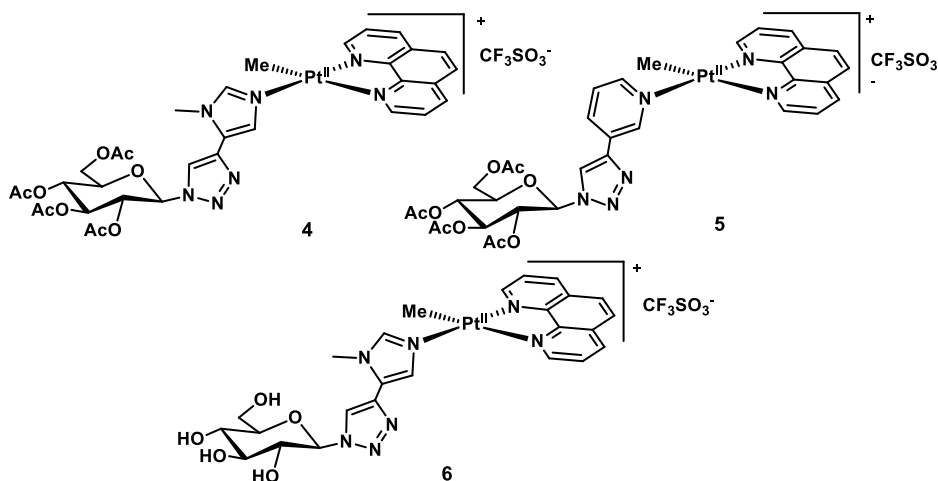


**Figure 2.2.** Complexes studied in this chapter

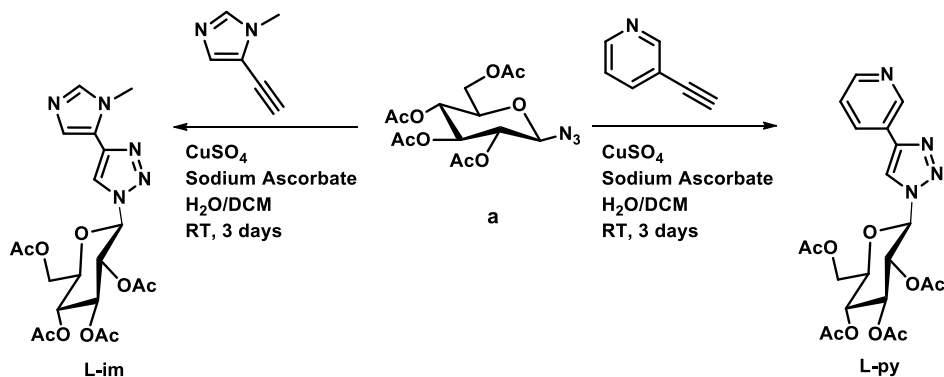
Compounds **4-6** are cationic Pt(II) complexes having the glucoconjugate pyridine or methylimidazole, and a methyl ligand as their five-coordinate analogues

(reported in **Figure 2.1**). In the *sp* coordination environment 1,10-phenanthroline (*phen*) replaced *dmphen* to avoid steric hindrance with the other ligands. Noteworthy, in this new class of compounds the planar geometry and the presence of aromatic fragments make compounds **4-6** potentially capable to intercalate in DNA base pairs by  $\pi$  stacking and weak electrostatic interactions.<sup>143–145</sup> The in-solution reactivity, the interaction with model biomolecules and the anticancer activity of compounds **4-6** was evaluated and compared to the corresponding *tbp* complexes **1-3** (in **Figure 2.1**) previously studied.

## 2.2 Results and Discussion

### 2.2.1 Synthesis of the glucoconjugate ligands

The sugar-based ligands have been synthesized as reported in **Scheme 2.1**:

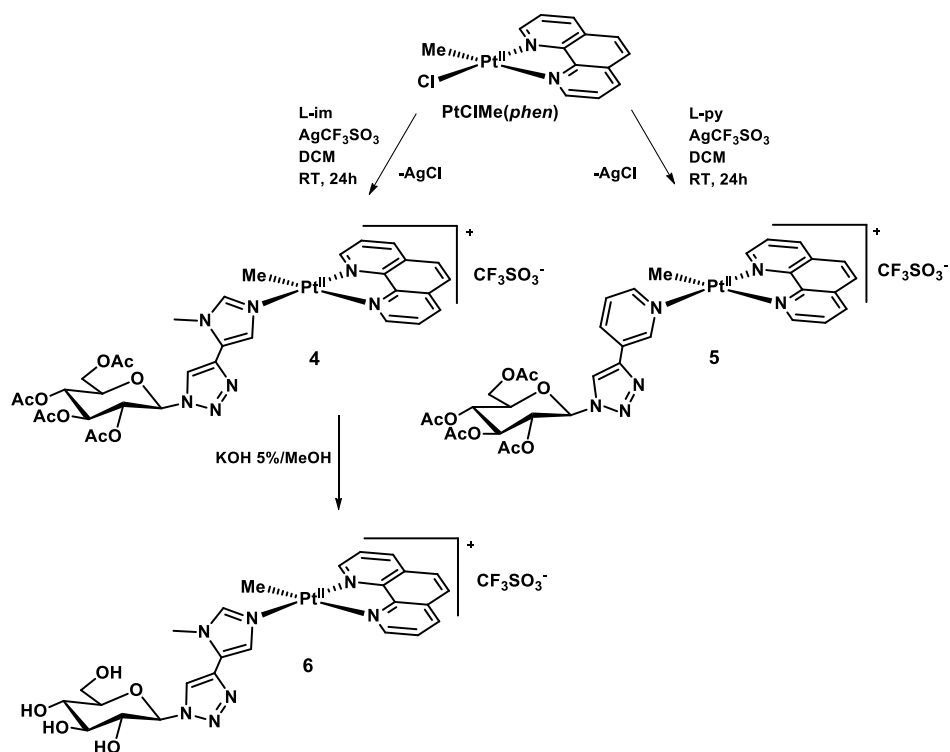


**Scheme 2.1.** Synthesis of the ligands

The ligands were obtained in high yields by reacting the glucosyl azide (**a** in **Scheme 2.1**) with the corresponding ethynyl imidazole or pyridine through a copper catalyzed click-chemistry reaction. The products were characterized by  $^1\text{H}$  and  $^{13}\text{C}$  NMR spectroscopy and elemental analysis. Proton spectra showed the presence of a singlet belonging to the triazole proton between 7.9 and 8.1 ppm while the coupling patterns of the sugar fragment was in agreement with a  $^4\text{C}_1$  chair glucose in  $\beta$  configuration for both **L-im** and **L-py**.

### 2.2.2 Synthesis and characterization of complexes 4-6

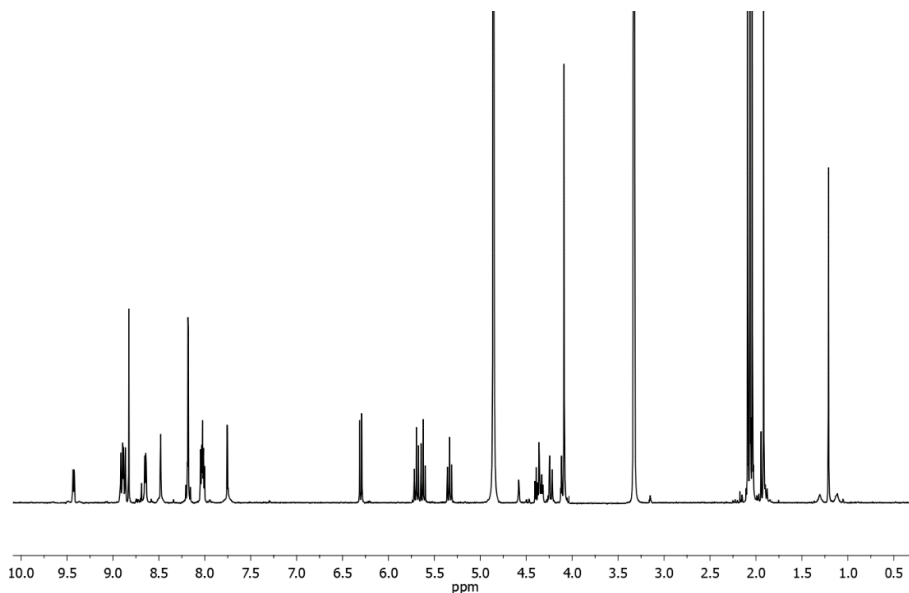
The synthesis of the platinum compounds 4-6 is reported in **Scheme 2.2**.



**Scheme 2.2.** Synthetic procedure to access compounds 4-6

The peracetylated complexes **4** and **5** were prepared starting from the precursor  $[\text{PtClMe(phen)}]$  through a substitution reaction in presence of silver triflate. Following filtration of precipitated  $\text{AgCl}$ , the complexes were isolated as bright yellow powder by reducing the volume of the filtrate and by adding diethyl ether. The de-acetylated species **6** was prepared starting by compound **4** which was dissolved in methanol containing a catalytic amount of potassium hydroxide.

Attempts to synthesize a square-planar 2,9-dimethyl-1,10-phenanthroline (*dmphen*) analogue to complex **4** were carried out by reacting the precursor [PtClMe(*dmphen*)] with **L-im** in the same conditions reported in **Scheme 2.1**. Unfortunately, the analysis of reaction mixture showed no clear evidence of the formation of the desired product, probably due to the steric hindrance brought in the plane by the methyl groups which prevents the formation of the complex.  $^1\text{H}$  NMR spectra of **4-6** are reported in **Figure 2.3**.



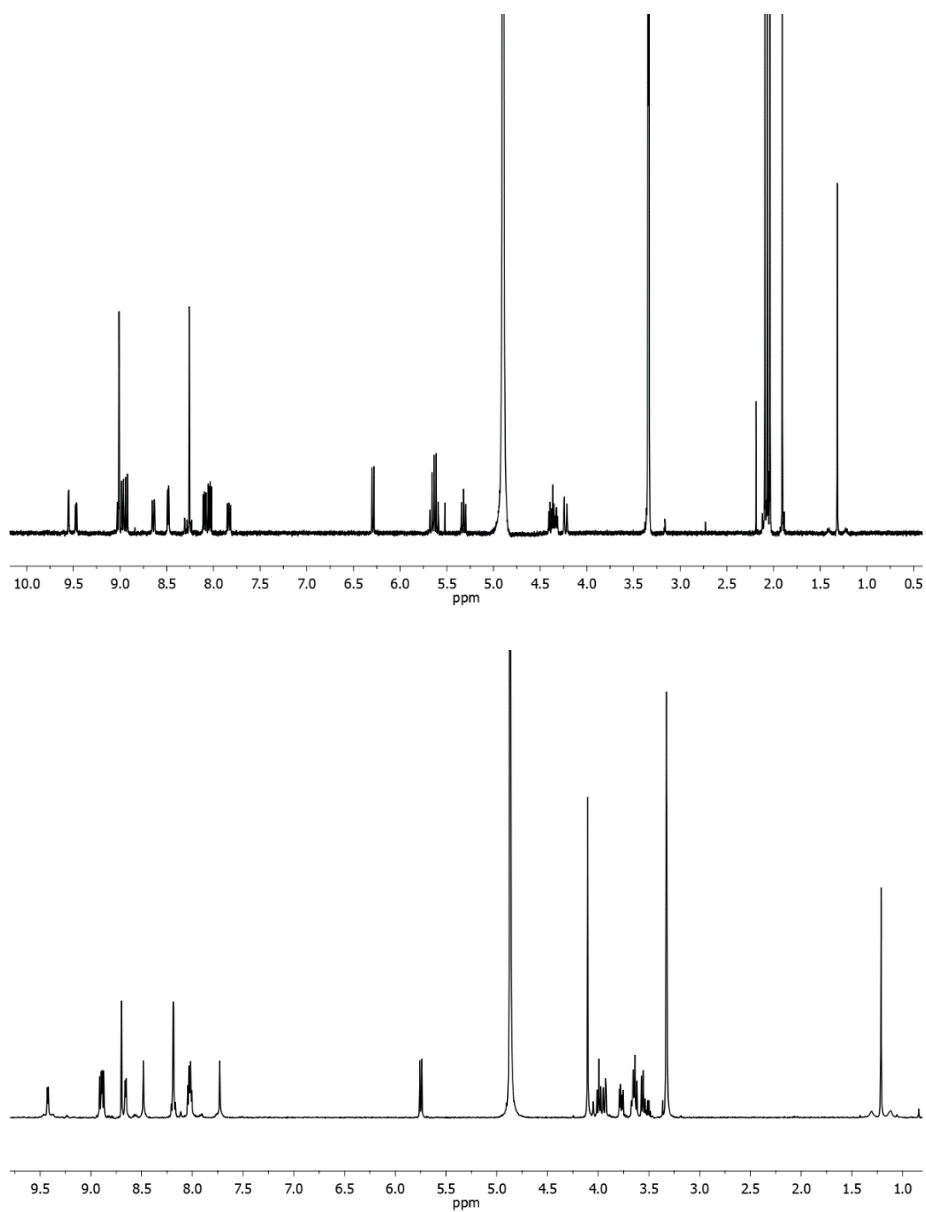


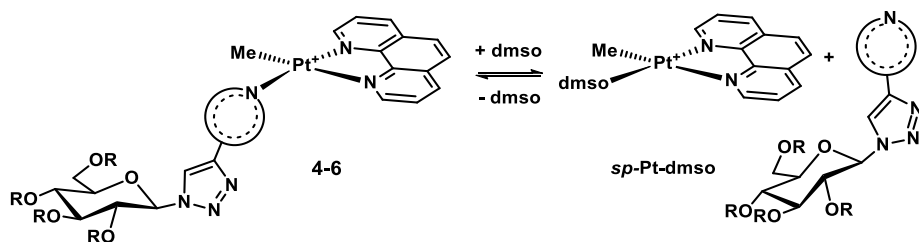
**Figure 2.3.**  $^1\text{H}$  NMR spectra of **4** (top), **5** (middle) and **6** (bottom) in  $\text{CD}_3\text{OD}$  at 400 MHz



As predictable, in all the complexes the two halves of the *phen* ligand are not equivalent. Hydrogens in adjacent position to coordinating nitrogens are affected by coupling with  $^{195}\text{Pt}$ , as well as the H2 proton on the pyridine ligand ( $J_{\text{Pt}} = 45\text{--}50\text{ Hz}$ ). The sugar proton signals maintain the coupling patterns already observed for the ligands **L-im** and **L-py**. In the peracetylated compounds **4** and **5**, glucose protons resonate in the typical range (between 6.5–4 ppm), shifting to lower frequencies (4–3 ppm with the exception of anomeric proton) in the deprotected compound **6**. The methyl on platinum is at higher frequencies (1.2–1.3 ppm) than in five-coordinate analogues (0–0.5 ppm) and display satellites due to the coupling with the  $^{195}\text{Pt}$  nuclei of ca. 70 Hz, typical of *sp* organoplatinum(II) complexes with *N,N'*-chelating ligands. The complete attribution of signals was performed by  $^1\text{H}$ - $^1\text{H}$  COSY NMR spectra, while signals attributable to the triflate ion were detected in the  $^{13}\text{C}$  NMR spectra. HRMS (ESI/QTOF) spectra recorded in methanol showed peaks relative to the whole cationic platinum complexes at  $m/z$  869.2225, 866.2106 and 701.1802 attributable to **4**, **5** and **6**, respectively.

### 2.2.3 *In-solution reactivity*

The in-solution reactivity of the synthesized complexes in organic and mixed aqueous-organic solvent mixtures was studied by  $^1\text{H}$  NMR in comparison to the analogue *tbp* complexes. When dissolved in strongly coordinating DMSO, *sp* compounds give rise to the exchange reaction reported in **Scheme 2.3**.



**Scheme 2.3.** Ligand exchange in DMSO-*d*<sub>6</sub> of complexes 4-6

In **Figure 2.4** <sup>1</sup>H NMR spectra recorded over 48 h for complex **4** are reported.

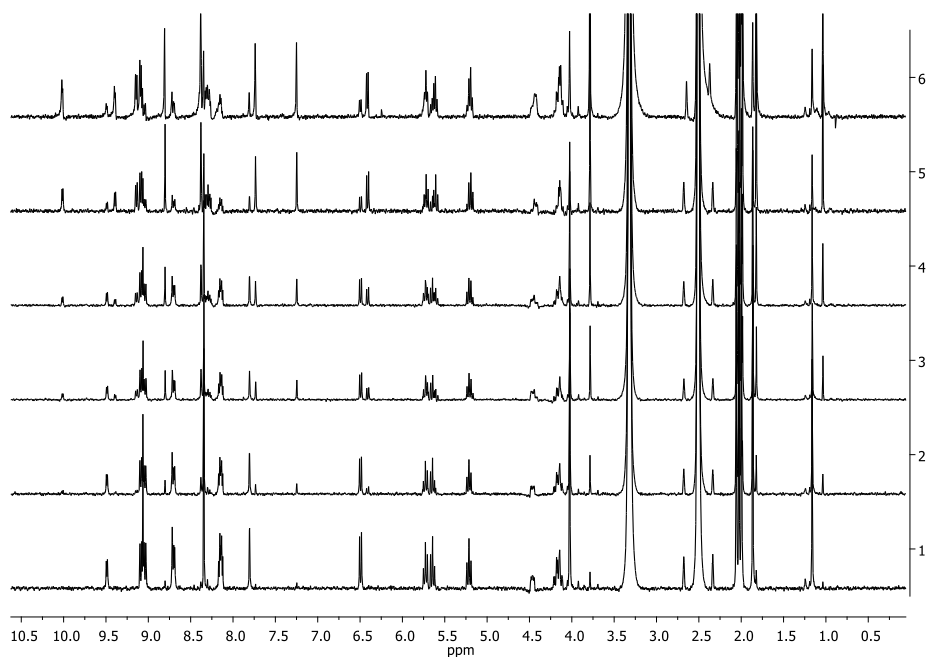


**Figure 2.4** <sup>1</sup>H-NMR spectra of **4** in DMSO-*d*<sub>6</sub> over time (trace 1 = start, 2 = 1h, 3 = 3h, 4 = 4.5 h, 5 = 24h, 6 = 48 h) at 500 MHz.

Interestingly, an equilibrium condition was reached after 24 h at 37 °C with 75-80% of the starting complex converted to the solvato-species. The occurrence of an equilibrium was evident by reducing the amount of DMSO and dissolving the

complexes in 50%-50% D<sub>2</sub>O-DMSO-*d*<sub>6</sub> (spectra collected for **4** in **Figure 2.5**). After 48 hours 50% of conversion of the starting complex to the solvato-species was observed. Analogue results were collected for complex **5**. In DMSO the kinetic of ligand substitution for *tbp* analogues was highly accelerated with 80% of equilibrium conversion reached after 2 h in solution.

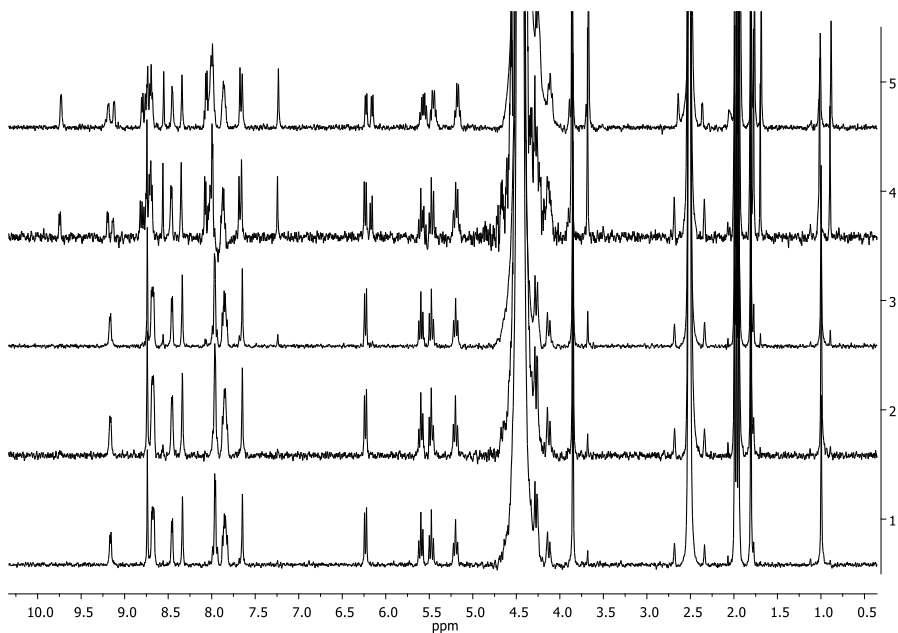


**Figure 2.5.** <sup>1</sup>H NMR spectra of **4** in 50%-50% D<sub>2</sub>O-DMSO-*d*<sub>6</sub> over time (trace 1 = start, 2 = 1h, 3 = 3h, 4 = 24h, 5 = 48 h) at 500 MHz.

The enhanced robustness of square-planar complexes was also observable in 50%-50% D<sub>2</sub>O-acetone-*d*<sub>6</sub>. Over 72 h no change in the spectrum was observed (**Figure 2.6**) and the addition of the free ligands to the NMR tube confirmed that no exchange occurred.

In this solvent mixture, *tbp* compounds underwent to an immediate ligand substitution with a solvent molecule, as observable in NMR spectra reported for complex **2** in **Figure 2.7**.

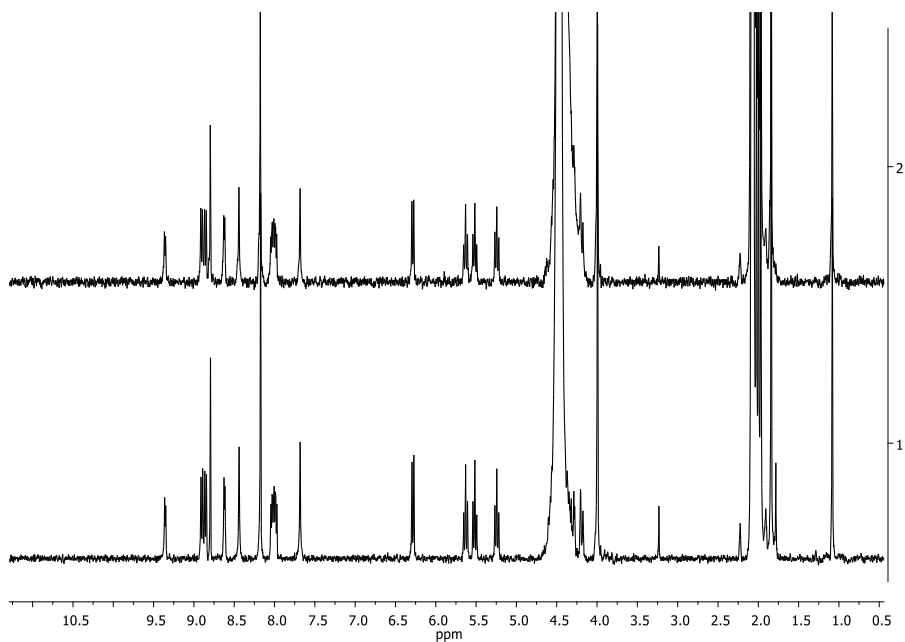


**Figure 2.6.**  $^1\text{H}$ -NMR spectra of **4** 50%-50% acetone- $d_6$ - $\text{D}_2\text{O}$  over time (trace 1 = start, 2 = 72 h) at 400 MHz.

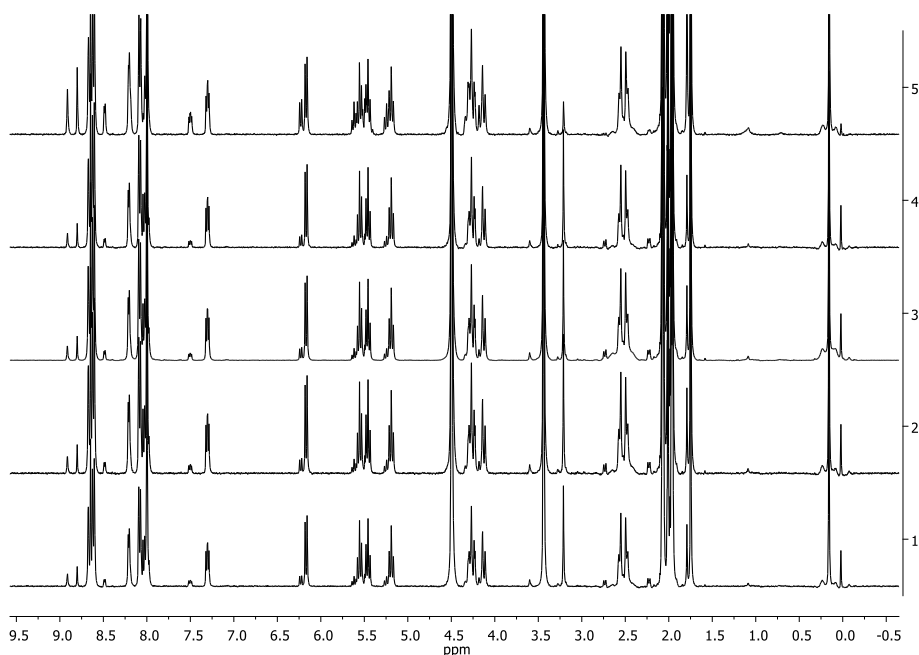


**Figure 2.7.**  $^1\text{H}$ -NMR spectra of **2** in 50%-50% acetone- $d_6$ - $\text{D}_2\text{O}$  over time (trace 1 = start, 2 = 10 min, 3 = 20 min, 4 = 30 min, 5 = 30 min following the addition of free **L-py**) at 500 MHz.

Finally, the stability of square-planar complexes was assessed in pseudo-physiological conditions, at 37 °C, in 90%-10% phosphate buffer (PB, pH 7.4)-DMSO (to solubilize the compounds), by recording  $^1\text{H}$ -NMR spectra over 48 h. No appreciable change in the spectra was observed (spectra of **4** are reported in **Figure 2.8**), suggesting that the complexes can preserve their integrity in biological environment.

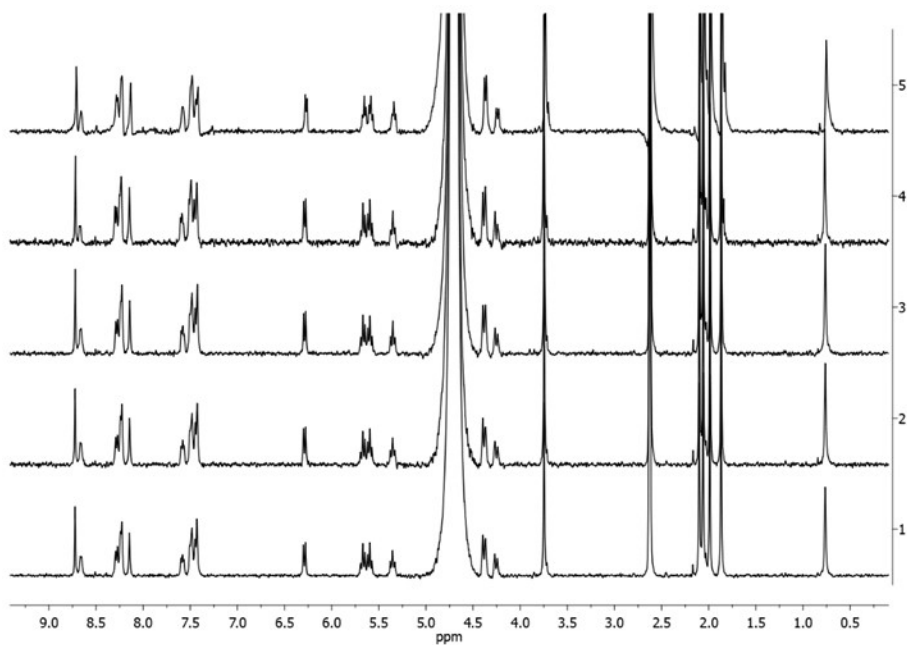
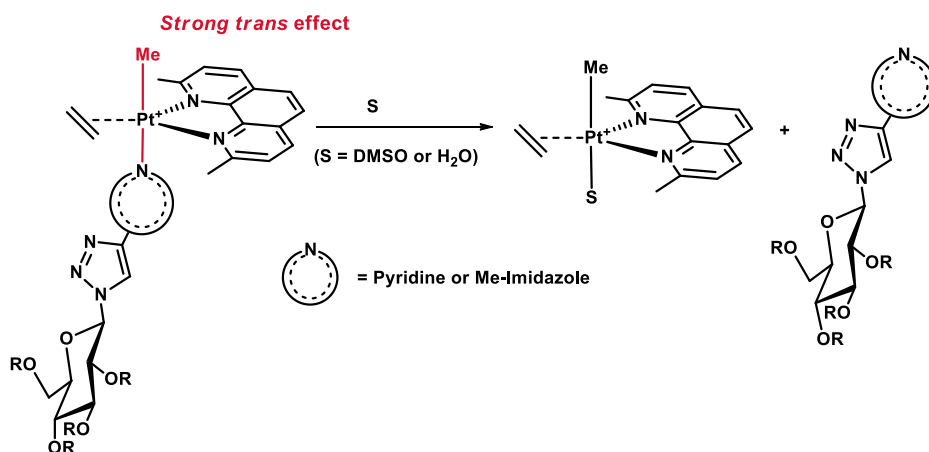


**Figure 2.8.**  $^1\text{H}$ -NMR spectra of **4** in 90%-10% PB:DMSO- $d_6$  at different time (1 = start, 2 = 1h, 3 = 3h, 4 = 24h, 5 = 48 h).

The different reactivity of the two classes of compounds can be rationalized by their structure. The ease of substitution of *N*-based ligands in *tbp* complexes in presence of coordinating solvents is probably facilitated by the strong *trans*-effect of the methyl ligand (**Scheme 2.4**)



**Scheme 2.4.** *Trans* effect of the methyl promotes the substitution of the sugar ligand in *tbp* complexes

The presence of the methyl labilizes the Pt-N bond and accelerates the substitution reaction. Such reactivity could explain the biological activity observed for *tbp* complexes which displayed no selectivity for cancer cells. Indeed, the loss of the neutral nitrogen ligands in solution suggested that the active compound that entered to the cell did not contain anymore the sugar label, and it was not able to selectively target cancer cells. The increased inertness displayed by the square-planar complexes **4-6** could apport a beneficial effect on the selectivity of the complexes, with the occurrence of a possible recognition action exerted by the sugar portion on the cellular target.

#### 2.2.4 Biological studies

The biological activity of the compounds **4-6** was tested on two couples of cell lines with each couple constituted by a cancerous line and a biologically related non-cancerous counterpart. The same lines were used for testing *tbp* analogue complexes, allowing to perform a homogeneous comparison between **1-3** and **4-**

6. Human tumor cell line A431 (epidermoid carcinoma cells) and related non-tumor HaCaT (human keratinocyte cells), MCF-7 (breast cancer cells) and non-tumorigenic H9c2 (rat cardiomyoblast cells) were selected. The cytotoxicity was evaluated by determining the IC<sub>50</sub> values (the concentration of complex able to reduce to 50% the cell viability) through MTT assay. The selectivity of the compounds was expressed as IC<sub>50</sub>(Healthy cells)/IC<sub>50</sub>(Cancer cells). After 48 h of incubation, a cytotoxic effect was observed on all the analyzed cell lines, as revealed by the IC<sub>50</sub> values reported in **Table 2.1**.

**Table 2.1.** IC<sub>50</sub> values (μM) obtained for **1-6** on immortalized and cancer cells after 48 h incubation. Selectivity Index (SI), indicated by the ratio between the IC<sub>50</sub> of immortalized cells and cancer cells

Complex	IC <sub>50</sub> (μM)				SI	SI
	HaCaT	A431	H9c2	MCF7	HaCat /A431	H9c2/ MCF7
<b>1</b>	0.80 ± 0.14	1.10 ± 0.14	0.35 ± 0.07	0.88 ± 0.11	0.73	0.40
<b>2</b>	0.58 ± 0.04	1.00 ± 0.14	0.35 ± 0.07	0.60 ± 0.09	0.58	0.58
<b>3</b>	1.03 ± 0.25	1.10 ± 0.01	0.38 ± 0.04	0.63 ± 0.11	0.94	0.59
<b>4</b>	27 ± 7	16 ± 8	53 ± 11	43 ± 7	1.7	1.2
<b>5</b>	66 ± 11	12 ± 2	22 ± 10	35 ± 4	5.5	0.63
<b>6</b>	> 200	> 200	> 200	> 200	N.A.	N.A.
<b>Cisplatin</b>	6.6 ± 0.3	39 ± 12	8 ± 2.1	18 ± 1.6	0.17	0.44

According to the different reactivity in solution, the square-planar species **4-6** exhibited different biological activity compared to their *thp* analogue. Compounds **1-3** demonstrated the same cytotoxicity on the tested cell lines, regardless the nature of the sugar ligand. Conversely, the square-planar complexes showed a certain degree of selectivity for cancer cells, as stated by the selectivity index (SI)



reported in **Table 2.1**. Even if *sp* compounds are less potent than *thp* species, with IC<sub>50</sub> values generally higher, compound **5** showed greater IC<sub>50</sub> value for HaCaT compared to A431 cells, indicating some selectivity for cancer cells. Moreover, both **4** and **5** had much higher IC<sub>50</sub> values on healthy cells than cisplatin, indicative of enhanced biocompatibility. A decrease in the IC<sub>50</sub> value, with respect to cisplatin, was observed for A431 cells, stating for a general greater selectivity of the compounds compared to cisplatin. The deprotected complex **3** showed no cytotoxic activity either on cancer or non-cancer cells, indicating a crucial effect exerted by the nature of the sugar portion.

Studies on the mechanism of action were performed on **5** in A431 cells. First, the involvement of GLUT receptors in the internalization process was studied by evaluating the cytotoxicity of **5** on A431, previously incubated with a non-lethal concentration of quercetin, which is an inhibitor of glucose transporters.<sup>146,147</sup> The presence of quercetin did not inhibit the cytotoxic action of **5**, thus the involvement of GLUT receptors in the internalization of **5** was excluded. The mechanism of cell death was also investigated. The occurrence of necrosis was evaluated by measuring the release of LDH (lactate dehydrogenase) which is a marker of this mechanism. A431 were treated with complex **5** at 10  $\mu$ M (close to IC<sub>50</sub>) and 20  $\mu$ M, and no LDH release was observed after cell incubation, excluding necrosis. The triggering of the apoptotic mechanism was analyzed by Western blotting and by measuring the mitochondrial membrane potential, as it is well known that mitochondrial outer membrane permeabilization is essential to initiate mitochondrial apoptosis. Western blot analysis was performed to assess the activation of caspase-3 and caspase-9 which are key enzymes in the cascade processes which trigger cell death, and markers of the apoptosis. Normally, caspases are found in the cell in the inactive form of pro-caspases. When the apoptotic process begins pro-caspases are activated by cleavage into different

protein subunits. The activation of caspases-3 and caspases-9 was confirmed following the incubation of A431 cells with **5** for 48 h, with the Western blot analysis that showed a significant decrease in the signal associated to both procaspases 3 and 9. Finally, the measurement of the mitochondrial potential ( $\Delta\psi_m$ ) confirmed the apoptotic pathway with a significant decrease in A431 cells observed following the incubation with **5**.

### *2.2.5 Reactivity with model biomolecules*

#### *2.2.5.1 Interaction with model DNA*

The interaction of **4-6** with model double helix DNA was evaluated through ethidium bromide (EtBr) displacement fluorescence assay, using calf-thymus DNA (ctDNA). Ethidium bromide is an intercalating agent which forms fluorescent adduct with DNA. The displacement of EtBr by a metal complex results in the decreasing of fluorescence. DNA-EtBr adduct was titrated with solutions of compounds **4-6** and fluorescence was measured. Results undoubtedly indicate that the compounds bind DNA by displacing EtBr from ctDNA (**Figure 2.9**).<sup>148</sup>

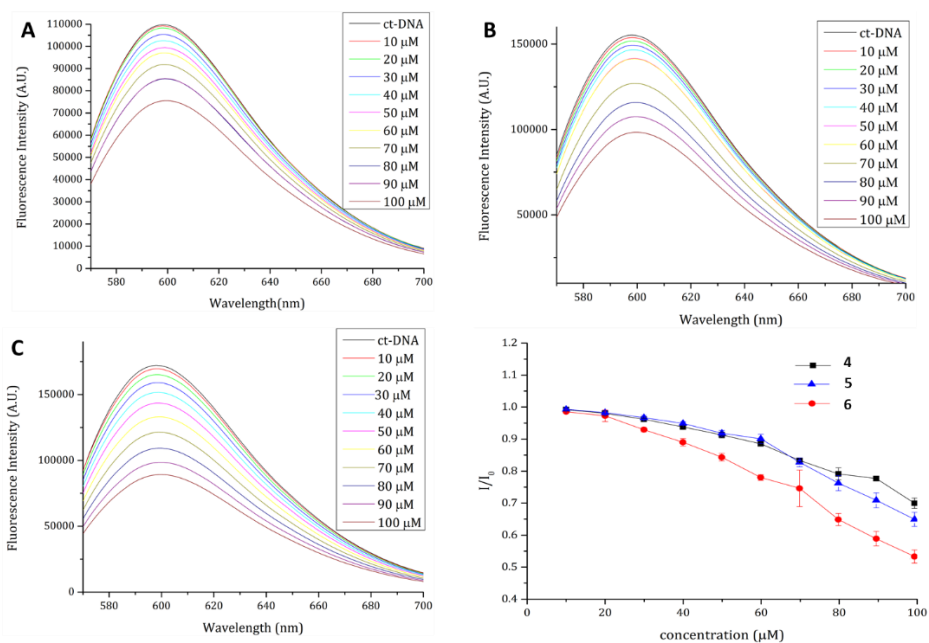


**Figure 2.9.** Fluorescence emission spectra of ct-DNA-EtBr adduct upon titration with a solution of **4** (A), **5** (B), **6** (C).  $I/I_0$  as function of compound concentration is reported.

Moreover, attempts to collect circular dichroism spectra of ctDNA in the presence of the compounds were performed to get information on conformational change in the double helix following interaction with Pt-complexes. Unfortunately, it was not possible to collect CD spectra due to the formation of a yellow precipitate when an excess of complexes was added to ct-DNA.

To shed light on the interaction between complexes and DNA, the reaction with the model nucleobase 2'-deoxyguanosine-5'-monophosphate (dGMP) was monitored by  $^1\text{H}$ -NMR spectroscopy and ESI mass spectrometry. **4** and **5** were reacted with 2.5 eq of dGMP at 37 °C in 90%-10% PB (pH 7.4)-DMSO- $d_6$  and spectra were recorded over 48h (spectra for complex **4** are reported in **Figure 2.10**).

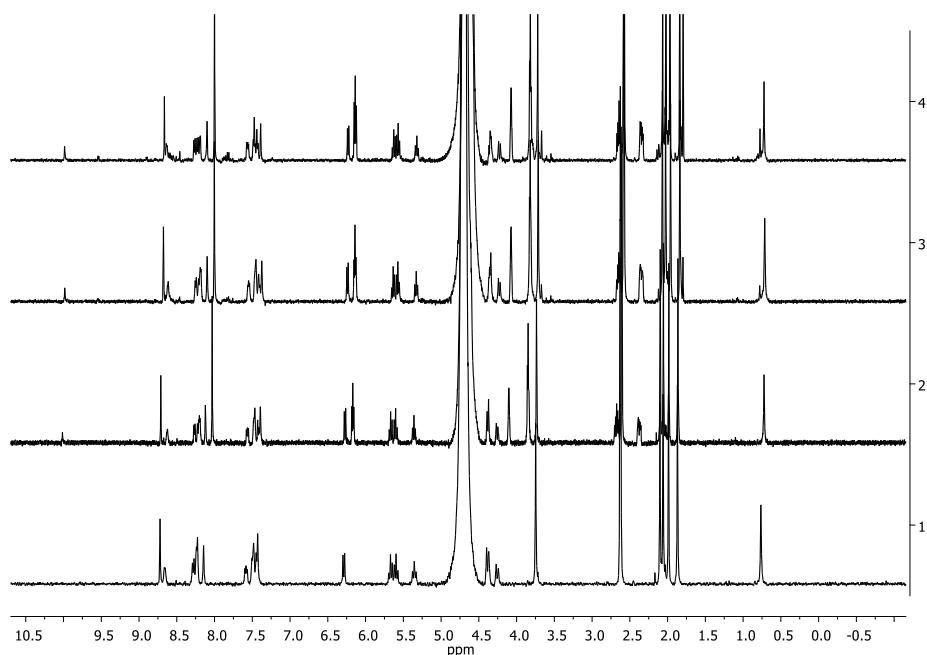


**Figure 2.10.**  $^1\text{H}$ -NMR spectra over time of **4** in 90%-10% PB-DMSO- $\text{d}_6$  (trace 1) and following the addition of 2.5 eq. of dGMP at 37 °C (trace 2 = start, 3 = 24 h, 4 = 48 h)

No coordination of dGMP to the platinum complex was observed. Such results were also confirmed by ESI mass spectrometry experiments performed in 90%-10%  $\text{H}_2\text{O}$ -DMSO. The analysis of the reaction mixture at  $t = 0$  and after 48 h of reaction at 37 °C confirmed no occurrence of coordination by dGMP, while the presence of the ***sp*-Pt-dmsO** complex was detected.

Such results, combined to the suppressed ligand exchange in physiological conditions observed for **4-6** (section 2.2.2), suggest that the family of *sp* interact with model DNA through an intercalative mechanism.<sup>149</sup> Indeed, the resistance toward ligand substitution either in aqueous systems or in presence of guanine nucleobase support the hypothesis that no coordination to DNA occurs, conversely to Pt(II) based drugs (e.g. cisplatin and derivatives). This kind of non-

covalent interaction may be favoured by the planar geometry and by the presence of aromatic ligands in the structures.<sup>150–152</sup>

#### *2.2.5.2 Reactivity with S-donor molecules*

The interaction of platinum drugs with sulphur-donor nucleophiles (thiol and thioether) resulted in sequestration/deactivation processes, which reduce their effectiveness. Therefore, the reactivity of complexes **4** and **5** with glutathione (GSH) and L-Methionine, an amino acid residue containing a thioether moiety, was studied to get insights in the biological activity of the compounds. The complexes were reacted with 2.5 eq. of L-methionine at 37 °C in 90%-10% PB (pH 7.4)-DMSO-d<sub>6</sub> and the reaction course was monitored by <sup>1</sup>H-NMR spectroscopy. Spectra collected over time showed no sign of coordination of methionine over 48 h for both complexes.

The compounds were reactive with GSH in the same conditions as observed by the <sup>1</sup>H NMR spectra for compound **4** (**Figure 2.11**).

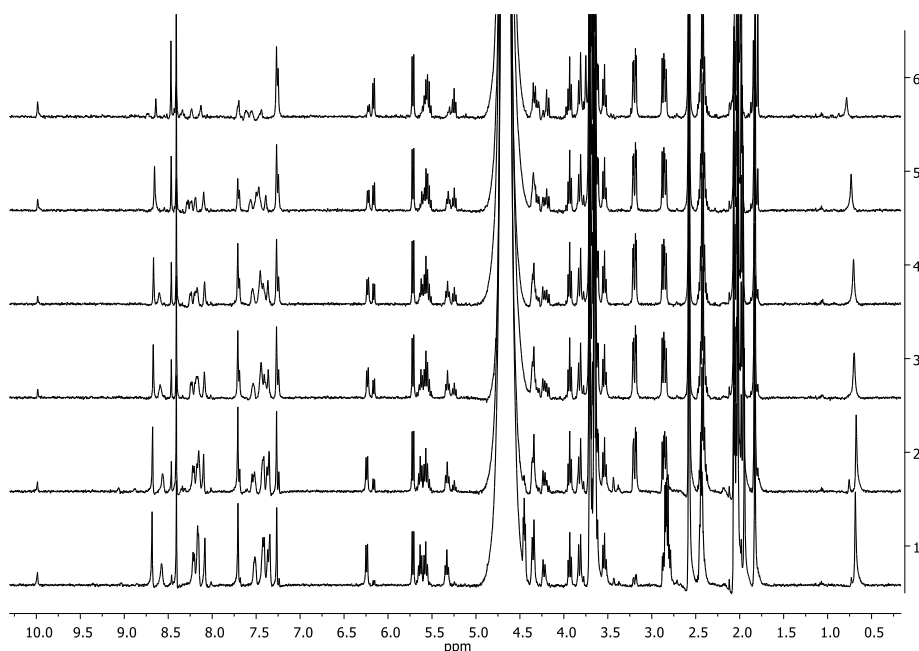


**Figure 2.11.**  $^1\text{H}$ -NMR spectra of **4** reacted with 2.5 eq. of GSH in 90%-10% PB (pH 7.4)-DMSO- $\text{d}_6$  at 37 °C at different time (1 = start, 2 = 2h, 3 = 4h, 4 = 6h, 5 = 24 h, 6 = 48 h).

Signals attributable to the free ligands were identified, but NMR did not allow to identify the new formed platinum species. The signals decreased in intensity over time until they almost disappeared (completely in case of **5**, probably because of precipitation of the reaction products). To identify this unknown species, the reaction mixture was analyzed by ESI-MS. Immediately after the dissolution of **4** and GSH in 90%-10%  $\text{H}_2\text{O}$ -DMSO, the spectrum showed the presence of the intact complex, with a peak at  $m/z$  869.22. The analysis repeated after 48 h at 37 °C revealed the presence of multiple peaks reported in **Table 2.2**.

**Table 2.2.** List of peaks found in the ESI-MS spectrum of the reaction mixture between **4** and GSH (2.5 eq.) after 48 h of at 37 °

Entry	Sequence	MF	Charge	MF Mass	m/z
1	[ <b>4</b> – CF <sub>3</sub> SO <sub>3</sub> <sup>−</sup> ]	C <sub>33</sub> H <sub>36</sub> N <sub>7</sub> O <sub>9</sub> Pt	(+)	869.2222	869.2217
2	[ <b>L-im</b> + <b>H</b> ]	C <sub>20</sub> H <sub>25</sub> N <sub>5</sub> O <sub>9</sub>	(+)	480.1652	480.1725
3	[ <i>sp</i> -Pt-dmsol]	C <sub>15</sub> H <sub>17</sub> N <sub>2</sub> OPtS	(+)	468.071	468.0704
4	[PtMephen]	C <sub>13</sub> H <sub>11</sub> N <sub>2</sub> Pt	(+)	390.057	390.0565
5	[Ptphen( <b>L-im</b> ) <sub>2</sub> ]	C <sub>52</sub> H <sub>58</sub> N <sub>12</sub> O <sub>18</sub> Pt	(+2)	1333.364	666.6814
6	[Pt <sub>2</sub> (phen) <sub>2</sub> (GS) <sub>2</sub> ]	C <sub>44</sub> H <sub>48</sub> N <sub>10</sub> O <sub>12</sub> Pt <sub>2</sub> S <sub>2</sub>	(+2)	1362.219	681.109

The decomposition of the complex was confirmed by the presence of various species including free ligand **L-im** and Pt-fragments lacking the methyl. The new Pt-species were identified as mononuclear adducts with two imidazole ligands (entry 5) or dinuclear species with two deprotonated glutathione molecules (Figure 2.12).

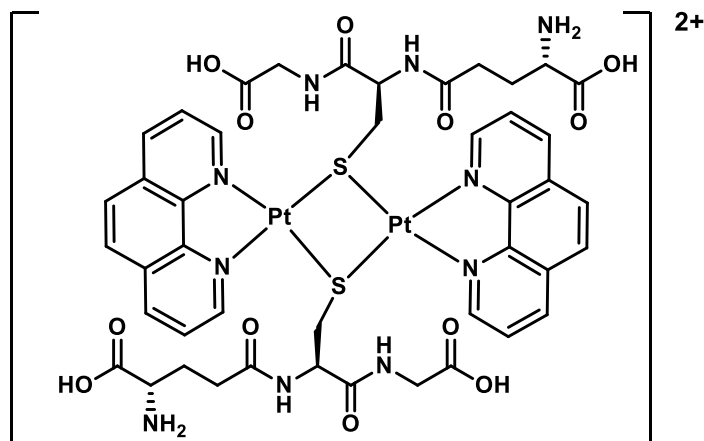


**Figure 2.12.** Dinuclear Pt-species with two deprotonated glutathione molecules.

The formation of these decomposition species is supported by literature studies: Pt(II) phenanthroline compounds were found to be reactive with GSH forming dinuclear adducts with bridging sulphur atoms.<sup>153</sup> Moreover, the formation of methane in methyl-organoplatinum(II) reacted with -SH ligands was reported,<sup>154</sup> supporting the occurrence of the described reactivity in the decomposition of **4**.



## 2.3 Experimental Part

### 2.3.1 General

Solvents and reagents were purchased from Sigma-Aldrich and were used without further purification. A431, H9c2 and MCF7 cells were purchased from American Type Culture Collection (ATCC). HaCaT cells were purchased from Innoprot (Spain). NMR spectra were recorded using a 400 Bruker AvanceUI-trashielded <sup>TM</sup> or 500 Varian Inova spectrometers. The chemical shifts are provided in parts per million (ppm,  $\delta$ ), referred to the solvent (<sup>1</sup>H NMR: CHD<sub>2</sub>OD,  $\delta$  = 3.34 ppm; <sup>13</sup>C NMR: <sup>13</sup>CHD<sub>2</sub>OD,  $\delta$  = 49 ppm). Coupling constants are expressed in Hz. The following abbreviations describe NMR multiplicities: singlet (s), doublet (d), triplet (t), quartet (q), double doublet (dd), broad (br) and multiplet (m). ESI-MS spectra were recorded on a Xevo G2-S QTOF (Waters) in positive ion mode. MS spectra were analyzed using the open-source software Aom2S.<sup>155</sup> Fluorescence spectra were collected on a HORIBA Fluoromax-4 spectrofluorometer. 1-azido-2,3,4,6-tetra-*O*-acetyl- $\beta$ -D-glucopyranoside<sup>156</sup> and PtClMe(*phen*)<sup>157,48</sup> were prepared starting from 1-bromo-2,3,4,6-tetra-*O*-acetyl- $\alpha$ -D-glucopyranoside and K<sub>2</sub>PtCl<sub>4</sub> respectively, as reported in literature procedures

### 2.3.2 Synthesis and characterization

#### 2.3.2.1 Synthesis of the ligands

A solution in DCM (5 mL) containing 1-azido-2,3,4,6-tetra-*O*-acetyl- $\beta$ -D-glucopyranoside (0.630 g, 1.68 mmol) and 3-ethynylpyridine (0.182 g, 1.76 mmol) or 5-ethynyl-1-methyl-1H-imidazole (0.187 g, 1.76 mmol) was stirred with a solution of CuSO<sub>4</sub>·5H<sub>2</sub>O (0.064 g, 0.26 mmol) and sodium ascorbate (0.151 mg,

0.762 mmol) in water (10 mL). After three days at room temperature, the two layers were separated, and the aqueous phase was extracted with DCM ( $2 \times 5$  mL). The combined organic phases were washed with an aqueous solution of sodium sulfide (0.5 M, 5 mL) and then with water ( $2 \times 5$  mL). The organic phase was dried over sodium sulfate, and the solvent was rotary evaporated to afford a yellowish powder.

**L-im:** yield 94% (0.791 g),  $^1\text{H}$  NMR (400 MHz, 298 K,  $\text{CDCl}_3$ ):  $\delta$  7.91 (s, 1H, H-Triazole), 7.51 (s, 1H, H2-imidazole), 7.30 (s, 1H, H4-imidazole), 5.91 (d, 1H,  $J_{\text{H1-H2}} = 11.5$  Hz, H1-glu), 5.51–5.41 (m, 2H, H2-glu and H3-glu), 5.26 (t, 1H,  $J_{\text{H4-H5}} = 10.0$  Hz, H4-glu), 4.33 (dd, 1H,  $J_{\text{H6-H6'}} = 12.6$  Hz,  $J_{\text{H5-H6}} = 5.0$  Hz, H6-glu), 4.17 (dd, 1H,  $J_{\text{H5-H6'}} = 2.1$  Hz, H6'-glu), 4.03 (dd, 1H, H5-glu), 3.89 (s, 3H, Me-Imidazole), 2.09 (s, 3H, OAc), 2.08 (s, 3H, OAc), 2.04 (s, 3H, OAc), 1.90 (s, 3H, OAc).  $^{13}\text{C}$  NMR (100 MHz, 298 K,  $\text{CDCl}_3$ ):  $\delta$  170.3, 169.8, 169.3, 168.8, 139.6, 139.1, 129.2, 122.7, 119.1, 85.7, 75.1, 72.4, 70.3, 67.6, 61.4, 33.4, 20.6, 20.4, 20.3, 20.0. Anal. Calcd (found): ( $\text{C}_{20}\text{H}_{25}\text{N}_5\text{O}_9$ ): C, 50.10 (50.33); H, 5.26 (5.15); N, 14.61 (14.84).

**L-py:** yield 96%, (0.804 g),  $^1\text{H}$  NMR (400 MHz, 298 K,  $\text{CDCl}_3$ ):  $\delta$  9.05 (br, 1H, H2-py), 8.60 (d, 1H,  $J_{\text{H5py-H6py}} = 4.6$  Hz, H6-py), 8.18 (d, 1H,  $J_{\text{H4py-H5py}} = 7.7$  Hz, H4-py), 8.10 (s, 1H, H-Triazole), 7.38 (dd, 1H, H5-py), 5.95 (d, 1H,  $J_{\text{H1-H2}} = 8.9$  Hz, H1-glu), 5.55–5.43 (m, 2H, H2-glu and H3-glu), 5.28 (t, 1H,  $J_{\text{H4-H5}} = 9.3$  Hz, H4-glu), 4.34 (dd, 1H,  $J_{\text{H6-H6'}} = 12.8$  Hz,  $J_{\text{H5-H6}} = 5.4$  Hz, H6-glu), 4.17 (dd, 1H,  $J_{\text{H5-H6'}} = 2.1$  Hz, H6'-glu), 4.08–4.01 (m, 1H, H5-glu), 2.10 (s, 3H, OAc), 2.08 (s, 3H, OAc), 2.05 (s, 3H, OAc), 1.90 (s, 3H, OAc).  $^{13}\text{C}$  NMR (100 MHz, 298 K,  $\text{CDCl}_3$ ):  $\delta$  170.4, 169.8, 169.3, 169.0, 149.6, 147.3, 145.5, 133.2, 126.1, 123.7, 118.3, 85.9, 75.3, 72.6, 70.4, 67.8, 61.6, 20.6, 20.5 ( $2\times$ ), 20.2. Anal. Calcd (found): ( $\text{C}_{21}\text{H}_{24}\text{N}_4\text{O}_9$ ): C, 52.94 (52.66); H, 5.08 (5.20); N, 11.76 (11.59).

### 2.3.2.2 Synthesis of compounds 4-5

To a suspension of PtClMephen (0.130 g, 0.306 mmol) in DCM (3 mL) the appropriate ligand (0.306 mmol) in DCM (3 mL), and CF<sub>3</sub>SO<sub>3</sub>Ag (0.075 g, 0.306 mmol) dissolved in the minimum volume of MeOH, were added. The mixture was stirred at RT for 24 h. After that, the solid residue was filtered on Celite® and the yellow filtrate was concentrated under vacuum to ca. 2 mL. The addition of diethyl ether afforded a yellow microcrystalline solid, which was isolated, washed several times with diethyl ether, and then dried.

**4:** yield: 73% (0.223 g). <sup>1</sup>H NMR (400 MHz, CD<sub>3</sub>OD) δ 9.44 (dd, J<sub>Pt</sub> = 53 Hz, 1H, H2 or H9 phen), 8.92 (dd, 1H, H4 or H7 phen), 8.88 (dd, 1H, H7 or H4 phen), 8.83 (s, 1H, H-Triazole), 8.66 (dd, 1H, H9 or H2 phen), 8.49 (br, 1H, H-Imidazole), 8.18 (ABq, 2H, H5 and H6 phen), 8.04 (dd, 1H, H3 or H8 phen), 8.02 (dd, 1H, H8 and H3 phen), 7.76 (d, 1H, H-imidazole), 6.30 (d, J<sub>H1-H2</sub> = 9.4 Hz, 1H, H1-glu), 5.70 (t, 1H, J<sub>H2-H3</sub> = 9.4 Hz, H2-glu), 5.62 (t, J<sub>H3-H4</sub> = 9.4 Hz, 1H, H3-glu), 5.34 (t, J<sub>H4-H5</sub> = 9.4 Hz, 1H, H4-glu), 4.42 – 4.32 (m, 2H, H5-glu and H6-glu), 4.23 (dd, J<sub>H5-H6'</sub> = 11.8 Hz, J<sub>H6-H6'</sub> = 1.3 Hz, 1H, H6'-glu), 4.09 (s, 3H, Me-Imidazole), 2.09 (s, 3H, OAc), 2.06 (s, 3H, OAc), 2.04 (s, 3H, OAc), 1.92 (s, 3H, OAc), 1.21 (s, 3H, J<sub>Pt</sub> = 74 Hz).

<sup>13</sup>C NMR (101 MHz, CD<sub>3</sub>OD) δ 170.8, 170.0, 169.8, 169.2, 149.6, 148.7, 147.7, 145.2, 141.6, 138.9, 138.3, 136.3, 131.0, 130.6, 128.5, 127.6 (x2), 127.4, 126.4, 125.6, 122.3, 120.4 (q, J<sub>C-F</sub> = 320 Hz) 85.5, 74.7, 72.5, 70.8, 67.8, 61.6, 33.6, 19.1 (x3), 18.7, -14.0. HRMS (ESI/QTOF), m/z 869.2225, [**4** – CF<sub>3</sub>SO<sub>3</sub><sup>-</sup>].

**5:** yield: 76%, (0.231 g). <sup>1</sup>H NMR (400 MHz, CD<sub>3</sub>OD) <sup>1</sup>H NMR (400 MHz, CD<sub>3</sub>OD) δ 9.55 (d, J<sub>H2Py-H4Py</sub> = 1.9 Hz, J<sub>Pt</sub> = 46 Hz, 1H, H2Py), 9.47 (dd, 1H, H2 or H9 phen), 9.03 (dd, J<sub>H6Py-H5Py</sub> = 5.6 Hz, J<sub>H6Py-H4Py</sub> = 1.3 Hz, 1H, H6Py), 9.01 (s,

1H, H-Triazole), 8.97 (dd, 1H, H4 or H7 phen), 8.93 (dd, 1H, H7 or H4 phen), 8.64 (ddd,  $J_{H4Py-H5Py} = 8$  Hz, 1H, H4Py), 8.48 (dd, 1H, H9 or H2 phen), 8.26 (ABq, 2H, H5 and H6 phen), 8.09 (dd, 1H, H3 or H8 phen), 8.04 (dd, 1H, H8 or H3 phen), 7.83 (ddd, 1H, H5Py), 6.29 (d,  $J_{H1-H2} = 8.8$  Hz, 1H, H1-glu), 5.66 (t,  $J_{H2-H3} = 9.3$  Hz, 1H, H2-glu), 5.61 (t,  $J_{H3-H4} = 9.3$  Hz, 1H, H3-glu), 5.32 (t,  $J_{H4-H5} = 9.4$  Hz, 1H, H4-glu), 4.39 (dd,  $J_{H6-H6'} = 12$  Hz,  $J_{H5-H6} = 5.0$  Hz, 1H, H6-glu), 4.33 (ddd,  $J_{H5-H6'} = 1.7$  Hz, 1H, H5-glu), 4.23 (dd, 1H, H6'-glu), 2.09 (s, 3H, OAc), 2.07 (s, 3H, OAc), 2.04 (s, 3H, OAc), 1.90 (s, 3H, OAc), 1.32 (s, 3H,  $J_{Pt} = 81$  Hz).

$^{13}C$  NMR (101 MHz,  $CD_3OD$ )  $\delta$  170.8, 170.0, 169.8, 169.2, 152.7, 150.0 (x2), 148.5, 147.5, 145.0, 142.7, 139.4, 138.7, 135.4, 131.0, 130.7, 130.3, 127.7, 127.6, 127.5, 126.6, 125.61, 121.9, 120.4 (q,  $J_{C-F} = 319$  Hz), 85.4, 74.7, 72.6, 70.8, 67.8, 61.6, 19.2, 19.1 (x2), 18.7, -12.1. HRMS (ESI/QTOF)  $m/z$  866.2106, [**5**–  $CF_3SO_3^-$ ]

### 2.3.2.3 Synthesis of **6**

Complex **4** (0.065 g, 0.064 mmol) was treated in 5.0 mL of methanol containing 5% mol/mol of KOH. After 1 hours stirring at room temperature, the complex was crystallized by slow addition of diethyl ether to the reaction mixture. Yield 90% (0.050 g).  $^1H$  NMR (400 MHz,  $CD_3OD$ )  $\delta$  9.46 (d,  $J_{Pt} = 49$  Hz, 1H, H2 or H9 phen), 8.94 (d, 1H, H4 or H7 phen), 8.90 (d, 1H, H7 or H4 phen), 8.71 (s, 1H, 1H, H-Triazole), 8.68 (dd, 1H, H9 or H2 phen), 8.49 (s, 1H, 1H, H-Imidazole), 8.22 (ABq, 2H, H5 and H6 phen), 8.05 (dd, 1H, H3 or H8 phen), 8.03 (dd, 1H, H8 or H3 phen), 7.75 (s, 1H, H-Triazole), 5.76 (d,  $J_{H1-H2} = 9.2$  Hz, 1H, H1-glu), 4.09 (s, 3H, Me-Imidazole), 4.01 (t,  $J_{H2-H3} = 9.1$  Hz, 1H, H2-glu), 3.95 (dd,  $J_{H6-H6'} = 11.6$  Hz,  $J_{H6-H5} = 1.4$  Hz, 1H, H6-glu), 3.79 (dd,  $J_{H6'-H5} = 5.3$  Hz, 1H,

H6'-glu), 3.70 3.50 (m, 2H, H3-glu and H4-glu), 1.26 (s, 3H, JPt = 76 Hz).  $^{13}\text{C}$  NMR (101 MHz,  $\text{CD}_3\text{OD}$ )  $\delta$  149.8, 148.8, 147.4, 145.2, 141.5, 139.0, 138.1, 135.8, 131.0, 130.7, 128.6, 127.6, 127.4, 126.4, 125.9, 125.6, 122.5, 120.5 (JC-F = 317 Hz), 88.6, 79.9, 77.0, 72.42, 69.9, 60.8, 33.2, -13.7. HRMS (ESI/QTOF)  $m/z$  701.1802, [**6** –  $\text{CF}_3\text{SO}_3^-$ ]

### 2.3.3 $^1\text{H}$ NMR and ESI-MS in-solution studies

Stock solutions of every complex were freshly prepared for each set of experiments. The appropriate complex (10 mM) was dissolved in 0.5 mL of  $\text{DMSO-}d_6$  or  $\text{Acetone-}d_6$ . Calculated volumes of solution were diluted to 600  $\mu\text{L}$  with the appropriate volumes of PB in  $\text{D}_2\text{O}$  (25 mM, pH 7.4), and/or  $\text{DMSO-}d_6$  to provide a final concentration of 1 mM of Pt-complex with the appropriate v/v ratio of solvents. Samples were incubated at 37  $^\circ\text{C}$  and NMR spectra were recorded at different times. Stock solutions (10 mM) of nucleophiles (dGMP, L-methionine and GSH) were prepared in PB in  $\text{D}_2\text{O}$  (25 mM, pH 7.4) and the correct volume was added to a freshly prepared solution of the complexes in 90%-10% PB- $\text{DMSO-}d_6$  to afford a final concentration of 1 mM of Pt-complex and 2.5 mM of nucleophile.

Samples for ESI-MS analysis were prepared as described for NMR samples using  $\text{DMSO}$  and  $\text{H}_2\text{O}$  instead of deuterated solvents. Prior to analysis, an aliquot of the reaction mixture was withdrawn and diluted 1:10 with water.

### 2.3.4 Evaluation of the biological activity

Cell culture and experiments involving cytotoxicity assays, LDH release, Western blot analysis, and measurement of mitochondrial membrane potential were

performed in collaboration with Prof. Daria M. Monti research group at University of Naples Federico II.

#### 2.3.4.1 *Cytotoxicity Experiments*

Cells were cultured in DMEM (Sigma-Aldrich, St. Louis, MO, USA), supplemented with 10% fetal bovine serum (HyClone, Thermo Scientific, Logan, UT, USA) and antibiotics, in a 5% CO<sub>2</sub> humidified atmosphere at 37 °C. The growth medium of H9c2 cells was implemented with 2 mM L-glutamine and 2 mM sodium pyruvate. Cells were seeded in 96-well plates at a density of  $2.5 \times 10^3$  cells per well. Compounds **4-6** were dissolved at 10 mM in 50%-50% H<sub>2</sub>O-Acetone and added at increasing concentrations (0.5  $\mu$ M – 200  $\mu$ M) to the cells, 24 hours after seeding, for dose-dependent assays. For the GLUT1 inhibitor mediated cytotoxicity assay, 24 h after seeding, the cells were treated with 0.5–200  $\mu$ M of **2** in the presence or absence of 5  $\mu$ M quercetin. Quercetin alone was used as the control. After 48 h incubation, cell viability was assessed by MTT assay as described in literature.<sup>158</sup> Control experiments were performed either by growing cells in the absence of the compound and by supplementing the cell cultures with identical volume of solvent mixture (50%-50% H<sub>2</sub>O-Acetone). Each value is the mean of three independent experiments, each with three determinations. Significance was determined by the Student's t-test.

#### 2.3.4.2 *LDH release*

The occurrence of necrosis was determined by measuring the release of lactate dehydrogenase (LDH) in the culture medium as described by Sucha *et al.*<sup>159</sup> The LDH content of the medium from untreated cells was referred to as spontaneous

release, whereas the LDH total cellular content was determined upon cell lysis. The percentage of LDH release was calculated as:

*LDH release (%)*

$$= [(experimental - spontaneous release)/(total content - spontaneous release)] \times 100$$

Each value is the mean of three independent experiments, each with three determinations. Significance was determined by the Student's t-test.

#### 2.3.4.3 *Western blot analyses*

A431 cells were plated at a density of  $3 \times 10^5$  cells  $\text{cm}^{-2}$  in complete medium for 24 h and then treated for 48 h with 12  $\mu\text{M}$  **5**. At the end of the incubation, both untreated and treated cells were analyzed for Western blot analyses. Upon determination of total protein concentration in the supernatant by the Bradford assay, samples were analyzed by SDS-PAGE and Western blot using specific antibodies directed towards procaspase-3 or -9.  $\beta$ -actin or GAPDH were used as loading control. Each value is the mean of three independent experiments, each with three determinations. Significance was determined by the Student's t-test.

#### 2.3.4.4 *Analysis of mitochondrial membrane potential*

Cells were plated at a density of  $2 \times 10^4$  cells per well and after 24 h, cells were incubated for 48 h with 12-20  $\mu\text{M}$  **5**. At the end of the treatment, the cells were incubated with 200 nM of the cationic lipophilic dye tetramethylrhodamine ethyl ester (TMRE) for 20 min at 37 °C. Then, the cells were gently washed with 0.2% BSA in PBS three times and the fluorescence was measured in a microplate reader with peak  $\lambda(\text{ex})/\lambda(\text{em}) = 549/575$  nm. Each value is the mean of three independent experiments, each with three determinations. Significance was determined by the Student's t-test.

### 2.3.5 *Ethidium bromide displacement fluorescence assay*

Fluorescence experiments and attempts to collect Circular Dichroism experiments were performed in collaboration with Prof. Antonello Merlino research group at University of Naples Federico II.

Fluorescence spectra were collected at 25 °C using 1 cm path length cuvettes. ctDNA was incubated with ethidium bromide (EtBr) in a 1:50 molar ratio for 30 min at room temperature. Then, the complex was diluted in 10 mM ammonium acetate buffer at pH 7.5 up to a ctDNA final concentration of 200  $\mu$ M. The ctDNA–EtBr complex was then titrated with a **4-6** solution (final concentration from 10 to 100  $\mu$ M, stock concentration 15 mM). Fluorescence emission spectra were recorded at an excitation at 545 nm after an equilibration time of 5 min following each addition of Pt-complex.



## 3 Pt(0) olefin complex with a glucoconjugated iminopyridine ligand

### 3.1 General Overview

Platinum(0) complexes are scarcely represented in anticancer research due to the major fragility with respect to Pt(II) and Pt(IV) congeners. Indeed, the decomposition of Pt(0) molecular compounds can easily lead to the deposition of metallic platinum, a particularly undesirable event in biological systems. However, some properties of this oxidation state could be an interesting option to be studied. With respect to Pt(II) and Pt(IV), Pt(0) complexes are less electrophilic, with consequent benefit on the indiscriminate reactivity toward nucleophiles in biological environment. This feature can be modulated by the choice of ligands, offering interesting opportunities in developing Pt(0) anticancer agents.

Compounds of general structure  $[\text{Pt}^0(\text{N,N-chelate})(\text{olefin})]$  are particularly attractive since they combine good stability with a wide panel of reactivity tuned by the nature of N-N' and of the olefin ligands. Among N,N'-chelating ligands, bidentate 2-iminopyridines (general structure in **Figure 3.1**) have been widely explored in several applications<sup>160–167</sup>,

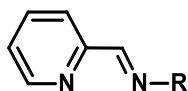


**Figure 3.1.** General structure of a bidentate 2-iminopyridine ligand

The good  $\sigma$ -donation and  $\pi$ -backdonation properties of 2-iminopyridine ensured by the presence of the two  $\text{sp}^2$ -hybridized nitrogen atoms stabilize a variety of metal ions in various oxidation states<sup>168</sup>. The selection of the residue R can be made depending on the availability of the amine  $\text{R-NH}_2$  precursor and its ease of

functionalization. Aminosugars represent a convenient and highly available option in the choice of the amine residue. Several metal complexes with glucoconjugated 2-iminopyridines (**L-glu** in **Figure 3.2**) are known and have been used in different applications. Among these, a Pt(II) complex having the glucoconjugate 2-iminopyridine (**L-glu<sup>OH</sup>**) ligand (**Figure 3.2**) has been previously evaluated as anticancer agents by Fanizzi, Ruffo et al.<sup>169</sup>

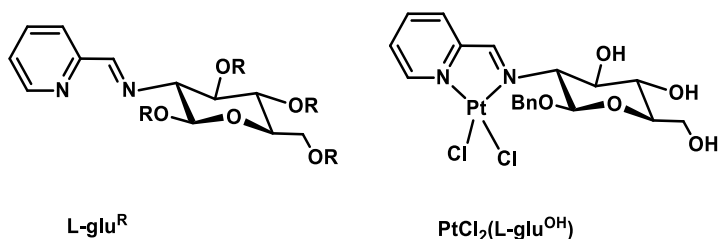


**Figure 3.2.** Structure of the glucoconjugated 2-iminopyridine ligand and of the relative Pt(II) complex studied as anticancer agent by Fanizzi, Ruffo et al.

Chemical characteristics of  $[\text{Pt}^0(\text{N,N-chelate})(\text{olefin})]$  are sometimes similar to  $\text{Pt}^{\text{II}}$  square-planar complexes. Such parallelism is rationalizable by considering the degree of the metal-to-olefin  $\pi$ -backdonation, which gives to the formal Pt(0) species (**a** in **Figure 3.3**) a consistent Pt(II) cyclopropanemetalate character (**b** in **Figure 3.3**).

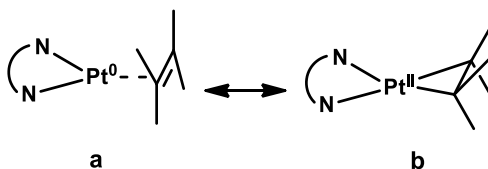


**Figure 3.3.** Possible mesomeric forms of  $[\text{Pt}^0(\text{N,N-chelate})(\text{olefin})]$  type complex

On these bases, the complex **7** (**Figure 3.4**) was designed to get preliminary information on the anticancer activity of Pt(0) complexes with glycoconjugate ligands.

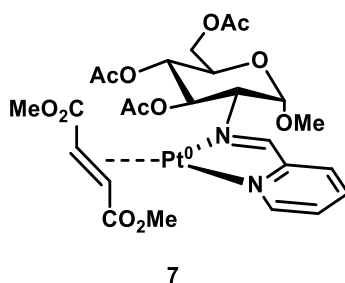


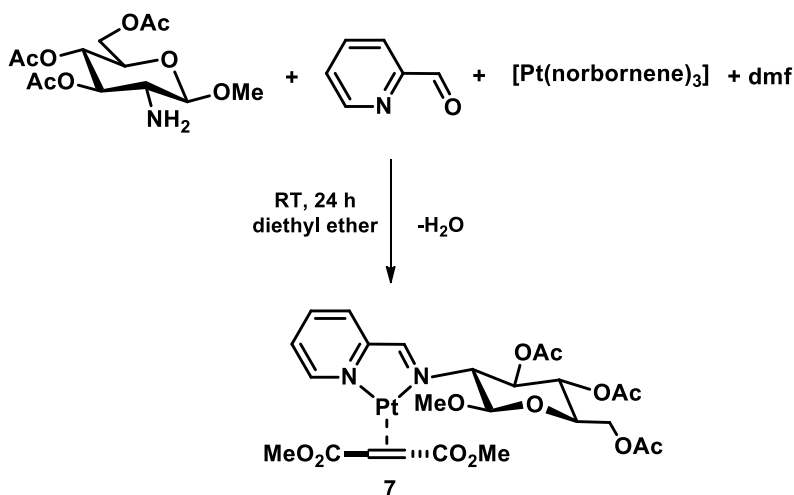
**Figure 3.4** Complex **7** studied in this chapter

Complex **7** displayed the N,N'-chelate **L-Glu<sup>Ac</sup>** and dimethyl fumarate, whose strong electron withdrawing ability is expected to enhance the overall stability of the complex. Although the presence of a chiral ligand and of a pro-chiral olefin could result in the possible formation of diverse diastereomers, NMR studies disclosed that the stereochemistry of coordination was highly selective. Moreover, the in-solution stability and the anticancer activity were studied.

## 3.2 Results and Discussion

### 3.2.1 Synthesis of complex 7

Complex **7** was prepared through a template synthesis by reacting 1-methyl-3,4,6-tri-*O*-acetyl-2-amino- $\beta$ -D-glucopyranose and pyridine-2-carboxaldehyde with [Pt(norbornene)<sub>3</sub>] in presence of the olefin dimethyl fumarate, in dry diethyl ether, as reported in **Scheme 3.1**.



**Scheme 3.1.** Synthesis of complex **7** (The bold and the hashed bonds in dmf are used only to indicate the trans configuration, without reference to the coordinated enantioface)

After 24 hours at RT the bright orange microcrystalline product was isolated by removing the solvent and purified through chromatography on Silica Gel. The complex was soluble in halogenated solvents, in acetone and appreciably soluble also in water (ca. 2 mg/mL). Despite the possible formation of diverse diastereomers due to multiple stereochemical motifs, the NMR characterization showed high diastereoselectivity of the reaction. The <sup>1</sup>H NMR spectra of the purified product disclosed the presence of two diastereomers with a solvent

dependent diastereomeric ratio with a good to excellent excess in  $\text{CDCl}_3$  (7:1) and in  $\text{D}_2\text{O}$  (18:1). Spectra are reported in **Figure 3.5**.

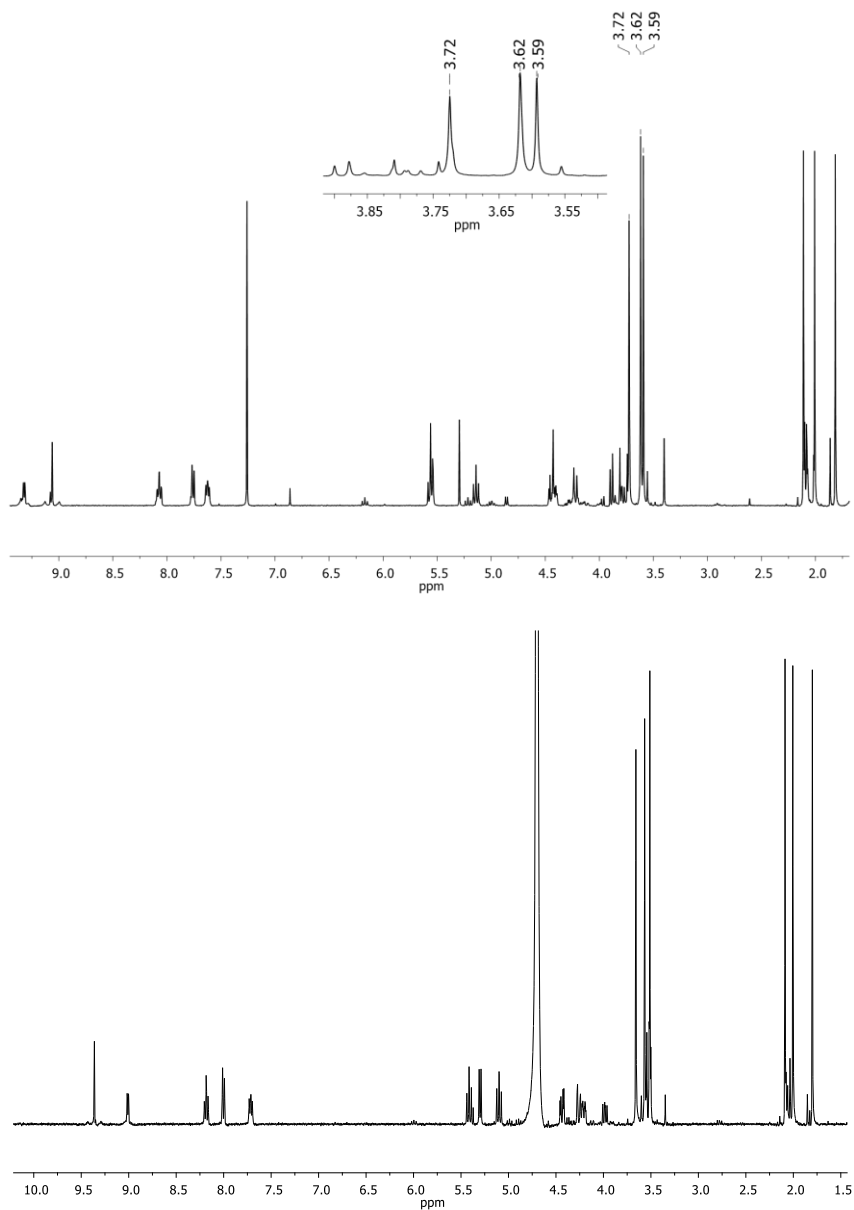


**Figure 3.5**  $^1\text{H}$  NMR spectra of **7** in  $\text{CDCl}_3$  (top) and in  $\text{D}_2\text{O}$  (bottom) at 400 MHz.

To verify that a thermodynamic equilibrium between the two isomers was reached, dmf- $d_6$ ,  $E$ - $CD_3O_2CH=CHCO_2CD_3$  was added to a solution of the complex in  $CDCl_3$ . The addition of the deuterated alkene gave rise to an exchange process with the coordinated alkene, causing the reduction of the intensities of the two corresponding methoxyl signals, without altering the ratio between the two diastereoisomers, as observed by integrating suitably corresponding signals.

The spectra showed the imine, the  $\alpha$ -pyridine and the olefin protons affected by the expected coupling to  $^{195}Pt$ , while the protons of the sugar ring revealed the  $J_{H-H}$  constants typical of  $\beta$  glucose configuration. The significant  $\pi$ -backdonation from Pt to alkene bond was evident by the shift of the olefin proton doublets, moved at low frequencies of about 3 ppm signals (between 3.9-3.7 ppm in  $CDCl_3$ ) with respect to free dmf. The carbon spectrum was in fully agreement and the C-alkene signals were found in  $CDCl_3$  at 26.4 and 26.1 ppm with  $J_{Pt-C}$  of ca. 400 Hz. To disclose the configuration of the major diastereomer, bi-dimensional NMR experiments were carried out. It is important to note that, in principle, it is possible to hypothesize at least four structures reported in **Figure 3.6**.

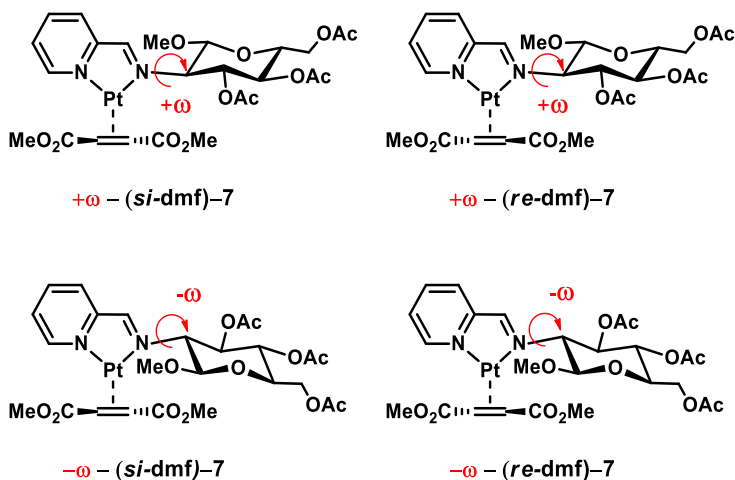


**Figure 3.6.** Possible diastereomers for 7

It is reasonable to assume that for steric reasons the glucoside residue arranges the middle plane of its chair orthogonally to the plane of the complex, resulting in two different possible conformations with respect to the rotation around the N-C2 bond (labelled as  $\omega$  or  $-\omega$ ). Moreover, due to its prochirality, the coordination of the alkene can occur with each of the two enantiofaces (*re* or *si*).

$^1\text{H}$ ,  $^1\text{H}$ - $^1\text{H}$  COSY and  $^1\text{H}$ - $^{13}\text{C}$  HSQC NMR experiments allowed to attribute every peak to the corresponding nuclei. The methoxyl signal on the sugar at C1 was identified among the three singlets at 3.72, 3.62 and 3.59, by the previous mentioned addition of dmf- $d_6$  in  $\text{CDCl}_3$  (**Figure 3.5**) The exchange with the coordinated alkene allowed to attribute the intact peak at  $\delta$  3.59 to the methoxyl sugar. NOESY spectra were carried out in  $\text{D}_2\text{O}$  or in  $\text{CDCl}_3$  (**Figure 3.7**). The presence of an evident contact between H2-glucose and the iminic proton allowed to identify as  $-\omega$  the orientation of the sugar residue with respect to the N-C2 bond and confirmed that the middle plane of the sugar chair was orthogonal to the Pt coordination plane.

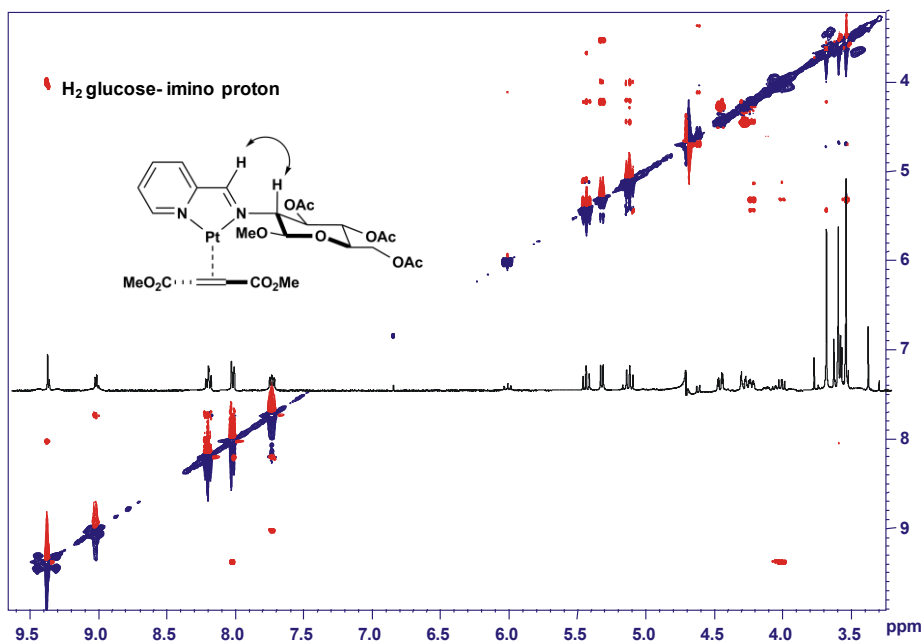


**Figure 3.7.** Section of the NOESY spectrum of **7** in D<sub>2</sub>O, showing the interaction between the imino proton and H<sub>2</sub>-glucose.

Following the definition of the conformation of the nitrogen ligand, selective NOE contacts between the olefin protons and other protons of the complex were searched to individuate the enantioface coordinated to metal centre in the main diastereoisomer. In the spectrum recorded in D<sub>2</sub>O (**Figure 3.8**) two distinct NOE contacts between H1-glucose with one dmf CH=, and between H3-glucose with one dmf OMe group were observed. The spatial proximity between these nuclei is diagnostic of the orientation of the alkene moiety. Indeed, this spatial interaction is only possible if the alkene is coordinated with its *si* face, orienting one CH= proton in the area intercepted by the anomeric position of the H1-glucose as depicted in **Figure 3.8**. Analogous NOE contacts were also observed in CDCl<sub>3</sub>.



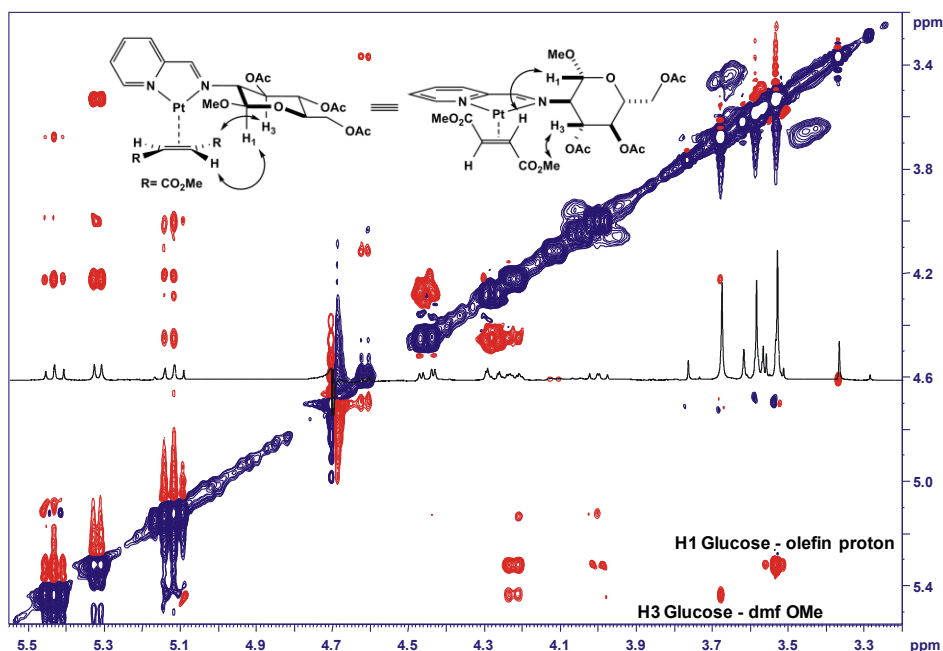


**Figure 3.8.** Section of the NOESY spectrum of **7** in D<sub>2</sub>O, showing the interaction between one olefin proton and H1-glucose.

### 3.2.2 *In-solution stability*

Pt(0) complexes require stabilizing ligand to avoid degradation in solution and consequent formation of metallic platinum. The choice of using dimethyl fumarate was aimed to improve the overall stability of the complex given the electron-attracting properties of this alkene which enhance the  $\pi$ -back donation to the metal center. In line with expectations, compound **7** showed to be highly stable in CDCl<sub>3</sub> for long period (over two weeks), while no degradation was observed over 3-4 days in water. Only after many days of aging, partial release of alkene and formation of complexes difficult to identify were observed in water. No tendency to give oxidative addition, neither of the C-Cl bond of chloroform, nor of the O-

H bond by water was observed. Therefore, oxidative phenomena in the biological environment can be excluded at least in a short time, encouraging the use of the complex in *in vitro* biological experiments.

### 3.2.3 Cytotoxic activity of **7**

The biological activity of **7** was assessed on two couples of cell lines, with each couple constituted by a cancerous line and a biologically related non-cancerous counterpart. Tumor cell line A431 (epidermoid carcinoma cells) and related non-tumor HaCaT (human keratinocyte cells), SVT2 cells (murine fibroblasts BALB/c-3T3 transformed with SV40 virus) and BALB/c3T3 were selected. The cytotoxicity was evaluated by determining the IC<sub>50</sub> values (the concentration of complex able to reduce to 50% the cell viability) through MTT assay after 48 h incubation. The selectivity of the compounds was evaluated by relating the IC<sub>50</sub> of the cancer line with its healthy counterpart. Cells were incubated with increasing concentrations of the complex and then cell survival was evaluated. A cytotoxic effect was observed on all the cell lines under test (**Table 3.1**).

**Table 3.1.** IC<sub>50</sub> values (μM) obtained for **7** on immortalized and cancer cells after 48 h incubation. Selectivity Index (SI), indicated by the ratio between the IC<sub>50</sub> of immortalized cells and cancer cells

Complex	IC <sub>50</sub> (μM)				SI	SI
	HaCaT	A431	BALB/c3T3	SVT2	HaCat /A431	BALB/c3T3 /SVT2
<b>7</b>	32 ± 6	36 ± 0.5	45 ± 3	61 ± 5	0.89	0.74
<b>Cisplatin</b>	6.6 ± 0.3	39 ± 12	240 ± 47	195 ± 7	0.17	1.23

From the IC<sub>50</sub> values reported in **Table 3.1** it is possible to observe that complex **7** did not display any selectivity toward cancer cells. Indeed, selectivity indexes are close to 1, indicating no differences in the action toward cancer and non-cancerous

cell lines. However, **7** showed to be by far more toxic than cisplatin on the couple BALC/c 3T3 and SVT2. Such activity should be considered , since few examples of Pt(0) molecular complexes tested as anticancer drug are reported in literature, although their tuneability of the chemical properties by the opportune choice of the coordination environment is an attractive feature for future developments.

### 3.3 Experimental Part

#### 3.3.1 General

All reagents and solvents were purchased from Sigma-Aldrich and were used without further purification. Human A431 epidermoid carcinoma, murine BALB/c-3T3 and SVT2 fibroblasts were from ATCC. Human HaCaT keratinocyte cells were from Innoprot. Cells were cultured in Dulbecco's modified Eagle's medium (DMEM) (Sigma-Aldrich, St Louis, MO, USA), supplemented with 10% foetal bovine serum (HyClone), 2 mM L-glutamine and antibiotics, under a 5% CO<sub>2</sub> humidified atmosphere at 37 °C. NMR spectra were recorded in D<sub>2</sub>O (HDO,  $\delta$  4.79 as internal standard) and CDCl<sub>3</sub> (CHCl<sub>3</sub>,  $\delta$  7.26, and <sup>13</sup>CDCl<sub>3</sub>,  $\delta$  77.0 as internal standards), using a 400 Bruker Avance Ultrashield 400 MHz and a 600 Bruker MHz equipped with cryoprobe. The following abbreviations were used for describing NMR multiplicities: s, singlet; d, doublet; dd, double doublet; t, triplet; m, multiplet. Methyl-tri-O-acetyl-2-amino-2-deoxy- $\beta$ -D-glucopyranoside<sup>170</sup> and [Pt(norbornene)<sub>3</sub>]<sup>171</sup> were prepared starting from D-glucosamine hydrochloride and from K<sub>2</sub>PtCl<sub>4</sub> respectively, as reported in literature procedures.

#### 3.3.2 Synthesis and characterization of **7**

[Pt(norbornene)<sub>3</sub>] (0.10 g, 0.21 mmol) was suspended in 2 mL of dry diethyl ether and stirred at RT with dmf (0.030 g, 0.21 mmol). After 10 minutes, a solution containing methyl-tri-O-acetyl-2-amino-2-deoxy- $\beta$ -D-glucopyranoside (0.083 g, 0.26 mmol) and pyridine-2-carboxaldehyde (25  $\mu$ L, 0.26 mmol) in dry diethyl ether (1 mL) was added. The mixture was stirred for 24 h at RT after that, the solvent was removed under reduced pressure. The product was obtained pure after

a chromatography on Silica gel using 100:4 DCM/methanol. Yield 72%(0.11 g). <sup>1</sup>H NMR, CDCl<sub>3</sub>, δ: 9.32 (d, 1H, J<sub>Pt</sub>= 30 Hz, H6-py), 9.06 (s, 1H, J<sub>Pt</sub>= 54 Hz, N=CH), 8.07 (t, 1H, H4-py), 7.76 (d, 1H, H3-py), 7.62 (dd, 1H, H5-py), 5.56 (t, 1H, J<sub>H2-H3</sub>= J<sub>H3-H4</sub>= 9.4 Hz, H3-glu), 5.55 (d, 1H, J<sub>H1-H2</sub>= 7.8 Hz, H1-glu), 5.14 (t, 1H, J<sub>H4-H5</sub> = 9.4 Hz, H4-glu), 4.47-4.38 (m, 2H, H5-glu and H6-glu), 4.26-4.19 (m, 1H, H6'-glu), 3.89 (d, 1H, J<sub>Pt</sub>= 90 Hz, CH= dmf ), 3.79 (dd, 1H, H2-glu), 3.74 (d, 1H, CH= dmf ), 3.72 (s, 3H, OMe-dmf), 3.62 (s, 3H, OMe-dmf), 3.59 (s, 3H, OMe-glu), 2.11 (s, 3H, OAc), 2.01 (s, 3H, OAc), 1.81 (s, 3H, OAc). <sup>1</sup>H NMR (400 MHz, D<sub>2</sub>O) δ 9.36 (s, 1H), 9.01 (d, J = 5.8 Hz, 1H), 8.18 (dd, J = 8.4, 7.1 Hz, 2H), 8.00 (d, J = 7.8 Hz, 2H), 7.78 – 7.65 (m, 2H), 5.40 (dd, J = 18.2, 8.5 Hz, 2H), 5.30 (d, J = 7.9 Hz, 1H), 5.10 (t, J = 9.7 Hz, 2H), 4.43 (dt, J = 16.7, 8.4 Hz, 2H), 4.23 (dd, J = 20.7, 10.6 Hz, 3H), 3.98 (dd, J = 9.7, 8.1 Hz, 1H), 3.66 (s, 5H), 3.56 (d, J = 6.7 Hz, 5H), 3.53 – 3.49 (m, 6H), 2.14 – 2.05 (m, 6H), 2.01 (s, 6H), 1.81 (d, J = 11.0 Hz, 5H). <sup>13</sup>C NMR, CDCl<sub>3</sub>, δ 176.8, 176.5, 170.8, 170.2, 168.9, 166.4, 154.1, 153.5, 138.2, 129.8, 126.7, 104.4, 74.8, 72.6, 71.2, 68.8, 62.2, 58.1, 51.4, 51.1, 26.4 (J<sub>Pt</sub> = 401 Hz), 26.1 (J<sub>Pt</sub> = 376 Hz), 20.8, 20.7, 20.5. Elem. Anal. Calcd. (Found) for C<sub>25</sub>H<sub>32</sub>N<sub>2</sub>O<sub>12</sub>Pt: C, 40.16 (40.38); H, 4.31 (4.27); N, 3.75 (3.70).

### 3.3.3 *Evaluation of the biological activity*

Cell culture and cytotoxicity assays were performed in collaboration with Prof. Daria M. Monti research group at University of Naples Federico II.

To test the cytotoxicity of **7**, cells were seeded at a density of  $2.5 \times 10^3$  cells per well in 96-well plates. After 24 h, increasing concentrations of compound dissolved in water, were added to the cells (0.1–67 μM). After 48 h incubation, cell viability was assessed by the MTT assay (3-(4,5-dimethylthiazol-2-yl)-2,5-

diphenyltetrazolium bromide), as reported in literature.<sup>158</sup> Cell survival was expressed as the percentage of viable cells in the presence of **7** compared to the controls, represented by untreated cells and cells supplemented with identical volumes of water. Each sample was tested in three independent analyses, each carried out in triplicate.

## 4 C-glycoconjugate *thp* Pt(II) complexes

### 4.1 General Overview

Recently, Merlino, Ruffo et al. reported a panel of coordinatively saturated Pt(II) *thp* complexes of general structure reported in **Figure 4.1**.<sup>172</sup>

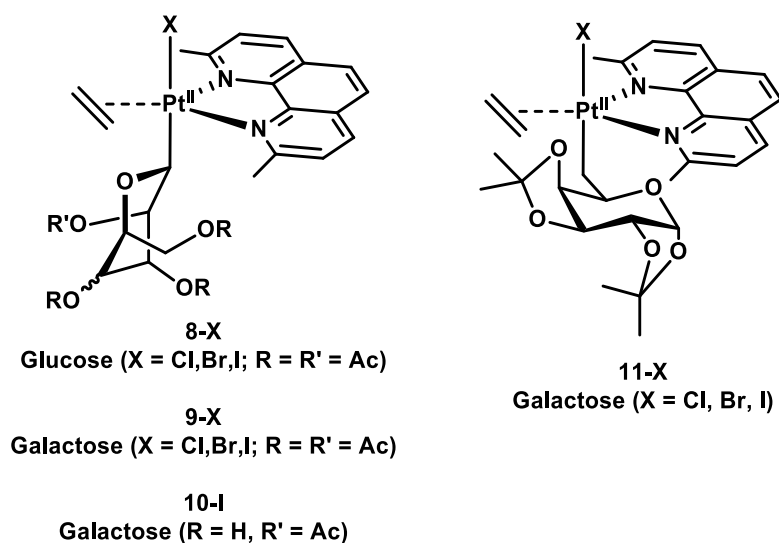
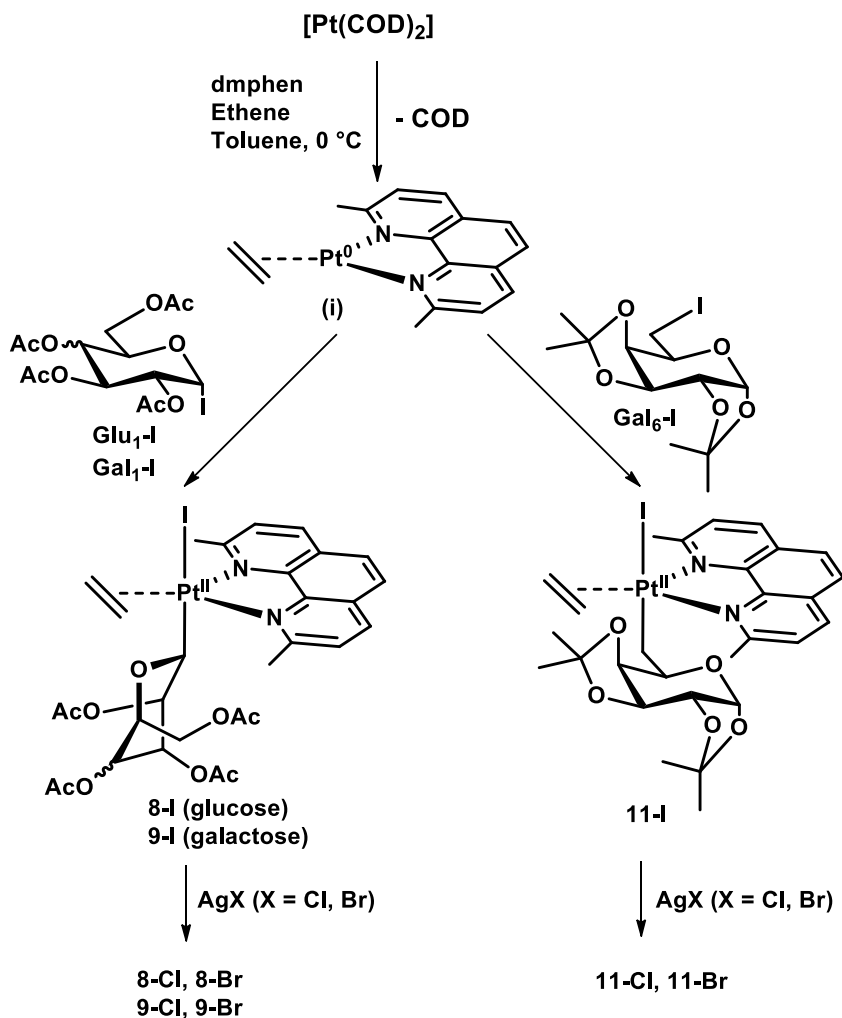


**Figure 4.1.** General structure of the complexes studied by Merlino and Ruffo.

The complexes can be divided in four subclasses having different sugar residues (glucosyl or galactosyl) directly linked to platinum through C1 (**8-X**, **9-X** and **10-I**) or C6 (**11-X**), with each type of subclass containing complexes with different halido ligands (X = Cl, Br, I). The compounds display a trigonal bipyramidal arrangement with the N,N-bidentate ligand *dmphen* and the alkene in the plane, and the halide and the sugar residue in the axial positions.

The iodo-compounds were obtained through the oxidative addition of the corresponding iodo- $\alpha$ -D-pyranoses (glucose or galactose) to the Pt(0) precursor

[Pt(dmphen)(ethene)] ((i) in **Scheme 4.1**), and then reacted in halide exchange reaction to prepare the other derivatives, as reported in **Scheme 4.1**.



**Scheme 4.1.** Synthetic strategy to access *tbp* C-glycosylated compounds

The stereochemical outcome of the oxidative addition of 1-iodo- $\alpha$ -D-tetra-O-acetylpyranoses (**Glu<sub>1</sub>-I** and **Gal<sub>1</sub>-I**) was particularly interesting. Indeed, in both cases, the major product was the compound with the retention of configuration at



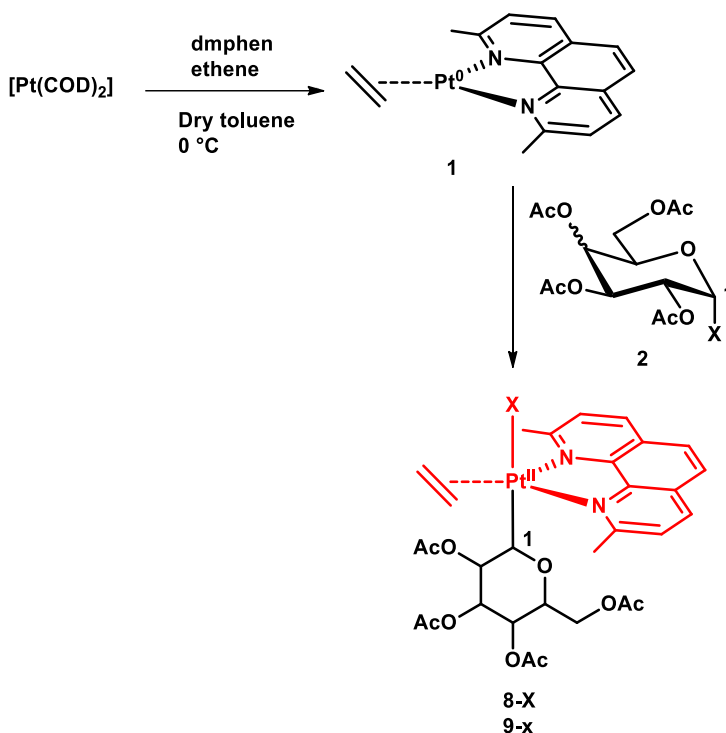
anomeric position ( $\alpha$  anomer) with the glycosyl fragments in the unusual  ${}^1C_4$  conformation (**8-X** and **9-X**). However, subsequent analysis of the reaction mixture between (**i**) and **Glu<sub>1</sub>-I** revealed the presence of another compound, identified as the  $\beta$ -anomer (inversion of configuration product).

These are the premises on which is based the work of the present chapter. The two stereoisomers **8 $^{\alpha}$ -I** and **8 $^{\beta}$ -I** have been separated and characterized by NMR and X-ray crystallography. Combined experimental and computational studies have been performed to shed light on the mechanistic aspects that result in the preferential formation of the retention products ( $\alpha$ -anomers). Moreover, the biological activity of the studied compounds will be discussed.

## 4.2 Results and Discussion

### 4.2.1 Synthesis and Experimental Mechanistic Study

The general strategy to synthesize compounds **8-X** and **9-X** is reported in **Scheme 4.2**.

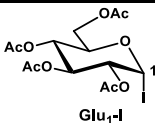
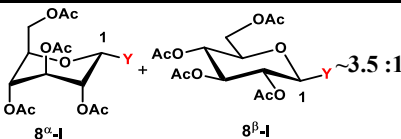
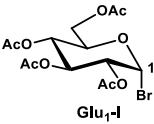
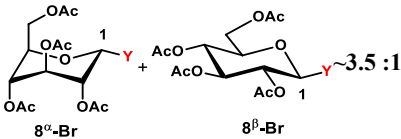
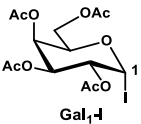
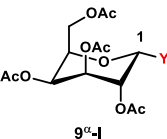
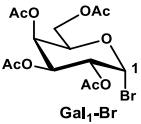
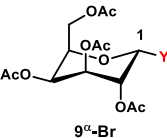


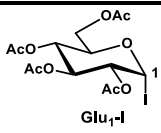
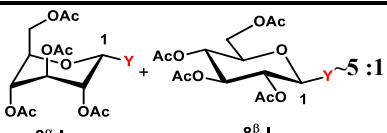
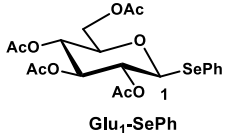
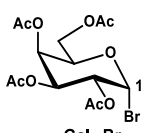
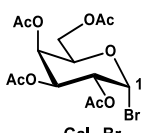
**Scheme 4.2.** Synthetic strategy to afford compounds **8-X** and **9-X**

The oxidative addition of the glycosyl halide **2** to the ethene Pt(0) precursor **1** was carried out at RT for a period of 16 h. The progress of the reactions could be roughly monitored through the switch from the intense red color, typical of precursor (**i**), to the yellow-brown tint of the product mixture. At the end of the reaction, hexane was added to the mixture and the crude product was isolated by

removing the mother liquor and washing the solid with hexane. To get insights on the mechanism of the reaction, different glycosyl substrates and different experimental conditions were investigated. The crude and the mother liquor were analyzed by  $^1\text{H}$  NMR, without any purification to observe the actual composition of the reaction mixture. The investigated experimental conditions are reported in **Table 4.1**.

**Table 4.1.** Investigated reaction conditions. In the column “**Products**” the **Y** states for the whole fragment **[-Pt(dmphen)(ethene)X]**. Such notation was adopted to evidence the stereochemical outcome on the sugar fragment

Entry	Glycosyl halide (2)	Experimental conditions	Products	$\alpha : \beta$ ratio
1	 Glu <sub>1</sub> -I	Toluene, RT 1.5 eq. of 2	 8 <sup><math>\alpha</math></sup> -I + 8 <sup><math>\beta</math></sup> -I	$\sim 3.5 : 1$
2	 Glu <sub>1</sub> -Br	Toluene, RT 1.5 eq. of 2	 8 <sup><math>\alpha</math></sup> -Br + 8 <sup><math>\beta</math></sup> -Br	$\sim 3.5 : 1$
3	 Gal <sub>1</sub> -I	Toluene, RT 1.5 eq. of 2	 9 <sup><math>\alpha</math></sup> -I	Only $\alpha$
4	 Gal <sub>1</sub> -Br	Toluene, RT 1.5 eq. of 2	 9 <sup><math>\alpha</math></sup> -Br	Only $\alpha$

5	 Glu <sub>1</sub> -I	Acetone, RT 1.5 eq. of 2	 8 <sup>α</sup> -I + 8 <sup>β</sup> -I
6	 Glu <sub>1</sub> -SePh	Toluene, RT 1.5 eq. of 2	No Product observed
7	 Gal <sub>1</sub> -Br	Toluene, RT 1.5 eq. of 2 0.1 eq. of TEMPO	No Product observed
8	 Gal <sub>1</sub> -Br	Toluene, RT 1.5 eq. of 2 0.1 eq. of TEMPO	No Product observed

First, the effect of the nature of the halide was evaluated either for glucosyl or galactosyl derivatives (**Entries 1-4**). As predictable, bromides reacted slower than iodides, as observable by the slower change in the color of the reaction mixture, although no differences in the composition of the reaction mixture were observed. Indeed, the spectra of crude **8-X** (X = I, Br, **Figure 4.2**) revealed the presence of two species with distinct glucose patterns, while only one species was observed in the crude of **9-X** (X = Br, I), as well as in the mother liquors. Either the product **9-X** (X = Br, I) or the major species of **8-X** were identified as the retention product ( $\alpha$  anomer). The spectra of the compounds (**9-I** is reported in **Figure 4.2**) displayed a set of coupling constants attributed to a  $^1C_4$  conformation of the hexopyranose ring, indicating that a chair inversion occurred, and the metal was in equatorial position. For instance, the  $^3J_{H2-H3}$  value of 3.5 Hz in **9-I** demonstrated

that the relative position of these two protons is not *trans-diaxial* as in the  ${}^4C_1$  chair of the starting galactosyl halides, where  ${}^3J_{H2-H3}$  is 10.6 Hz.

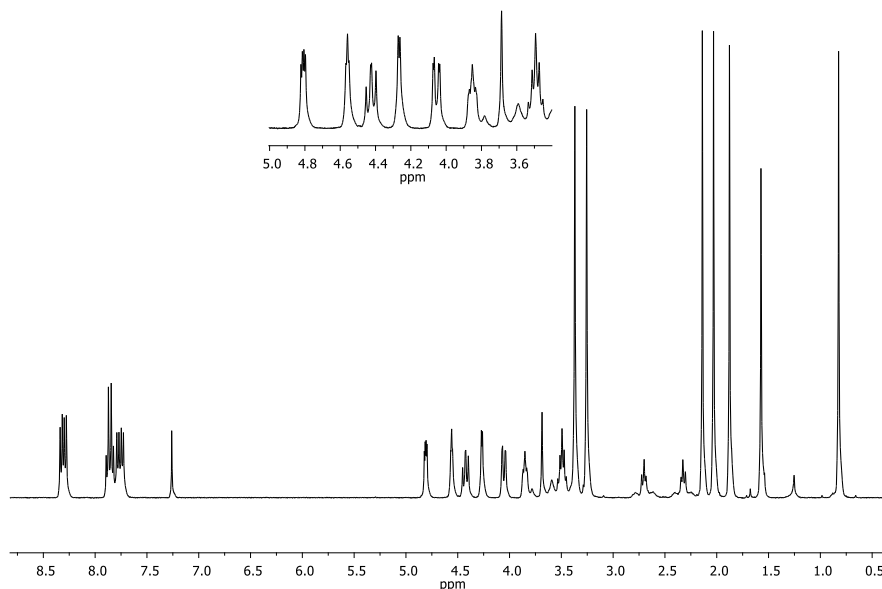


**Figure 4.2.**  ${}^1H$  NMR spectrum of **9-I** in  $CDCl_3$  at 400 MHz.

By multiple crystallization of the reaction mixture of **8-X** the two pure products were isolated. A first crystallization from DCM with diethyl ether of **8-I** led to the isolation of the pure complex, already reported as the  $\alpha$  anomer, **8 $^{\alpha}$ -I**. Subsequent recrystallization of the mother liquors led to the isolation of few milligrams of the second species. Both the compounds were characterized by  ${}^1H$  NMR (**Figure 4.3**) which showed the high-field shifts of the non-equivalent olefin protons ( $\delta$  2-3 ppm), due to the high  $\pi$ -backdonation from the platinum centre, typical of *tbp* Pt(II) complexes. Such effect was also noted in  ${}^{13}C$  NMR spectra, where the ethene

carbons signals are found at  $\delta$  values significantly lower than free ethene. In both  $^1\text{H}$  and  $^{13}\text{C}$  NMR spectra,  $^{195}\text{Pt}$  satellites were also clearly identifiable.

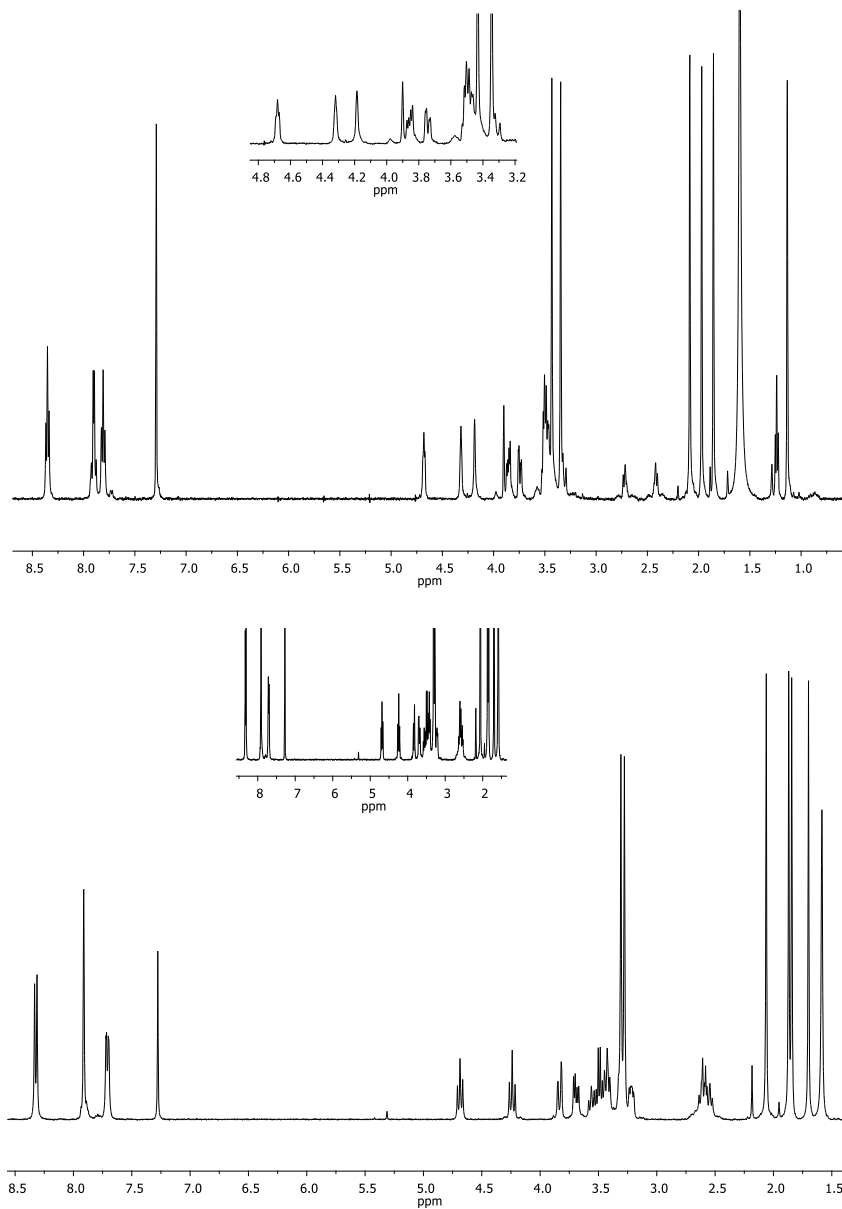


**Figure 4.3.**  $^1\text{H}$  NMR spectra of  $8^\alpha\text{-I}$  (top)  $8^\beta\text{-I}$  (bottom) in  $\text{CDCl}_3$  at 400 MHz.

Interestingly, the typical  ${}^4C_1$  arrangement was preserved in the minor species that was identified as the  $\beta$  anomer, **8 $\beta$ -I**, deriving from the inversion of configuration at the anomeric position. The  $\alpha$  :  $\beta$  ratio was found to be independent from the nature of the halogen used in the synthesis (Entries 1-4, **Table 4.1**). These results indicated that the reaction proceeded differently when **Gal $_1$ -X** or **Glu $_1$ -X** were used, since in the former case only retention and chair inversion were observed, while in the latter one both retention and inversion occurred.

The influence of the solvent on the reaction outcomes was evaluated, switching from toluene to acetone. **Glu $_1$ -I** was reacted with (**i**) yielding a mixture of the two anomers (Entry 5 vs 1) with a little difference in the  $\alpha$ : $\beta$  ratio. Indeed, the more polar solvent seemed to favour the  $\alpha$  isomer **8 $\alpha$ -I**, with a ratio  $\sim$ 5:1 with respect to the  $\sim$ 3.5:1 observed in toluene.

To evaluate the effect of the initial configuration of the glycosyl halide ( $\alpha$  vs  $\beta$ ) the oxidative addition was performed using the chalcogenide **Glu $^\beta_1$ -SePh** (entry 6). Indeed,  $\beta$ -glycosyl halides are not isolable, and by literature studies, **Glu $^\beta_1$ -SePh** was found to be used as glycosyl donor in oligosaccharides synthesis, similarly to glycosyl halides.<sup>173</sup> However, no reaction was observed, probably due to a low reactivity of the glycosyl precursor.

. In principle, it is possible to hypothesize four different reaction mechanisms herein briefly discussed:

- $S_N2$ -like attack of Pt ( $d_{z^2}$ ) on RBr (**Figure 4.4**) and subsequent rebound of bromide would result in inversion at C1. This path can be excluded for galactose where only retention product is observed, while it can occur to produce **8 $\beta$ -X**.

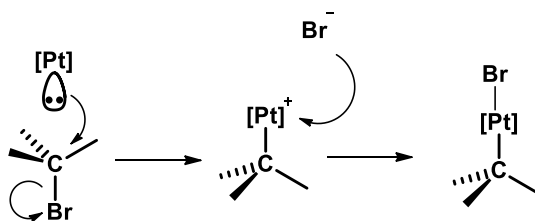


**Figure 4.4.** S<sub>N</sub>2-like attack mechanism

- Side-on concerted oxidative addition (**Figure 4.5**) would result in retention, but in this case, it would suffer from extreme steric crowding. Indeed, this path is actually accessible only for primary alkyl halides, and then ruled out for this system.

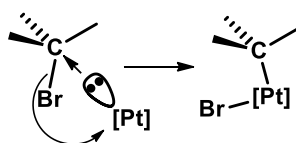


**Figure 4.5.** Side-on concerted mechanism

- Single electron transfer SET from Pt(0) to the anomeric carbon to form a radical anionic species, that undergo the cleavage of C-Br bond. Subsequent recombination between (R•)<sup>-</sup> and (Pt•)<sup>+</sup>, followed by the addition of the bromide (**Figure 4.6**) would result in the formation of the product. The stereoselectivity would be fixed at the **R-Pt** recombination stage, or it is possibly related to a <sup>4</sup>C<sub>1</sub>-<sup>1</sup>C<sub>4</sub> equilibrium of R• before coupling to (Pt•)<sup>+</sup>. This mechanism could be intercepted through the addition of a stoichiometric amount of a radical trap.<sup>[11]</sup>

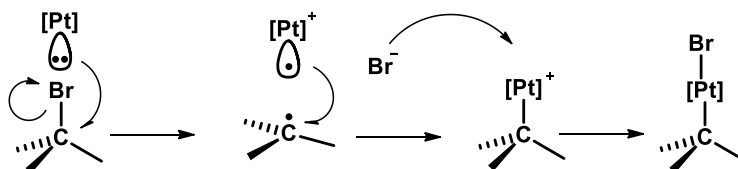




**Figure 4.6.** SET mechanism

- Radical chain mechanism (**Figure 4.7**). As for the SET, the stereochemistry would be fixed in the coupling stage between  $R^\bullet$  to Pt, or in a  $^4C_1$ - $^1C_4$  equilibrium of  $R^\bullet$ , preceding that step. In the radical chain mechanism, a radical trap could interfere even in sub-stoichiometric amounts.

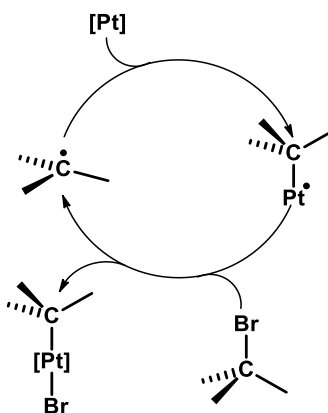


**Figure 4.7.** Radical chain mechanisms

By previous studies reported in literature, the radical mechanisms have frequently been invoked for the oxidative addition of glycosyl halides to organometallic substrates.<sup>174–177</sup> Therefore, the reactions between **(i)** and both **Glu<sub>1</sub>-Br** and **Gal<sub>1</sub>-Br** were performed in the presence of a catalytic amount of TEMPO ((2,2,6,6-tetramethylpiperidin-1-yl)oxyl), known to act as radical trap (Entries 7-8, **Table 4.1**). The presence of 10 mol% of TEMPO (with respect to the glycosyl halide) totally inhibited the formation of both the products **8-Br** and **9-Br**, supporting the occurrence of a radical chain mechanism in the oxidative addition. To support these experimental data, pointing toward a radical mechanism, some theoretical investigations were performed.

#### 4.2.2 Preliminary computational investigation

Preliminary density functional calculations were carried out to support in interpreting the experimental results. Calculations were performed for peracetylated glucose and galactose derivatives. First,  ${}^4\text{C}_1$  and  ${}^1\text{C}_4$  conformations for the pyranosyl radicals derived from Br abstraction were optimized. Results indicated the  ${}^4\text{C}_1$  conformations to be preferred, by only  $\sim 1.1$  kcal/mol for both glucose and galactose. These values correlated to the experimentally observed product distributions, although they did not explain observed differences between glucose and galactose. However, the possibility to get a definitive conclusion was prevented by the large number of potentially accessible conformations of the glycosyl fragment. It is possible to affirm that limiting  ${}^4\text{C}_1$ - ${}^1\text{C}_4$  interconversion at the RBr or R• stage differentiates between stereochemical outcomes.

Moreover, dissociation curves were calculated for breaking the C1-Pt bond considering R-Pt• in  $\alpha/{}^1\text{C}_4$  and  $\beta/{}^4\text{C}_1$  forms. Starting geometries were constructed from the X-ray structures of the glucose derivatives **8 $\alpha$ -I** and **8 $\beta$ -I**, described in the next section. These curves represent the reverse of R-Pt coupling stage, and it seemed possible that the barriers for Pt-C coupling would differ depending on the nature of the sugar fragment. However, all curves showed smooth and monotonous energy increase to the dissociation limit, apparently without any transition state, suggesting that attack of R• on the intact Pt reactant was barrierless, thus, not providing any clue to the observed stereoselectivity.

Although computational data are not conclusive in identifying the mechanism of the oxidative addition, it is intriguing that the reaction outcome may depend on several aspects. First, the structure of the pyranose should be considered. In glycosylation reactions proceeding through a standard ionic mechanism (usually

involving the generation of an intermediate glycosyl cation), it is known that the presence of ester groups placed at position 4 (or 6) in galactose building blocks, strongly favours the generation of  $\alpha$  glycoside, due to a remote participation effect. It has indeed been demonstrated that the carbonyl oxygen of the ester group forms a covalent bond with the intermediate cation at the anomeric carbon, resulting in preferential  $\alpha$  glycosylation (**Figure 4.8**).<sup>178</sup>

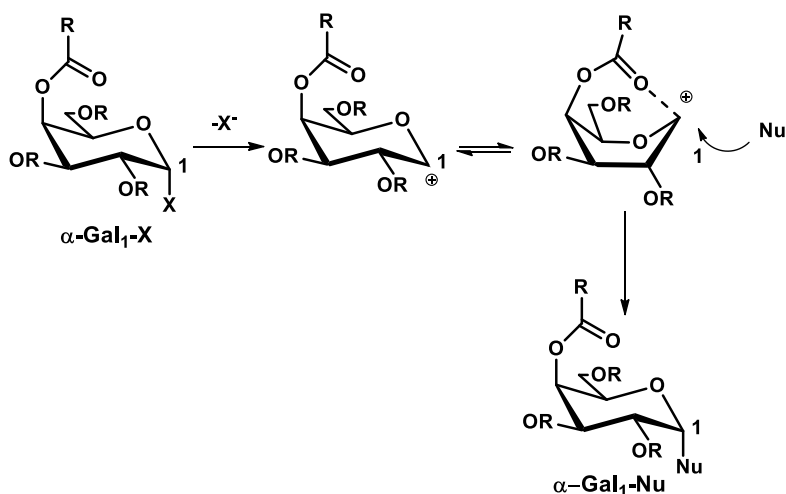


**Figure 4.8.** Remote participation of ester group at C4 in galactose glycosylation

In this view, it cannot be ruled out that a similar effect could work for a radical mechanism, involving the occurrence of noncovalent interaction between the putative anomeric radical and non-bonding electrons at the acetyl oxygen. However, such hypothesis is not easy to prove. The elucidation of these aspects would require a further study with the comparison of the reactivity of different sugars that should be properly synthesized, also with different protecting groups installed at the hypothetically involved positions. Therefore, a deep investigation

of this intriguing sugar-dependent stereochemistry will be the topic of follow-up studies.

#### 4.2.3 X-ray crystallographic structures of **8 $\alpha$ -I** and **8 $\beta$ -I**

Single crystals of both **8 $\alpha$ -I** and **8 $\beta$ -I** were obtained by slow diffusion of diethyl ether in DCM solutions, and their structure determination confirmed the  $^1C_4$  arrangement of **8 $\alpha$ -I** (**Figure 4.9**) and the  $^4C_1$  arrangement of **8 $\beta$ -I** (**Figure 4.10**)

**8 $\alpha$ -I** and **8 $\beta$ -I** crystallize in the  $P2_1$  and  $P2_12_12_1$  space group respectively, with one molecule contained in the asymmetric unit. In both compounds the platinum ion adopts a trigonal bipyramidal geometry with the *dmphen* and ethene ligands in the equatorial plane. The axial positions are occupied by the iodine atom and the C1 atom of the glucosyl group. In both the compounds platinum is in the more favourable equatorial position of the glucosyl chair. In **8 $\alpha$ -I** all the acetyl groups on the pyranose ring are in the axial positions according to the  $^1C_4$  arrangement and the sugar mean plane is almost orthogonal to the coordination plane (**Figure 4.9**).

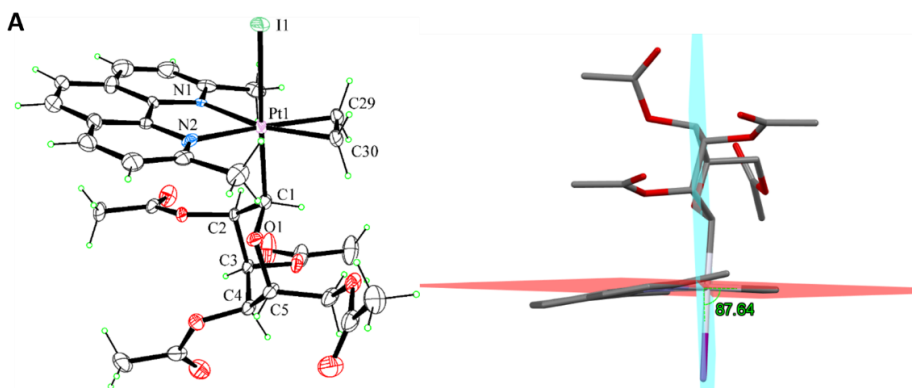


**Figure 4.9.** (Left) ORTEP view of **8 $\alpha$ -I** with thermal ellipsoids drawn at 30% probability level. Only the major part of the disordered ligands is drawn for clarity. Selected bond distances and angles: Pt1–I1 = 2.7551(6), Pt1–N1 = 2.26(2), Pt1–N2 = 2.11(3), Pt1–C1 = 2.060(7), Pt1–C29 = 2.078(19), Pt1–C30 = 2.046(16) Å; I1–Pt1–C1 = 175.0(2), N1 Pt1 I1

= 88.8(6) N2 Pt1 I1 = 86.6(8), C29 Pt1 I1 = 90.2(5), C30 Pt1 I1 = 90.1(5)°. **(Right)** View of **8<sup>a</sup>-I** down the edge of coordination plane. The angle between the sucrose mean plane C1/C2/C3/C4/C5/O1 (cyan) and the coordination mean plane N1/N2/Pt1/C29/C30 (red) is shown.

In **8<sup>b</sup>-I** all the substituents are in the equatorial positions according with in the <sup>4</sup>C<sub>1</sub> arrangement. The glucosyl group assumes an overall flat shape that allows a significant inclination of the sugar mean plane with respect to the coordination plane **(Figure 4.10)**.

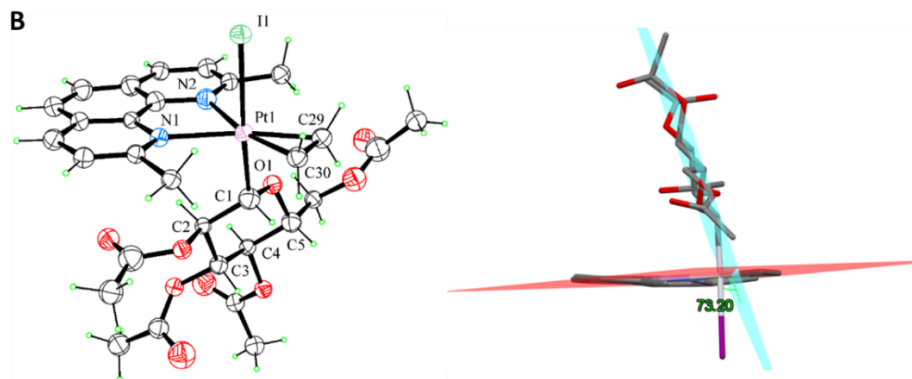


**Figure 4.10. (Left)** ORTEP view of **8<sup>b</sup>-I** with thermal ellipsoids drawn at 30% probability level. Selected bond distances: Pt1-I1 = 2.761(4), Pt1-N1 = 2.23(4), Pt1-N2 = 2.19(4), Pt1-C1 = 2.04(5), Pt1-C29 = 2.06(5) Pt1-C30 = 2.00(5) Å; I1-Pt1-C1 = 175.7(15), N1 Pt1 I1 = 87.1(9), N2 Pt1 I1 = 87.7(12), C29 Pt1 I1 = 93.1(14), C30 Pt1 I1 = 90.2(15)°. **(Right)** View of **8<sup>b</sup>-I** down the edge of the coordination plane. The angle between the coordination mean plane N1/N2/Pt1/C29/C30 (red) and the sucrose mean plane C1/C2/C3/C4/C5/O1 (cyan) is shown

Crystal and structural refinements for both the structures are reported in Appendix **(Table A1)**.

#### 4.2.4 Biological studies

The cytotoxic effect of the compounds belonging to the classes **8-X**, **9-X**, **11-X** (X = Cl, Br, I), and of the deprotected complex **10-I**, was evaluated on a couple of cell lines, the immortalized murine fibroblast BALB/c-3T3 and tumoral SVT2 (BALB/c-3T3 transformed with SV40 virus). Cells were incubated for 48 h with increasing concentrations of the compounds, and then, the cell viability was measured by MTT assay. IC<sub>50</sub> values are reported in **Table 4.1**.

**Table 4.1.** IC<sub>50</sub> values (μM) obtained for **8-X**, **9-X**, **11-X** (X = Cl, Br, I), and **10-I** after 48 h incubation. Selectivity Index (SI), indicated by the ratio between the IC<sub>50</sub> of immortalized cells and cancer cells.

Complex	IC <sub>50</sub> (μM)		SI
	BALB/c3T3	SVT2	
<b>8-Cl</b>	4.5 ± 0.5	3.2 ± 0.5	1.4
<b>8-Br</b>	4.1 ± 0.1	4.3 ± 0.1	0.95
<b>8<sup>α</sup>-I</b>	1.3 ± 0.6	1.7 ± 0.2	0.76
<b>8<sup>β</sup>-I</b>	6.7 ± 0.4	4.4 ± 0.6	1.5
<b>9-Cl</b>	19.4 ± 0.3	4.9 ± 0.3	3.9
<b>9-Br</b>	26 ± 2	6.3 ± 0.4	4.1
<b>9-I</b>	21 ± 1	4.5 ± 0.3	4.7
<b>10-I</b>	3.7 ± 0.4	3.1 ± 0.15	1.2
<b>11-Cl</b>	2.72 ± 0.07	0.89 ± 0.07	3.1
<b>11-Br</b>	2.7 ± 0.3	1.03 ± 0.01	2.6
<b>11-I</b>	4.41 ± 0.07	0.98 ± 0.14	4.5
<b>Cisplatin</b>	239 ± 14	193 ± 2	1.2

Results showed that the C1-galactosyl subclass **9-X** were more toxic towards the cancer cell line than towards the immortalized ones, displaying the highest values of SI. Similarly, **11-X** where the galactose is linked through C6 was selective, while no selectivity was observed with glucosylated **8-X** compounds deprotected galactose compound **10-I**. Noteworthy, **8<sup>β</sup>-I** and **8<sup>α</sup>-I** showed similar activity and selectivity. Such observations confirmed that the sugar fragment has an active role in the cytotoxic activity of the complex.

The change of the halogen ligand did not influence the cytotoxicity of the complexes, all found to be more active than cisplatin.

Investigations on the mechanism of action were then performed. The involvement of the transporter GLUT1 in **9-I** cytotoxic activity was studied, by using quercetin as GLUT inhibitor. Therefore, both cell lines were exposed to different concentrations of **9-I** in the presence or absence of quercetin for 48 h. No difference in cell viability was observed on immortalized fibroblasts, while a decrease in the activity of **9-I** was detected on cancer cells, when incubated in the presence of quercetin. This result suggests the involvement of glucose transporter in **9-I** endocytosis.

The measurement of LDH and of pro-caspase-3 level was performed to understand which cell death pattern was activated. No release of LDH was observed at any concentration analyzed, whereas the activation of pro-caspase-3 was detected only in cancer cells, suggested the occurrence of an apoptotic pathway.

## 4.3 Experimental Part

### 4.3.1 General

All reagents and solvents were purchased from Sigma-Aldrich and were used without further purification. Murine BALB/c-3T3 and SVT2 fibroblasts were obtained from ATCC and cultured in Dulbecco's modified Eagle's medium (DMEM) (Sigma-Aldrich, St Louis, MO, USA), supplemented with 10% foetal bovine serum (HyClone), 2 mM L-glutamine and antibiotics, all from Sigma-Aldrich, under a 5% CO<sub>2</sub> humidified atmosphere at 37 °C. NMR spectra were recorded in CDCl<sub>3</sub> (CHCl<sub>3</sub>,  $\delta$  7.26, as internal standard), using a 400 Bruker Avance Ultrashield 400. The following abbreviations were used for describing NMR multiplicities: s, singlet; d, doublet; dd, double doublet; t, triplet; m, multiplet. [Pt(1,5-cyclooctadiene)<sub>2</sub>]<sup>171</sup> and the sugar precursors<sup>179–181</sup> were synthesized following literature procedures. NMR characterization of pure **8-X** (X = Cl, Br), **9-X** (X = Cl, Br, I), **10-I** and **11-X** (X = Cl, Br, I) are reported in ref 161.

### 4.3.2 Oxidative addition of **Glu<sub>1</sub>-X** and **Gal<sub>1</sub>-X** (X = Br, I) to [Pt(dmphen)ethene]

[Pt(1,5-cyclooctadiene)<sub>2</sub>] (0.104 g, 0.241 mmol) was suspended in 2 mL of dry toluene under an ethene atmosphere at 0 °C. After 15 minutes, anhydrous 2,9-dimethyl-1,10-phenanthroline (0.052 g, 0.241 mmol) was added to the clear yellow solution, resulting in a red suspension containing [Pt(dmphen)(ethene)]. The suspension was allowed to warm at room temperature, and then the solvent was carefully removed with a pipette Pasteur. The red product was washed with toluene (1 mL) and quickly dried. A solution of the appropriate glycosyl halide



(0.360 mmol) in 2.5 mL of dry toluene or acetone (entry 5 in Table 4.1) was then added to the red solid. After 16 hours of stirring at room temperature, hexane was added to the resulting yellow-orange suspension, and the crude product was filtered and washed twice with hexane. Yield: > 90%. Crude materials were analyzed by NMR without further manipulations. In the case of **8-I**, a work-up process was performed. The crude was dissolved in DCM and the resulting brown solution was filtered through Celite to remove metal impurities. The resulting yellow solution was then sequentially crystallized by adding diethyl ether.

**8<sup>α</sup>-I** : <sup>1</sup>H NMR (400 MHz, CDCl<sub>3</sub>) δ .33 (d, 1H), 8.31 (d, 1H), 7.87 (dABq, 2H), 7.79 (d, 1H), 7.77 (d, 1H), 4.65 (dd, 1H, <sup>3</sup>J<sub>H3-H4</sub> = 4.4 Hz, <sup>3</sup>J<sub>H4-H5</sub> = 6.5 Hz, H4-glu), 4.29 (dd, 1H, <sup>3</sup>J<sub>H2-H3</sub> = 3.5 Hz, H3-glu), 4.15 (d, H, 1H, H2-glu), 3.87 (s, 1H, <sup>2</sup>J<sub>Pt-H</sub> = 76 Hz, H1-glu), 3.83 (dd, 1H, <sup>3</sup>J<sub>H5-H6</sub> = 5.9 Hz, <sup>3</sup>J<sub>H6-H6'</sub> = 12.0 Hz, H6-glu), 3.71 (dd, 1H, <sup>3</sup>J<sub>H5-H6</sub> = 3.9 Hz, H6'-glu), 3.49 (app d, C<sub>2</sub>H<sub>4</sub>, <sup>2</sup>J<sub>Pt-H</sub> = 76 Hz, 2H), 3.43 (m, H5, 1H), 3.40 (s, *Me*-dmphen, 3H), 3.31 (s, *Me*-dmphen, 3H), 2.69 (m, C<sub>2</sub>H<sub>4</sub>, <sup>2</sup>J<sub>Pt-H</sub> = 71 Hz, 1H), 2.39 (m, C<sub>2</sub>H<sub>4</sub>, <sup>2</sup>J<sub>Pt-H</sub> = 64 Hz, 1H), 2.05 (s, Me, 3H), 1.94 (s, Me, 3H), 1.82 (s, Me, 3H), 1.10 (s, Me, 3H). <sup>13</sup>C NMR (100 MHz, 298 K, CDCl<sub>3</sub>): δ 170.6, 169.3, 168.9, 168.8, 162-125 (aromatics), 74.2, 71.4, 70.5, 68.2, 61.9, 53.4 (<sup>1</sup>J<sub>Pt-C</sub> = 859 Hz), 31.2 (<sup>1</sup>J<sub>Pt-C</sub> = 364 Hz), 30.8 (<sup>1</sup>J<sub>Pt-C</sub> = 366 Hz), 29.3, 29.1, 20.8 (×2), 20.7, 20.0. Anal. Calcd (found): (C<sub>30</sub>H<sub>35</sub>IN<sub>2</sub>O<sub>9</sub>Pt): C, 40.50 (40.34); H, 3.97 (3.86); N, 3.15 (3.09).

**8<sup>β</sup>-I**: <sup>1</sup>H NMR (400 MHz, CDCl<sub>3</sub>): δ d): 8.30 (d, 2H), 7.90 (s, 2H), 7.68 (dd, 2H), 4.67 (t, 1H, <sup>2</sup>J<sub>H2-H3</sub> = <sup>2</sup>J<sub>H3-H4</sub> = 9.0 Hz, H3-glu), 4.22 (t, 1H, <sup>2</sup>J<sub>H4-H5</sub> = 9.8 Hz, H4-glu), 3.81 (d, 1H, <sup>2</sup>J<sub>H6-H6'</sub> = 12.0 Hz, H6-glu), 3.67 (dd, 1H, <sup>2</sup>J<sub>H5-H6'</sub> = 5.7 Hz, H6'-glu), 3.54 (m, 1H, ethene), 3.41 (m, 2H, ethene and H2-glu), 3.29 (s, 3H, *Me*-dmphen), 3.26 (s, 3H, *Me*-dmphen), 3.21 (m, 1H, H5-glu), 2.58 (m, 3H, ethene and H1-glu), 2.05 (s, 3H, OAc), 1.85 (s, 3H, OAc), 1.83 (s, 3H, OAc), 1.68 (s, 3H, OAc). <sup>13</sup>C-NMR data (CDCl<sub>3</sub>, ): 170.48, 170.27, 169.48, 168.84, 162.38, 161.54, 145.00,

144.81, 137.85, 137.38, 128.82, 128.39, 126.27, 126.06, 125.62(2C), 74.79, 72.75, 68.18, 64.93, 62.75, 31.20, 29.77, 29.07, 28.99, 21.23, 20.78, 20.51, 20.42.

#### *4.3.3 Oxidative additions of 2-glu-Br or 2-gal-Br to [Pt(dmphen)(ethene)] with TEMPO*

Pt(1,5-cyclooctadiene)<sub>2</sub>] (0.52 g, 0.12 mmol) was suspended in 1 mL of dry toluene under an ethene atmosphere at 0 °C. After 15 minutes, anhydrous 2,9-dimethyl-1,10-phenanthroline (0.026 g, 0.12 mmol) was added to the clear yellow solution, resulting in a red suspension containing [Pt(dmphen)(ethene)]. The suspension was allowed to warm at room temperature, and then the solvent was carefully removed with a pipette Pasteur. The red product was washed with toluene (1 mL) and quickly dried. The appropriate glycosyl bromide (0.074 g, 0.18 mmol) and TEMPO (2.8 mg, 0.018 mmol) were dissolved in 1 mL of dry toluene and the resulting solution was added to the red solid. After 16 hours of stirring hexane was added to the red-brown suspension and the precipitate was filtered and washed twice with hexane. The NMR spectra of the solids did not show appreciable signals of five-coordinate complexes, but mainly signals due to extensive decomposition.

#### *4.3.4 X-ray crystallography*

X-ray crystallographic analysis were performed in collaboration with Prof. Angela Tuzi from the University of Naples Federico II.

Data were measured in flowing N<sub>2</sub> at 173 K using a Bruker-Nonius KappaCCD four-circle diffractometer equipped with a Oxford Cryostream apparatus (graphite

monochromated radiation  $\text{MoK}\alpha = 0.71073 \text{ \AA}$ ). Reduction of data and semiempirical absorption correction were done using the SADABS program.<sup>182</sup> Both structures were solved by direct methods (SIR97 program)<sup>183</sup> and refined by the full-matrix least-squares method on  $F^2$  using the SHELXL-2018/3 program with the aid of the program WinGX.<sup>184</sup> Anisotropic parameters were used for non-H atoms. Ethene hydrogen atoms were located in difference Fourier maps in- **8 $\alpha$ -I** and refined as riding model with isotropic thermic parameter  $U_{\text{iso}}(\text{H})$  equal to  $1.2 \cdot U_{\text{eq}}$  of the carrier atom. All the other H atoms were generated stereochemically and refined accordingly to the riding model with C–H distances in the range 0.93–0.98 Å and  $U_{\text{iso}}(\text{H})$  equal to  $1.2 \cdot U_{\text{eq}}$  of the carrier atom ( $1.5 \cdot U_{\text{eq}}$  for  $\text{C}_{\text{methyl}}$ ). In **8 $\alpha$ -I** the ligands were splitted in two positions with refined occupancy factors 0.52 and 0.48 (Figure S9). For **8 $\beta$ -I** only a few poor-quality single crystals were obtained, containing disordered lattice solvent that could not be modeled. The PLATON SQUEEZE procedure was used to exclude the contribution of solvent to the structure. Some constraints on displacement parameters were introduced in the last stage of refinement to obtain reasonable values. The figures were generated using ORTEP-3<sup>185</sup> and Mercury CSD 3.9.<sup>186</sup> Crystallographic data for **8 $\alpha$ -I** and **8 $\beta$ -I** were deposited in the Cambridge Crystallographic Data Centre with deposition number CCDC 2045989 and 2045990. These data can be obtained free of charge from [www.ccdc.cam.ac.uk/data\\_request/cif](http://www.ccdc.cam.ac.uk/data_request/cif).

#### 4.3.5 DFT-Calculations.

DFT calculations were performed in collaboration with Prof. P.H.M. Budzelaar from the University of Naples Federico II.

Geometries were optimized at the tpssh/def2-SV(P) level (corresponding ECP at Pt) using Turbomole 7.3 coupled to an external optimizer. The purely organic

pyranosyl radicals were also re-optimized at the tpssh/def2-TZVPP level but changes in geometries were small. Frequency analyses were carried out to check the nature of all stationary points (minima: no imaginary frequencies). Improved single-point energies were evaluated at the PCM(toluene)/M06 +DFTD3/cc-pVTZ level using Gaussian-16. These energies were combined with thermal corrections from the frequency calculations mentioned above to arrive at final free energies.

#### *4.3.6 Evaluation of the biological activity*

Cell culture and experiments involving cytotoxicity assays, LDH release, and measurement of pro-caspase-3 were performed in collaboration with Prof. Daria M. Monti research group at University of Naples Federico II

##### *4.3.6.1 Cytotoxicity Experiments*

For dose-response experiments, cells were seeded in 96-well plates at a density of  $2.5 \times 10^3$  cells per well. 24 h after seeding, increasing concentrations of compounds were added to the cells. Cell viability was assessed by the MTT (3-(4,5-dimethylthiazol-2-yl)-2,5-diphenyltetrazolium bromide) assay after 48 h. For GLUT inhibitor mediated cytotoxicity assay, 24 h after seeding, cells were treated with **9-I** in the presence or absence of 3  $\mu$ M quercetin. Quercetin alone was used as a control. After 48 h incubation, the MTT assay was performed as reported in literature.<sup>158</sup> Cell survival was expressed as the percentage of viable cells in the presence of the compound under test compared to controls. Two groups of cells were used as controls, i.e. untreated cells and cells supplemented with identical volumes of DMSO. Each sample was tested in three independent analyses, each carried out in triplicate.

#### *4.3.6.2 Analysis of the mechanism of action.*

For western blotting analyses, cells were treated as described above. After 48 h of incubation, cell lysates were analysed by western blot. To normalize protein intensity levels, a specific antibody against internal standards was used, i.e. anti-GAPDH (Thermo Fisher, Rockford, IL, USA) or anti-actin (Sigma-Aldrich). The chemiluminescence detection system (SuperSignal® West Pico) was from Thermo Fisher. The occurrence of necrosis was determined by measuring the release of lactate dehydrogenase (LDH) in the culture medium using the *in vitro* toxicology assay kit LDH based (Sigma-Aldrich).

## 5 Pt(II) versus Pt(IV) in NHC glycoconjugates complexes

### 5.1 General overview

Trigonal bipyramidal complexes described in Chapters 2 and 4 (**Figure 5.1**) revealed to be promising anticancer agents displaying interesting biological properties.

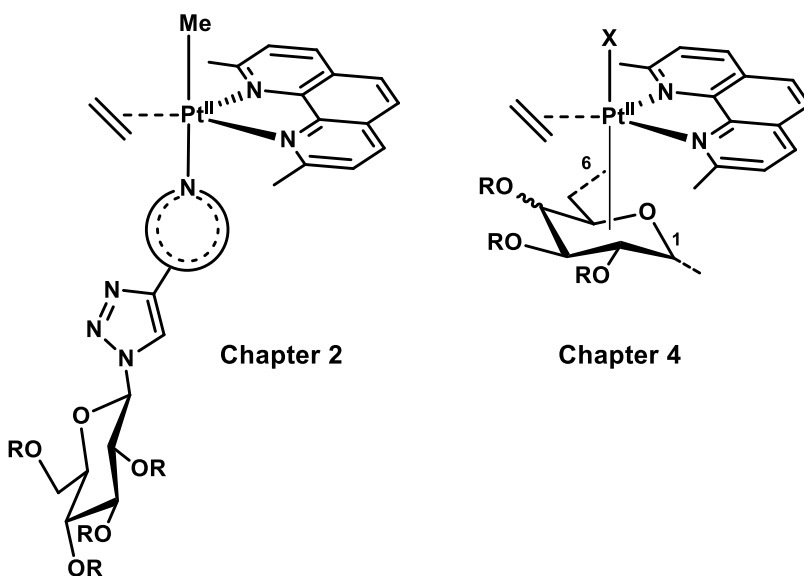


**Figure 5.1.** *tbp* Pt(II) complexes described in the other chapters of this work

Indeed, cationic *tbp* methyl-platinum compounds having neutral *N*-based ligands (Chapter 2) were found to be by far more active than cisplatin with IC<sub>50</sub> values in the sub-micromolar range, although the loss of the sugar-based ligand in physiological conditions resulted in scarce selectivity. Similarly, C-glycosylated *tbp* complexes described in Chapter 4 showed to be active and in some case

selective for cancer cells. Aiming to combine beneficial features of both these structures, the first panel of compounds described in this chapter was designed (Figure 5.2).

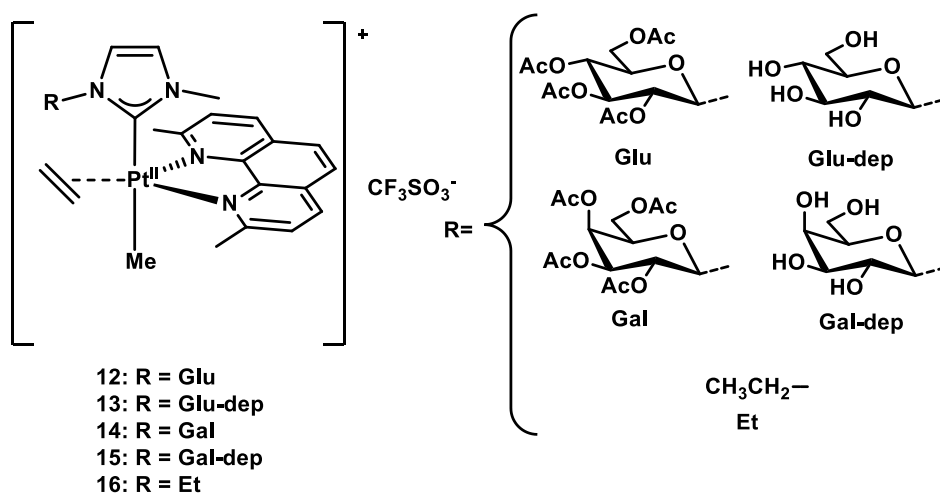


**Figure 5.2.** Structures of Pt(II) *thp* compounds studied in this chapter.

These compounds are Pt(II) *thp* species with *dmphen* and ethene ligands in the equatorial plane. They combine the simultaneous presence of a methyl and a glycoconjugate *N*-heterocyclic carbene (NHC) ligand, that ensure the complex to be cationic species. Methyl imidazole was selected as NHC scaffold and conjugated to different sugar fragments. Glucose and galactose, either in peracetylated or fully deprotected fashions, were selected. Moreover, an ethyl derivative (complex **16**) was designed to disclose the impact of the sugar portion on the properties of the complexes.

NHC ligands are strong  $\sigma$ -donor, as well as  $\pi$ -donor and in minor extent as  $\pi$ -acceptor ligands,<sup>187</sup> that give rise to a plethora of highly stable metal complexes. The wide tuneability of this class of ligands results in the possibility to easily access to several metal complexes, spanning over different type of metals and oxidation states. NHC metal complexes have been intensively explored as

anticancer agents in medicinal chemistry, due to the enhanced robustness in physiological conditions, as well as wide tuneability of the chemical and biological properties, which result in several modes of action.<sup>188</sup> This encouraged to extend the exploration of NHC platinum complexes by preparing the Pt(IV) analogues reported in **Figure 5.3**.

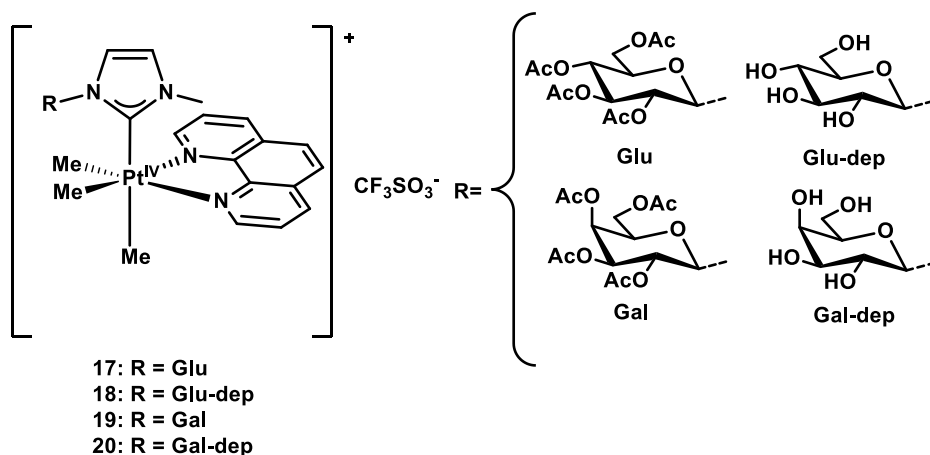


**Figure 5.3.** Structures of Pt(IV) analogues to Pt(II) studied in this chapter.

The compounds display a Pt(IV) center with a phenanthroline ligand (instead of *dmphen*) and two methyl groups delineating the equatorial plane of the octahedron. Another methyl and the glycoconjugate NHC occupy the axial positions. This change in the oxidation state of the metal allowed to make a rather rare homogeneous comparison within the two oxidation states, Pt(II)/Pt(IV).<sup>189–192</sup> In fact, the *tbp* platinum(II) complexes **12-16** and the octahedral platinum(IV) species **17-20** share considerable structural similarities (**Figure 5.4**).



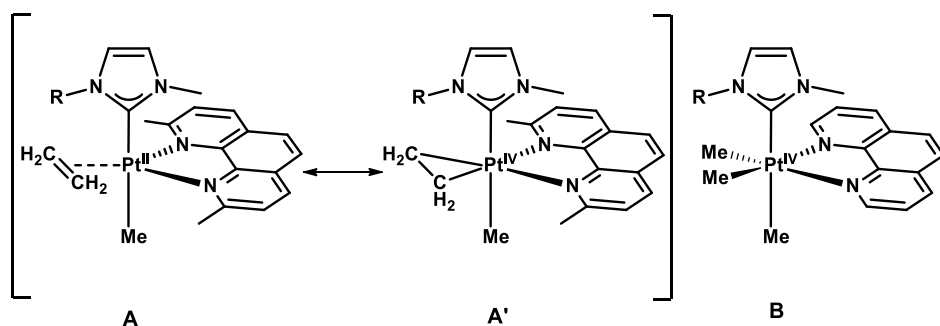


**Figure 5.4.** Structural analogy between *tbp* and octahedral complexes

In the *tbp* complexes, the strong Pt-to-ethene  $\pi$ -backdonation results in a partial  $sp^2 \rightarrow sp^3$  rehybridization of the alkene carbons, and the whole structure can be considered as a hybrid between two limit structures (**Figure 5.4**). This confers to the formal Pt(II) species (**A**) a partial Pt(IV) cyclometallate character (**A'**). In the octahedral complexes (**B**), two methyl groups substitute ethene in the equatorial plane of the structure, rendering the two coordination environments strictly overlapping.

Indeed, it should be underlined that usually the switch to the higher oxidation state involves huge structural variations, passing from square-planar to octahedral geometry. This makes a direct comparison between analogous Pt(II) and Pt(IV) compounds less uniform and more difficult to interpret. Therefore, the availability of species in the two different states of oxidation, but with similar coordination environment, provides the opportunity to evaluate the “true” effect of the oxidation state on the chemical and biological properties of the resulting complexes.

The structural properties, the in-solution reactivity, the anticancer activity, and the reactivity with model biomolecules of complexes **12-20** were studied and compared to delineate parallelisms, analogies as well as differences between the two different oxidation states. This study allowed also to gain insights in the

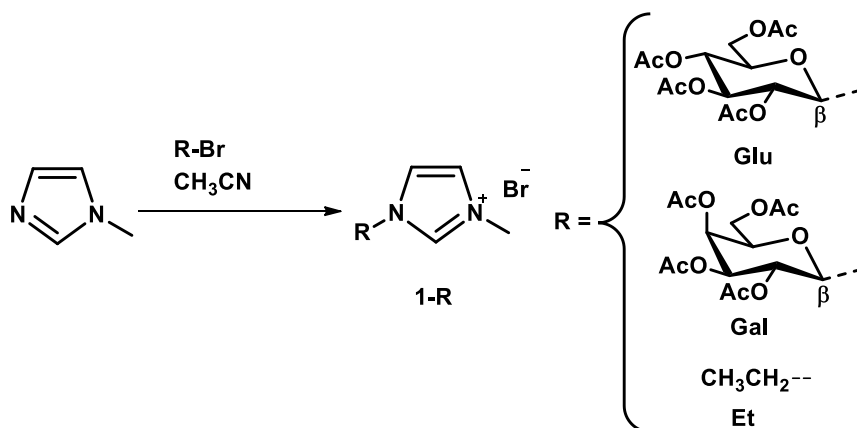
biological behaviour and in the mechanism of action of coordinatively saturated glycoconjugate Pt anticancer agents.

## 5.2 Results and Discussion

### 5.2.1 Synthesis and Structural Characterization of the Complexes

#### 5.2.1.1 Synthesis of the pro-carbene ligands

The glycoconjugate pro-carbene were synthesized following the general procedure reported in **Scheme 5.1**.



**Scheme 5.1.** Synthetic procedure to synthesize the pro-carbene ligands

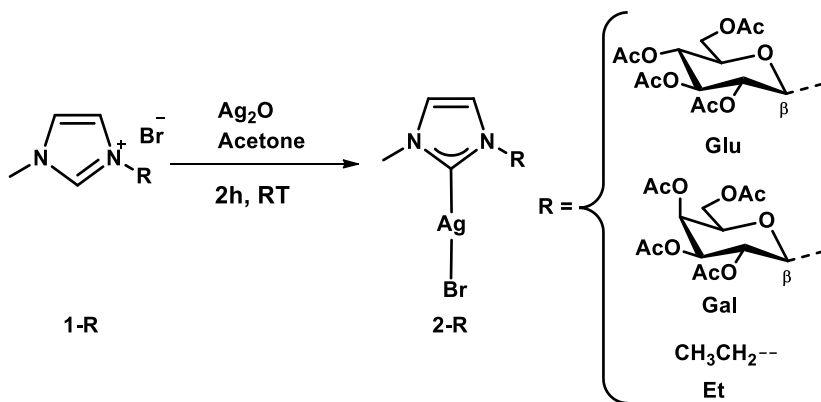
1-bromo- $\alpha$ -D-tetra-*O*-acetylpyranoses (glucose or galactose) were reacted with methylimidazole in acetonitrile, to perform a nucleophilic substitution reaction. Slight differences were observed according to the glucosyl reagent. Indeed, as reported in literature,<sup>193</sup> the glucosyl derivative **1-Glu** was obtained as a white powder by treating the reaction mixture with cold acetone, removing the mother liquor, and drying. The same procedure applied to the galactosyl species was unsuccessful since no precipitation occurred. Attempts to precipitate the product with diethyl ether or hexane led the isolation of crude materials containing several unidentified species, and purification procedures to isolate pure **1-Gal** failed. The

reaction was then performed in  $\text{CD}_3\text{CN}$  and monitored by  $^1\text{H}$  NMR. Unexpectedly, only the desired product **1-Gal** was detected in the first 10 minutes of reaction, while the additional unidentified signals appeared later. The synthesis was then performed by quenching the reaction after 10 minutes by adding diethyl ether. The product precipitated as white solid and it was characterized through  $^1\text{H}$  NMR, COSY and  $^{13}\text{C}$  NMR. Both the proton spectra of the pro-ligands displayed the expected coupling patterns of glucosyl or galactosyl derivatives. The values of  $^3J_{\text{H1-H2}} \sim 9$  Hz typical of a 1,2 *trans*-diaxial coupling were diagnostic of the  $\beta$ -configuration of both **1-Gal** and **1-Glu**, suggesting that the reaction probably occurred through a  $\text{S}_\text{N}2$  mechanism.

The pro-carbene **1-Et** was synthesized by reacting methylimidazole and ethyl bromide in refluxing THF.

#### 5.2.1.2 Synthesis of the Ag-NHC intermediates

Transmetalation via Ag(I) NHC is by far the most used synthetic strategy to access NHC metal complexes. Silver intermediates were prepared according to **Scheme 5.2**.



**Scheme 5.2.** Synthetic scheme to prepare Ag(I) NHC intermediates.

Imidazolinium bromides were reacted with Ag<sub>2</sub>O in acetone for 2 h. The products were quantitatively recovered by removing the solvent under vacuum.

Proton spectra confirmed the positive outcome of the reactions. The complete disappearance of the signal at  $\delta$  10.8 (**Figure 5.5**), attributed to the N-CH-N proton, was diagnostic of the formation of the NHC complex. Elemental analysis confirmed the identity of **2-R** compounds.

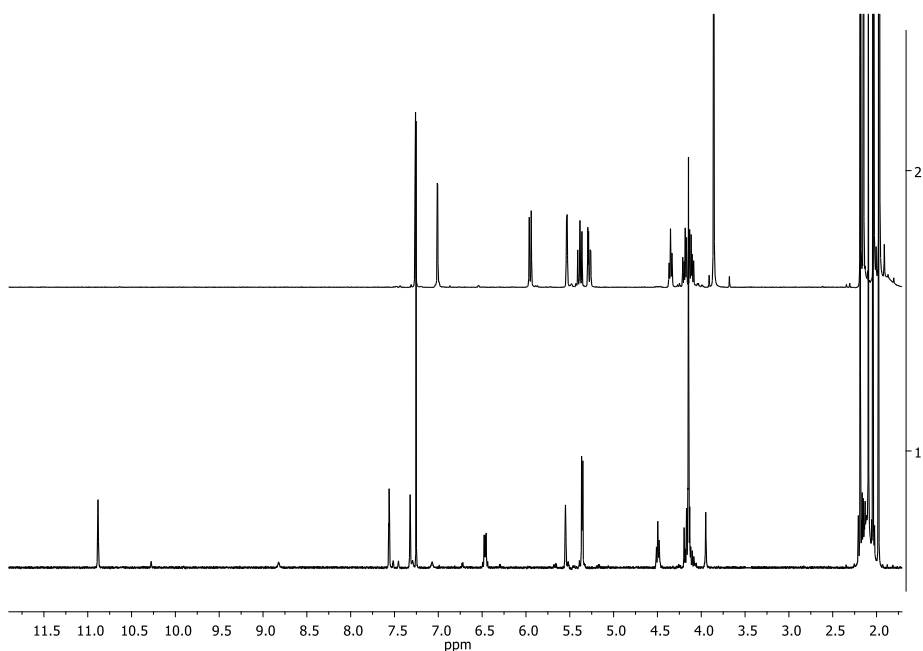
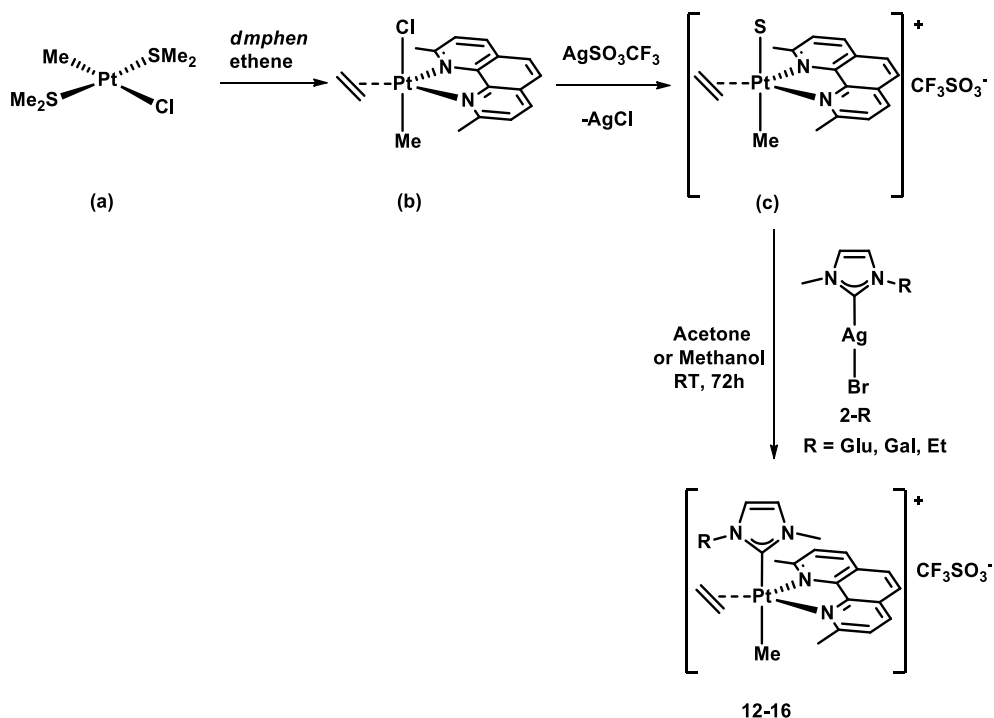


**Figure 5.5.** <sup>1</sup>H NMR spectrum of **1-Gal** (Trace 1) and **2-Gal** (Trace 2) in CDCl<sub>3</sub> at 400 MHz.

### 5.2.1.3 Synthesis of Pt(II) complexes **12-16**

Complexes **12-16** were prepared according to the procedure reported in **Scheme 5.3**.



**Scheme 5.3.** Synthetic procedure to prepare Pt(II) *thp* NHC complexes

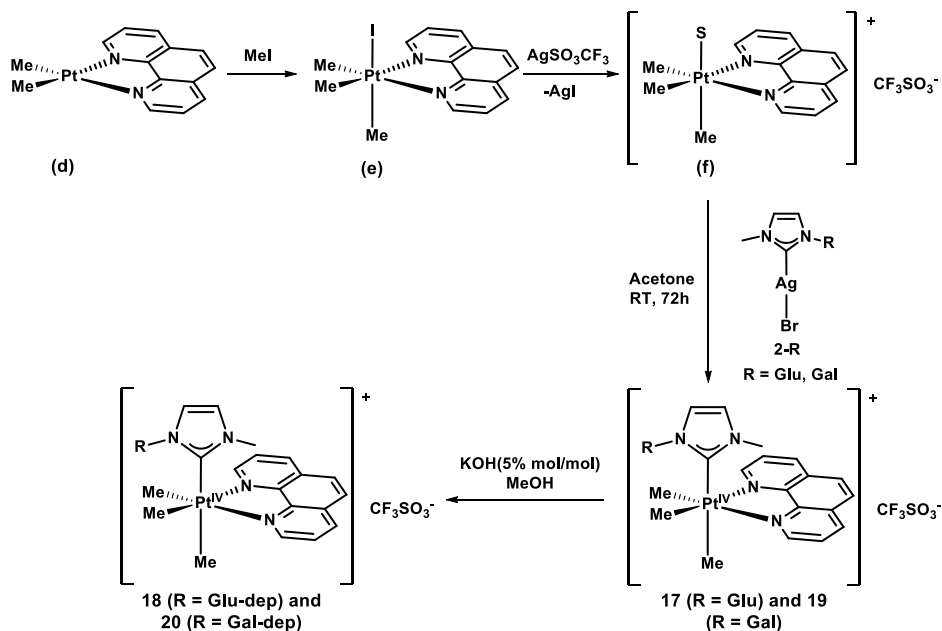
The platinum precursor (**a**) was reacted with *dmphen* and ethene to get the five coordinate *thp* chlorido-compound (**b**). This latter was converted into the cationic intermediate (**c**) by precipitating the  $\text{Cl}^-$  ligand in presence of  $\text{AgCF}_3\text{SO}_3$ . The cationic solvato-species was then reacted for 72h at RT with the appropriate silver carbene **2-R**, to perform a transmetalation which resulted in the formation of the desired products. Interestingly, the outcome of the reaction was solvent dependent. When the peracetylated species **2-R** (R = Glu or Gal) was reacted in

acetone, the peracetylated complexes (**12** or **14**) were isolated. When the same reaction was performed in methanol, the corresponding sugar deprotected complexes (**13** or **15**) were isolated, probably due to a silver-catalyzed transesterification of the acetate groups. The ethyl derivative **16** was prepared following the same procedure in acetone.

All the complexes were recrystallized as white powders from DCM solutions, by adding diethyl ether. Their structure was confirmed through LC/MS–QTOF analysis and NMR spectroscopy (see section 5.2.1.5).

#### 5.2.1.4 Synthesis of Pt(IV) complexes 17-20

The Pt(IV) analogues **17-20** were synthesized following a similar strategy to the one used for the *tbp* complexes and reported in **Scheme 5.4**.



**Scheme 5.4** Synthetic scheme to prepare Pt(IV) complexe **17-20**

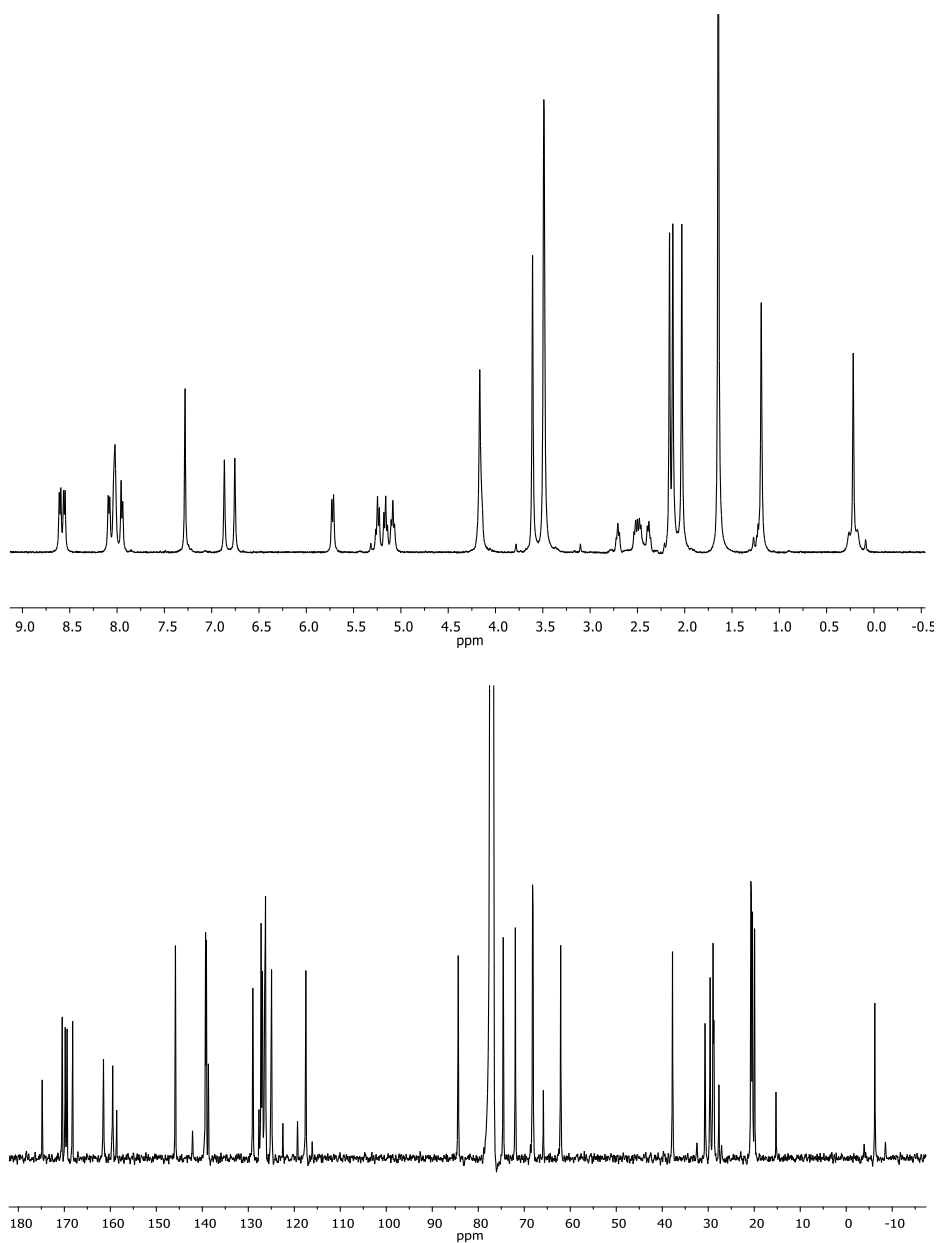
The Pt(II) dimethyl *phenanthroline* compound (**d**) was oxidized with methyl iodide, yielding the intermediate (**e**). The latter one was then ionized with  $\text{AgCF}_3\text{SO}_3$ , and the resulting solvato-species (**f**) was reacted in acetone with the appropriate **2-R** (Glu or Gal), to afford the corresponding peracetylated complexes **17** or **19**. The compounds were obtained in pure form by chromatography on Silica gel and following recrystallization from DCM with diethyl ether.

The deprotected compounds, **18** and **20** were obtained by treating the relative peracetylated species in methanol solutions containing a catalytic amount of KOH. Elemental analysis and NMR spectroscopy confirmed the identity and the purity of all the compounds.

#### 5.2.1.5 Structural characterization of Pt(II) and Pt(IV) complexes

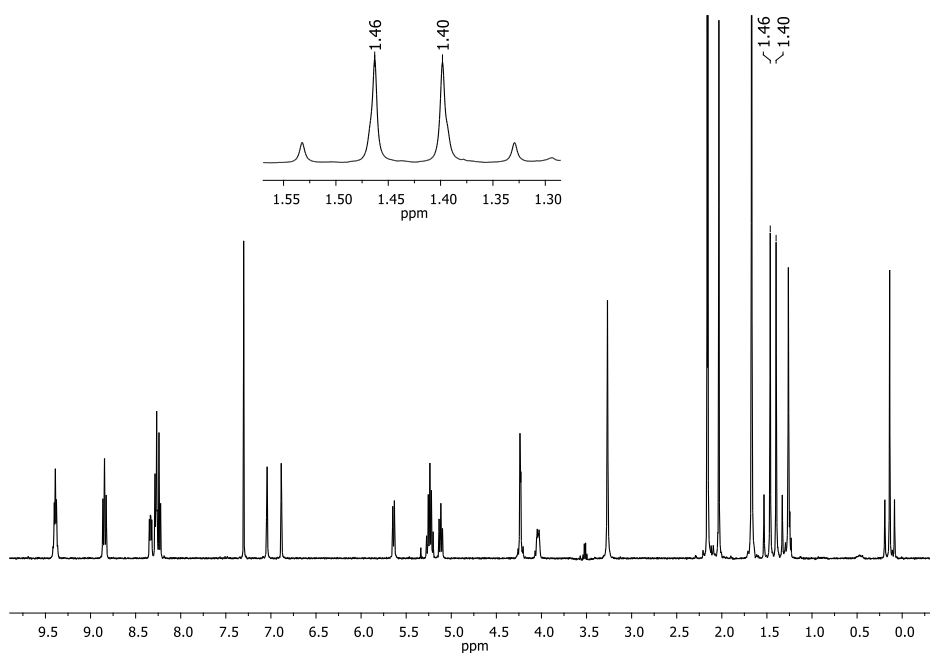
NMR, UV-vis spectroscopy, and X-ray diffraction analysis disclosed strict structural analogies between the two families of compounds. As expected, both the  $^1\text{H}$  and  $^{13}\text{C}$  NMR spectra of **12-16** (spectra of **12** in **Figure 5.6**) showed the signals of the coordinated ethene at higher fields, due to the  $\pi$ -backdonation contribution in the metal-olefin bond. The methyl was found at ca. 0.2-0.3 ppm in the proton and -7 ppm in the  $^{13}\text{C}$  NMR spectra respectively, as typical for *tbp* methyl platinum(II) complexes. The carbene carbon resonated around 170 ppm with a  $^1J_{\text{Pt-C}}$  ca. 700 Hz; all the mentioned signals displayed the satellites due to the coupling to  $^{195}\text{Pt}$  nuclei.





**Figure 5.6.**  $^1\text{H}$  and  $^{13}\text{C}$  NMR spectra of **12** in  $\text{CDCl}_3$  at 400 MHz.

In the proton spectra of Pt(IV) complexes **17-20**, the axial methyl resonated as a singlet close to  $\delta$  0, similarly to the methyl in the analogue *tbp* species. The equatorial methyl ligands, equivalent in the precursor (**e**), were found as two distinct singlets around  $\delta$  1.5 (spectra of **17** in **Figure 5.7**) with satellites due to the coupling to  $^{195}\text{Pt}$ , due to the lack of symmetry led by the sugar ligand.



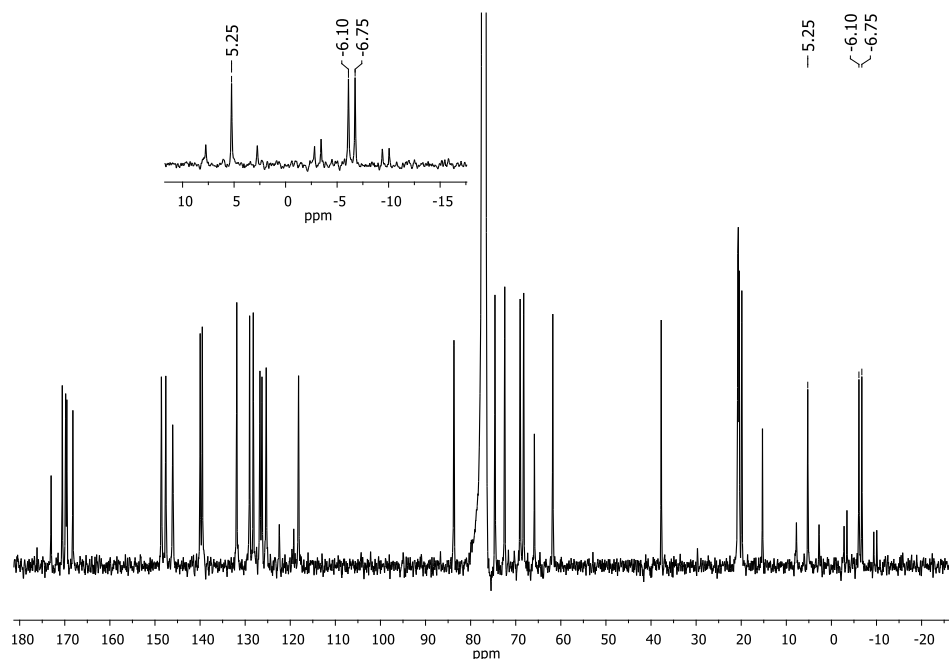


**Figure 5.7.**  $^1\text{H}$  and  $^{13}\text{C}$  NMR spectra of **17** in  $\text{CDCl}_3$  at 400 MHz.

In the  $^{13}\text{C}$  spectrum the non-equivalent equatorial methyls were shifted at lower frequencies than the axial one, as shown in **Figure 5.7**. Also for Pt(IV) complexes the carbene atom resonances were found around 170 ppm (analogue frequencies observed for the Pt(II) *tbp* complexes with a slight minor values for  $^1J_{\text{Pt-C}}$  of *ca.* 600 Hz).

The spectra of the glycoconjugate complexes displayed the multiplets of the sugar protons with the expected coupling constants, as well as two strict doublets at *ca.*  $\delta$  7 for the protons riding on the carbene ligands.

UV-vis spectra were found to be almost superimposable, with absorption maximum around 270 nm and 300 nm for both the families of compounds.

The analogies observed in the in-solution characterization were confirmed by the crystal structures resolved for **12** and **19** (Figure 5.8 and Figure 5.9).

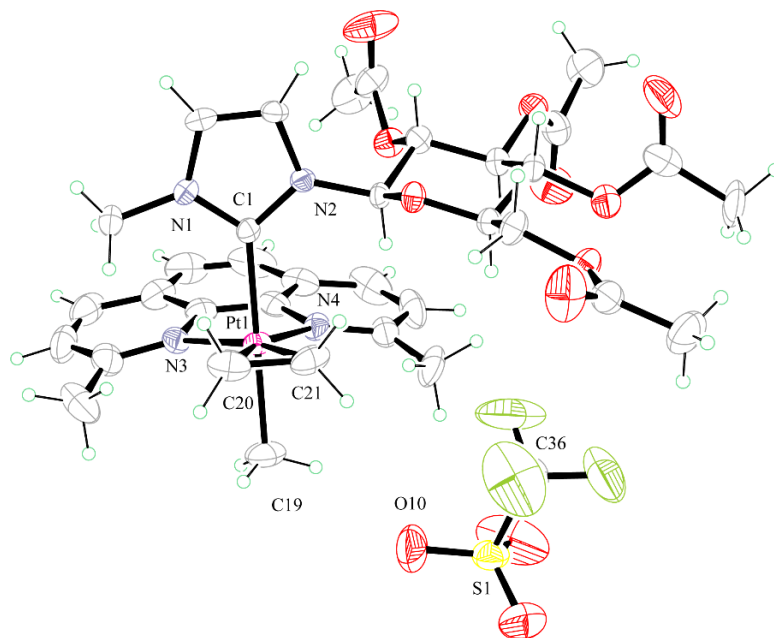


**Figure 5.8.** ORTEP view of **12** with thermal ellipsoid drawn at 30% probability level

Complex **12** crystallized in  $P2_12_12_1$  space group with one cation and one anion in the independent unit. The Pt atom adopts a fairly regular trigonal bipyramidal geometry with *dmphen* and the olefin ligands in the equatorial plane. The axial positions are occupied by the central carbon atom of NHC ligand and by the methyl group. The glucosyl group at N2 is in the expected chair conformation and  $\beta$  configuration, with all substituents in the equatorial positions. Triflate anion places near Pt(II) in between the axial methyl group and the equatorial ethene ligand with the shortest distance  $\text{Pt}\cdots\text{O-S}$  of 4.94(1) Å. The crystal packing is also stabilized by normal van der Waals and  $\text{C-H}\cdots\text{O}$  weak interactions.

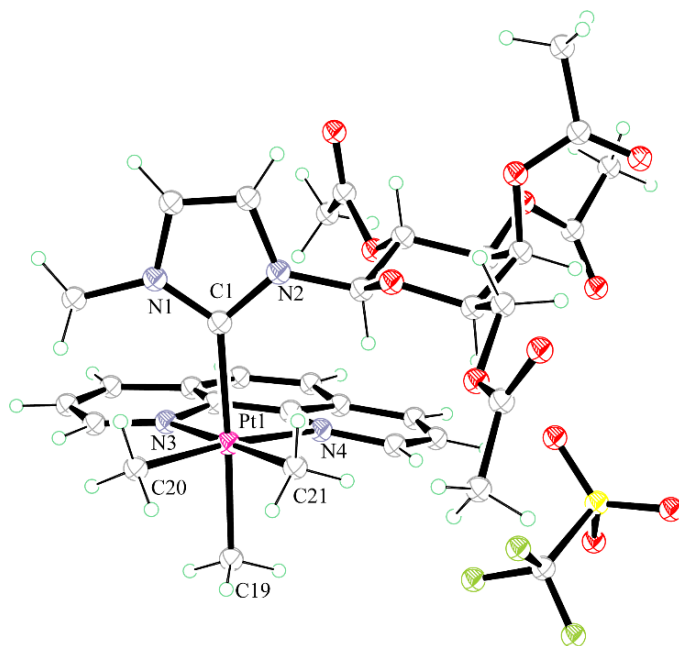


**Figure 5.9.** ORTEP view of one of the four independent molecules of **18**. Thermal ellipsoids are drawn at 30% probability level

Compound **19** crystallizes in the triclinic P1 space group with four independent pairs of cations and anions in the unitary cell. No significative differences in the geometric parameters were found between the four independent pairs of molecular ions. The Pt atom adopts a fairly regular octahedral geometry with the bidentate *phen* ligand and two methyl groups in the equatorial plane. The two Pt-Me distances (2.05(2) and 2.07(2) Å) are in line with previous literature data. The axial positions are occupied by the central carbon atom of carbene ligand and by a third methyl group. The galactosyl group at N2 atom is in the expected chair conformation in  $\beta$  configuration, with three equatorial and one axial substituent. In the crystal the triflate anions place in the neighborhood of Pt(IV), with mean

Pt $\cdots$ O(triflate) distance of 5.91(3) Å. The crystal packing is dominated by electrostatic interactions and is also stabilized by weak C-H $\cdots$ O interactions.

The two crystal structures revealed a close analogy, with the coordination environments overlapping, despite the different oxidation state of platinum. In **Table 5.1** the most relevant bond distances and angles are reported and compared.

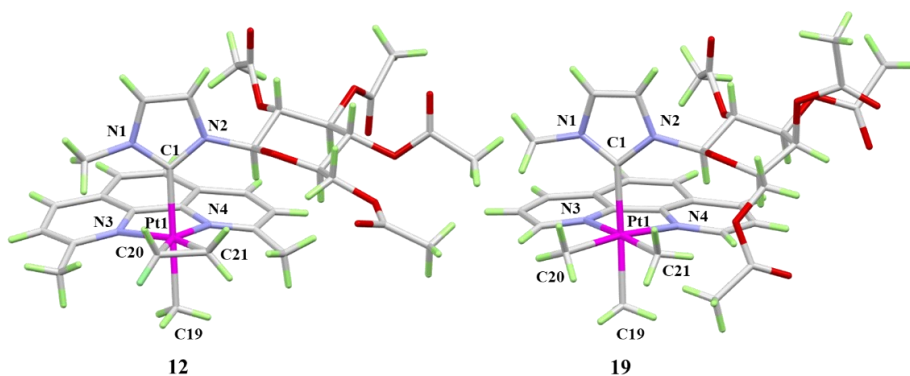


**Table 5.1.** Most relevant bond distances and angles measured in **12** and **19** crystallographic structures

Bond distance	12	19
Pt1-C1	2.101(7) Å	2.132 Å
Pt-C19	2.070(9) Å	2.102 Å
Pt-C20	2.079(10) Å	2.042 Å
Pt-C21	2.073(10) Å	2.021 Å
Pt-N3	2.213(8) Å	2.175 Å
Pt-N4	2.232(8) Å	2.195 Å
C20-C21 (ethene)	1.444(16) Å	-
<b>Bond angles</b>		
C1-Pt1-C19	177.1(4) °	176.1(1) °
N3-Pt1-N4	73.4(4) °	77.6(2) °
N1-C1-N2	103.1(4) °	102.4(3) °
C20-Pt1-C21	40.7(0) °	82.9(3) °

The glycosyl fragments on the NHC ligands only differ for the inverted axial (galactosyl) or equatorial (glucosyl) position of the acetyl group at the C4 of the ring. In **12** the glucose fragment was found in a flat shape and placed far away from *dmphen* to avoid unfavorable intermolecular interactions. A bowl-like distortion of *dmphen* was observed, with dihedral angle between mean planes of outer rings of  $16.1(3)^\circ$  (**Figure 5.10 A**). In the structure of **19** a not flat shape is adopted by the galactosyl group, due to the axial substituent that placed far away from the *phen* ligand plane to avoid steric effects. A less evident bowl-like distortion of the bidentate ligand was observed with respect to **12**, with dihedral angle between mean planes of the outer rings ranging from  $8(2)^\circ$  to  $11(2)^\circ$  in the four independent cations (**Figure 5.11 B**).

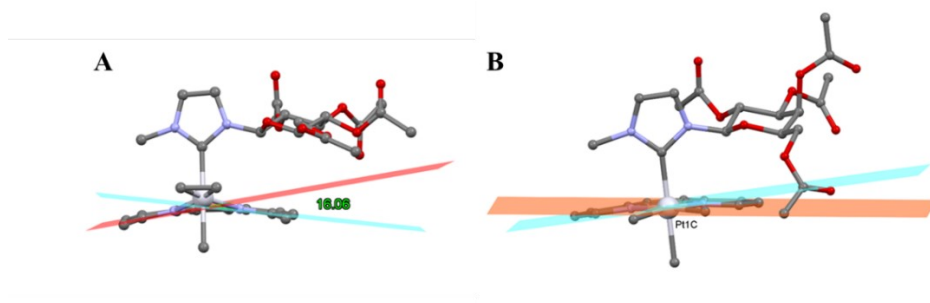


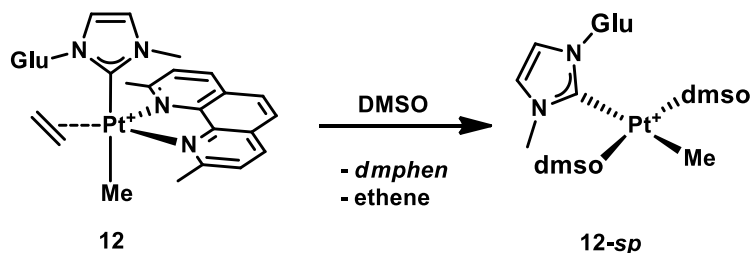
**Figure 5.11.** (A) Bowl-like distortion of *dmphen* ligand in **12** (angle between mean planes of outer rings is  $16.0(6)^\circ$ ). (B) Small bowl-like distortion of *phen* plane. The angle between the mean planes of outer rings is  $8(2)^\circ$ .

## 5.2.2 In-solution reactivity

### 5.2.2.1 Stability in aqueous media and coordinating solvents

The stability of the compounds was studied in pseudo-physiological conditions, (90%-10% PB-DMSO pH 7.5 and 50%-50% PB-DMSO pH 7.5) and pure in DMSO at 37 °C, by  $^1\text{H}$  NMR and UV-vis absorption spectroscopy. Compounds **12** and **17** were considered as representative members of the Pt(II) and Pt(IV) classes, respectively.

Interestingly, **12** and **17** showed very different reactivity in solution. Indeed, **12** was found to be reactive in pure DMSO, according to **Scheme 5.5**.



**Scheme 5.5.** Exchange reaction observed for **12** in DMSO at 37 °C.

Immediately after the dissolution in DMSO, *dmphen* and ethene were replaced by solvent molecules, resulting in the change of the coordination environment and the formation of a square-planar NHC species. The process was completed after 24 h at 37 °C (**Figure 5.12**).



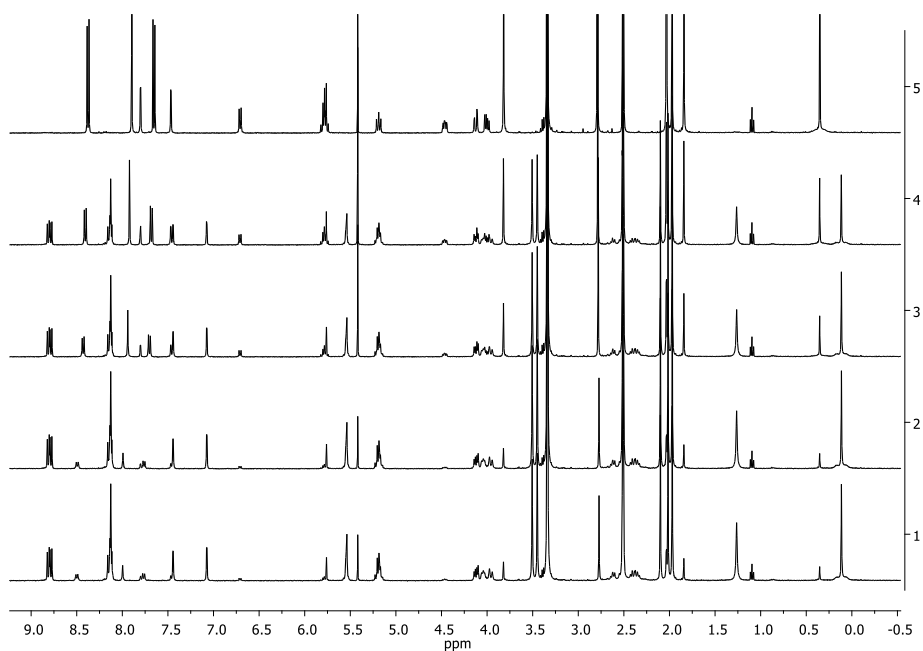


**Figure 5.12**  $^1\text{H}$  NMR spectra of **12** in  $\text{DMSO}-d_6$  at different time (1 = start, 2 = 1h, 3 = 4h, 4 = 6h, 5 = 24 h) at 500 MHz..

Conversely, the analogue Pt(IV) complex, **17** was stable in DMSO over several days, as observable in **Figure 5.13**.

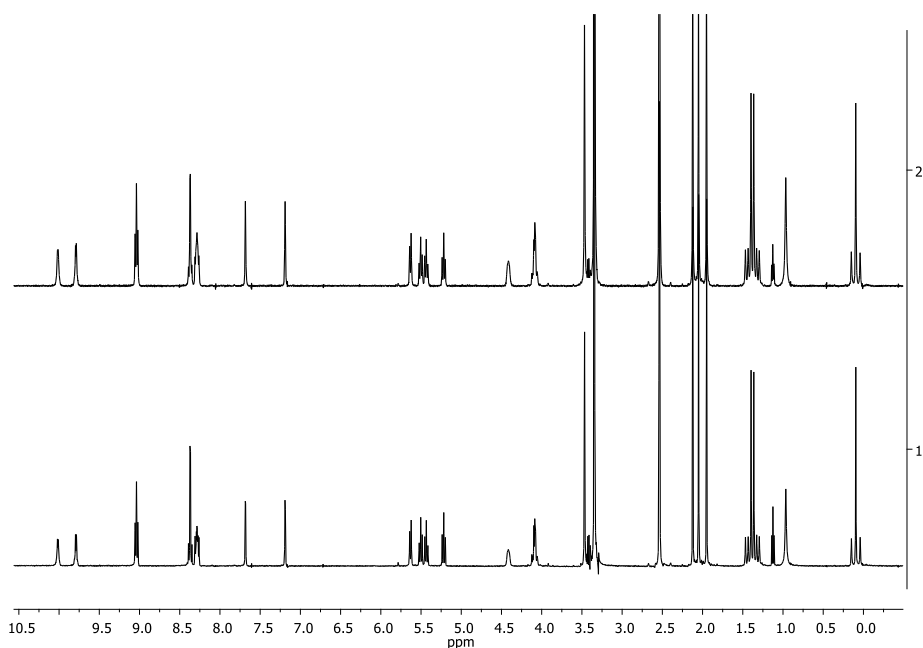


**Figure 5.13.**  $^1\text{H}$  NMR spectra of **17** in  $\text{DMSO-}d_6$  at different time (1 = start, 2 = 4 days) at 500 MHz.

No changes were detected in the spectra collected over time, suggesting that the octahedral Pt(IV) complexes benefit from an increased robustness in non-protic strong coordinating solvents, with respect to their Pt(II) counterparts.

Such behavior changed in aqueous media. Indeed, **12** was highly stable in pseudo physiological medium (37 °C, 90%-10% PB-DMSO pH 7.5) showing only traces of substitution of the ligands (probably by DMSO, as reported in **Scheme 5.5**) after 6 days in solution (**Figure 5.14**).

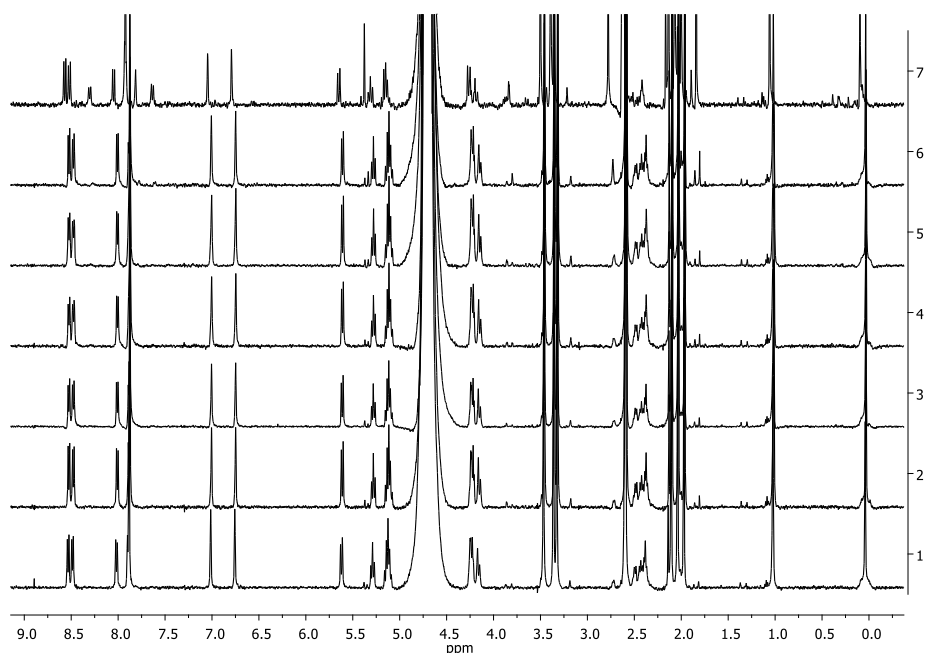
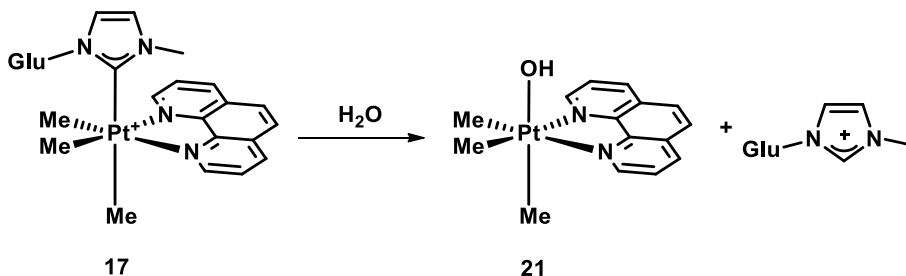


**Figure 5.14.**  $^1\text{H}$  NMR spectra of **12** in 90%-10% PB-DMSO- $d_6$  pH 7.4 at different time (trace 1 = start, 2 = 1h, 3 = 2 h, 4 = 8 h, 5 = 24 h, 6 = 48 h, 7 = 6 days) at 500 MHz...

In the same conditions, **17** was unexpectedly reactive toward hydrolysis, according to **Scheme 5.6**.



**Scheme 5.6.** Unexpected hydrolysis of Pt(IV) complex (**17**) in aqueous solvent

**17** underwent hydrolysis of the carbene moiety, yielding a hydroxyl Pt(IV)-species (**21** in **Scheme 5.6**) and the imidazolinium salt.<sup>166,194,195</sup> The process was completed within 48 hours at 37 °C (**Figure 5.15**).

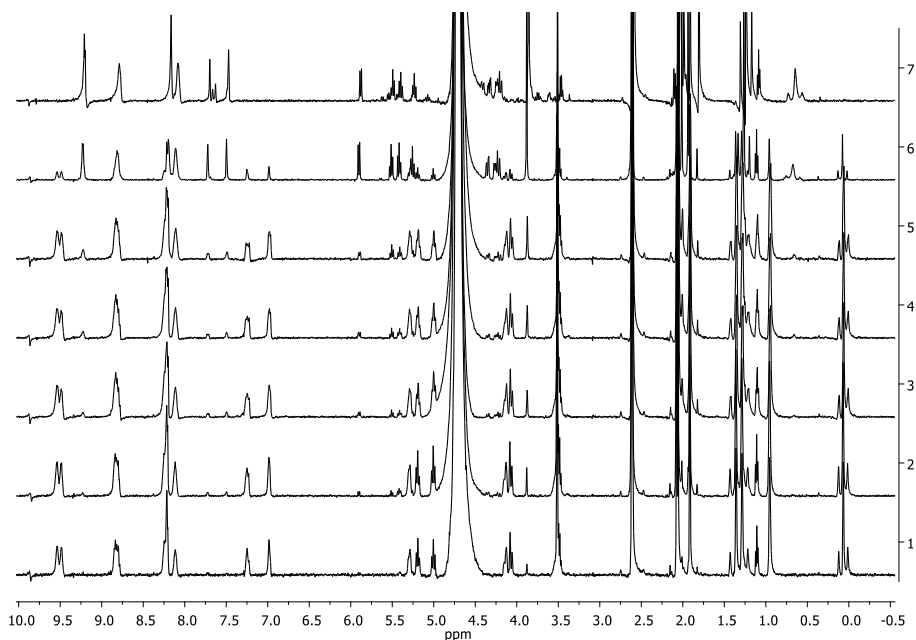


**Figure 5.15.**  $^1\text{H}$  NMR spectra of **17** in 90%-10% PB:DMSO- $d_6$  pH 7.5 at different time (trace 1 = start, 2 = 1h, 3 = 2 h, 4 = 3 h, 5 = 5h, 6 = 24h, 7 = 48h) at 500 MHz.

The two products were identified and fully characterized by comparing their NMR spectra with those of authentic synthesized samples. An influence of pH was observed, as using  $\text{D}_2\text{O}$  instead of phosphate buffer (pH 7.5), the same process occurred slowly.

The consistent differences observed for the two families can be rationalised considering that **12** was sensitive to DMSO, a strong coordinating aprotic solvent, probably due to the aptitude of the equatorial neutral ligand ethene to act as a leaving group. Its release probably starts the substitution process described in **Scheme 5.5** as the square-planar complex  $[\text{Pt}(\text{dmphen})(\text{NHC})\text{Me}]^+$  is sterically

hindered and rapidly substitutes *dmphen* for DMSO. In **17** the absence of such neutral leaving group, as well as the inertness of Pt(IV) complexes deriving by their  $d^6$  electronic configuration in octahedral environment, stabilized the complex toward ligand substitution. Contrarywise, the situation was reversed in water, a weaker ligand for platinum with respect to DMSO. The Pt(II) compounds remained intact, while the Pt(IV)-carbene bond was responsive to an hydrolysis process. Pt(IV) complexes with N,N'-chelating and four hydrocarbyl ligands (of type  $[\text{Pt}(\text{N},\text{N}')(\text{R})_4]$ ) were found to be susceptible to the cleavage of an axial Pt-C bond in protic solvents, with formation of the alkane (RH) and of a Pt(IV) species of type  $[\text{Pt}(\text{N},\text{N}')(\text{X})(\text{R})_3]$ . The cleavage of the axial R group was ascribed to the mutual *trans*-influence of R ligands in apical positions, which enriches the Pt-C bond of electron density.<sup>196</sup> It is reasonable to affirm that in compounds **17-20** the axial methyl performs a stronger *trans*-influence than the NHC ligand. This latter is then more susceptible to cleavage, and reacts with water to give **21**. It can also be reasonable to hypothesize that a different electronic distribution in **12-16**, due to the formal oxidation state Pt(II) and to the presence of ethene in the equatorial plane, results in different thermodynamics and/or kinetics stabilities of the complexes, that do not lead to the cleavage of the carbene ligand.

#### 5.2.2.2 Reactivity in presence of reducing agents

Pt(IV) prodrugs are activated by reduction in cytosol. Therefore, the reactivity of **17** toward reduction was studied in presence of ascorbic acid and glutathione, the most representative reducing agents in the cell. In absence of reducing agents, no sign of reduction was observed. The formation of Pt(II) species would likely involve two different paths:

- the reductive elimination of ethane, with formation of a Pt(II) complex of type  $[\text{Pt}(\text{phen})\text{Me}(\text{NHC})]^+$ . This kind of reactivity was observed in alkyl platinum(IV) complexes with chelating di-phosphines ligands;<sup>197</sup>
- the reductive elimination of a Me-NHC coupling product, and the formation of a dimethyl Pt(II) species ( $[\text{Pt}(\text{phen})(\text{Me})_2]$ ), as reported in literature for Pt(IV) and Pd(IV) alkyl complexes.<sup>198,199</sup>

**17** was incubated at 37 °C in 90%-10% PB:DMSO-*d*<sub>6</sub> pH 7.5, with different excesses of the reducing agent, and <sup>1</sup>H NMR spectra were recorded at different time of incubation. In these conditions no sign of reduction was observed for **17** neither for its hydrolysate form **21** (Scheme 5.6) with both ascorbic acid and glutathione.

The reduction of **17** and **21** was studied electrochemically, by cyclic voltammetry. The reduction peaks detected in the voltammogram are reported in Table 5.3.

**Table 5.3.** Reduction peaks of **17**<sup>a</sup> and **21** (1mM in DMSO-0.10 M  $[\text{Et}_3\text{MeN}][\text{BF}_4]$ ).

Complex	$E_{red1}$	$E_{red2}$	$E_{red3}$	$E_{red4}$
<b>17</b>	-1.54	-1.89	/	/
<b>21</b>	-0.89 <sup>b</sup>	-1.40	-1.59	-1.89

<sup>a</sup>1-methyl-3-(2,3,4,6-tetra-*O*-acetyl-β-D-glucopyranosyl)imidazolylidene bromide and 1,10-phenanthroline are not electroactive above -2 V. <sup>b</sup>Attributed to the reduction of O-H.

Reduction peaks were found at significantly more negative values than those of Pt(IV) complexes known to undergo chemical reduction.<sup>200</sup> In DMSO, peaks of reduction were observed at -1.54 and -1.89 V for **17**, and -1.40, -1.59 and -1.89 V for **21**. These values matched with those observed for other cyclometalated

organometallic Pt(IV) compounds containing aryl substituents, which similarly were not chemically reduced as well.<sup>201</sup>

It is reasonable to assume that the stability toward reduction of the Pt(IV) complexes, either in the presence of glutathione or ascorbate, is due to the absence of ligands as chlorido, acetate or hydroxido able to form bridges with the reductant, resulting in quick inner sphere electron transfer.<sup>75</sup>

It should be underlined that no coordination of glutathione was observed neither with **17**, **21** nor with the Pt(II) analogue **12**, despite the known ability of this tripeptide ligand to coordinate platinum complexes. Such observation may be considered a beneficial characteristic of these coordinatively saturated compounds since coordination to glutathione is one of the main deactivation pathways of the drug in cell.

### 5.2.3 *Biological studies*

#### 5.2.3.1 *Cytotoxicity and Cellular Uptake*

The biological activity of the NHC platinum(II) **12-16**, platinum(IV) **17-20** and of the hydrolysate Pt(IV)-OH product **21** was assessed on two couples of cell lines, with each couple constituted by a cancerous line and a biologically related non-cancerous counterpart. Tumor cell line A431 (epidermoid carcinoma cells) and related non-tumor HaCaT (human keratinocyte cells), SVT2 cells (murine fibroblasts BALB/c-3T3 transformed with SV40 virus) and BALB/c3T3 were selected. The cytotoxicity was evaluated by determining the IC<sub>50</sub> values (the concentration of complex able to reduce to 50% the cell viability) through MTT assay after 48 h incubation. The selectivity of the compounds was evaluated by relating the IC<sub>50</sub> of the cancer line with its healthy counterpart. Cells were

incubated with increasing concentrations of the complex and then cell survival was evaluated. The IC<sub>50</sub> values are reported in **Table 5.2**.

**Table 5.2.** IC<sub>50</sub> values (μM) obtained for **12-21** after 48 h incubation. Selectivity Index (SI), indicated by the ratio between the IC<sub>50</sub> of immortalized cells and cancer cells.

Complex	IC <sub>50</sub> (μM)				SI	SI
					HaCat/A431	BALB /c3T3/ SVT2
	HaCaT	A431	BALB/c3T3	SVT2		
<b>12</b>	13 ± 1.7	0.40 ± 0.01	6.3 ± 0.4	0.65 ± 0.07	32	10
<b>13</b>	66 ± 3	94 ± 8	62 ± 4	4.8 ± 0.8	0.70	13
<b>14</b>	16 ± 3	94 ± 4	37 ± 8	15 ± 2	0.17	2.5
<b>15</b>	92 ± 8	76 ± 16	61.0 ± 0.9	52 ± 2	1.2	1.2
<b>16</b>	3.2 ± 0.7	15 ± 2	5 ± 1.6	3 ± 1.3	0.21	1.7
<b>17</b>	43.8 ± 4.3	43.8 ± 2.8	196 ± 14	176 ± 13	1.0	1.1
<b>18</b>	55 ± 9	41.8 ± 1.7	59.6 ± 2.6	122 ± 5	1.3	0.50
<b>19</b>	N.D.	N.D.	N.D.	N.D.	N.D.	N.D.
<b>20</b>	N.D.	N.D.	N.D.	N.D.	N.D.	N.D.
<b>21</b>	13.6 ± 1.6	14.9 ± 0.6	7.2 ± 0.7	6.4 ± 0.6	0.91	1.12
<b>Cisplatin</b>	6.6 ± 0.3	39 ± 12	240 ± 47	195 ± 7	0.17	1.23

Interestingly, the peracetylated glucosyl Pt(II) derivative **12** showed to be the most promising member of the whole family being 100-times more cytotoxic than cisplatin toward A431 cells. Furthermore, it was more toxic on A431 cancer cells than on the non-cancerous counterpart HaCaT with SI = 32, which is more than 180-fold higher than that of cisplatin (SI = 0.17).



Noteworthy, the nature of the sugar fragments had an enormous impact on the biological activity. Indeed, the Pt(II) galactosyl (**14**) and the Pt(II) deprotected compounds (**13** and **15**) were by far less active and selective than **12**. The ethyl derivative **16** was still active but not able to discriminate between normal and cancer cell lines, and its toxicity was similar on all the analyzed cell lines.

Surprisingly, despite the structural similarities, the change of the oxidation greatly reduced the performances of the NHC compounds. The glucosylated Pt(IV) complex, **17**, was about 100 times less toxic than its Pt(II) analogue **12**, and it completely lost selectivity. The hydrolyzed Pt-OH products **21** was found to be more toxic than the other glycosylated Pt(IV) compounds but no selectivity was observed.

No IC<sub>50</sub> was detected for galactosyl derivatives **19-20**, confirming that the activity of this class of compounds was strictly dependent on the nature of sugar portion and very sensible upon its small variations.

It is not easy to establish the specific reasons of the different behavior observed for these molecules since many factors may contribute to their performances. Considering the effect of the sugar residues, a role could be played by the different polarity obtained by installing protecting groups on the hydroxyls of the sugar residue. Indeed, this aspect may certainly affect the internalization process. Although it cannot be deduced which mechanism of internalization took place in this case, it is reasonable to affirm that the increased lipophilicity provided by acetyl groups in **12** could favor the affinity for cellular membrane or the interaction with proteins, involved in an active transportation. It cannot be excluded that this aspect could also affect the interaction with biological targets which triggers the biological response. However, the reduced activity of the galactosyl derivatives definitively confirm an active role of the sugar fragment on the whole biological activity of these complexes.

The switch from Pt(II) to Pt(IV) had a dramatic impact on the biological activity of the NHC complexes. Considering the established concept that Pt(IV) agents need reduction to be effective, it can be assumed that the lack of reduction in the cytosol, described in the previous section, was a major reason for the poor activity of **17-21** with respect to the Pt(II) congeners **12-16**.

To shed light on the differences in the mechanism of action of the two classes of compounds, the cellular uptake of the glucosylated **12** and **17** in A431 cells was analyzed. Cancer cells were incubated with the complexes at the concentration needed to reach the IC<sub>50</sub> values. Cisplatin was used as a reference. After 48 h incubation, the Pt content was measured by ICP-MS. The amount of Pt uptake in A431 cells was 0.65% ± 0.15 for **12**, with respect to 0.39% ± 0.09 for **17** and 0.79% ± 0.25 for cisplatin. These data indicate that in the case of **12** the percentage of Pt internalized by the cells is about 2 times higher than that found in the case of cells treated with **17**. Then, a lower degree of internalization displayed by the Pt(IV) complexes could be considered another major cause of the drastic decrease in the biological activity of complexes **17-21**.

#### *5.2.3.2 Study of the mechanism of Cell Death induced by 12*

Preliminary investigations on the mechanism of cell death induced by **12** on A431 cells were performed. First, the intracellular ROS levels were measured to evaluate the redox state of the cells following the incubation of the drug. When A431 cells were incubated with **12** at 0.4 μM (IC<sub>50</sub> concentration), for different times (from 5 min to 48 h) a significant increase in ROS levels was observed already after 6 h of incubation. The ability of **12** to act as photosensitizer (PS) producing singlet oxygen and consequently ROS in the cell, was assessed in preliminary cell-free

experiments. However, results suggested that the Pt complex was not able to produce singlet oxygen.

The oxidative pathway was confirmed by Western blot analysis. After 16 h of incubation, a significant increase in the phosphorylation level of p38 was observed. The phosphorylation of this protein is a marker that cell is undergoing an oxidative stress, which generally results in the depolarization of mitochondrial membrane ( $\Delta\psi_m$ ). As consequence of this pathway, the apoptotic mechanism is triggered. A significant depolarization level was observed in cells incubated with **12** for 48 h.

The activation of apoptosis was studied by Western Blot analysis which revealed the typical markers of this cell death mechanism. Indeed, a decrease in the levels of the survival factor Bcl-2 and in the inactivated forms of pro-caspase -3, -7 and -9 was detected, confirming that apoptosis was active in A431 cells.

#### 5.2.4 *Interaction with model biomolecules*

##### 5.2.4.1 *Reactivity with model DNA*

The interaction of the Pt(II) and Pt(IV) NHC complexes with DNA was studied by fluorescence, circular dichroism, ESI mass spectrometry and  $^1\text{H}$  NMR.

The binding to the double helix was studied using calf-thymus DNA (ctDNA) by ethidium bromide (EtBr) displacement fluorescence assay.

Interestingly, the results showed an increasing of fluorescence when the DNA-EtBr adduct was titrated with the Pt complexes, differently from what observed for cisplatin and *dmphen* ligand, that led to a decrease of fluorescence intensity (**Figure 5.16**). These results suggested that both **12** and **17** did not displace EtBr

from the ctDNA major groove, providing a different type of interaction when compared to cisplatin and its analogues.

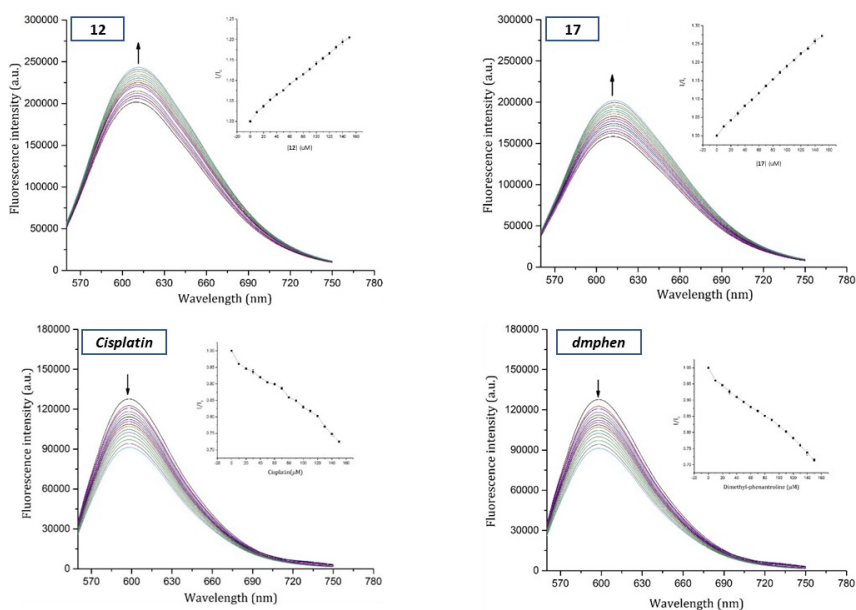


**Figure 5.16.** Fluorescence spectra recorded for **12**, **17**, cisplatin and *dmphen* in ethidium bromide displacement assay.

To disclose the occurrence of an interaction between complexes and DNA circular dichroism (CD) spectra of ctDNA in the presence of **12** and **17** at different molar ratios were registered, and compared to the spectrum of DNA without the agents (**Figure 5.17**),

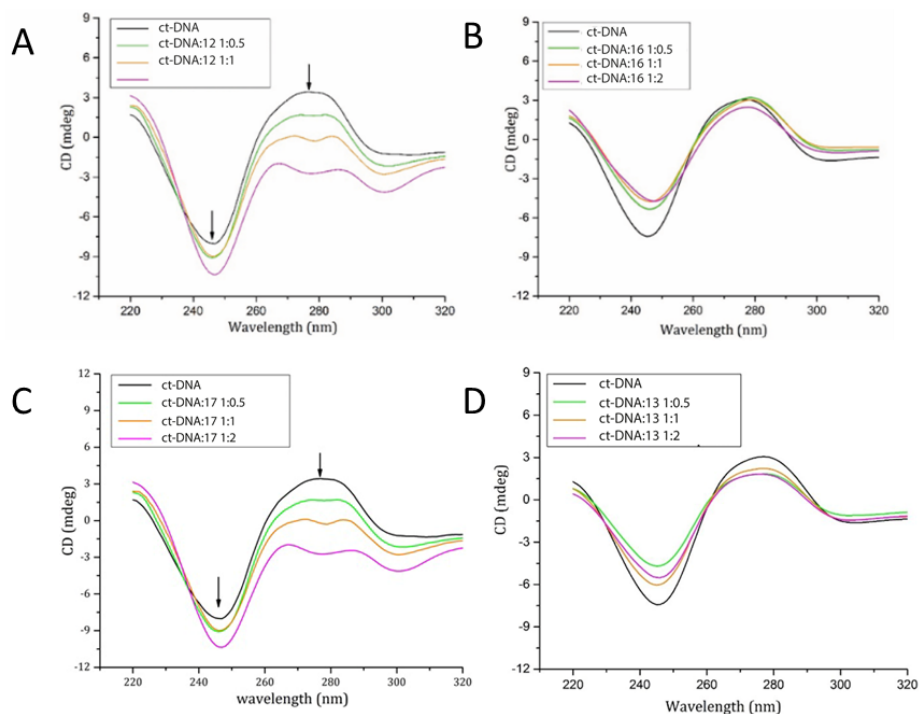


**Figure 5.17.** CD spectra of ct-DNA in presence of different concentrations of complexes **12** (A), **16**(B), **17**(C) and **13** (D)

CD spectra of ctDNA consists of a positive band at 275 nm due to base stacking and a negative band at 245 nm due to helicity. These features are typical of DNA in right-handed B form. In the presence of **12** and **17** the intensities of both positive and negative bands shifted to lower ellipticity values, indicating that the complexes interact with DNA altering the structure of the double helix.

Interestingly, when ctDNA was treated with the deprotected Pt(II) **13** or with the ethyl analogue **16**, the intensity of negative bands increased and that of the positive band decreased without any changes in the wavelength, suggesting that the nature of the sugar residue have an active role in the interaction with the double helix.

Altogether these data suggest that Pt-NHC complexes probably display a different mechanism of action when compared to canonical Pt-based drugs, and that minimal variations in the structure can affect the nature of the interaction with biological targets. This observations match with the biological activity data described in the previous section.

Successively, to shed light on the interaction between complexes and DNA at molecular level, the binding of **12** and **17** to a 20mer double stranded oligonucleotide (dsDNA) was investigated by ESI mass spectrometry. All signals detected in the ESI-MS spectra of **12** and **17** with dsDNA are reported in **Table 5.3**.

**Table 5.3.** Results of ESI-MS analysis of species formed upon reaction of DNA with **12** and **17**. The m/z values detected in MS spectra and their relative charges, as well as experimental (Exp) and theoretical (Theor) monoisotopic mass values and the corresponding ion species are reported. dsDNA = double stranded DNA; ssDNA = single stranded DNA.

Complex	Signal (m/z)	Signal charge	Exp MW (Da)	Theoretical MW (Da)	Species
<b>12</b>	1195.36	(-5)			
	1494.45	(-4)	5982.92±0.80	5983.9	ssDNA <sub>1</sub>
	1993.02	(-3)			
	1249.57	(-5)			
			6254.45±0.50	6255.1	ssDNA <sub>2</sub>
	1562.22	(-4)			
	1358.99	(-9)			
	1528.98	(-8)	12240.33±0.30	12239	dsDNA
	1747.71	(-7)			

17	2039.04	(-6)			
	1636.21	(-9)			
	1869.85	(-8)	13096.53±2.20	13097.81	dsDNA + 12
	2182.45	(-7)			
		(-6)			
	1195.42	(-5)			
	1494.52	(-4)	5982.15±0.03	5983.9	ssDNA <sub>1</sub>
	1041.25	(-6)			
	1249.65	(-5)	6253.58±0.27	6255.1	ssDNA <sub>2</sub>
	1562.47	(-4)			
	1358.87	(-9)			
	1528.80	(-8)	12238.82±0.27	12239	dsDNA
	1747.43	(-7)			
	1135.23	(-6)			
	1362.28	(-5)	6817.08±0.46	6816.15	ssDNA <sub>1</sub> + 17
	1703.24	(-4)			
	1180.24	(-6)	7087.04±0.42	7087.35	ssDNA <sub>2</sub> + 17
	1416.32	(-5)			
	1451.31	(-9)			
	1632.80	(-8)	13071.34±0.87	13071.25	dsDNA + 17
	1866.53	(-7)			

Mass spectra revealed that both **12** and **17** formed adducts with DNA, although some differences were observed. Indeed, dsDNA was obtained by annealing procedure starting from two complementary single-stranded DNA (ssDNA). In the ESI spectra of **17** two peaks were detected, at  $6817.08 \pm 0.46$  Da and at  $7087.04 \pm 0.42$  Da, indicative of a binding of the Pt(IV) complex to the two ssDNA molecule. No peaks attributable to adducts with the single strand DNA were observed in the spectra collected following the incubation of **12** with dsDNA under the same experimental conditions.

However, in both cases one molecule of each Pt compound bound the dsDNA, as demonstrated by the presence of the species at molecular weight  $13096.53 \pm 2.20$  Da and  $13071.34 \pm 0.87$  Da. Both the compounds were intact in the adduct with dsDNA, with all the original ligands retained.

These data suggest that both Pt(II) and Pt(IV) compounds bind DNA through non-covalent interactions. Indeed, both are coordinatively saturated and do not have available sites of coordination for DNA nucleobases. Such hypothesis confirmed the occurrence of a different mechanism of interaction of these molecules with DNA when compared to cisplatin and other Pt-drugs. Indeed, under the same experimental conditions, up to three cisplatin molecules bound the dsDNA, and upon binding, each cisplatin molecule lost both Cl<sup>-</sup> ligands.

To confirm the hypothesis of the interaction via non coordinative mechanism, the reactivity of the complexes **12** and **17** with 2-deoxyguanosine monophosphate (dGMP) was investigated by <sup>1</sup>H NMR, at 37 °C in 90%-10% PB-DMSO pH 7.5. In case of the Pt(IV) complex **17**, the reactivity with dGMP was monitored also in presence of ascorbic acid. Under these conditions, coordination of guanosine was not observed up to 2 weeks for both the complexes. For **17** neither coordination nor reduction was observed, beyond the hydrolysis reaction to form **21**.



Mass spectrometry data also suggested that the interaction between DNA and Pt(IV) complexes stabilized them toward the hydrolysis of the NHC ligand. Indeed, no traces of adducts between DNA and the hydrolysed product **21** were observed in mass spectra. To confirm the hypothesis of the stabilization, a time course in the UV-vis spectra of **12** and **17** in the presence of DNA was performed (Figure 5.18).

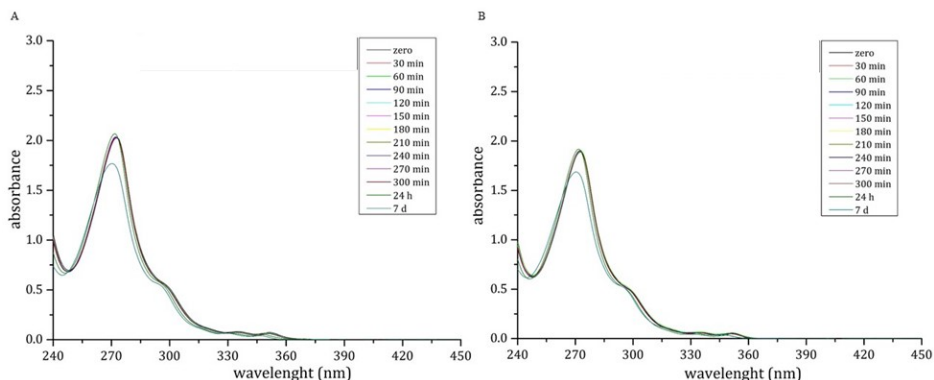


**Figure 5.18.** Time course UV-vis spectra of 50  $\mu\text{M}$  **12** (A) and 50  $\mu\text{M}$  **17** (B) in 90%-10% PB:DMSO pH 7.5 in the presence of ctDNA.

The UV-vis spectra remained unchanged over 24 h, with a minimal shift of the maximum absorption peak from 273 to 270 nm observed only after 7 days. This experiment confirmed that the Pt(IV) complexes were more stable in aqueous media in the presence of DNA, probably due to the formation of an adduct not susceptible of hydrolysis.

#### 5.2.4.2 Reactivity with model proteins

The reaction between platinum complexes and the model protein hen egg white lysozyme (HEWL) and human serum albumin (HSA) was studied by UV-vis absorption spectroscopy and circular dichroism. **12** and **17** were selected as representative of the two subclasses. UV-vis spectra of the two compounds in the absence and in the presence of HEWL and HSA were collected over 7 days under different experimental conditions. Spectral profiles did not show appreciable changes suggesting that both **12** and **17** were rather stable in the presence of the two proteins, in agreement with what observed for **17** in the presence of DNA.

To evaluate in detail the potential interaction of **12** and **17** with HEWL and HSA, the secondary structure content of the two proteins was evaluated by CD spectroscopy at increasing concentration of the metal compounds. Far UV-CD spectra were collected upon 24h incubation at room temperature. CD spectra reported in **Figure 5.19** showed decrease of the molar ellipticity at increasing concentrations of **12** and **17** for both HEWL and HSA. This is indicative of a potential binding of the Pt compounds to the proteins.

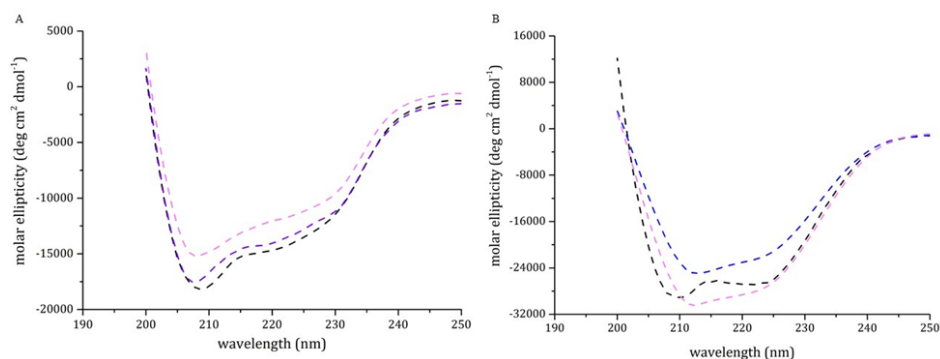


**Figure 5.14.** Far UV-CD spectra of HEWL (A) and HSA (B) incubated for 24 h in the presence of **12** (blue dashed curve/spectrum) and **17** (purple dashed curve/spectrum) in 90%-10% PB:DMSO pH 7.4 in a 1:3 protein to metal molar ratio. Free protein is represented by black dashed curves/spectra.

In summary, NHC platinum compounds showed a great variety in reacting with model biomolecules. Both Pt(II) and Pt(IV) species react with DNA probably via non-covalent interactions since they retained their ligands upon formation of adducts with DNA, as observed by mass spectrometry. This evidence was confirmed by the lack of coordination with the nucleobase dGMP observed by  $^1\text{H}$  NMR. Moreover, fluorescence experiments suggested that the compounds performed a type of interaction different from common Pt-based drugs, since they were not able to displace ethidium bromide. Interestingly, the interaction with DNA and proteins seems to stabilize Pt(IV) complexes toward the hydrolysis, observed when the compounds were dissolved in aqueous media.

Pt(II) complexes were highly stable in pseudo-physiological conditions supporting the hypothesis of non-covalent interactions, at least in the case of DNA. Moreover, both Pt(II) and Pt(IV) were not coordinated by glutathione, which is known to be responsible of several deactivation and detoxification processes of platinum drugs in the cell, limiting the efficacy of anticancer therapies. These findings confirm that coordinatively saturated species can be valid alternatives with respect to cisplatin and its derivatives, offering increased general stability in biological environment along with non-canonical reactivity which can result in alternative mechanisms of interaction with biomolecules and improved anticancer activity.

## 5.3 Experimental Part

### 5.3.1 General

Reagents and solvents were purchased from Sigma-Aldrich and were used without further purification. Human A431 epidermoid carcinoma, murine BALB/c-3T3 and SVT2 fibroblasts were from ATCC. Human HaCaT keratinocyte cells were from Innoprot. Cells were cultured in Dulbecco's modified Eagle's medium (DMEM) (Sigma-Aldrich, St Louis, MO, USA), supplemented with 10% foetal bovine serum (HyClone), 2 mM L-glutamine and antibiotics, all from Sigma-Aldrich, under a 5% CO<sub>2</sub> humidified atmosphere at 37 °C. NMR spectra were acquired on a 400 Bruker Avance UltrashieldTM 400 and on a 500 Varian Inova, located at the Dipartimento di Scienze Chimiche, Università di Napoli Federico II, Napoli (Italy). The solvents were CDCl<sub>3</sub> (CHCl<sub>3</sub>,  $\delta$  7.26, and <sup>13</sup>CDCl<sub>3</sub>,  $\delta$  77.0, as internal standards), (CD<sub>3</sub>)<sub>2</sub>SO ((CD<sub>2</sub>H)<sub>2</sub>SO),  $\delta$  2.49, as internal standard), D<sub>2</sub>O (HDO,  $\delta$  4.80 as internal standard), CD<sub>3</sub>CN (CHD<sub>2</sub>CN,  $\delta$  1.94), and CD<sub>3</sub>OD (CD<sub>2</sub>HOD,  $\delta$  3.30, <sup>13</sup>CD<sub>3</sub>OD,  $\delta$  49.0, <sup>195</sup>PtCl<sub>6</sub><sup>2-</sup>,  $\delta$  0, as internal standards). The following abbreviations were used for describing NMR multiplicities: s, singlet; d, doublet; dd, double doublet; triplet; app, apparent; m, multiplet; ABq, AB quartet. Electrochemical measurements were recorded on a Reference 3000 Gamry instrument controlled by Framework software. Data analyses were performed with EChem Analyst electrochemical software. UV-visible spectra were collected on a Jasco V-650 UV-vis spectrophotometer at room temperature using 1 cm path length cuvettes. Fluorescence spectra were collected on a HORIBA Fluoromax-4 spectrofluorometer at 25°C using a 1 cm path length cuvette. Mass spectra were recorded in negative mode using a Q-ToF Premier (Waters, Milford, MA, USA) mass spectrometer. Platinum precursors **a**<sup>157</sup> and **d**<sup>202</sup> were prepared as described in literature starting from K<sub>2</sub>PtCl<sub>4</sub>.

### 5.3.2 Synthesis and Characterization

#### 5.3.2.1 Synthesis of the pro-carbene ligands **1-R**

**1-Glu:** To a solution of 2,3,4,6-tetra-*O*-acetyl-1-Br- $\alpha$ -D-glucopyranoside (3.2 g, 7.8 mmol) in acetonitrile (0.75 mL) was added 1-methylimidazole (0.62 mL, 7.8 mmol). The mixture was stirred for 4 hours at room temperature, and then cold acetone was added. The product precipitated as a white solid, which was filtered and washed with cold acetone. Yield: 30% (1.1 g).

$^1\text{H}$  NMR,  $\text{CDCl}_3$ ,  $\delta$ : 10.9 (s, 1H, NCHN), 7.54 (br, 1H, H-Im), 7.35 (br, 1H, H-Im), 6.62 (d, 1H,  $J_{\text{H1-H2}} = 9.30\text{ Hz}$ , H1-glu), 5.47 (t, 1H,  $J_{\text{H2-H3}} = 9.27\text{ Hz}$ , H2-glu), 5.29 (t, 1H,  $J_{\text{H3-H4}} = 9.20\text{ Hz}$ , H3-glu), 5.23 (t, 1H,  $J_{\text{H4-H5}} = 9.52\text{ Hz}$ , H4-glu), 4.36-4.28 (m, 2H, H5-glu, H6-glu), 4.14-4.16 (m, 1H, H6'-glu), 4.14 (s, 3H, Me-Im), 2.07 (s, 3H, OAc), 2.06 (s, 3H, OAc), 2.04 (s, 3H, OAc), 1.99 (s, 3H, OAc).

**1-Gal:** To a solution of 2,3,4,6-tetra-*O*-acetyl-1-Br- $\alpha$ -D-galactopyranoside (3.2 g, 7.8 mmol) in acetonitrile (0.75 mL) was added 1-methylimidazole (0.62 mL, 7.8 mmol). The mixture was stirred for 10 minutes at room temperature, and then diethyl ether was added. The product precipitated as a clear oil, which was washed with cold ethyl acetate and dried. Yield: 10% (0.36 g).

$^1\text{H}$  NMR,  $\text{CDCl}_3$ ,  $\delta$ : 10.9 (s, 1H, NCHN), 7.57 (br, 1H, H-Im), 7.33 (br, 1H, H-Im), 6.47 (d, 1H,  $J_{\text{H1-H2}} = 9.30\text{ Hz}$ , H1-gal), 5.55 (m, 1H, H4-gal), 5.38-5.34 (m, 1H, H3-gal), 4.50 (t,  $J_{\text{H2-H3}} = 6.37\text{ Hz}$ , 1H, H2-gal), 4.21-4.12 (m, 2H, H5-gal, H6-gal), 3.96 (d, 1H, H6'-gal), 4.14 (s, 3H, Me-Im), 2.19 (s, 3H, OAc), 2.09 (s, 3H, OAc), 2.04 (s, 3H, OAc), 1.98 (s, 3H, OAc).

**1-Et:** 1-methylimidazole (1 g, 12.2 mmol) and bromoethane (2 g, 18.3 mmol) were refluxed in 5 mL of THF for 24 h. The product is obtained as white solid by removing the solvent under vacuum. Yield: 99% (2.3 g).

$^1\text{H}$  NMR ( $\text{CD}_3\text{CN}$ )  $\delta$  8.91 (s, 1H, H-Im), 7.44 (br, 1H), 7.38 (br, 1H, H-Im), 4.21 (q,  $J = 7.3$  Hz, 2H,  $\text{CH}_2\text{Me Im}$ ), 3.86 (s, 3H, Me-Im), 1.46 (t, 3H,  $\text{CH}_2\text{Me-Im}$ ).

#### 5.3.2.2 Synthesis of the Ag(I) NHC precursors **2-R**

The appropriate imidazolium salt **1-R** (1 mmol) was suspended in acetone (12 mL) and  $\text{Ag}_2\text{O}$  (0.290 g, 1.25 mmol) was added. The reaction mixture was stirred for 3 hours at room temperature. The residual  $\text{Ag}_2\text{O}$  was filtered on a pad of Celite® the filtrate was dried under vacuum to yield the product as a white powder (yield: 98-99%).

**2-Glu:**  $^1\text{H}$  NMR,  $\text{CDCl}_3$ ,  $\delta$ : 7.24 (d, 1H, H-Im), 7.02 (d, 1H, H-Im), 5.88 (d, 1H,  $J_{\text{H1-H2}} = 9.0$  Hz, H1-glu), 5.41 (t, 1H,  $J_{\text{H2-H3}} = 9.63$  Hz, H2-glu), 5.27 (t, 1H,  $J_{\text{H3-H4}} = 9.27$  Hz, H3-glu), 5.21 (t, 1H,  $J_{\text{H4-H5}} = 9.92$  Hz, H4-glu), 4.31 (dd, 1H), 4.18-4.17 (m, 1H), 4.15-4.08 (m, 1H), 3.86 (s, 3H, Me-Im), 2.10 (s, 3H, OAc), 2.07 (s, 3H, OAc), 2.00 (s, 3H, OAc), 1.96 (s, 3H, OAc).

**2-Gal:**  $^1\text{H}$  NMR,  $\text{CDCl}_3$ ,  $\delta$ : 7.26 (d, 1H, H-Im), 7.01 (d, 1H, H-Im), 5.95 (d,  $J_{\text{H1-H2}} = 9.53$  Hz, 1H, H1-gal), 5.53 (d, 1H,  $J_{\text{H3-H4}} = 2.94$  Hz, H4-gal), 5.38 (t, 1H,  $J_{\text{H2-H3}} = 10.57$  Hz, H2-gal), 5.27 (dd, 1H, H-3), 4.35 (t, 1H,  $J_{\text{H4-H5}} = 6.40$  Hz, H5-gal), 4.22-4.15 (m, 1H, H6-gal), 4.14-4.12 (m, 1H, H6'-gal), 3.85 (s, 3H, Me-Im), 2.18 (s, 3H, OAc), 2.14 (s, 3H, OAc), 2.03 (s, 3H, OAc), 1.96 (s, 3H, OAc).

**2-Et:**  $^1\text{H}$  NMR ( $\text{CDCl}_3$ )  $\delta$  6.99 (d, 1H, H-Im), 6.97 (d, 1H, H-Im), 4.15 (q, 2H  $\text{CH}_2\text{Me-Im}$ ), 3.83 (s, 3H, Me-Im), 1.44 (t, 3H,  $\text{CH}_2\text{Me-Im}$ ).

#### 5.3.2.3 Synthesis of the Pt(II) precursor (**b**)

[PtClMe(SMe<sub>2</sub>)<sub>2</sub>] (0.262 g, 0.70 mmol) and *dmphen* (0.150 g, 0.72 mmol) were dissolved in DCM (5 mL) under ethene atmosphere at 0 °C. The mixture was let to warm at RT and stirred for 24 h. Then, the solvent was reduced in volume until a clear solid precipitated. The precipitation was completed by adding diethyl ether. The product was obtained as a white powder, washed with diethyl ether, and dried under vacuum. Yield: 75% (0.25 g)

<sup>1</sup>H NMR (400 MHz, CDCl<sub>3</sub>) δ 8.32 (d, 2H, *dmphen*), 7.85 (s, 2H, *dmphen*), 7.78 (d, 2H, *dmphen*), 3.35 (s, 6H, Me-*dmphen*), 3.18 – 2.91 (m, 2H, ethene,  $J_{Pt} = 84$  Hz), 2.42 – 2.12 (m, 1H,  $J_{Pt} = 67$  Hz), -0.02 (s, 3H,  $J_{Pt} = 70$  Hz).

#### 5.3.2.4 Synthesis of Pt(II) NHC complexes **12-14-16**

A solution of silver triflate (0.17 g, 0.48 mmol) in acetone (2 mL) was added under stirring to a solution of the five-coordinate chloro-precursor (**i**) (0.23 g, 0.48 mmol) in the same solvent (6 mL). After 10 minutes, silver chloride was filtered off, and a solution of the appropriate **2-R** (0.48 mmol) in acetone (2 mL) was added to the clear filtrate. The mixture was stirred at room temperature for 72 hours protected from light. The resulting solid was filtered off and the solvent was removed under vacuum to obtain a yellow solid, which was recrystallized from DCM/diethyl ether as a white powder.

**12:** Yield 75% (0.36 g). <sup>1</sup>H NMR (400 MHz, CD<sub>3</sub>OD) δ 8.72 (d, 1H, H-4 or H-7 *dmphen*), 8.69 (d, 1H, H-7 or H-4 *dmphen*), 8.19 (d, 1H, H-3 or H-8 *dmphen*), 8.08 (br, 2H, H-5 and H-6 *dmphen*), 8.05 (d, 1H, H-8 or H-3 *dmphen*, partially hidden), 7.26 (d, 1H, H-Im), 6.93 (d, 1H, H-Im), 5.75 (d,  $J_{H1-H2} = 9.6$  Hz, 1H, H1-glu), 5.44 (t,  $J_{H2-H3} = 9.7$  Hz, 1H, H2-glu), 5.31 (t,  $J_{H3-H4} = 9.6$  Hz, 1H, H3-glu), 5.20 (t,  $J_{H4-H5} = 9.5$  Hz, 1H, H4-glu), 4.29 - 4.22 (m, 2H, H5-glu and H6-glu), 4.17

(m, 1 H, H6'-glu), 3.64 (s, 3H, Me-Im), 3.53 (s, 3H, 2-Me or 9-Me dmphen), 3.47 (s, 3H, 9-Me or 2-Me dmphen), 2.79 (m, 1H,  $J_{Pt}$  = 70.7 Hz, ethene), 2.61 - 2.38 (m, 3H, ethene), 2.16 (s, 3H, OAc), 2.10 (s, 3H, OAc), 2.03 (s, 3H, OAc), 1.16 (s, 3H, OAc), 0.27 (s, 3H,  $J_{Pt}$  = 50.6 Hz, Pt-Me).  $^{13}\text{C}$  NMR (100 MHz,  $\text{CD}_3\text{OD}$ )  $\delta$  174.8 ( $J_{Pt}$  = 703 Hz), 170.5, 169.8, 169.4, 168.2, 161.5, 159.5, 145.9, 139.3, 139.1, 138.7, 129.0, 127.2, 126.9, 126.4, 126.3, 125.0, 124.9, 120.8 (q,  $J_{C-F}$  = 328 Hz), 117.5, 84.4, 74.6, 71.9, 68.2, 68.1, 62.1, 37.8, 30.7 ( $J_{Pt}$  = 352 Hz), 29.6, 28.9, 28.8 ( $J_{Pt}$  = 340 Hz), 20.7, 20.6, 20.4, 19.9, -6.2 ( $J_{Pt}$  = 467 Hz).

**14:** Yield 71% (0.34 g)  $^1\text{H}$  NMR (400 MHz,  $\text{CD}_3\text{OD}$ )  $\delta$  8.71 (d, 1H, H-4 or H-7 dmphen), 8.69 (d, 1H, H-7 or H-4 dmphen), 8.13 (d, 1H, H-3 or H-8 dmphen), 8.09 (d, 1H, H-8 or H-3 dmphen, partially hidden), 8.07 (br, 2H, H-5 and H-6 dmphen), 7.13 (d, 1H, H-Im), 6.94 (d, 1H, H-Im), 5.72 (d,  $J_{H1-H2}$  = 9.4 Hz, 1H, H1-glu), 5.62 (d,  $J_{H3-H4}$  = 2.9 Hz, 1H, H4-glu), 5.44 (t,  $J_{H2-H3}$  = 10.1 Hz, 1H, H2-glu), 5.24 (dd, 1H, H3-glu), 4.44 (t,  $J_{H5-H6}$  = 6.5 Hz, 1H, H-5), 4.09 (m, 2H, H-6 and H-6'), 3.62 (s, 3H, Me-Im), 3.54 (s, 3H, 2-Me or 9-Me dmphen), 3.49 (s, 3H, 9-Me or 2-Me dmphen), 2.80 (m, 1H,  $J_{Pt}$  = 75.6 Hz, ethene), 2.60 (m, 1H,  $J_{Pt}$  = 79.8 Hz, ethene), 2.56 - 2.43 (m, 2H, ethene), 2.19 (s, 3H, OAc), 2.13 (s, 3H, OAc), 2.00 (s, 3H, OAc), 1.25 (s, 3H, OAc), 0.25 (s, 3H,  $J_{Pt}$  = 49.8 Hz, Pt - Me).  $^{13}\text{C}$  NMR (100 MHz,  $\text{CD}_3\text{OD}$ )  $\delta$  174.4 ( $J_{Pt}$  = 691 Hz), 170.6, 170.3, 169.7, 168.4, 161.6, 160.7, 145.7, 139.1, 138.9, 138.5, 129.1, 128.9, 126.7, 126.4, 126.2, 126.1, 124.2, 120.4 (q,  $J_{C-F}$  = 329 Hz), 118.1, 84.7, 73.4, 70.5, 67.4, 66.6, 61.2, 36.9, 29.7 ( $J_{Pt}$  = 352 Hz), 28.8 ( $J_{Pt}$  = 348 Hz), 28.3, 27.8, 19.3, 19.0 (x2), 18.7, -7.3 ( $J_{Pt}$  = 463 Hz).

**16:** Yield 81% (0.27 g)  $^1\text{H}$  NMR (400 MHz,  $\text{CD}_3\text{OD}$ )  $\delta$  8.75 (d, 2H, H-4 and H-7 dmphen, 1H), 8.14 (d, 2H, H-3 and H-8 dmphen, partially hidden), 8.12 (s, 2H, H-5 and H-6 dmphen), 6.99 (d, 1H, H-Im), 6.92 (d, 1H, H-Im), 4.08 (q, 2H,  $\text{CH}_2\text{Me-Im}$ ), 3.53 (s, 3H, Me Im), 3.36 (s, 6H, 2-Me and 9-Me dmphen), 2.47 (s,



$J_{Pt} = 76.8$  Hz, 4H, ethene), 0.71 (t, 3H, CH<sub>2</sub>Me-Im), 0.17 (s,  $J_{Pt} = 49.2$  Hz, 3H, Pt-Me). <sup>13</sup>C NMR (100 MHz, acetone-d<sub>6</sub>)  $\delta$  169.5 ( $J_{Pt} = 710$  Hz), 161.7 ( $J_{Pt} = 32$  Hz), 145.7, 138.7, 128.7, 126.4, 124.6 (q, JC-F = 321 Hz), 123.7, 119.8, 44.2, 36.6, 28.8 ( $J_{Pt} = 360$  Hz), 27.9 (JPt = 23 Hz), 15.1, -7.4 ( $J_{Pt} = 469$  Hz).

### 5.3.2.5 Synthesis of the deprotected Pt(II) NHC complexes **13-15**

The complexes were obtained according to the procedure described above, but using methanol as solvent. The compounds were re-crystallized from methanol/diethyl ether.

**13:** Yield 68% (0.26 g). <sup>1</sup>H NMR (400 MHz, CD<sub>3</sub>OD)  $\delta$  8.59 (d, 1H, H-4 or H-7 dmphen), 8.53 (d, 1H, H-7 or H-4 dmphen), 7.97 (d, 1H, H-3 or H-8 dmphen), 7.96 (s, 2H, H-5 and H-6 dmphen), 7.95 (d, 1H, H-8 or H-3 dmphen), 7.04 (d, 1H, H-Im), 6.83 (d, 1H, H-Im), 5.35 (d,  $J_{H1-H2} = 9.0$  Hz, 1H, H1-glu), 3.64 (m, 2H), 3.48 (s, 3H, Me-Im), 3.46 (s, 3H, 2-Me or 9-Me dmphen), 3.45-3.26 (m, 4H), 3.41 (s, 3H, 9-Me or 2-Me dmphen), 2.79 (m, 1H,  $J_{Pt} = 79.2$  Hz, ethene), 2.68 (m, 1H,  $J_{Pt} = 77.2$  Hz, ethene), 2.40 (m, 2H,  $J_{Pt} = 76.5$  Hz, ethene), 0.15 (s, 3H, JPt = 49.2 Hz, Pt-Me). <sup>13</sup>C NMR (100 MHz, CD<sub>3</sub>OD)  $\delta$  173.3 ( $J_{Pt} = 704$  Hz), 161.0, 160.8, 145.9, 145.7, 138.6, 128.9, 128.6, 126.4, 126.3, 125.8 (x2), 123.3, 120.6 (q, JC-F = 319 Hz), 117.9, 87.2, 78.8, 76.6, 72.5, 69.1, 59.9, 36.6, 29.8 ( $J_{Pt} = 350$  Hz), 28.9 ( $J_{Pt} = 352$  Hz), 28.0, 27.7, -7.7 ( $J_{Pt} = 464$  Hz).

**15:** Yield 65% (0.25 g). <sup>1</sup>H NMR (400 MHz, CD<sub>3</sub>OD)  $\delta$  8.64 (d, 1H, H-4 or H-7 dmphen), 8.57 (d, 1H, H-7 or H-4 dmphen), 8.02 (d, 1H, H-3 or H-8 dmphen), 8.00 (s, 2H, H-5 and H-6 dmphen), 7.98 (d, 1H, H-8 or H-3 dmphen, partially hidden), 7.05 (d, 1H, , H-Im), 6.86 (d, 2H, H-Im), 5.33 (d,  $J_{H1-H2} = 8.9$  Hz, 1H, H1-glu), 4.02 (m, 1H), 3.70-3.60 (m, 4H), 3.51 (s, 3H, Me-Im), 3.50 (s, 3H, 2-Me or

9-Me *dmphen* ), 3.47 (m, 1H), 3.44 (s, 3H, 9-Me or 2-Me *dmphen*), 2.85 (m, 1H,  $J_{Pt} = 80.6$  Hz, ethene), 2.72 (m, 1H, ethene), 2.44 (m, 2H,  $J_{Pt} = 75.8$  Hz, ethene), 0.19 (s, 3H,  $J_{Pt} = 49.1$  Hz, Pt-Me).  $^{13}C$  NMR (100 MHz,  $CD_3OD$ )  $\delta$  172.6 ( $J_{Pt} = 709$  Hz), 161.0, 160.9, 145.9, 145.7, 138.6, 138.5, 129.0, 128.6, 126.3, 126.2, 125.7 (x2), 123.3, 120.4 (q,  $J_{C-F} = 316$  Hz), 118.1, 87.5, 77.4, 73.6, 69.4, 68.4, 60.4, 36.6, 29.9 ( $J_{Pt} = 352$  Hz), 29.0 ( $J_{Pt} = 352$  Hz), 27.9, 27.7, -7.6 ( $J_{Pt} = 468$  Hz).

#### 5.3.2.6 Synthesis of the Pt(IV) precursor (*e*)

A suspension of red  $[PtMe_2(phen)]$  (0.3 g, 0.70 mmol) was suspended in acetone (8mL) and MeI (0.5 mL, 8 mmol) was added. Immediately the colour of the mixture turned to yellow, and the product was isolated by removing the solvent under vacuum (yield > 99%).

$^1H$  NMR (400 MHz, Acetone)  $\delta$  9.40 (dd, 2H,  $J_{Pt} = 19$ Hz, H-*phen*), 8.92 (m, 2H, H-*phen*), 8.34 (s, 2H, H-*phen*), 8.22 (m, 2H, H-*phen*), 1.62 (s, 6H,  $J_{Pt} = 72$  Hz,  $Me_{eq}$ -Pt), 0.64 (s, 3H,  $J_{Pt} = 71$  Hz,  $Me_{ax}$ -Pt).

#### 5.3.2.7 Synthesis of the Pt(IV) NHC complexes **17** and **19**

The precursor *e* (0.14 g 0.26 mmol) was suspended in acetone (8 mL) and silver triflate (0.066 g, 0.26 mmol) was added. After stirring 10 minutes AgI was filtered off and to the filtrate was added a solution of the appropriate **2-R** (0.15 g, 0.26 mmol) in acetone (2 mL). The mixture was stirred protected from light for 3 days at RT. Then, solid was filtered off and the solvent was removed under vacuum yielding a yellow oil. The product was obtained purified by  $SiO_2$  chromatography using 97:3 DCM/methanol.

**17:** Yield 94% (0.26 g).  $^1\text{H}$  NMR, (400 MHz,  $\text{CDCl}_3$ )  $\delta$ : 9.36 (m, 2H, H-2 *phen* and H-9 *phen*), 8.81 (d, 2H, H-4 and H-7 *phen*), 8.29 (dd, 1H, H-3 or H-8 *phen*), 8.24 (dd, 1H, H-8 or H-3 *phen*), 8.22 (ABq, 2H, H-5 and H-6 *phen*), 7.00 (d, 1H, H-Im), 6.82 (d, 1H, H-Im), 5.58 (d, 1H,  $J_{\text{H1-H2}} = 8.6$  Hz, H1-glu), 5.18 (m, 2H, H2-glu and H3-glu), 5.06 (t, 1H,  $J_{\text{H4-H3}} = 9.8$  Hz, H4-glu), 4.20 (m, 2H, H6-glu and H6'-glu), 4.01 (m, 1H, H5-glu), 3.23 (s, 3H, Me-Im), 2.11 (s, 3H, OAc), 2.10 (s, 3H, OAc), 1.98 (s, 3H, OAc), 1.20 (s, 3H, OAc), 1.41 (s, 3H,  $J_{\text{Pt}} = 70$  Hz,  $\text{Me}_{\text{eq-Pt}}$ ), 1.34 (s, 3H,  $J_{\text{Pt}} = 70$  Hz,  $\text{Me}_{\text{eq-Pt}}$ ), 0.08 (s, 3H,  $J_{\text{Pt}} = 55$  Hz,  $\text{Me}_{\text{ax-Pt}}$ ).  $^{13}\text{C}$  NMR,  $\text{CDCl}_3$ ,  $\delta$ : 173.1 ( $J_{\text{Pt}} = 648$  Hz), 170.5, 169.8, 169.5, 168.2, 148.0, 147.6, 146.0, 140.0, 139.4 (x2), 131.8 (x2), 128.9, 128.2, 126.7, 126.3, 125.3, 120.8 (q  $J_{\text{C-F}} = 322$  Hz), 117.9, 83.7, 74.5, 72.4, 69.0, 68.2, 65.9, 61.6, 37.7, 20.7, 20.6, 20.4, 19.8, 5.3 ( $J_{\text{Pt}} = 506$  Hz), -6.1 ( $J_{\text{Pt}} = 664$  Hz), -6.8 ( $J_{\text{Pt}} = 664$  Hz).  $^{195}\text{Pt}$  NMR,  $\text{CD}_3\text{OD}$ ,  $\delta$ : -2777. Anal. Calcd (found): ( $\text{C}_{34}\text{H}_{41}\text{F}_3\text{N}_4\text{O}_{12}\text{PtS}$ ): C, 41.59 (41.81); H, 4.21 (4.26); N, 5.71 (5.67).

**19:** Yield 93% (0.26 g)  $^1\text{H}$  NMR (400 MHz  $\text{CDCl}_3$ )  $\delta$ : 9.34 (m, 2H, H-2 and H-9 *phen*), 8.84 (m, 1H, H-4 or H-7 *phen*), 8.80 (m, 1H, H-7 or H-4 *phen*), 8.28 (dd, 1H, H-3 *phen* or H-8 *phen*), 8.24 (dd, 1H, H-8 or H-3 *phen*), 8.22 (s, 2H, H-5 and H-6 *phen*), 7.07 (d, 1H, H-Im), 6.86 (d, 1H, H-Im), 5.53 (d, 1H,  $J_{\text{H1-H2}} = 9.4$  Hz, H1-gal), 5.49 (d, 1H,  $J_{\text{H4-H3}} = 3.2$  Hz, H4-gal), 5.39 (t, 1H,  $J_{\text{H2-H3}} = 9.4$  Hz H-2 galactose), 5.02 (dd, 1H, H-3 galactose), 4.13 (m, 2H, H5-gal and H6-gal), 4.03 (m, 1H, H6'-gal), 3.20 (s, 3H, Me-Im), 2.18 (s, 3H, OAc), 2.10 (s, 3H, OAc), 1.97 (s, 3H, OAc), 1.41 (s, 3H,  $J_{\text{Pt}} = 68$  Hz,  $\text{Me}_{\text{eq-Pt}}$ ), 1.36 (s, 3H,  $J_{\text{Pt}} = 70$  Hz,  $\text{Me}_{\text{eq-Pt}}$ ), 1.31 (s, 3H, OAc), 0.06 (s, 3H,  $J_{\text{Pt}} = 55$  Hz,  $\text{Me}_{\text{ax-Pt}}$ ).  $^{13}\text{C}$  NMR,  $\text{CDCl}_3$ ,  $\delta$ : 172.9 ( $J_{\text{Pt}} = 640$  Hz), 170.5, 169.9, 169.7, 168.4, 148.5, 147.8, 146.0, 139.7, 139.5, 131.8, 128.9 (x2), 128.3 (x2), 126.4, 126.2, 125.3, 124.0 (q  $J_{\text{C-F}} = 327$  Hz), 118.7, 84.2, 73.5, 70.7, 67.3, 67.0, 61.3, 37.6, 20.8, 20.7, 20.4, 20.0, 5.4 ( $J_{\text{Pt}} = 508$  Hz), -

6.3 ( $J_{Pt} = 659$  Hz), -6.6 ( $J_{Pt} = 658$  Hz).  $^{195}\text{Pt}$  NMR,  $\text{CD}_3\text{OD}$ ,  $\delta$ : -2789. Anal. Calcd (found): ( $\text{C}_{34}\text{H}_{42}\text{F}_3\text{N}_4\text{O}_{12}\text{PtS}$ ): C, 41.59 (41.75); H, 4.21 (4.10); N, 5.71 (5.83).

#### 5.3.2.8 Synthesis of the deprotected Pt(IV) NHC complexes **18** and **20**

The corresponding peracetylated complex (**17** or **19**) (0.10 g, 0.10 mmol) was treated in 5.0 mL of methanol containing 5% mol/mol of KOH. After 10 minutes stirring at room temperature, the complexes were crystallized by slow addition of diethyl ether to the reaction mixture.

**18**: Yield 92% (0.073 g).  $^1\text{H}$  NMR,  $\text{CD}_3\text{OD}$ ,  $\delta$ : 9.42 (m, 2H, H-2 *phen* and H-9 *phen*), 8.87 (m, 2H, H-4 and H-7 *phen*), 8.27 (s, 2H, H-5 and H-6 *phen*), 8.19 (dd, 1H, H-3 or H-8 *phen*), 8.14 (dd, 1H, H-8 and H-3 *phen*), 7.28 (d, 1H, H-Im), 7.09 (d, 1H, H-Im), 4.86 (d, 1H,  $J_{H1-H2} = 6.3$  Hz, H1-glu), 3.63 (m, 1H, H6-glu), 3.49 (m, 1H, H6'-glu), 3.59 (s, 3H, Me-Im), 3.25 (app t, 2H, H2-glu and H4-glu), 2.71 (t, 1H, H3-glu), 2.66 (m, 1H, H5-glu), 1.46 (s, 3H,  $J_{Pt} = 69$  Hz,  $\text{Me}_{eq}\text{-Pt}$ ), 1.42 (s, 3H,  $J_{Pt} = 69$  Hz,  $\text{Me}_{eq}\text{-Pt}$ ), 0.03 (s, 3H,  $J_{Pt} = 53$  Hz,  $\text{Me}_{ax}\text{-Pt}$ ).  $^{13}\text{C}$  NMR,  $\text{CD}_3\text{OD}$ ,  $\delta$ : 170.8 ( $J_{Pt} = 645$  Hz), 148.9, 148.5, 146.1, 139.2, 139.1, 138.5, 131.9, 131.7, 128.0, 127.8, 126.2, 125.6, 124.4, 121.1 (q  $J_{C-F} = 322$  Hz), 118.3, 85.8, 78.9, 76.5, 72.1, 68.9, 60.8, 36.8, 3.7 ( $J_{Pt} = 511$  Hz), -7.1 ( $J_{Pt} = 663$  Hz), -7.4 ( $J_{Pt} = 663$  Hz).  $^{195}\text{Pt}$  NMR,  $\text{CD}_3\text{OD}$ ,  $\delta$ : -2777. Anal. Calcd (found): ( $\text{C}_{26}\text{H}_{33}\text{F}_3\text{N}_4\text{O}_8\text{PtS}$ ): C, 38.38 (38.12); H, 4.09 (4.19); N, 6.89 (6.67).

**20**: Yield 83% (0.068 g).  $^1\text{H}$  NMR (400 MHz,  $\text{CD}_3\text{OD}$ )  $\delta$ : 9.43 (d, 1H, H-2 or H-9 *phen*), 9.42 (d, 1H, H-9 or H-2 *phen*), 8.85 (d, 1H, H-4 or H-7 *phen*), 8.82 (d, 1H, H-7 *phen* or H-4 *phen*), 8.24 (s, 2H, H-5 and H-6 *phen*), 8.16 (dd, 1H, H-3 or H-8 *phen*), 8.13 (dd, 1H, H-8 or H-3 *phen*), 7.34 (d, 1H, H-Im), 7.05 (d, 1H, H-Im), 4.86 (d, 1H, partially hidden, H1-gal), 3.77 (d, 1H), 3.59-3.44 (m, 2H), 3.55 (s,

3H, Me-Im), 3.32-3.29 (m, 2H), 3.30 (t, 1H), 2.91 (dd, 1H), 1.43 (s, 3H,  $J_{Pt} = 69$  Hz, Me<sub>eq</sub>-Pt), 1.42 ( $J_{Pt} = 69$  Hz, Me<sub>eq</sub>-Pt), 0.02 ( $J_{Pt} = 55$  Hz, Me<sub>ax</sub>-Pt). <sup>13</sup>C NMR, CD<sub>3</sub>OD,  $\delta$ : 172.45 x2 ( $J_{Pt} = 655$  Hz), 150.4, 150.1, 147.45, 140.5 x2, 133.2, 133.1, 129.4, 129.1, 127.7, 127.0, 125.7, 120.0, 87.7, 79.1, 74.8, 70.6, 69.8, 62.0, 38.2, 5.06 ( $J_{Pt} = 502$  Hz), -5.67 ( $J_{Pt} = 664$  Hz), -5.98 ( $J_{Pt} = 671$  Hz). d: -2779. Anal. Calcd (found): (C<sub>26</sub>H<sub>33</sub>F<sub>3</sub>N<sub>4</sub>O<sub>8</sub>PtS): C, 38.38 (38.21); H, 4.09 (4.15); N, 6.89 (6.77).

### 5.3.3 X-ray crystallography

X-ray crystallographic analysis were performed in collaboration with Prof. Angela Tuzi from the University of Naples Federico II.

Single crystals of **12** were obtained under slow diffusion of diethyl ether into a methanol solution at room temperature. Crystals of **19** were obtained under slow diffusion of diethyl ether stratified on a DCM solution of the complex, at room temperature. Data were measured at room temperature using a Bruker-Nonius KappaCCD four-circle diffractometer (graphite monochromated Mo K $\alpha$  radiation,  $\lambda = 0.71073$  Å, CCD rotation images, thick slices,  $\varphi$  and  $\omega$  scans to fill asymmetric unit. Reduction of data and semiempirical absorption correction were done using SADABS program. Structure was solved by direct methods (SIR97 program<sup>51</sup>) and refined by the full-matrix least-squares method on F<sup>2</sup> using SHELXL-2018/3 program<sup>52</sup> with the aid of the program WinGX.<sup>53</sup> Anisotropic parameters were used for non-H atoms. All the H atoms were generated stereochemically and refined accordingly to the riding model with C–H distances in the range 0.93–0.98 Å and U<sub>iso</sub>(H) equal to 1.2·U<sub>eq</sub> of the carrier atom (1.5·U<sub>eq</sub> for C<sub>methyl</sub>). Some acetate groups and triflate anions are affected by thermal disorder that accounts for the rather high values of the displacement parameters. Some constraints were

introduced in the last stage of refinement to regularize the geometry and the displacement parameters using DFIX, SAME, SIMU and DELU instructions of SHELXL program. Disordered lattice solvent is present. It was not possible to model the disorder and the PLATON SQUEEZE procedure was used to exclude the contribution of solvent to the structure. The figures were generated using ORTEP-3 53 and Mercury CSD 4.2 54 programs.

Crystallographic data for **12** and **19** were deposited in the Cambridge Crystallographic Data Centre with deposition number CCDC 1904738 and CCDC1972544 respectively. These data can be obtained free of charge from [www.ccdc.cam.ac.uk/data\\_request/cif](http://www.ccdc.cam.ac.uk/data_request/cif).

#### 5.3.4 NMR studies

##### 5.3.4.1 In-solution reactivity

**12** and **17** (10 mmol) were dissolved in DMSO-d<sub>6</sub> (1 mL). The calculated volumes (60 µL) of the two solutions were diluted with the appropriate volume of 25 mM PB buffer in D<sub>2</sub>O (pH 7.5) or DMSO-d<sub>6</sub> to provide final 1 mM concentration of the complex. Spectra were recorded at different time to evaluate the solution stability over 7 days.

##### 5.3.4.2 Studies of reduction of **17**

Reduction experiments were performed by adding ascorbic acid or glutathione to the complex **17** in PB-DMSO pH 7.5, resulting in 1 mM concentrations of the complex and 10-25 mM of ascorbic acid or 2 mM of glutathione. The solutions were incubated at 37° C and spectra were measured over time along 7 days.

### 5.3.5 *Electrochemical Studies*

Electrochemical data were obtained by cyclic voltammetry (CV) and differential pulse voltammetry (DPV) under N<sub>2</sub> at 20 °C using DMSO as solvent and [Et<sub>3</sub>MeN][BF<sub>4</sub>] (0.10 M) as supporting electrolyte. CV and DPV were performed in a three-electrode cell configuration consisting of a working glassy carbon (GC) electrode and two platinum wires as counter electrode and quasi-reference electrode. Prior to voltammetric experiments, the working electrode was polished with alumina, rinsed twice with water and acetone and then dried. The analytes were introduced into the cell with concentration of 1mM. In CV the scanning rate was 0.01 Vs<sup>-1</sup> and in DPV the pulse size was 0.025 V. All potentials are referred to the ferrocene/ferrocenium(Fc/Fc<sup>+</sup>) couple.

### 5.3.6 *Evaluation of the biological activity*

Cell culture and experiments involving cytotoxicity assays, Western blot analysis, and analysis on the mechanism of cell death were performed in collaboration with Prof. Daria M. Monti research group at University of Naples Federico II. Cellular uptake experiments were performed in collaboration with Prof. Angela Amoresano research group at University of Naples Federico II.

#### 5.3.6.1 *Cytotoxicity Experiments*

To test the cytotoxicity of **12-21**, cells were seeded at a density of  $2.5 \times 10^3$  cells per well in 96-well plates. 24 h after seeding, increasing concentrations of compounds were added to the cells (0.1–200 μM). Cell viability was assessed by the MTT (3-(4,5-dimethylthiazol-2-yl)-2,5-diphenyltetrazolium bromide) assay after 48 h, as previously described.<sup>158</sup> Cell survival was expressed as the

percentage of viable cells in the presence of the Pt drug compared to the controls, represented by untreated cells and cells supplemented with identical volumes of DMSO (maximum 1% final volume). Each sample was tested in three independent analyses, each carried out in triplicate.

#### *5.3.6.2 Uptake Experiments*

To study the uptake of Pt drugs, A431 cells were incubated for 48 h in the presence of each drug, tested at the IC<sub>50</sub> concentration. At the end of the incubation, Pt content was quantified by ICP-MS following a method previously reported.<sup>203</sup> Briefly, Pt concentration was measured with three replicates using an Agilent 7700 ICP-MS instrument (Agilent Technologies) equipped with a frequency-matching radio frequency (RF) generator and 3rd generation Octopole Reaction System (ORS3), operating with helium gas in ORF and the following parameters: RF power: 1550 W, plasma gas flow: 14 L min<sup>-1</sup>; carrier gas flow: 0.99 L min<sup>-1</sup>; He gas flow: 4.3 mL min<sup>-1</sup>. <sup>103</sup>Rh was used as an internal standard (final concentration: 50 µg L<sup>-1</sup>). Standard solutions have been prepared in 5 % nitric acid at four different concentrations (1, 10, 50, and 100 µg L<sup>-1</sup>).

#### *5.3.6.3 Analysis of cell death mechanism*

To determine ROS levels a fluorescent probe 2',7'-dichlorodihydrofluorescein diacetate (DCFDA, Sigma-Aldrich) was used. After treatment with 0.4 µM of **12** for different times (from 5 min to 48 h), cells were incubated with cell-permeable DCFDA probe, which fluorescence, upon oxidation by ROS, was measured using a PerkinElmer LS50 spectrofluorometer (525 nm emission wavelength, 488 nm excitation wavelength, 300 nm min<sup>-1</sup> scanning speed and 5 nm slit width for both excitation and emission). ROS production was expressed as a percentage of DCF



fluorescence intensity of the sample under test, with respect to the untreated sample. Each value was assessed by three independent experiments, each with three determinations. Significance was determined by the Student's t-test. To measure the mitochondrial membrane potential ( $\Delta\psi_m$ ) cells were plated at a density of  $2 \times 10^4$  cells per well and after 24 h were treated as described above. At the end of the treatment, the cells were incubated with 200 nM of the cationic lipophilic dye tetramethylrhodamine ethyl ester (TMRE) for 20 min at 37 °C. Then, cells were gently washed with 0.2% BSA in PBS three times and the fluorescence was measured in a microplate reader with peak  $\lambda(\text{ex})/\lambda(\text{em}) = 549/575$  nm. Each value is the mean of three independent experiments, each with three determinations. Significance was determined by the Student's t-test. For western blotting analyses, cells were treated with 0.4  $\mu\text{M}$  of **12** and then incubated at 37 °C. Then, western blotting, performed as reported by Galano et al.<sup>41</sup>, was used to determine intracellular levels of phosphorylated p38 (after 16 h of incubation), pro-caspase -3, -7, -9 and Bcl-2 (after 48 h of incubation). All antibodies were purchased from Cell Signal Technology (Danvers, MA, USA). To normalize the protein intensity levels, a specific antibody against internal standards was used, i.e. anti-GAPDH (Thermo Fisher, Rockford, IL, USA) or anti-actin (Sigma-Aldrich). The chemiluminescence detection system (SuperSignal® West Pico) was purchased from Thermo Fischer.

### 5.3.7 *Reactivity with model biomolecules*

UV-vis, fluorescence, and CD experiments were performed in collaboration with Prof. A. Merlino research group at University of Naples Federico II. ESI-MS experiments were performed in collaboration with Prof. Maria Monti research group at University of Naples Federico II.

#### *5.3.7.1 UV-vis measurements*

The complexes were first dissolved in pure DMSO and then diluted in the selected buffers at a final concentration of 50  $\mu$ M. Spectra have been collected using the following setup: 240-450 nm wavelength range, 400 nm/min scanning speed, 2.0 nm band width, 1.0 nm data pitch. UV-vis measurements of **12** and of **17** with HEWL and HSA were performed by diluting the compounds stock solutions to 50  $\mu$ M in in 90%-10% PB:DMSO pH 7.4. HEWL and HSA were added at about 17  $\mu$ M to yield a final metal/protein ratio of 3:1. Spectra were recorded over 7 days at room temperature. The same procedure was used in order to collect UV-vis spectra of ctDNA in the presence of the two platinum compounds. A solution of 10  $\mu$ M ct-DNA was added to a 50  $\mu$ M Pt solution containing in 90%-10% PB:DMSO pH 7.4. Spectra were collected over 7 days.

#### *5.3.7.2 Fluorescence experiments*

ctDNA was incubated with EtBr in a 1:50 molar ratio for 30 minutes at room temperature. Then, the complex was diluted in 10 mM ammonium acetate buffer at pH 7.5 up to a DNA final concentration of 200  $\mu$ M. The DNA-EtBr complex was then titrated with complexes solution at a concentration of 15 mM and fluorescence emission spectra were recorded exciting at 545 nm. The spectra were registered after an equilibration time of 5 minutes following each addition.

#### *5.3.7.3 Circular Dichroism experiments*

CD spectra of ctDNA were registered from 220 to 320 nm on a Jasco J-810 spectropolarimeter at 25°C in the presence of different amount of compound. Quartz cells with 0.1 cm path length were used. Each spectrum was obtained averaging three scans and subtracting contributions from the corresponding

reference (10 mM ammonium acetate buffer at pH 7.5). Spectra were collected using samples obtained upon 24 h incubation of DNA with metal complexes at a 1:0.5, 1:1 and 1:2 molar ratios. Other experimental settings were: 50 nm/min scan speed, 2.0 nm band width, 0.2 nm resolution, 50 mdeg sensitivity and 4 s response. CD spectra of HSA and HEWL were registered upon a 24 h incubation in the presence of **12** and **17** in a 1:3 protein to metal molar ratio.

#### *5.3.7.4 NMR experiments*

The interaction with 2-deoxyguanosine monophosphate was studied by adding the appropriate volume of a dGMP solution in PBS (25 mM) to the **12** or **17** in DMSO- $d_6$  to obtain final concentrations of 1 mM for the complexes and 4 mM for dGMP. Solutions were incubated at 37° C and spectra were recorded over 7 days.

#### *5.3.7.5 ESI-MS experiments*

A 20-mer double strand DNA (dsDNA) was obtained by annealing procedure starting from two complementary single-stranded DNA (ssDNA) with a nucleotide base sequence corresponding to 3'-CCA CCC GGA CCC CGT ACC TG-5' for single strand 1 (ssDNA1) and to 3'-CAG GTA CGG GGT CCG GGT GG-5' for single strand 2 (ssDNA2). The annealing reaction was carried out in water, mixing the single stranded oligonucleotides in equal molar amount for 2 minutes at 95°C and then cooling the mixture at room temperature for 45 minutes. 1Pt-Glu and 2Pt-Glu were dissolved in dimethyl sulfoxide (DMSO) (Bioshop, Burlington, ON, Canada) to a final concentration of 25 nmol/μl. Pt complexes were incubated with dsDNA in 10-fold molar excess at room temperature for 24h. Sample mixtures were diluted 1:10 in 15 mM ammonium acetate buffer at pH 6.8; spectra were recorded in negative mode using a Q-ToF Premier (Waters, Milford,

MA, USA) mass spectrometer. The acquisition was executed by direct injection at 10  $\mu\text{l min}^{-1}$  flow rate spanning the  $m/z$  range from 1000 to 3000. The capillary voltage was fixed to 2.7 kV, and source and desolvation gas temperatures at 70°C. Raw data were processed by MassLynx 4.1 (Waters, Milford, MA, USA) software

## 6 Glucosylated NHC Ru(II)-Arene complexes

### 6.1 General Overview

Ru(II)-arene NHC complexes attracted great interest in recent years, due to their flexible tunability which resulted in variegated biological activities.<sup>102,107,204–208</sup> The promising results, described in Chapter 5, obtained with platinum NHC complexes inspired the work reported in this section. Indeed, a panel of Ru(II)-arene complexes, whose structures is reported in **Figure 6.1**, has been designed.

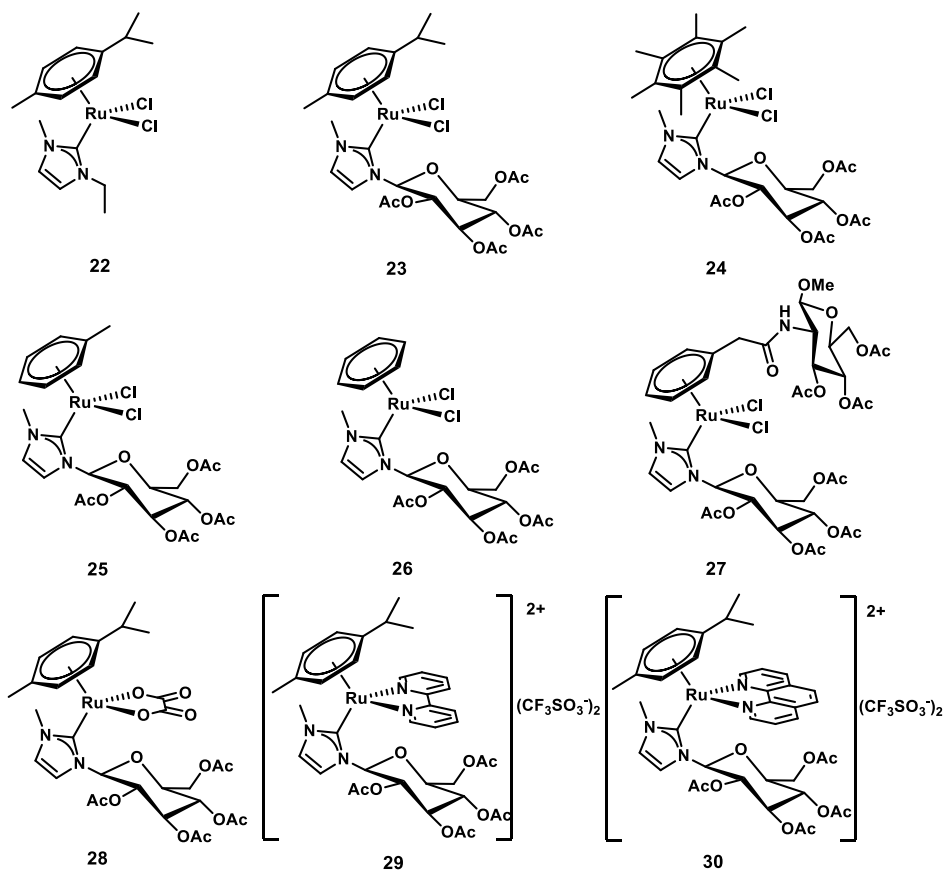


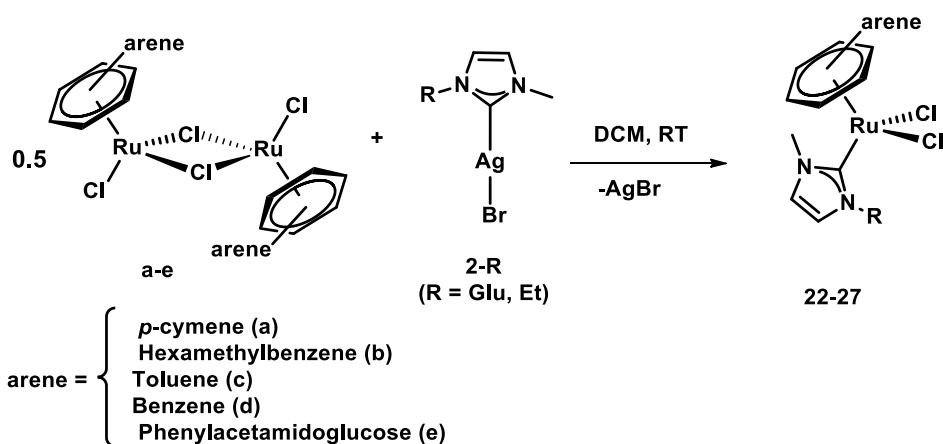
**Figure 6.1.** Ru(II)-arene complexes reported in this chapter

The complexes (**23-30**) displayed the same glucoconjugate NHC ligand used for platinum complexes **12** and **17** in Chapter 5, while the ethyl-carbene **22**, analogous to complex **16**, was designed as proof of concept to verify the impact of glycoconjugate ligands. Diversified substituent patterns on the arene ligands were explored, ranging from more electron rich *p*-cymene (**22-23**) and hexamethylbenzene (**24**), to less substituted toluene (**25**) and benzene (**26**). The derivative (**27**) was designed to have a second sugar unit on the arene ligand. Moreover, the *p*-cymene derivative was further modified to access complexes **28-30**: in the first one, the chlorido ligands were replaced by the anionic oxalate, in the latter ones by a neutral N,N'-chelating di-imine (2,2'-Bipyridine and 1,10-phenanthroline). The synthesis and the spectroscopic characterization of the novel complexes was performed. Structure-activity relationships for the members of this panel were collected by evaluating their hydrolytic behaviour, their reactivity with relevant biological nucleophiles, model proteins and DNA, as well as their cytotoxic activity. This part of the work was carried out during a period of research spent at the EPFL in Lausanne, under the supervision of Prof. Paul Dyson.

## 6.2 Results and Discussion

### 6.2.1 Synthesis and Spectroscopic Characterization of the complexes

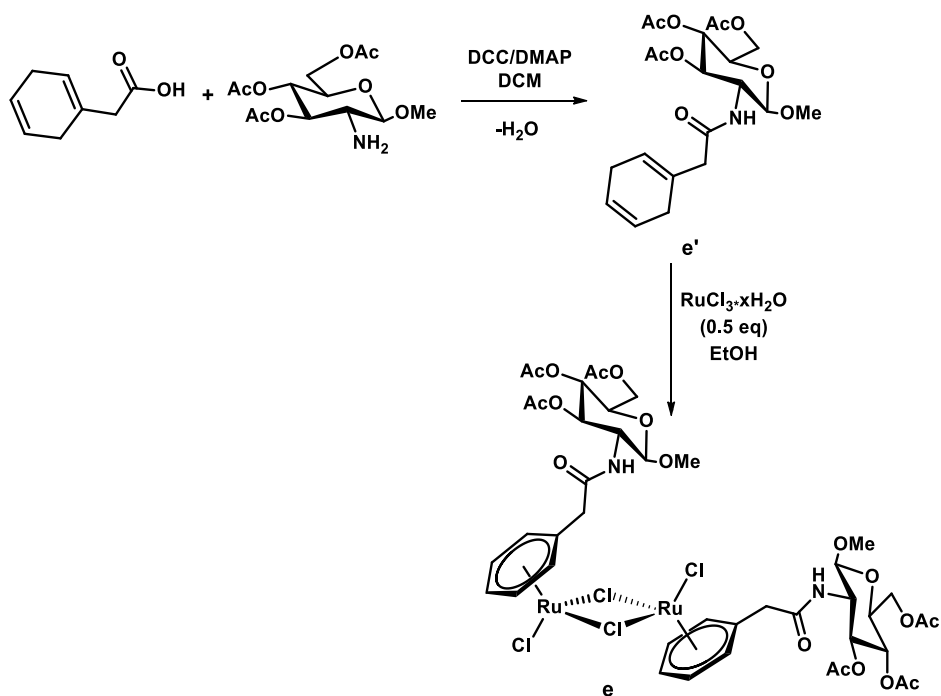
The dichlorido complexes **22-27** were prepared according to **Scheme 6.1**.



**Scheme 6.1.** Synthetic procedure to prepare **22-27**

The appropriate ruthenium(II) arene dimer **a-e** was reacted with 2 eq. of silver carbene **2-R** (R = Et or Glu) in DCM. After 36 h at RT AgBr was filtered off and the products were crystallized as red-orange powders by adding diethyl ether.

The precursor **e**, used to get complex **27** was synthesized as reported in **Scheme 6.2**.

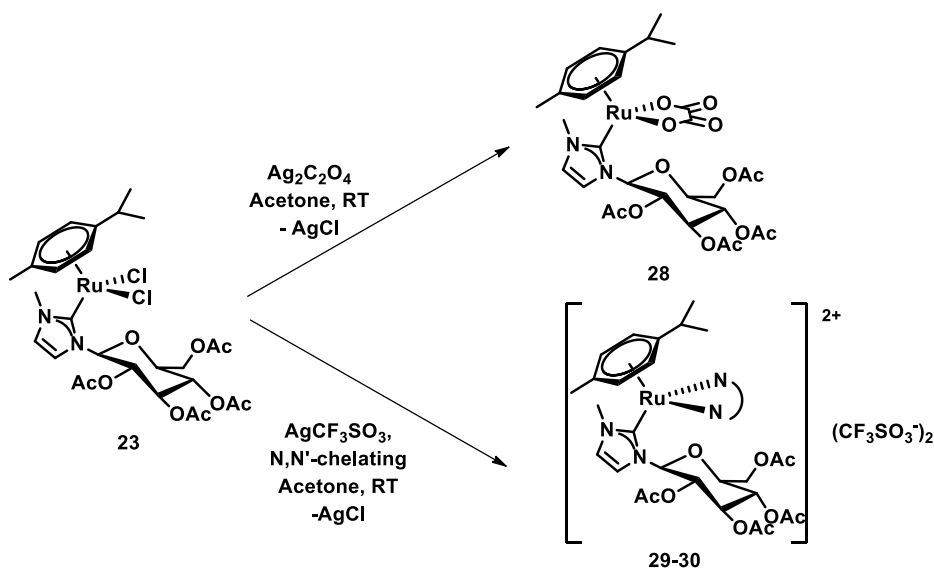


**Scheme 6.2.** Synthesis of Ru(II) arene dimer **e**

A DCC/DMAP-mediated coupling reaction of 2-(cyclohexa-1,4-dien-1-yl)acetic acid with the appropriate glucosamine derivative, yielded the diene **e'**. The diene was refluxed with RuCl<sub>3</sub>·xH<sub>2</sub>O in ethanol to afford the Ru(II) arene dimer **e**.



Finally, the derivatives **28-30** were synthesized starting from complex **23**, as reported in **Scheme 6.3**.

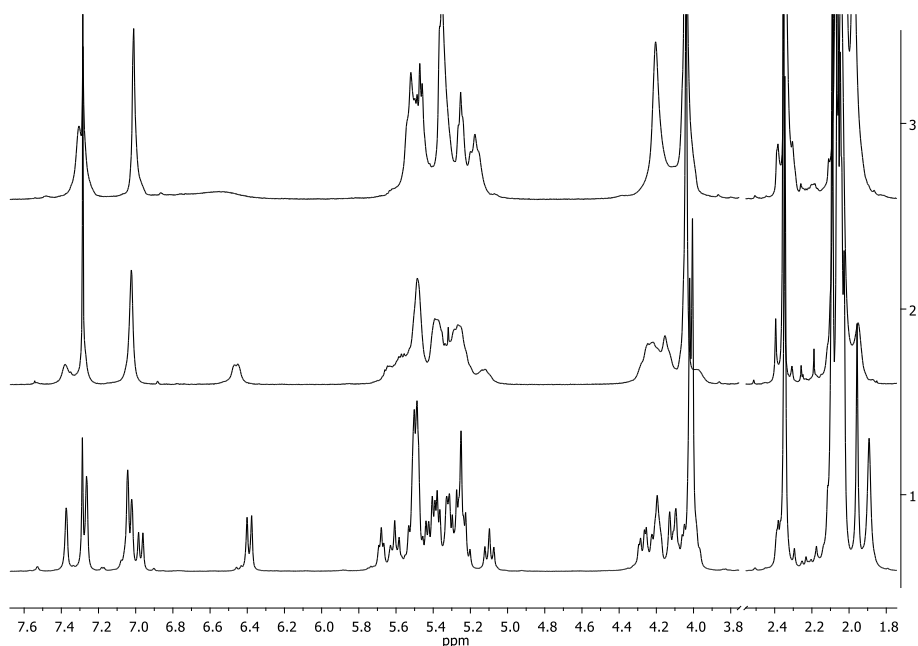


**Scheme 6.3.** Synthetic procedure to prepare **28-30**

The oxalate complex **28** was obtained by dissolving **23** in acetone in presence of a slight excess of silver oxalate. After 16 hours at RT, the suspension was filtered, and the solvent was removed under vacuum to afford **28** as a yellow solid. Compounds **29-30** were obtained by treating **23** with 2 eq. of silver triflate in acetone and by removing  $\text{AgCl}$ . The addition of 2,2'-Bipyridine (*bipy*) or 1,10-phenanthroline (*phen*) led to the formation of the products that were isolated after removal of the solvent, and recrystallization by DCM/diethyl ether.

All the compounds were characterized by mono- and bi-dimensional NMR spectroscopy. Notably, some of the  $^1\text{H}$  NMR spectra of compounds **22-27** showed diffused broadness in the signals when recorded at RT.

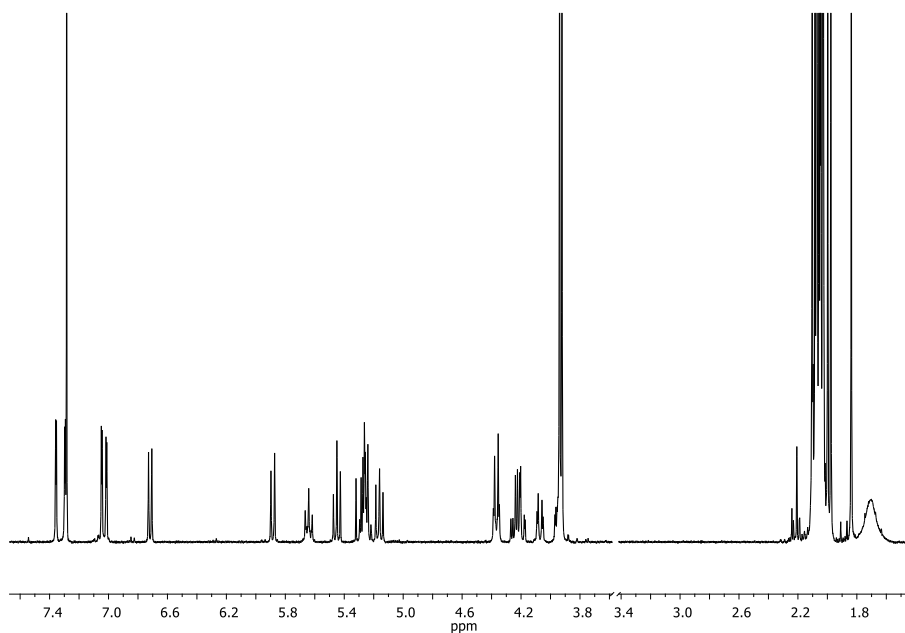
The broadening resolved in two distinct sets of signals when the spectra were collected at -10 °C, while coalescence of the signals to one single pattern was observed at 50 °C (**Figure 6.2**).



**Figure 6.2.**  $^1\text{H}$  NMR spectra of complex **25** in  $\text{CDCl}_3$  at -10 °C (trace 1), 25 °C (trace 2) and 50 °C (trace 3) and 400 MHz.

The two patterns of signals (trace 1 in **Figure 6.2**) were attributed to two different glucoconjugate species. The coalescence at high temperature (trace 3 in **Figure 6.2**) suggested that a slow dynamic process occurred in solution. Such phenomenon was individuated in the slow rotation of the NHC ligand about the  $\text{C}_{\text{carbene}}\text{-Ru}$  bond. The chirality led by the sugar fragment allowed to distinguish the two locked rotamers, since they displayed two distinct resonance patterns at low temperature. Similar observations were already reported in Ru(II) and Rh(III) complexes with chiral NHC.<sup>209–211</sup> Interestingly, the energy barriers associated to the rotation were strictly dependent on the substitution pattern on the arene ring,

and on the presence of chlorido or chelating ligands. Indeed, the broadening was not detected in the spectra of the hexamethyl complex **24** and of the *p*-cymene derivatives with chelating ligands **28-30** (Figure 6.3), which displayed two distinguished sets of signals at RT.



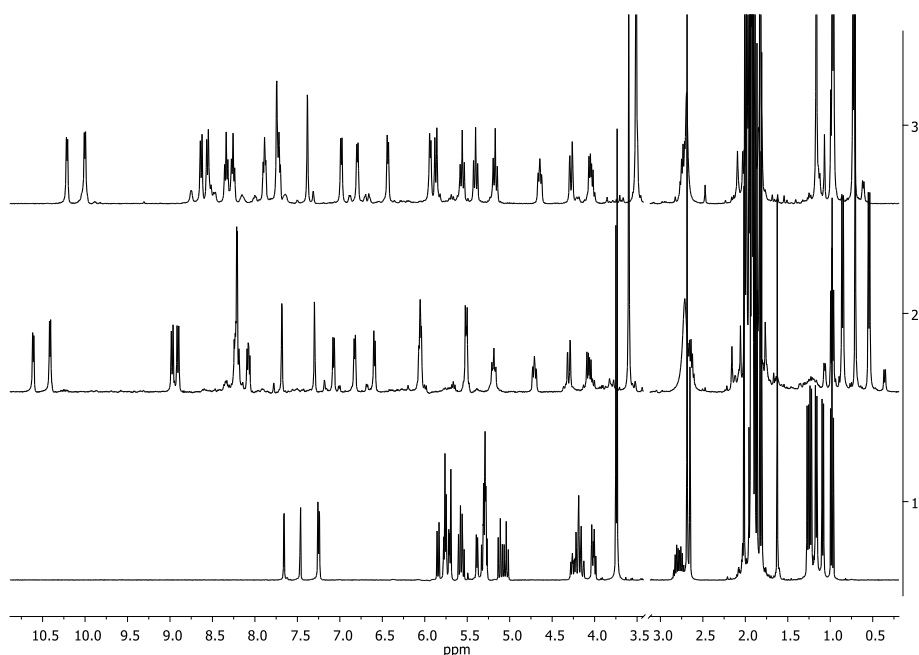


**Figure 6.3.**  $^1\text{H}$  NMR spectra of **24** (top) in  $\text{CDCl}_3$ , and **28** (trace 1), **29** (trace 2) and **30** (trace 3) in  $\text{Acetone-d}_6$ , at 400 MHz.

Moreover, the presence of the chiral NHC ligand made non-equivalent the two halves of *bipy* and *phen* in **29** and **30** respectively. In all the complexes, the protons of the arene ligands shifted upfield with respect the uncoordinated arenes. For instance, *p*-cymene protons resonated as four distinct doublets at *ca.* 5-6 ppm. Similarly, the  $^{13}\text{C}$  NMR spectra displayed broadening at RT due to the slow rotation of the carbene ligand. The NHC carbon resonated between at *ca.* 170-180 ppm, in agreement with literature data.<sup>212</sup> The identity of the compounds was confirmed by ESI-MS, elemental analysis and by the X-ray crystallography.

Single crystals of complexes **23** (Figure 6.4), **25** (Figure 6.5) and **28** (Figure 6.6) were obtained by slow diffusion of diethyl ether in DCM (**23**) and acetonitrile (**25** and **28**) solutions.

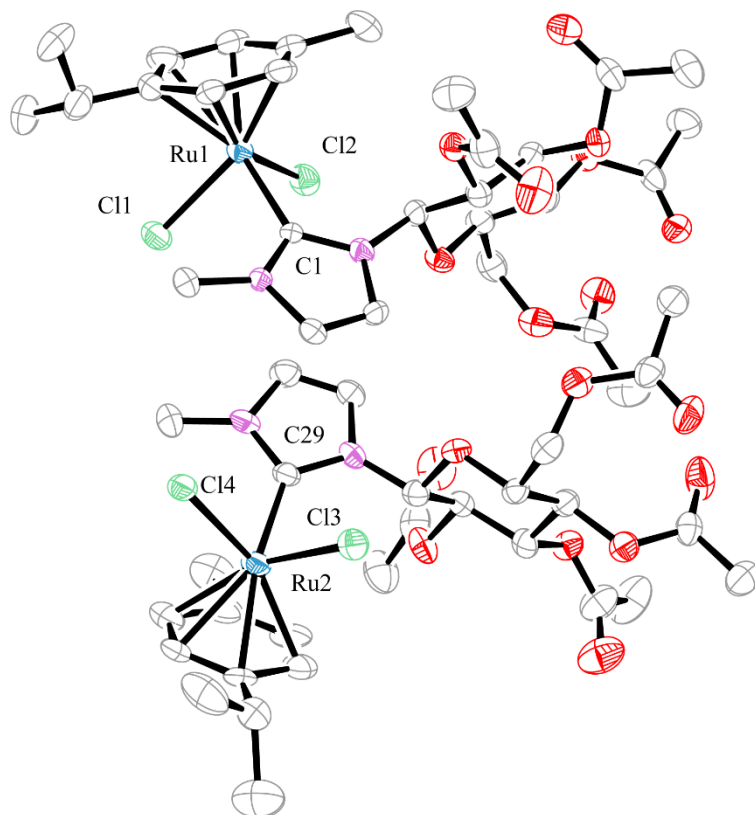


**Figure 6.4.** Crystal structure of compound **23**. Ellipsoids at 30% probability levels. Selected bond lengths [Å]: Ru1–Cl1 2.446(4), Ru1–Cl2 2.460(5), Ru1–C1 2.066(15)

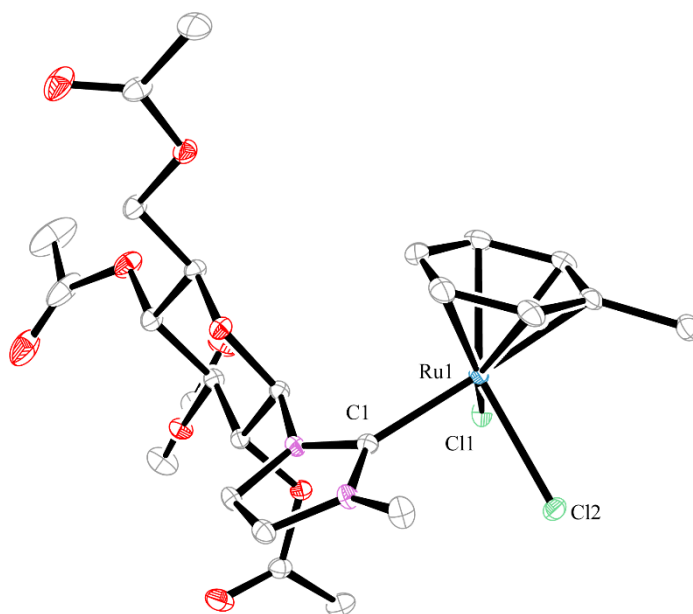


**Figure 6.5.** Crystal structure of compound **25**. Ellipsoids at 30% probability levels. Selected bond lengths [Å]: Ru1–Cl1 2.4016(10), Ru1–Cl2 2.4421(9), Ru1–C1 2.049(4).

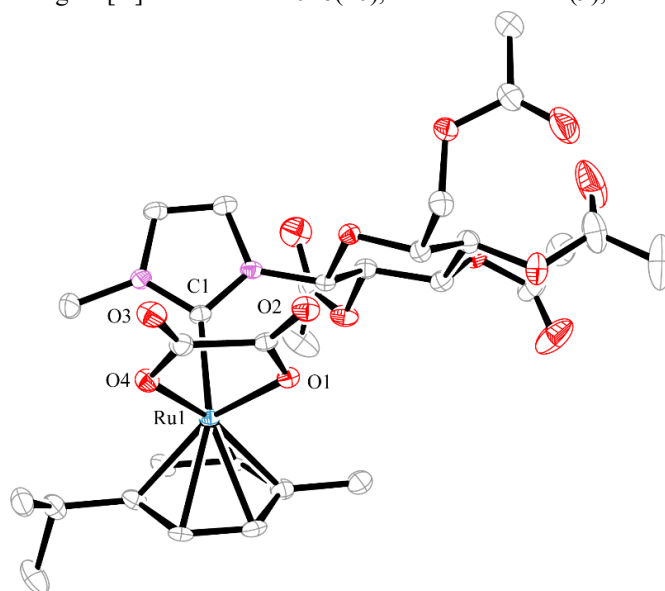


**Figure 6.6.** Crystal structure of compound **28**. Ellipsoids at 30% probability levels. Selected bond lengths [Å]: Ru1–O2 2.088(4), Ru1–O1 2.090(4) Ru1–O4 2.092(5)

The complexes crystallized in orthorhombic  $P2_12_12_1$  (#19) (**25**), triclinic  $P1$  (#1) (**23**), and monoclinic  $P2_1$  (#4) (**28**) space groups. They displayed the characteristic “piano-stool” geometry with the chlorido and the NHC ligands in “three-legs” positions. All bond angles and distances were found in the ranges detected for other Ru(II) arene complexes. The angles involving Ru and the legs of the stool are near  $90^\circ$  (with a range of  $84\text{--}92^\circ$ ) in the di-chlorido complexes **23** and **25**.<sup>206,213,214</sup> In the oxalate derivative **28** the angle observed bond for O1-Ru1-O4 was  $77.75^\circ$  indicating a strained five-membered chelated metallacycle.<sup>101</sup> O-Ru-C<sub>Carbene</sub> angles were found in the range  $84\text{--}86^\circ$ .

The glucosyl group was in a flat shape chair conformation, in  $\beta$  configuration with all the substituents on the pyranose ring in equatorial positions. The sugar mean plane was almost orthogonal to plane of the imidazole ring.

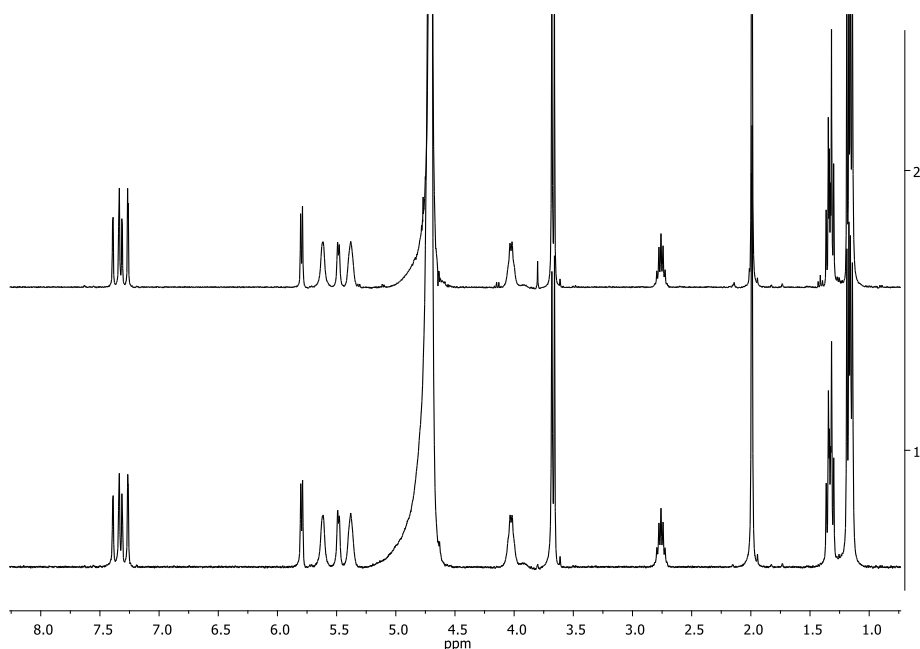
The acetyl groups and the alkyl substituents on the arene were placed far away to avoid unfavorable intermolecular interactions. In the crystals of complex **23** (**Figure 6.4**) two units with different orientations of the *p*-cymene, mutually rotated of  $90^\circ$ , were observed. In both the isopropyl group was oriented away from the sugar residue. Crystallographic data are reported in Appendix.

### 6.2.2 *Hydrolytic behaviour*

The reactivity of the complexes in aqueous media was studied by NMR, ESI-MS, and UV-vis spectroscopy. UV-vis absorption spectra of **22-30** in different aqueous buffers involving water, 100 mM sodium acetate pH 4.0 or 10mM sodium citrate pH 5.1 showed a profile that did not significantly change over 24 h, suggesting a good general stability of the compounds.  $^1\text{H}$  NMR and ESI-MS spectra were collected by keeping the complexes at 37 °C, over 3 days.

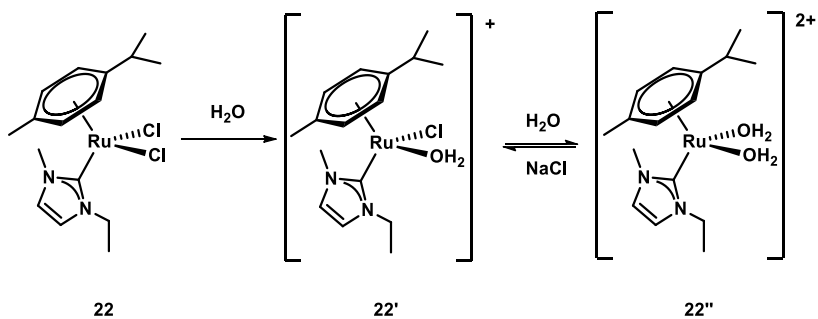
As observed for RAPTA-type complexes, the substitution of the chlorido ligands for water molecules was observed in compounds **22-27**. In glycoconjugate complexes this substitution gave rise to diastereoisomeric species with overlapping signals, upon formation of an additional chiral centre at the ruthenium atom. The coexistence of multiple diastereoisomers complicated the NMR spectra, and therefore some general considerations will be illustrated for the ethyl complex **22**. Following its dissolution in water, the  $^1\text{H}$  NMR spectrum showed the presence of two different species and no change in the spectra was observed over 72 h at 37° C (**Figure 6.7**).





**Figure 6.7.**  $^1\text{H}$  NMR spectra of **22** in  $\text{D}_2\text{O}$  (trace 1 = Start, trace 2 = 72 h) at 400 MHz.

The two species were unequivocally identified, by comparing the  $^1\text{H}$  NMR spectra recorded after the addition of 1 eq., and then 2 eq. of  $\text{AgNO}_3$ , to a freshly dissolved sample of **22** (Figure 6.8).



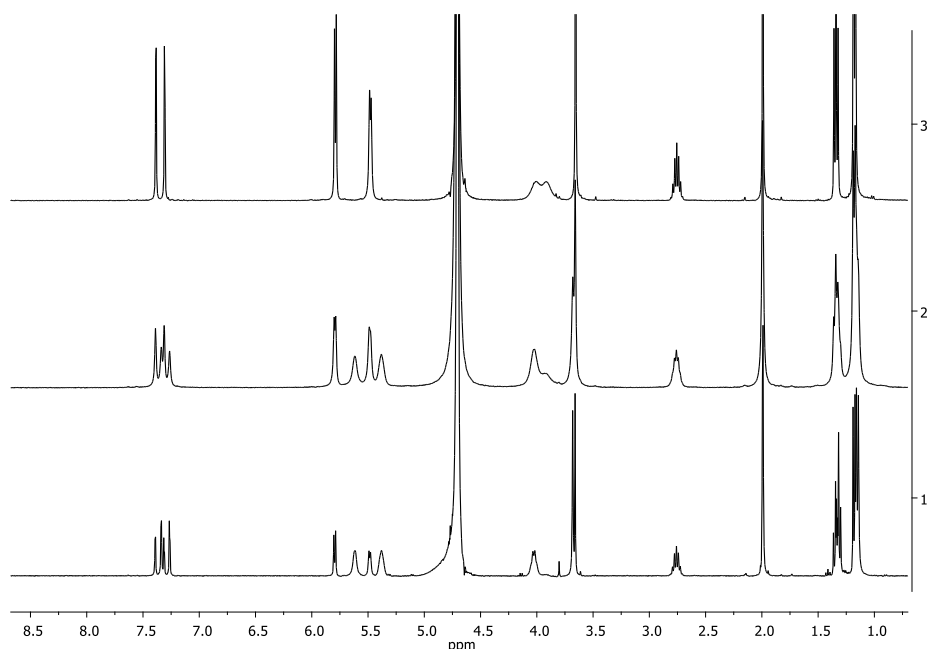


**Figure 6.8.** Schematic representation of the hydrolysis of **22** (top);  $^1\text{H}$  NMR spectra of **22**: in  $\text{D}_2\text{O}$  (trace 1), after the addition of 1 eq. of  $\text{AgNO}_3$  (trace 2), and after the addition of 2 eq. of  $\text{AgNO}_3$  (trace 3) at 400 MHz.

Compared to the spectra previously recorded in water (trace 1 in **Figure 6.8**), no change in the position and in the number of peaks was detected after the addition of the first equivalent of  $\text{AgNO}_3$  (trace 2 in **Figure 6.8**). This excluded the presence of the di-chlorido complex (**22**) in solution. Following the second addition, only one of the two species was detected (trace 3 in **Figure 6.8**) and the identified as the di-aqua complex (**22''** in **Figure 6.8**) while the other set of signals was attributed to the mono-aqua species (**22'** in **Figure 6.8**). The two species are in equilibrium, reversible upon addition of an excess of  $\text{NaCl}$ .

The stability over-time in chloride solution was also evaluated, by monitoring the complex in 100 mM  $\text{NaCl}$ , which is the typical concentration in plasma, and in 4 mM  $\text{NaCl}$ , which mimics the intracellular concentration of chloride, at 37 °C. In

4 mM NaCl the same behaviour as in pure water was observed. In 100 mM NaCl, compound **22** gave rise to the mono-aqua species, while the hydrolysis of the second chlorido was suppressed (**Figure 6.9**).

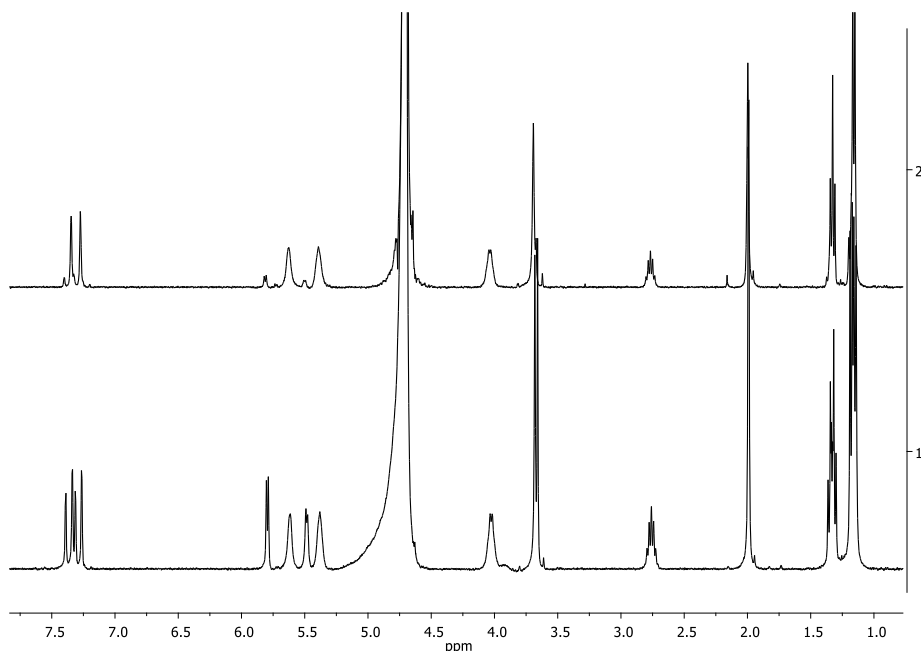


**Figure 6.9.**  $^1\text{H}$  NMR spectrum of **22** in  $\text{D}_2\text{O}$  (trace 1) and in 100 mM NaCl (trace 2) at 400 MHz.

The other dichlorido complexes displayed a similar behaviour regarding the hydrolysis of the  $\text{Cl}^-$  ligands. However, by reproducing the same experiments described for **22** with compounds **23-27**, other features emerged. Immediately after the dissolution, spectra showed the presence of two species, identified as the mono- and the di- aqua complexes by the addition of  $\text{AgNO}_3$ . Over time, spectra changed giving rise to additional set of signals as shown in **Figure 6.10** for complex **23**.

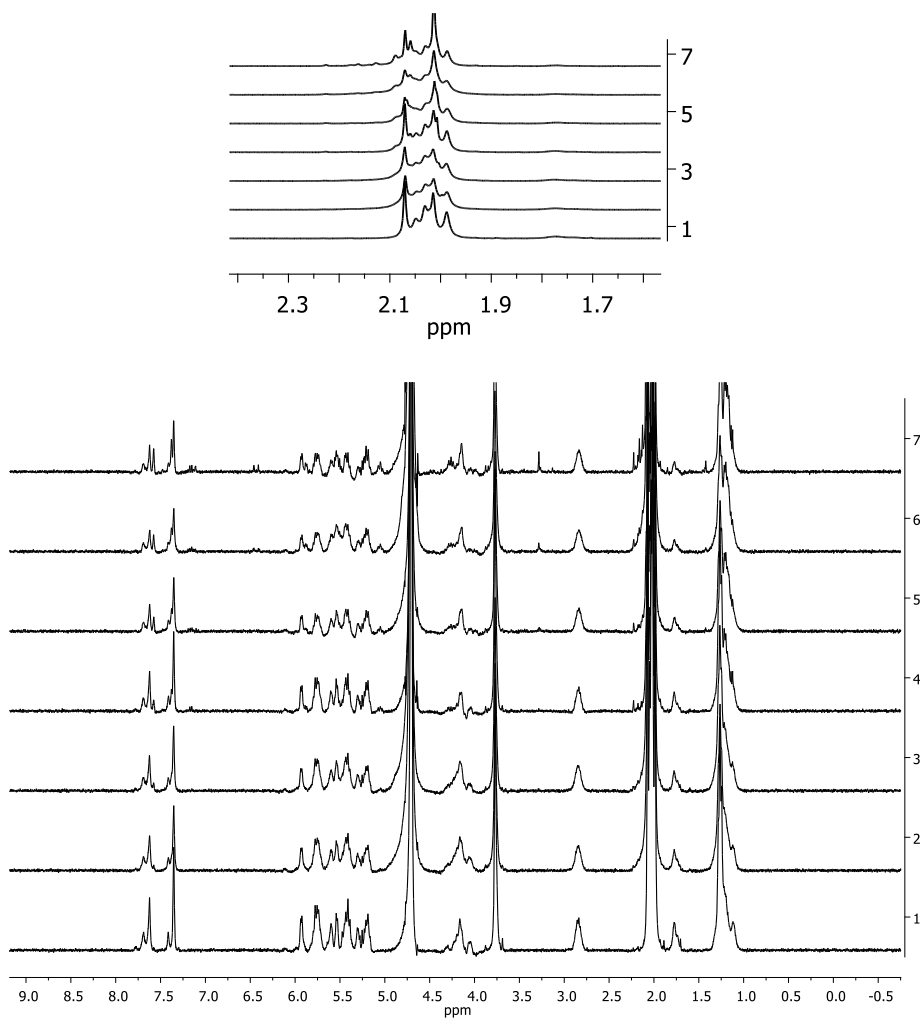


**Figure 6.10.**  $^1\text{H}$  NMR spectra of **23** in  $\text{D}_2\text{O}$  at  $37\text{ }^\circ\text{C}$  and 400 MHz, recorded at different times.

The appearance of signals around 3-4 ppm and of an intense singlet at *ca.* 2 ppm was suggestive of a hydrolysis of the acetyl groups of the sugar fragment. However, probably due to the slow rate of the process, after one week at  $37\text{ }^\circ\text{C}$  it

was not possible to confirm this hypothesis by NMR, due to the presence of multiple species and overlapping peaks. Therefore, to lead the process to completion, **23** was dissolved in D<sub>2</sub>O and the pH was increased at 8.4 by addition of NaHCO<sub>3</sub> and then to >12 upon addition of Na<sub>2</sub>CO<sub>3</sub>. Increasing pH quickened the hydrolysis, indeed after 12h at pH >12 and 37° only a single pattern was observed in solution. The complex was identified and characterized as the fully de-acetylated complex by <sup>1</sup>H and <sup>13</sup>C mono and bidimensional NMR spectroscopy (Figure 6.11).

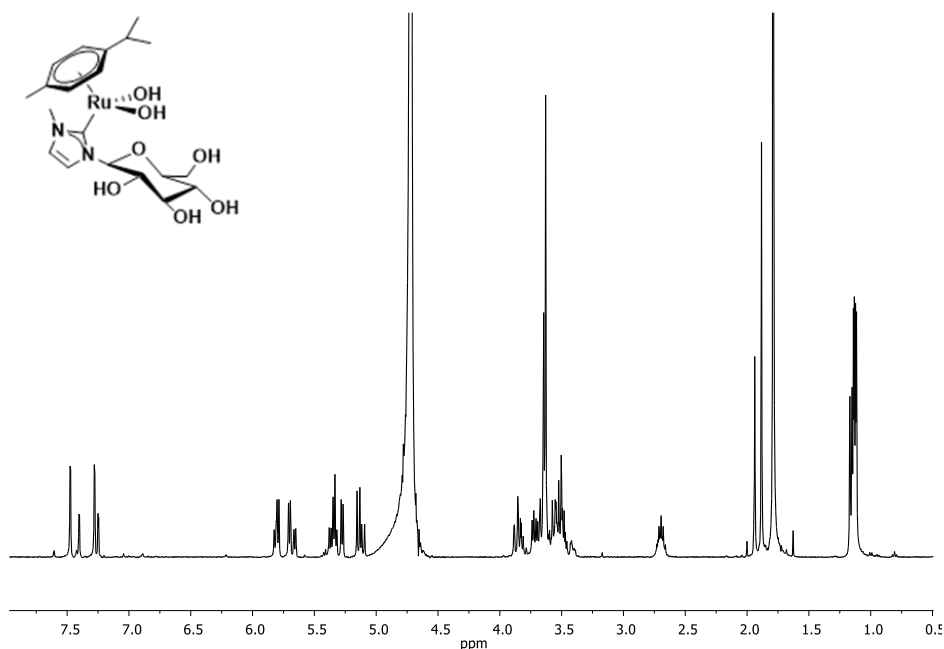
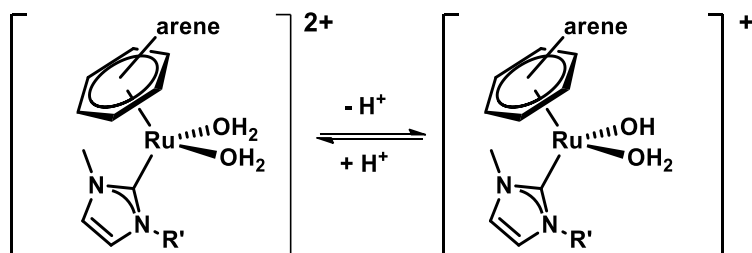


**Figure 6.11.** <sup>1</sup>H NMR spectrum of the de-acetylated form of complex **23** in D<sub>2</sub>O pH > 12, at 400 MHz.

Moreover, partial release of the arene was observed in compounds **25-27**, whose NMR spectra showed the progressive appearance of signals in the aromatic region attributable to the corresponding free aromatic rings. The phenomenon was even

accentuated in 100 mM NaCl. This reactivity can be correlated to the energies of the ruthenium-arene bond. The more electron-rich *p*-cymene and hexamethylbenzene gave rise to more robust complexes than benzene, toluene and the amido-glycoconjugate derivative in complex **27**. A similar trend was already reported for ruthenium and osmium arene *pta* complexes, whose binding energies were calculated.<sup>215</sup> Finally, compounds **28-30** showed no sign of hydrolysis over 72 h, both in water and in NaCl 100 mM, displaying enhanced robustness, probably provided by the presence of chelating ligands.

ESI-MS spectra recorded in water after incubation at 37 °C over 3 days, confirmed the NMR observations. Peaks identified as [M - Cl] and [M - 2Cl] were observed immediately after the dissolution, representative of species of type **22'** and **22''** (Figure 6.8). Moreover, molecular ions attributable to sugar complexes lacking some of the acetyl groups were detected over time, confirming the occurrence of a slow hydrolysis. This is probably favoured by certain degree of acidity of the solution, since ruthenium can act either as Lewis acid or as Bronsted acid in its hydrolysate form (Scheme 6.4).



**Scheme 6.4.** Bronsted acidity of Ru(II) complexes in the hydrolysate form

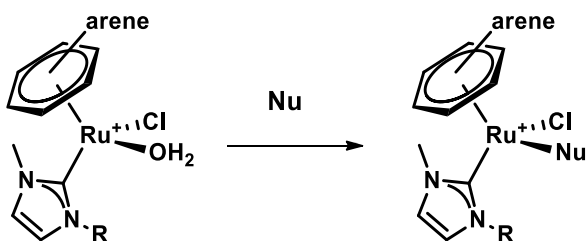
In summary, the synthesized compounds showed a wide variety in their hydrolytic behaviour, and different stabilities were observed. Such differences can have an important impact on the propensity to react with biological molecules as well as

on the type of adducts formed, and consequently to influence their biological activity.

### 6.2.3 Interaction with biological molecules

#### 6.2.3.1 Reactivity with model nucleophiles

The reactivity of complexes **22-30** with 9-ethylguanine (EtG), as model nucleobase, L-Histidine (Hist) and L-Aspartate (Asp) as model amino acids was studied by ESI mass spectrometry. These experiments allowed to delineate at molecular level how different ligands influenced the type of adducts that the complexes could form with proteins and DNA. Attempts to follow these reaction courses by  $^1\text{H}$  NMR were unsuccessful, due to the complexity of the spectra containing overlapping resonance patterns, derived by the presence of multiple stereoisomers. The reactions were performed in water by incubating each complex with 2.5 eq. of nucleophiles at 37 °C for 48 h. In principle, it could be supposed that the aqua-species resulting from the hydrolysis of the chlorido ligands were reactive toward nucleophiles (**Nu**), and coordinated them by substituting a water molecule (**Scheme 6.5**).



**Scheme 6.5.** Reactivity of aqua-complexes toward nucleophiles.

Nevertheless, mass spectra also revealed the presence of other species, and depending on the ligands in the coordination environment some general considerations could be done.

When incubated with EtG, compounds **22-24** formed adducts by replacing the Cl<sup>-</sup> ligands, as reported in **Scheme 6.5**, since molecular ions of type **I** in **Figure 6.12** were detected in the spectra. In addition to these adducts, in compounds **25-27** EtG replaced the arene, forming species with two nucleobases (molecular ions of type **II** in **Figure 6.12**), not observed for **22-24**.

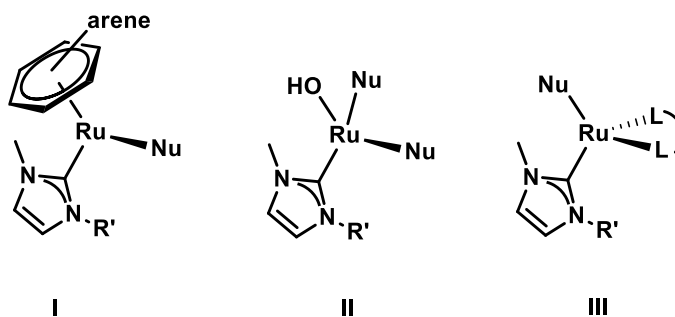


**Figure 6.12.** General structures of the molecular ions observed upon reaction with model nucleophiles

The complexes with chelating ligands **28-30**, gave rise to adducts of type **I** as observed for **28** and **30** that replaced oxalate and *phen* respectively.

Similar outcomes emerged by the reaction with L-Histidine. Indeed, molecular ions of type **II** were observed for **25-27**, while the compounds **22-24** only formed species of type **I**. Such data agreed with previous observation that less electron-reach arenes ligands can be more easily replaced. Noteworthy, for **22-24**, Hist-Ru-arene adducts lacking the NHC ligand were also observed.



Adducts of type **I** were generally observed following the incubation with L-Aspartate for all the complexes, except for complex **30**, in which *p*-cymene was substituted with retaining of the *phen* ligand (type **III** in **Figure 6.12**).

Such observations suggested that the mechanism of interaction with biomolecules strongly depends on the nature of the coordinating nucleophile and on both arene and ancillary ligands. Indeed, less electron-rich arenes were more easily substituted by L-Histidine and EtG and adducts with two coordinated nucleophiles were observed. Electron-donating arenes were generally retained, and in presence of Histidine the cleavage of the metal-NHC bond can occur. Such feature was not observed in presence of EtG and Asp. The neutral *phen* seemed to be preferentially substituted by neutral EtG and Hist, while *p*-cymene was replaced in the reaction with Asp. Finally, the oxalate seemed to act as leaving group in presence of nucleophiles, similarly to chlorido ligands. However, the chelating effect could result in enhanced kinetic inertness as observed for other carboxylate-ruthenium compounds.<sup>101</sup>

#### 6.2.3.2 Reactivity with model proteins

The reactivity of the Ru(II) compounds with model proteins was studied by mass spectrometry, intrinsic fluorescence, and X-ray crystallography.

First, the reactivity of the compounds with the model protein Ubiquitin (Ubi) was monitored by ESI-MS, following the incubation of the protein with metal complexes at protein to metal ratio 1:3 in water, at 37 °C for 24 h. The aqua-species derived by the hydrolysis of **22-27** were highly reactive with Ubi, forming adducts of type **IV** in **Figure 6.13**.

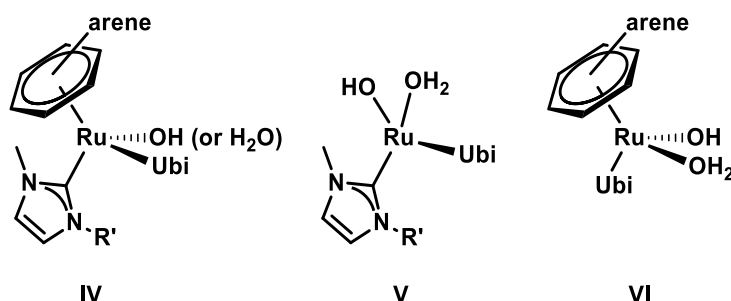


**Figure 6.13.** Type of adducts formed upon reaction of Ru complexes with Ubiquitin

Interestingly, even adducts derived by the loss of the arene (V) or by the cleavage of the NHC (VI) were detected, in agreement with the multi-modal modes of interaction of this class of compounds in reacting with proteins. Interestingly, no adducts were observed for cationic compounds **28-30**.

Then, the binding of **23-28** to Human serum albumin (HSA) was investigated by intrinsic fluorescence spectroscopy, following the emission of Trp214, which is the only tryptophane residue of the protein. Binding of potential metallodrugs to plasma proteins plays an important role in the evaluation of their bioavailability. HSA, which accounts for ~60% of total plasma proteins, is the major vehicle for these molecules in the human blood plasma.

Emission spectra of the protein in the absence and in the presence of increasing concentrations of complexes are reported in **Figure 6.14**. By adding increasing concentrations of metal complexes, the intensity of this band regularly decreased, although slightly. This indicates that the compounds quenched the fluorescence of HSA by a concentration-dependent manner. However, the shape of the peaks and the position of the maximum emission wavelength in the spectra of HSA were almost the same upon the addition of the Ru complexes, suggesting that the

interaction between the protein and **23-28** did not affect the polar environment of Trp214.

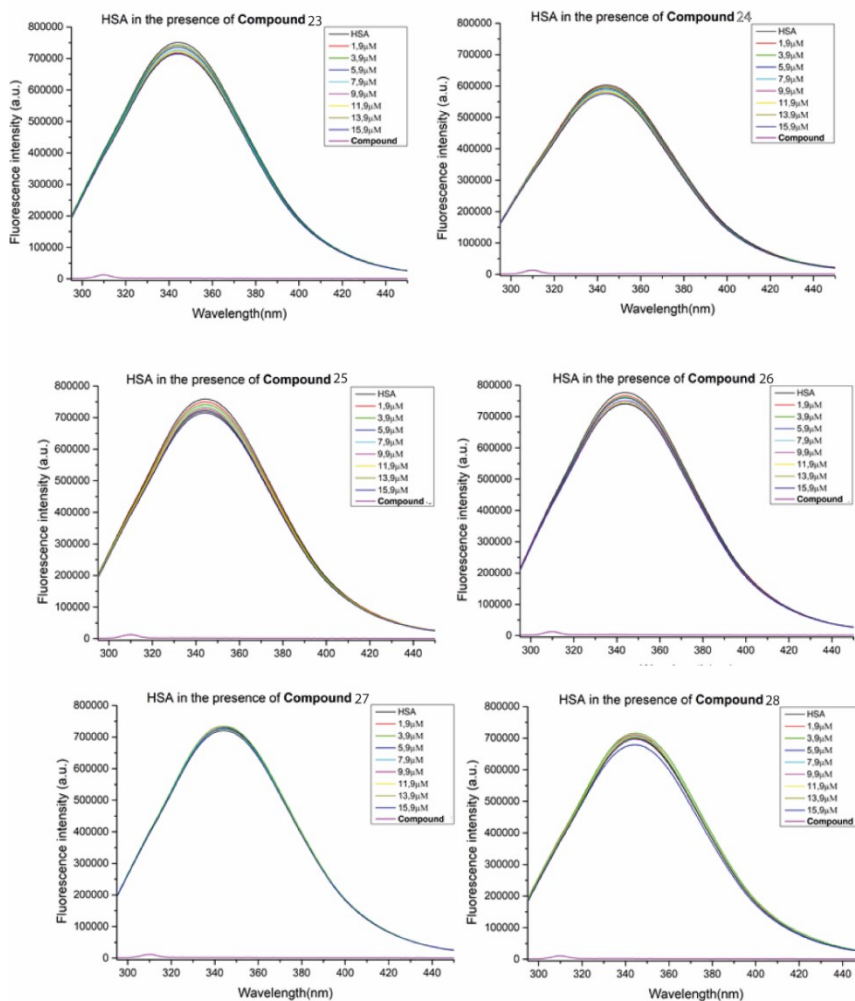


**Figure 6.14.** Fluorescence spectra of HSA in the presence of the Ru complexes **23-28**, upon excitation at 280 nm, using samples with increasing concentration of the metal complexes.

Moreover, the reactivity with the model proteins was further investigated using Hen Egg White Lysozyme (HEWL) and bovine pancreatic Ribonuclease (RNase A).

The reactivity of **22-27** with HEWL was investigated by collecting fluorescence spectra of the protein in the presence of increasing concentrations of each Ru-complex. When the metal complexes were added in protein to metal ratio 1:3, the fluorescence intensity of HEWL showed a slight decrease that did not change when the concentration of the complexes was increased. This observation suggested that protein binding sites on the protein surface were already occupied by the metal complex at protein to metal ratio is 1:3.

Complexes **22-27** were reactive with His and Asp, as observed by the ESI-MS studies. Such residues were previously identified as possible binding sites of ruthenium compounds, in reported crystallographic structures of the adducts between Ru(II) compounds with HEWL and RNase A. Considering that fluorescence data suggested an interaction between metal complexes and proteins, X-ray crystallographic studies were performed.

Complexes **22-27** formed adducts suitable for X-ray analysis, upon reaction HEWL and RNase A. The structures between the two proteins and complex **26** are here discussed. The structure determination allowed to analyse which were the real protein binding sites for these complexes.

Crystals of the adducts between **26** and proteins were obtained by soaking strategy: metal-free protein crystals of HEWL and RNase A were exposed to a solution containing the metal complex.

Crystals of HEWL and RNase A exposed to **26** diffract X-ray at 1.2 and 1.37 Å resolution. The structure of the protein in the adduct with HEWL was very similar to that in the absence of the metal compound. In the adduct, a ruthenium centre was identified close to the side chain of Asp119. This residue was already

identified as binding site for ruthenium complexes in previous studies. At this binding site, Ru had an occupancy value = 0.8 and retains the NHC ligand. The coordination sphere of Ru is completed by water molecules and a nitrate (present crystallization medium), while the benzene ring was lost (**Figure 6.15**).

---

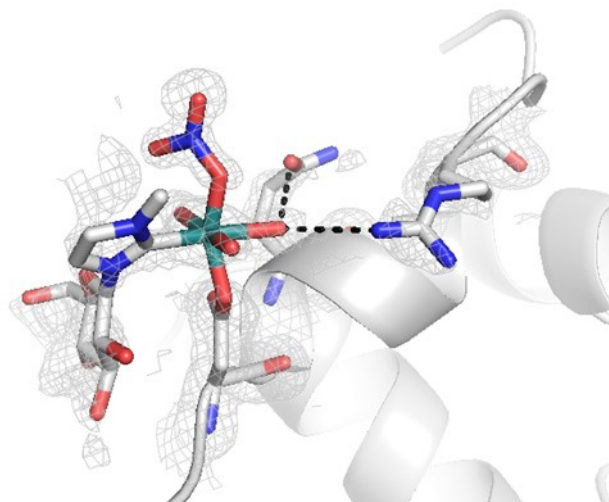


**Figure 6.15.** Ru-containing fragment binding sites in the structure of the adduct formed upon reaction of the HEWL with **26**. Electron density maps are reported at 1.0  $\sigma$  levels in grey.

Crystals of the adduct formed upon reaction of **26** with RNase A (figure not shown) contained two molecules in the asymmetric unit (hereafter referred as molecules A and B). In molecule A, two Ru centres were identified. They were found close to the side chains of His105, which is on the protein surface, and of His119, which is in the protein active site. In molecule B, only one Ru centre was found, close to the side chain of His105. The active site of molecule B was occluded by a phosphate/sulphate ion, which hampered the binding of the Ru compound. These results were not surprising considering that RNase A has a very high affinity for phosphates/sulphates. The electron density maps close to the

metal centres in this structure were not sufficiently well defined to define with accuracy the metal ligands.

X-ray crystallography studies perfectly matched with results collected by fluorescence and mass spectrometry. Indeed, under the investigated experimental conditions complexes **22-27** reacted with proteins leading to the formation of different adducts. Chlorido ligands were the most available to be replaced, although the arene and in some cases the NHC ligands were lost.

#### *6.2.3.3 Reactivity with model DNA*

Binding studies of Ru(II) complexes **23-30** with DNA were performed by ethidium bromide (EtBr) displacement fluorescence assay.

EtBr was incubated with ct-DNA for 30 min and then emission spectra of the resulting fluorescent adduct in the absence and presence of increasing concentration of the Ru complexes were recorded (**Figure 6.16**).

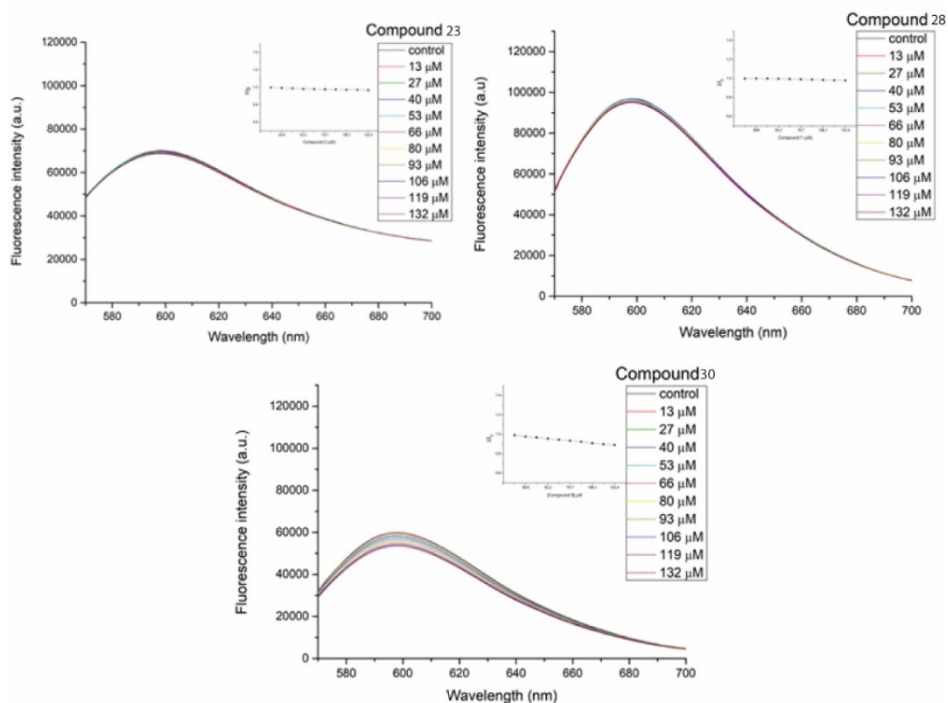


**Figure 6.16.** Emission spectra of EtBr-ctDNA system in the absence and in the presence of Compound **23**, **28** and **30**, upon excitation at 350 nm.

The addition of the Ru complexes did not induce a significant quenching of fluorescence, indicating that no competitive effect of the complexes with EtBr for binding DNA at major groove occurred. Only with the phenanthroline derivative **30** a slight decrease in the fluorescence intensity was observed, although such small effect could not be considered a definitive indication of binding.

To further verify the results, CD spectra of DNA were collected in the presence of the complexes. CD spectra of DNA incubated with **22-29** did not reveal appreciable variations in the spectral profile of DNA, supporting the conclusion that these compounds did bind the double helix. The spectrum of complex **30**

(**Figure 6.17**) suggested a slight alteration in DNA structure, although less evident with respect the spectral profile observed when metallodrugs bind ct-DNA.

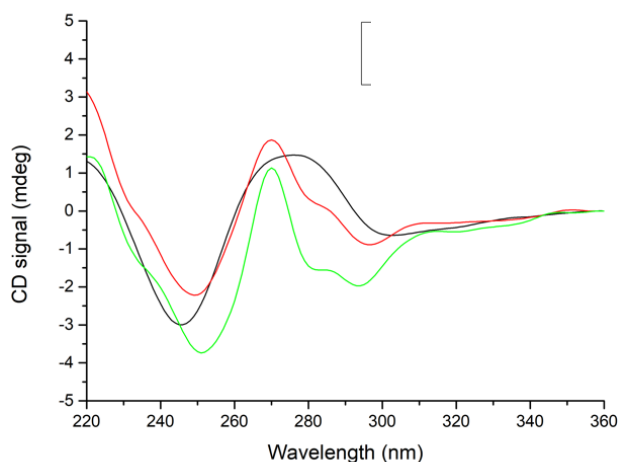


**Figure 6.17.** CD spectra of ct-DNA (black curve) and in presence of **30** at metal to DNA ratio 1:1 (red curve) and 1:2 (green curve).

These results confirmed that small change in the coordination environments, as the substitution pattern of the arene, or the presence of chelating ligands instead of chlorido ligands had an important impact on the reactivity of the complexes. The hydrolysis studies already disclosed differences that were reflected in the reactivity with model biomolecules. Indeed, it is possible to make some general considerations:

- the dichlorido complexes **22-27** undergo hydrolysis forming aqua-species, highly reactive with biomolecules. Both amino acids and nucleobases coordinated the complexes;
- less electron rich arenes, present in complexes **25-27** are more easily lost, as already observed when the complexes were monitored at 37 °C in water and in 100 NaCl solutions. Indeed, both mass experiments and X-ray



crystallography revealed the formation of adducts lacking the arene ligand. A similar outcome was reported by studying the binding of ruthenium arene (RAPTA) and analogue osmium (OSPTA) complexes with model oligonucleotides.<sup>215,216</sup> Such differences have to be considered in studying the anticancer properties of metal complexes since different kinds of molecular interactions can lead to diverse biological responses;

- these studies also suggested that the family of compounds **22-30** preferentially reacts with proteins, similarly to RAPTA complexes, rather than DNA. Only **30** seemed to interact with the double helix *in vitro*, although no definitive evidences was observed. **30** was also less reactive with proteins compared to the other compounds. This inertness may be beneficial for the behaviour of the complex in *in vivo* conditions, conferring a robustness which allows to reach intact its target.

#### 6.2.4 Evaluation of the Cytotoxic Activity

The *in vitro* cytotoxicity of the compounds **23-30** was evaluated by determining the IC<sub>50</sub> concentration on human ovarian carcinoma A2780 cells, the A2780cisR variant, with acquired resistance to cisplatin, and on human embryonic kidney (HEK293T) cells. IC<sub>50</sub> values were determined after 72 h of drug exposure to the cells using the MTT assay. Cisplatin was used as positive control while RAPTA-C and untreated cells were used as negative control. Collected data are reported in **Table 6.1**.

**Table 6.1.** IC<sub>50</sub> values (μM) obtained for **22-30** after 72 h of incubation.

Complex	IC <sub>50</sub> (μM)		
	A2780	A2780cisR	HEK293T
<b>22</b>	>100	>100	>100
<b>23</b>	>100	>100	>100
<b>24</b>	>100	>100	>100
<b>25</b>	>100	>100	>100
<b>26</b>	>100	>100	>100
<b>27</b>	>100	>100	>100
<b>28</b>	>100	>100	>100
<b>29</b>	>100	>100	>100
<b>30</b>	38 ± 14	> 100	> 100
<b>RAPTA-C</b>	> 200	> 200	> 200
<b>Cisplatin</b>	1.0 ± 0.2	6.4 ± 3.3	2.4 ± 1.1

The complexes showed no cytotoxicity up to 100 μM on the analysed cells, with the exception for complex **30** that displayed some activity on A2780 line. No activity was observed on non-cancerous HEK293T, stating for a certain degree of selectivity of this complex. It is not easy to rationalize these data of cytotoxicity since many factors may contribute to the whole effect of the complexes. Previously discussed studies evidenced some analogies of the dichlorido **22-27** to RAPTA type complexes. RAPTA are known to be angiogenesis<sup>98</sup> and antimetastatic<sup>217</sup> inhibitors, not displaying cytotoxicity when tested *in vitro*.<sup>96</sup> Further investigations would be needed to evaluate the *in vivo* activity of the glucoconjugate Ru(II) complexes, to disclose other similarities with RAPTA compounds. About complex **30**, it could be supposed that the presence of the *phenanthroline* ligand enhanced the hydrophobicity which is considered to have a beneficial role in the *in vitro* cytotoxicity of metal complexes.<sup>218–221</sup> Moreover,

**30** did not undergo hydrolysis and it was found to be scarcely reactive toward model biomolecules, although some preliminary indication of binding to DNA was observed. These aspects will be deeply investigated, since can be indicative for a different mechanism of action occurring biological conditions, that result in a different cytotoxicity.

## 6.3 Experimental Part

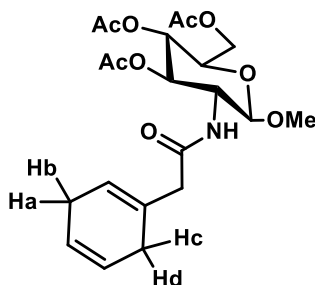
### 6.3.1 General

Reagents and solvents were purchased from Sigma-Aldrich and were used without further purification. The human ovarian carcinoma cell lines (A2780CisR and A2780) were purchased from the European Collection of Cell Cultures (ECACC). The human embryonic kidney 293T (HEK-293T) cell line was kindly provided by the biological screening facility (EPFL, Switzerland). Penicillin streptomycin, RPMI 1640 GlutaMAX (where RPMI = Roswell Park Memorial Institute), and DMEM GlutaMAX media (where DMEM = Dulbecco's modified Eagle medium) were obtained from Life Technologies, and fetal bovine serum (FBS) was obtained from Merck. Fluorescence spectra were collected using a Fluoromax 4 spectrofluorophotometer from Horiba equipped with a thermostat bath. NMR spectra were acquired on 400 MHz Bruker AVANCE-IIIHD-400 and AVANCENE0-400 located at the Institute of Chemical Sciences and Engineering of the École Polytechnique Fédérale de Lausanne (Switzerland). The solvents were  $\text{CDCl}_3$  ( $\text{CHCl}_3$ ,  $\delta$  7.26, and  $^{13}\text{CDCl}_3$ ,  $\delta$  77.0, as internal standards),  $(\text{CD}_3)_2\text{CO}$  ( $(\text{CD}_2\text{H})_2\text{CO}$ ),  $\delta$  2.09, as internal standard),  $\text{D}_2\text{O}$  ( $\text{HDO}$ ,  $\delta$  4.80 as internal standard), and  $\text{CD}_3\text{OD}$  ( $\text{CD}_2\text{HOD}$ ,  $\delta$  3.30,  $^{13}\text{CD}^3\text{OD}$ ,  $\delta$  49.0, as internal standard). The following abbreviations were used for describing NMR multiplicities: s, singlet; d, doublet; dd, double doublet; triplet; app, apparent; m, multiplet; ABq, AB quartet. Ru(II) arene dimers were prepared according to literature procedures.<sup>222</sup> Methyl-tri-O-acetyl-2-amino-2-deoxy- $\beta$ -D-glucopyranoside<sup>170</sup>, 2-(cyclohexa-1,4-dien-1-yl)acetic acid<sup>223</sup> and silver oxalate<sup>101</sup> were prepared according to literature.

## 6.3.2 Synthesis and Characterization

### 6.3.2.1 Synthesis of the arene precursor (*e'*)

2-(cyclohexa-1,4-dien-1-yl)acetic acid (0.84 g, 6.0 mmol), methyl-tri-O-acetyl-2-amino-2-deoxy- $\beta$ -D-glucopyranoside (1.55 g, 4.8 mmol), DCC (2.1 g, 10 mmol) and DMAP (0.61 g, 5.1 mmol) were stirred in 25 mL of DCM for 16 h. Then the mixture was filtered, and the filtrate was reduced in volume. Addition of n-hexane resulted in the precipitation of the product. Yield: 64% (1.35 g).



$^1\text{H}$  NMR (400 MHz,  $\text{CDCl}_3$ )  $\delta$  5.73 (d, 1H, NH), 5.69-5.58 (m, 3H,  $\text{C}=\text{CH}$ ), 5.30 (dd, 1H,  $J_{\text{H}2-\text{H}3} = 10.3$  Hz  $J_{\text{H}3-\text{H}4} = 9.7$  Hz, H3-glu), 5.05 (t, 1H, H4-glu), 4.61 (d,  $J_{\text{H}1-\text{H}2} = 18.2, 8.4$  Hz, 1H, H1-glu), 4.27 (dd,  $J_{\text{H}6-\text{H}6'} = 12.3$  Hz  $J_{\text{H}5-\text{H}6} = 4.7$  Hz, 1H, H6-glu), 4.14 (dd,  $J_{\text{H}5-\text{H}6'} = 2.2$  Hz, 1H, H6'-glu), 4.07 (dd,  $J = 12.2, 2.4$  Hz, 1H), 3.80 (m, 1H, H2-glu), 3.70 (ddd, 1H, H5-glu), 3.49 (s, 3H, OMe), 2.87 (s, 2H,  $-\text{CH}_2\text{CONH}-$ ), 2.74 (m, 2H, Ha and Hc), 2.57 (m, 2H, Hb and Hd), 2.08 (s, 3H, OAc), 2.01 (s, 3H, OAc), 2.00 (s, 3H, OAc).  $^{13}\text{C}$  NMR (101 MHz,  $\text{CDCl}_3$ )  $\delta$  171.2, 170.9, 170.8, 169.5, 129.9 (IV), 124.5, 123.9 (x2), 101.8, 72.2, 72.0, 68.9, 62.3, 57.0, 54.8, 46.2, 28.9, 26.9, 20.9, 20.8 (x2). ESI-MS (+)  $\text{CH}_3\text{OH}$  ( $m/z$  (relative intensity, %)): 462 (100)  $[\text{M} + \text{Na}]^+$ , 440 (76)  $[\text{M} + \text{H}]^+$ .

#### 6.3.2.2 Synthesis of the Ru(II) arene dimer **e**

The diene **e'** (0.68 g, 1.5 mmol) and RuCl<sub>3</sub>·xH<sub>2</sub>O (0.10 g, 0.38 mmol) were refluxed in ethanol (80 mL) for 16 h. The mixture is allowed to cool at room temperature and the volume of solvent was reduced under pressure. After storage at -20 °C overnight, the product was isolated as bright orange powder by filtration, washed with ethanol, diethyl ether and dried. Yield: 79% (0.18 g).

<sup>1</sup>H NMR (400 MHz, CDCl<sub>3</sub>) δ 7.42 (d, *J* = 9.4 Hz, H, NH), 5.88 (t, 1H, H-Ar), 5.70 (d, 1H, H-Ar), 5.64 (t, 1H, H-Ar), 5.59 (t, 1H, H-Ar), 5.48 (t, *J* = 9.8 Hz, 1H, H3-glu), 5.30 (br, 1H, H-Ar), 5.09 (t, *J* = 9.6 Hz, 1H, H4-glu), 4.83 (d, *J* = 8.9 Hz, 1H, H1-glu), 4.31 (dd, *J* = 12.5, 4.6 Hz, 1H, H6-glu), 4.18 (m, 1H, H6'-glu), 4.10 (m, 1H, H2-glu), 3.94 – 3.69 (m, 1H, H5-glu), 3.58 (s, 3H, OMe), 3.55 (ABq, *J* = 16.5 Hz, 2H, CH<sub>2</sub>CONH), 2.10 (s, 3H, OAc), 2.06 (s, 3H, OAc), 2.04 (s, 3H, OAc). Anal. Calcd. (found) for C<sub>42</sub>H<sub>54</sub>O<sub>18</sub>N<sub>2</sub>Cl<sub>4</sub>Ru<sub>2</sub>·2H<sub>2</sub>O: C, 40.20 (40.04), H, 4.66 (4.49), N, 2.23 (2.17).

#### 6.3.2.3 Synthesis of Complexes **22-27**

A solution of the appropriate silver carbene 2-R (1.1 mmol) in DCM (10 mL) was added to the appropriate Ru(II) arene dimer (0.55 mmol) suspended in DCM (10 mL). The mixture was stirred at RT, protected from light for 48 h. Then, AgBr was filtered off, and the volume of the clear filtrate was reduced under pressure. The addition of diethyl ether resulted in the precipitation of the products as red-orange microcrystalline solids, washed with ether and dried under vacuum. Yields: 75-85%

**22:** <sup>1</sup>H NMR (400 MHz, Acetone, 25 °C) δ 7.42 (d, 1H, H-Im), 7.35 (d, 1H, H-Im), 5.50 (d, *J* = 5.9 Hz, 2H, Ar), 5.18 (d, *J* = 5.8 Hz, 2H, Ar), 4.49 (br, 2H,

NCH<sub>2</sub>Me), 3.01 (heptet, 1H, Ar-CH-Me<sub>2</sub>), 2.85 (br, 3H, Me-Im), 1.99 (s, 3H, Me-Ar), 1.42 (t, *J* = 7.2 Hz, 3H, NCH<sub>2</sub>Me), 1.31 (d, *J* = 6.9 Hz, 6H, Ar-CH-Me<sub>2</sub>). Anal. Calcd. (Found) for C<sub>16</sub>H<sub>25</sub>Cl<sub>2</sub>N<sub>2</sub>Ru: C, 46.05 (46.00); H, 6.04 (5.87); N, 6.71 (6.55). ESI-MS (+) CH<sub>3</sub>OH (m/z (relative intensity, %)): 380 (100), [Ru(*p*-cym)NHCCl]<sup>+</sup>

**23:** <sup>1</sup>H NMR (400 MHz, Acetone, 25 °C) δ 7.64 (br, 1H, H-Im), 7.31 (d, 1H, H-Im), 6.67 (br, 1H, H1-glu), 5.81 – 5.52 (m, 3H, Ar(x2) and H2-glu), 5.32 (t, *J*<sub>H2-H3</sub> = 9.3 Hz, 1H, H3-glu), 5.23 (d, *J* = 6.0 Hz, 1H, Ar), 5.18 (d, *J* = 6.1 Hz, 1H, Ar), 5.13 (t, 1H, H4-glu), 4.24 – 4.02 (m, 3H, H5-glu, H6-glu, H6'-glu), 4.04 (s, 3H, Me-Im), 3.04 (heptet, 1H, Ar-CHMe<sub>2</sub>), 1.99 (s, 3H, Me-Ar), 1.96 (s, 3H, OAc), 1.94 (s, 6H, OAc(x2)), 1.92 (s, 3H, OAc), 1.29 (d, 6H, Ar-CHMe<sub>2</sub>). <sup>13</sup>C NMR (101 MHz, Acetone, , 25 °C) δ 181.06, 170.71, 170.25, 170.21, 169.69, 125.77, 121.19, 109.42, 100.59, 98.22, 91.03, 88.00, 86.08, 81.58, 80.76, 74.55, 71.03, 69.42, 66.03, 62.77, 40.12, 31.53, 24.28, 20.90 (x2), 20.70, 20.59, 18.84. ESI-MS (+) CH<sub>3</sub>OH (m/z (relative intensity, %)): 683 (100), [Ru(*p*-cym)NHCCl]<sup>+</sup>, Anal. Calcd. (found) for C<sub>28</sub>H<sub>38</sub>Cl<sub>2</sub>N<sub>2</sub>O<sub>9</sub>Ru · 0.25 CH<sub>2</sub>Cl<sub>2</sub>: C, 45.82 (45.96), H, 5.32 ( 5.20), N, 3.76 (3.78).

**24:** <sup>1</sup>H NMR (400 MHz, CDCl<sub>3</sub>, 25 °C) δ 7.32 (d, *J* = 2.3 Hz, 1H, H-Im), 7.28 (d, *J* = 2.1 Hz 1H, H-Im), 7.01 (d, *J* = 2.3 Hz, 1H, H-Im), 6.99 (d, *J* = 2.1 Hz, 1H, H-Im), 6.70 (d, *J* = 9.1 Hz, 1H, H1-glu), 5.86 (d, *J* = 9.5 Hz, 1H, H1-glu), 5.62 (t, *J* = 9.6 Hz, 1H, H2-glu), 5.43 (t, *J* = 9.4 Hz, 1H, H3-glu), 5.25 (m, 3H, H2-glu, H3-glu and H-4glu), 5.14 (t, *J* = 9.7 Hz, 1H, H4-glu), 4.35 (m, 2H, H5-glu, H6-glu), 4.20 (m, 2H, H6-glu and H6'-glu), 4.05 (m, 1H, H6'-glu), 3.93 (hidden, H5-glu), 3.92 (s, 3H, NMe), 3.90 (s, 3H, NMe), 2.08 (s, 3H, OAc), 2.06 (s, 3H, OAc), 2.0 (s, 18H, Ar-Me), 2.04 (s, 3H, OAc), 2.03 (s, 3H, OAc), 2.02 (s, 3H, OAc), 2.01 (HIDDEN, s, 3H, OAc), 2.01 (s, 18H, Ar-Me), 1.97 (s, 3H, OAc), 1.95 (s, 3H, OAc). <sup>13</sup>C NMR (101 MHz, CDCl<sub>3</sub>, 25 °C) δ 182.62, 181.18, 170.92 (OAc), 170.8,

170.44, 170.22, 169.986, 169.64, 169.61, 168.85, 124.51 (C-Im), 124.16 (C-Im), 120.98 (C-Im), 120.11 (C-Im), 94.36 (Ar x 6), 94.26 (Ar x 6), 84.64 (C1-glu), 84.29 (C1-glu), 74.38 (C5-glu), 74.31, 73.33, 72.89 (C3-glu), 70.24, 69.72 (C2-glu), 69.06, 68.10 (C4-glu), 62.80, 61.28, 39.92 (Me-Im), 39.72 (Me-Im), 20.97, 20.92, 20.89, 20.78, 20.76, 20.73 (x3), 15.98, 15.75.

ESI-MS (+) CH<sub>3</sub>OH (m/z (relative intensity, %)): 711 (100), [Ru(*hexa*)NHCCl]<sup>+</sup>, Anal. Calcd. (found) for C<sub>30</sub>H<sub>42</sub>Cl<sub>2</sub>N<sub>2</sub>O<sub>9</sub>Ru: C, 48.26 (47.85), H, 5.75 ( 5.75), N, 3.75 (3.68).

**25:** <sup>1</sup>H NMR (400 MHz, CDCl<sub>3</sub>, 50°C) δ 7.29 (br, 1H, H-Im), 6.99 (d, 1H, H-Im), 6.51 (br, 1H, H1-glu), 5.49 (m, 2H), 5.45 (t, 1H), 5.32 (m, 3H), 5.22 (m, 1H), 5.16 (t, J = 9.1 Hz, 1H, H4-glu), 4.51-4.30 (br, 3H), 4.03 (s, 3H- Me-Im), 2.33 (s, 3H, Me-Ar), 2.05 (s, 3H, OAc), 2.04 (s, 3H, OAc), 2.01 (s, 3H, OAc), 1.97(s, 3H, OAc). <sup>13</sup>C NMR (101 MHz, CDCl<sub>3</sub>, 50°C), δ 176.71, 170.64, 170.07, 169.81 (x2), 124.92, 120.20, 107.15, 87.97, 87.22, 86.57, 85.92, 85.52, 78.62, 74.50, 68.86, 65.94, 62.93, 62.07, 39.96, 20.92 (x2) (20.69 (x2), 19.16. ESI-MS (+) CH<sub>3</sub>OH (m/z (relative intensity, %)): 641 (100), [Ru(*tol*)NHCCl]<sup>+</sup>, Anal. Calcd. (found) for C<sub>25</sub>H<sub>32</sub>Cl<sub>2</sub>N<sub>2</sub>O<sub>9</sub>Ru · 0.25CH<sub>2</sub>Cl<sub>2</sub>: C, 43.43 (43.37), H, 4.66 ( 4.77), N, 4.01 (4.07).

**26:** <sup>1</sup>H NMR (400 MHz, Acetone, 50°C) δ 7.65 (d, 1H, H-Im), 7.33 (d, 1H, H-Im), 6.86 (br, 1H, H1-glu), 5.82-5.59 (m, 1H, partially hidden, H2-glu), 5.71 (s, 6H), 5.38 (t, 1H, J= 9.6 Hz, H3-glu), 5.16 (t, 1H, H4-glu), 4.33 – 4.06 (m, 3H, H5- glu, H6-glu and H6'-glu), 4.04 (s, 3H, Me-Im), 2.03 – 1.97 (m, 12H, OAc). <sup>13</sup>C NMR (101 MHz, Acetone, 50°C) δ 178.86, 170.77, 170.20 (x2), 169.51, 126.09, 120.55, 87.41 (x6), 75.08, 74.62, 71.49, 69.42, 63.62, 62.53, 39.89, 20.92, 20.87, 20.70, 20.63. ESI-MS (+) CH<sub>3</sub>OH (m/z (relative intensity, %)): 627 (100), [Ru(*benz*)NHCCl]<sup>+</sup>, Anal. Calcd. (found) for C<sub>24</sub>H<sub>30</sub>Cl<sub>2</sub>N<sub>2</sub>O<sub>9</sub>Ru · 0.5 CH<sub>2</sub>Cl<sub>2</sub>: C, 41.71 (41.65), H, 4.43 ( 4.54), N, 3.97 (4.04).



**27:**  $^1\text{H}$  NMR (400 MHz,  $\text{CDCl}_3$ ,  $-10^\circ\text{C}$ )  $\delta$  8.09 (d,  $J = 8.6$  Hz, 1H, *NH*), 7.92 (d,  $J = 8.6$  Hz, 1H, *NH*), 7.41 (br, 1H, H-Im), 7.31 (br, 1H, H-Im), 7.09 (br, 1H, H-Im), 7.07 (br, 1H, H-Im), 6.80 (d,  $J = 9.1$  Hz, 1H, H1-glu(NHC)), 6.30 (d,  $J = 9.7$  Hz, 1H, H1-glu(NHC)), 5.97 – 4.69 (m, 22H), 4.46 – 3.49 (m, 21H), 4.01 (s, 3H), 3.99 (s, 3H), 3.67 (s), 2.30 – 1.79 (m, 42H OAc (x 14)).  $^{13}\text{C}$  NMR (101 MHz,  $\text{CDCl}_3$ ,  $-10^\circ\text{C}$ )  $\delta$  176.90 (NHC), 174.56 (NHC), 171.23 (x2), 171.05 (x2), 170.81 (x2), 170.52 (x2), 170.36, 169.98 (x4), 168.51 (x2), 168.35, 125.14 (C-Im), 124.47 (C-Im), 120.50 (C-Im), 119.88 (C-Im), 108.03, 107.94, 101.76, 101.64 (x2), 89.60, 88.79, 86.20, 85.87, 85.53, 85.09 (x3), 83.89, 82.84, 82.15, 73.97 (x2), 73.91, 73.07 (x2), 71.12 (x2), 70.47, 68.56, 67.92, 67.49, 63.09 (x2), 62.04, 61.16 (x2), 57.24 (x2), 54.25, 54.06, 41.35 – 38.28 (x6), 21.41 – 20.62 (x14 COMe), ESI-MS (+)  $\text{CH}_3\text{OH}$  ( $m/z$  (relative intensity %)): 986 (100),  $[\text{Ru}(\text{Arene})\text{NHCCl}]^+$ , Anal. Calcd. (found) for  $\text{C}_{39}\text{H}_{51}\text{Cl}_2\text{N}_3\text{O}_{18}\text{Ru}\cdot 0.25\text{CH}_2\text{Cl}_2$ : C, 45.15 (45.11), H, 4.94 (5.10), N, 4.03 (3.99).

#### 6.3.2.4 Synthesis of Complex **28**

$\text{Ag}_2\text{C}_2\text{O}_4$  (0.040 g, 0.13 mmol) was added to a solution containing complex **23** (0.050 g, 0.070 mmol), in 1 mL of Acetone. The mixture was stirred for 16 h, after that the solid was filtered off and the solvent was removed to afford the product as a yellow powder. Yield: >99%

$^1\text{H}$  NMR (400 MHz, Acetone)  $\delta$  7.83 (d,  $J = 2.1$  Hz, 1H, H-Im), 7.62 (d,  $J = 2.0$  Hz, 1H, H-Im), 7.42 (m, 2H, H-Im), 6.01 (d,  $J = 9.4$  Hz, 1H), 5.96-5.91 (m, 3H), 5.90 – 5.84 (m, 2H), 5.78-5.70 (m, 2H), 5.56 (d,  $J = 5.9$  Hz, 1H), 5.53 – 5.41 (m, 5H), 5.28 (t,  $J = 10.0$  Hz, 1H), 5.21 (t,  $J = 9.8$  Hz, 1H), 4.50 – 4.27 (m, 4H), 4.26 – 4.08 (m, 2H), 3.92 (s, 3H, *Me*-Im), 3.90 (s, 3H, *Me*-Im), 3.03 – 2.88 (m, 2H, Ar-*CHMe*<sub>2</sub>), 2.18 (s, 3H), 2.06 (s, 3H), 2.05(s, 3H), 2.03 (s, 3H), 2.00 (s, 3H), 1.98

(s, 3H), 1.43 (d,  $J = 6.9$  Hz, 3H, Ar-CHMe<sub>2</sub>), 1.40 (d,  $J = 6.9$  Hz, 3H, Ar-CHMe<sub>2</sub>), 1.34 (t,  $J = 6.8$  Hz, 3H, Ar-CHMe<sub>2</sub>), 1.26 (d,  $J = 6.8$  Hz, 3H, Ar-CHMe<sub>2</sub>). <sup>13</sup>C NMR (101 MHz, Acetone)  $\delta$  180.59, 179.60, 169.76, 169.67, 169.53 (x2), 169.37, 169.18, 169.00, 168.58, 164.52, 164.42, 164.29, 164.19, 124.95, 124.42, 120.16, 119.45, 108.50, 104.80, 99.97, 97.19, 88.02, 87.75, 85.94, 85.78, 85.24, 85.19, 82.20, 81.18, 78.94, 77.69, 74.16, 73.99, 73.81, 73.04, 69.64, 68.80, 68.41, 67.53, 62.78, 60.62, 37.06, 37.01, 31.23, 31.06, 23.12, 22.87, 21.32, 20.93, 19.91, 19.89, 19.76 (x2), 19.72, 19.66, 19.59, 19.46, 17.89, 17.55.

ESI-MS (+) CH<sub>3</sub>OH (m/z (relative intensity, %)): 737 (100), [M + H]<sup>+</sup>, 759 (72), [M + Na]<sup>+</sup> Anal. Calcd. (found) for C<sub>30</sub>H<sub>38</sub>N<sub>2</sub>O<sub>13</sub>Ru · 0.5H<sub>2</sub>O: C, 48.34 (48.22), H, 5.23 (5.34), N, 3.75 (3.79).

#### 6.3.2.5 Synthesis of Complexes **29-30**

Complex **23** (0.075 g, 0.10 mmol) was dissolved in 1.5 mL of Acetone and CF<sub>3</sub>SO<sub>3</sub>Ag (0.055 g, 0.20 mmol) was added, leading to the immediate precipitation of silver chloride. The solid was filtered off and *bipy* or *phen* (0.11 mmol) were added to the clear red solution. After 16 h at RT, the dark red resulting solution was concentrated, and diethyl ether was added to afford the product as an orange solid. Yields: 83-85%

**29**: <sup>1</sup>H NMR (400 MHz, Acetone)  $\delta$  10.39 (d, 1H, H3 or H6), 10.18 (d, 1H, H3' or H6'), 8.80 (d, 1H, H6 or H3), 8.73 (d, 1H, H6' or H3'), 8.52 (t, 1H, H4 or H5), 8.44 (t, 1H, H4' or H5'), 8.06 (t, 1H, H5 or H4), 7.92, (d, 1H, H-Im), 7.91 (t, 1H, H5 or H4), 7.55 (d, 1H, H-Im), 7.13 (d, 1H, H-Ar), 6.97 (d, 1H, H-Ar), 6.62 (d, 1H, H-Ar), 6.11 (d, 1H, H-Ar), 6.05 (d,  $J_{H1-H2} = 9.6$  Hz, 1H, H1-glu), 5.75 (t,  $J_{H2-H3} = 9.7$  Hz, 1H, H2-glu), 5.58 (t,  $J_{H3-H4} = 9.7$  Hz, 1H, H3-glu), 5.35 (t,  $J_{H4-H5} = 9.7$  Hz, 1H, H4-glu), 4.82 - 4.75 (m, 1H, H5-glu), 4.46 (dd,  $J_{H5-H6} = 12.3$  Hz,  $J_{H6-H6'} =$

1.5 Hz, 1H, H6-glu), 4.21 (dd,  $J_{H5-H6'} = 7.0$  Hz, 1H, H6'-glu), 3.68 (s, 3H, MeIm), 2.91 (heptet, 1H, CHMe<sub>2</sub>), 2.16 (s, 3H), 2.12 (s, 3H), 2.10 (s, 3H), 2.00 (s, 3H) 1.32 (s, 3H), 1.15 (d, 3H, CHMe<sub>2</sub>), 0.89 (d, 3H, CHMe<sub>2</sub>). <sup>13</sup>C NMR (101 MHz, Acetone)  $\delta$  171.38, 170.98, 170.90, 170.19, 169.78, 160.96, 159.63, 158.16, 157.89, 142.59, 142.51, 130.61, 129.74, 128.87, 127.17, 126.85, 123.16, 113.77, 113.50, 98.35, 97.47, 86.48, 85.36, 83.40, 76.81, 73.19, 70.57, 69.41, 64.26, 40.77, 32.55, 24.89, 22.23, 21.51, 21.41, 21.38, 21.15, 19.33. ESI-MS (+) CH<sub>3</sub>OH (m/z (relative intensity, %)): 402 (100), [Ru(p-cym)NHC(*bipy*)]<sup>2+</sup>, Anal. Calcd. (found) for C<sub>40</sub>H<sub>46</sub>F<sub>6</sub>N<sub>4</sub>O<sub>15</sub>RuS<sub>2</sub>: C, 43.60 (43.76), H, 4.21 (4.42), N, 5.08 (5.01), S, 5.82 (6.12).

**30:** <sup>1</sup>H NMR (400 MHz, Acetone)  $\delta$  10.74 (d, 1H, H2-phen or H-9 phen), 10.54 (d, 1H, H9-phen or H-2 phen), 9.10 (d, 1H, H-4 phen or H-7 phen), 9.04 (d, 1H, H-7 phen or H-4 phen), 8.35 (dd, 1H, H-3 phen or H-8 phen), 8.34 (d, 2H H-5 and H-6 phen), 8.21 (dd, 1H, H-8 phen or H-3 phen), 7.81 (d, 1H, H-Im), 7.43 (d, 1H, H-Im), 7.18 (d, 1H, *H*-Ar), 6.95 (d, 1H, *H*-Ar), 6.72 (d, 1H, *H*-Ar), 6.30 – 6.10 (m, 2H, *H*-Ar and H1-glu), 5.74 - 5.63 (m, 2H, H2-glu and H3-glu), 5.32 (t,  $J_{H3-H4} = J_{H4-H5} = 9.6$  Hz, 1H, H4-glu), 4.88 (dd,  $J_{H6-H6'} = 12.4$  Hz  $J_{H5-H6'} = 1.7$  Hz 1H, H6-glu), 4.24 (dd,  $J_{H5-H6'} = 7.0$  Hz, 1H, H6'-glu), 4.31 – 4.16 (m, , H5-glu), 3.77 (s, 3H, Me-Im), 2.82 (heptet, CHMe<sub>2</sub>), 2.18 (s, 3H, OAc), 2.16 (s, 3H, OAc), 2.12 (s, 3H, MeAr), 2.00 (s, 3H, OAc), 1.03 (d, 3H, CHMe<sub>2</sub>), 0.87 (s, 3H, OAc), 0.67 (d, 3H, MeAr). <sup>13</sup>C NMR (101 MHz, Acetone)  $\delta$  171.41, 171.02, 170.91, 169.88, 169.45, 161.70, 160.23, 148.65, 148.57, 141.69, 141.43, 133.34, 133.20, 130.13, 129.48, 129.39 (C-Im), 129.14, 127.57, 123.04 (C-Im), 113.71 (cym), 113.23 (cym), 97.36, 96.42, 86.54, 84.93, 83.67, 76.43, 73.47, 70.56, 69.39 (C3), 64.29, 41.43, 32.48, 24.29, 22.14, 21.53, 21.39, 21.16, 20.72, 19.48.

ESI-MS (+) CH<sub>3</sub>OH (m/z (relative intensity, %)): 414 (100), [Ru(p-cym)NHC(*phen*)]<sup>2+</sup>, Anal. Calcd. (found) for C<sub>42</sub>H<sub>46</sub>F<sub>6</sub>N<sub>4</sub>O<sub>15</sub>RuS<sub>2</sub> · H<sub>2</sub>O: C, 44.09 (44.12), H, 4.23 (4.35), N, 4.90 (4.91), S, 5.61(6.04).

### 6.3.3 X-ray crystallography of the complexes

X-ray crystallographic studies were performed in collaboration with Dr Rosario Scopelliti and Dr. Farzaneh Fadaei Tirani Institute of Chemical Sciences and Engineering of the École Polytechnique Fédérale de Lausanne, Switzerland.

Suitable crystals were selected and mounted on a SuperNova, Dual, Cu at home/near, AtlasS2 diffractometer. The crystal was kept at a steady  $T = 140.00(10)$  K during data collection. The structure was solved with the ShelXT 2018/2 (Sheldrick, 2015) solution program using dual methods and by using Olex2 (Dolomanov et al., 2009) as the graphical interface. The model was refined with ShelXL 2018/3 (Sheldrick, 2015) using full matrix least squares minimisation on  $F^2$ .

Data were measured using  $\omega$  scans using Cu K $_{\alpha}$  radiation. Data reduction, scaling and absorption corrections were performed using CrysAlisPro (Rigaku, V1.171.40.84a, 2020). A gaussian absorption correction was performed using CrysAlisPro 1.171.40.84a (Rigaku Oxford Diffraction, 2020). The numerical absorption correction was based on gaussian integration over a multifaceted crystal model. The empirical absorption correction was carried out using spherical harmonics, implemented in SCALE3 ABSPACK scaling algorithm. All non-hydrogen atoms were refined anisotropically. Hydrogen atom positions were calculated geometrically and refined using the riding model.

### *6.3.4 Reactivity in aqueous media*

#### *6.3.4.1 NMR Experiments*

Each complex was dissolved in 600  $\mu\text{L}$  of the appropriate solvent mixture to provide a final concentration of 3 mM. Samples were incubated at 37 °C and NMR spectra were recorded at different times over 3-7 days.

#### *6.3.4.2 UV-vis measurements*

The stabilities of complexes **22-30** (0.15mM) were evaluated in aqueous solutions using a Varian Cary 5000 UV-vis-NIR spectrophotometer having a cell compartment thermostated by a temperature controller with accuracy of  $\pm 0.05^\circ\text{C}$  and the following parameters: wavelength range 240–700 nm, data pitch 1 nm, scanning speed 600 nm min<sup>-1</sup>, quartz cuvette with 1 cm path length. The electronic spectral changes were recorded over a period of 24 h and after 7 days at room temperature.

#### *6.3.5 Reactivity with model biomolecules*

UV-vis, fluorescence, CD, protein X-ray crystallographic experiments were performed in collaboration with Prof. A. Merlino research group at University of Naples Federico II. ESI-MS experiments were performed thanks to Dr. Daniel Ortiz at the Institute of Chemical Sciences and Engineering of the École Polytechnique Fédérale de Lausanne, Switzerland.

#### *6.3.5.1 ESI-MS experiments with model nucleophiles*

Stock solutions (10 mM) of each nucleophile were prepared in H<sub>2</sub>O. The correct volume of stock was added to a freshly prepared solution of each complex to afford 1 mM as final concentration of metal with a ratio of 1:2.5, metal to nucleophile. The reactions were carried out at 37 °C for 48 h. Samples for ESI-MS analysis were prepared by diluting 1:10 with water prior to analysis. Spectra were recorded using a Waters Xevo® G2-S QToF ESI mas spectrometer in positive mode. Data analysis was performed using the open-source software Aom2S.

#### *6.3.5.2 ESI-MS experiments with Ubiquitin*

Ubiquitin was dissolved in water at 1 mg/mL. Each complex was dissolved in water at final concentration mM. The appropriate volume of each metal complex solution was then added to a calculated volume of protein solution, to afford a final protein:metal ratio of 1:3. Mass spectrometry analyses were performed on a LTQ Orbitrap Elite FTMS instrument (Thermo Scientific, Bremen, Germany) operated in the positive mode coupled with a robotic chip-based nano-ESI source (TriVersa Nanomate, Advion Biosciences, Ithaca, NY, U.S.A.). A standard data acquisition and instrument control system was utilized (Thermo Scientific) whereas the ion source was controlled by Chipsoft 8.3.1 software (Advion BioScience). Samples were loaded onto a 96-well plate (Eppendorf, Hamburg, Germany) within an injection volume of 5 µl. The experimental conditions for the ionization voltage was +1.4kV and the gas pressure was set at 0.30 psi. The temperature of ion transfer capillary was 200 °C. Operate with the ion transfer capillary at very low temperature that can be used to prevent decomposition of labile molecules. FTMS spectra were obtained in the 100-2000 m/z range in the reduce profile mode with a resolution set to 120,000 and automatic gain control

(AGC) value set at 1E6. A total of 100 scans each consisting in 10  $\mu$ scans was acquired and averaged. Data were analyzed using Apm2 s software tool developed by Patiny et al.<sup>155</sup>

Search parameters were as follows: Ionizations 1-10, Threshold 1%, Mass accuracy 5 ppm, Zone -0.5-2.5, Minimum similarity 80%.

#### *6.3.5.3 Fluorescence experiments with proteins and DNA*

Fluorescence spectra were recorded after 10 min of incubation of each complex (0-16 Mm) with different concentrations of HEWL or HSA, at excitation wavelengths of 280 and 295 nm. When needed, fluorescence spectra correction was employed to the spectrophotometric titrations to compensate for the existing primary and/or secondary inner filter effects using the following equation:

$$F_{\text{corr}} = F_{\text{obs}} 10^{(A_{\text{ex}} + A_{\text{em}})/2}$$

where  $F_{\text{corr}}$  and  $F_{\text{obs}}$  are the corrected and observed fluorescence intensities, respectively, whereas  $A_{\text{ex}}$  and  $A_{\text{em}}$  are the absorbance values at the excitation and emission wavelengths, respectively.

Competitive DNA binding experiments by Ethidium Bromide displacement were carried out following the incubation of 5 mM calf thymus DNA (ct-DNA) with EtBr in 0.050 M ammonium acetate at pH 7.5 at ct-DNA : EtBr molar ratio of 1 : 50 for 30 min in the dark at room temperature. Then, the fluorescence quenching of EtBr-DNA was evaluated in the absence and in the presence of increasing amounts of **22-30** (0-30 mM). Samples were equilibrated for 5 min before collecting each spectrum. Other experimental settings: 1.0 cm quartz cell, excitation/emission slit 5.0 nm, 560–750 nm range, 50 nm min<sup>-1</sup> scanning speed. Data have been obtained as the average of three independent measurements.

#### 6.3.5.4 Crystallographic studies

Crystals of the adducts formed upon reaction of HEWL and RNase A with **26** were obtained using the soaking methods, i.e. exposing metal-free protein crystals to a solution of the reservoir containing the metal complex at 5 mM concentration. Crystals of metal-free HEWL were grown by the hanging drop vapour diffusion method using a reservoir consisting of 20% ethene glycol, 0.6 M NaNO<sub>3</sub> and 0.1 M sodium acetate at pH 4.0. Metal-free RNase A crystals were grown by hanging-drop vapor diffusion using RNase A at 20 mg mL<sup>-1</sup> and a reservoir solution containing 20% PEG4000 and 10 mM sodium citrate buffer at pH 5.1.

Data for the single crystals of the adducts formed upon reaction of HEWL and RNase A with **26** were collected at 100 K at the XRD2 beamline of Elettra, Italy. Crystals were flash-frozen at 100 K using nitrogen gas produced by an Oxford Cryosystem (and maintained at 100 K during the data collection). X-ray diffraction data were processed using Autoproc. The structures were solved by molecular replacement using the models derived from PDB codes 193L and 1JVT (molecule A). Building of the models was carried out using Coot. The structures were refined using REFMAC. Ruthenium ligand assignments were based on the interpretation of the Fo-Fc electron density maps. Ligands were not assigned if the electron density was not clear. Figures were created using PyMOL (v.1.3r1; <http://www.pymol.org>).

#### 6.3.5.5 Circular Dicroism Experiments

CD spectra of ctDNA were registered on a Jasco J-810 spectropolarimeter at 25°C in the presence of different amount of compound. Quartz cells with 0.1 cm path length were used. Each spectrum was obtained averaging three scans and subtracting contributions from the corresponding reference (10 mM ammonium acetate buffer at pH 7.0). Spectra were collected using samples obtained upon 24



h incubation of DNA in the presence of the Ru complexes, and then dialyzed to remove the unbound metal compounds.

#### *6.3.6 Evaluation of the biological activity*

Cell culture and experiments cytotoxicity assays were performed in collaboration with Mouna Hadji from Prof. Paul Dyson research group at the Institute of Chemical Sciences and Engineering of the École Polytechnique Fédérale de Lausanne, Switzerland.

The cells were cultured at 37 °C and CO<sub>2</sub> (5%) in RPMI 1640 GlutaMAX for the A2780 and A2780cisR cell lines and DMEM GlutaMAX media for the HEK-293 cell line. Culture media were supplemented with 10% heat-inactivated FBS and 1% penicillin streptomycin. To maintain resistance, cisplatin was routinely added to the culture medium of the A2780cisR cell line to obtain a final concentration of 2 µM. The cytotoxicity of the compounds was studied using the MTT (3-(4,5-Dimethylthiazol-2-yl)-2,5-Diphenyltetrazolium Bromide) assay. Stock solutions of the compounds were prepared in water and were sequentially diluted in water to give a final compound concentration range of 0–1 mM. 10 µL aliquots of the resulting solutions were added in triplicates to a 96-well plate to which 90 µL of the cell suspension was added at approximately  $1.4 \times 10^4$  cells/well (final volume 100 µL / concentrations range 0–100 µM). Cisplatin and RAPTA-C were used as positive (0–100 µM) and negative (0–200 µM) controls respectively. After 72 h of incubation at 37 °C and 5% CO<sub>2</sub>, 20 µL of an MTT solution (5 mg/mL in Dulbecco's phosphate buffered saline) were added to each well, and the plates were incubated for additional 4 h at the same conditions. The culture media was carefully aspirated and the purple formazan crystals were dissolved in DMSO (100 µL/well). The absorbance of the resulting solutions, directly proportional to

the number of surviving cells, was quantified at 590 nm using a SpectroMax M5e multimode microplate reader (SoftMax Pro software, version 6.2.2). The percentage of surviving cells was calculated (Graphpad prism software, version 9.2.0) from the absorbance of wells corresponding to the untreated control cells. The reported IC<sub>50</sub> values are based on the means from three independent experiments, each comprising 3 tests per concentration level.

## 7 Glycoconjugate Au(I) NHC complexes

### 7.1 General overview

Gold(I) NHC complexes are widely represented in current literature.<sup>188,205</sup> Some glycoconjugate NHC Au(I) compounds have been already mentioned in Section 1.3.2. However, others previous examples strictly related to the work of this chapter are here reported.

In 2017 D'Amora et al.<sup>224</sup> described on the synthesis and the study of the anticancer activity of a series of neutral and cationic Au(I) complexes (**Figure 7.1**), with the glycoconjugate NHC ligand presented in Chapters 5-6 of this work.

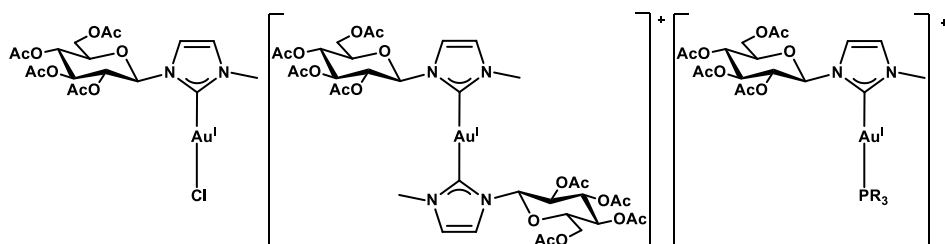


**Figure 7.1.** Gold(I) NHC complexes reported by D'Amora et.al.

The cationic phosphine compounds displayed anticancer activity comparable to cisplatin in terms of cytotoxicity, while both the chlorido derivative and the bis carbene complexes were inactive.

During the course of this PhD work, another series of similar compounds (**Figure 7.2**) were synthesized and studied in collaboration with Prof. Cristina Tubaro research group (University of Padova).<sup>225</sup>

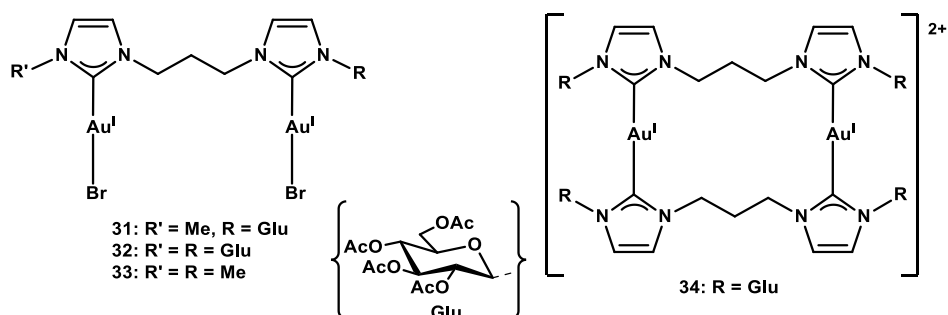


**Figure 7.2.** Gold(I) NHC complexes synthesized in collaboration with C. Tubaro group.

To further investigate the properties of glycoconjugate anticancer Au(I) NHC complexes, a new class of compounds (**Figure 7.3**) were designed.

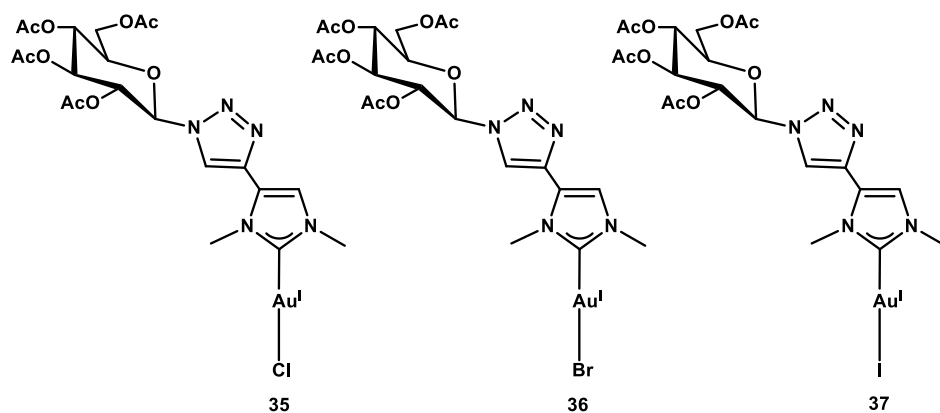


**Figure 7.3.** Au(I) NHC complexes described in this chapter.

The complexes **35-37** are linear Au(I) species with a carbene and a halido ligand. The NHC is an imidazole-2-ylidene ligand, still derived by a methyl imidazole scaffold. However, the glucosyl fragment is linked *via* a triazole obtained by a cycloaddition between an alkyne moiety and an azide function in C1 positions of

the glucopyranose ring. The three complexes display Cl, Br, and I ligands respectively. The synthesis and the spectroscopic characterization of the compounds was performed along with preliminary investigations on their in-solution reactivity. The biological activity of compounds **35-37** was evaluated and the results will be discussed in comparison with complexes **31-34**, to evaluate the effect of a different NHC glycoconjugate scaffold on the biological activity of the gold complexes.

## 7.2 Results and Discussion

### 7.2.1 Synthesis and Characterization of the Pro-Carbene Ligand

The carbene ligand used for the gold complexes **35-37** was obtained by the glucoconjugate imidazole ligand (**L-im**) reported in Chapter 2.

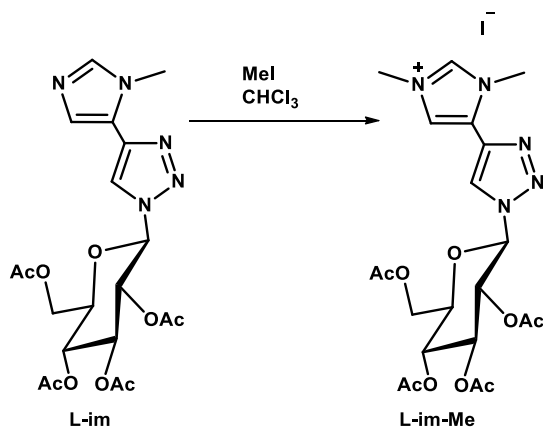


**Figure 7.4.** Synthesis of the pro-carbene ligand

The pro-carbene was easily prepared by reacting **L-im** with an excess of iodomethane in chloroform for 24 h. The alkylated product was isolated by removing the solvent.

NMR and elemental analysis confirmed the positive outcome of the reaction. <sup>1</sup>H NMR spectra of **L-im** and **L-im-Me** are compared in **Figure 7.4**.

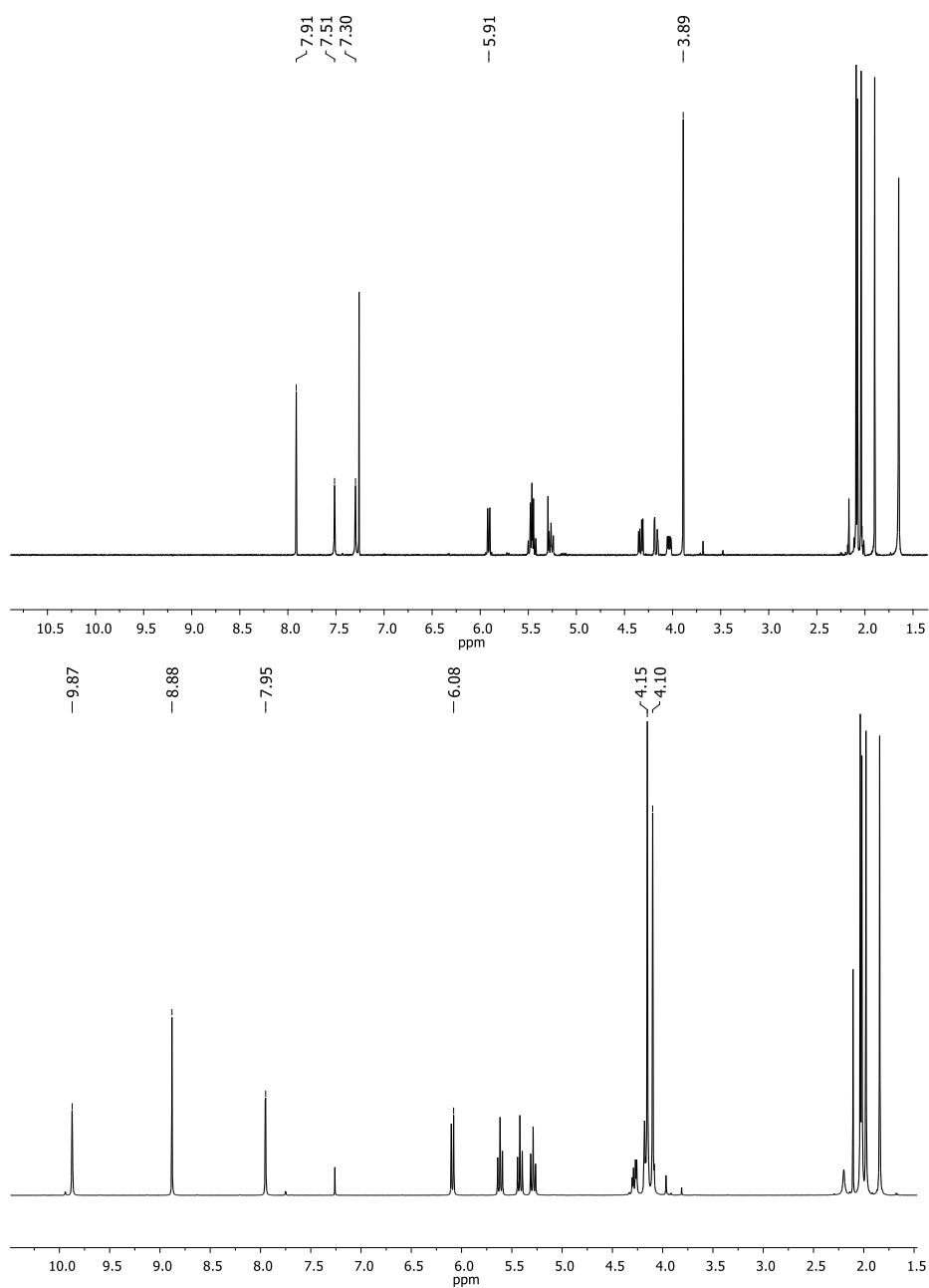


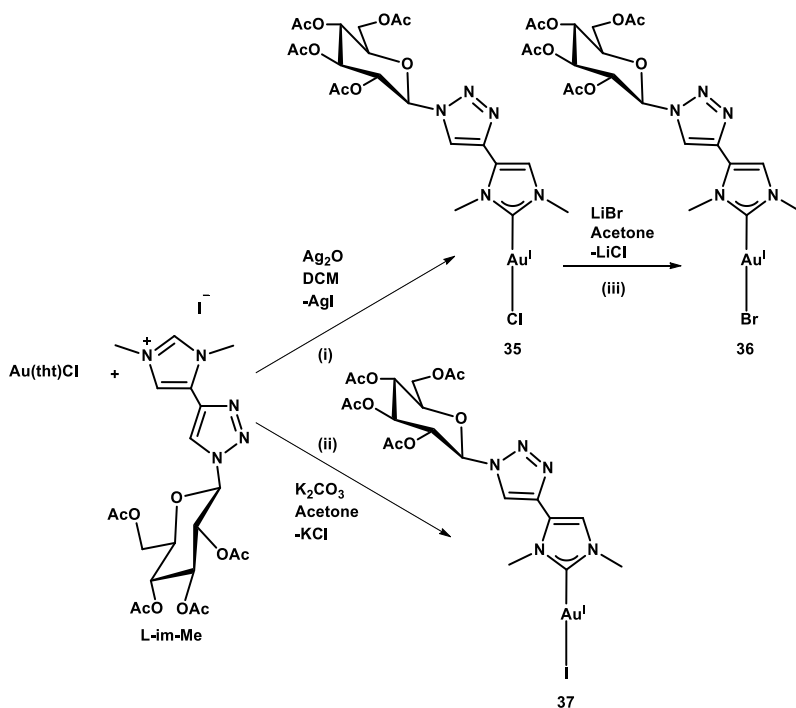
**Figure 7.4.**  $^1\text{H}$  NMR spectra of **L-im** (top) and the methylated pro-carbene **L-im-Me** (bottom), in  $\text{CDCl}_3$  at 400 MHz.

The formation of the cationic quaternary nitrogen atom resulted in a general downfield shift of the signals. The *NCHN* atom was the most affected, shifting from 7.51 ppm in **L-im** to 9.87 ppm in **L-im-Me**, while the singlet of the triazole and the doublet of the backbone imidazole protons shifted from 7.91 ppm to 8.88 ppm and from 7.30 to 7.95 ppm respectively. The two non-equivalent methyl groups were found at 4.10 and 4.15 ppm, with respect the singlet of neutral **L-im** observed at 3.89 pm. The identity of the pro-carbene was confirmed by elemental analysis.



### 7.2.2 Synthesis and Characterization of the Complexes

The gold complexes **35-37** were synthesized according to **Scheme 7.1**.



**Scheme 7.1.** Synthesis of gold(I) NHC complexes

Generally, the compounds were prepared by reacting the precursor  $[\text{Au}(\text{tht})\text{Cl}]$  (tht = tetrahydrothiophene) with the pro-carbene **L-im-Me**. However, different strategies were used depending on the halide co-ligand. The transmetalation via  $\text{Ag}(\text{I})$  NHC intermediate (path **i**) resulted in the formation of the chlorido complex **35**. Indeed, the reaction occurred with precipitation of  $\text{AgI}$ , which avoid the formation of mixed chloro/iodo species.

Conversely, the iodido derivative **37** was prepared *via* “free carbene route” (path **ii**). This strategy consisted in the *in situ* deprotonation of the imidazolinium salt

**L-im-Me** by  $K_2CO_3$  and coordination of the resulting carbene to gold. This strategy resulted only in the formation of the iodido derivative **37**. Finally, the bromo derivative **36** was isolated through a halide exchange, by treating **35** in presence of LiBr in acetone.

Such outcomes agreed with the expectations and can be explained considering that in path **i** the precipitation of the silver salt worked as thermodynamic driving force for the reaction. Then, the by far lower solubility of AgI with respect AgCl led to the formation only of **35**. In path **ii** (and **iii**) the major affinity of gold for softer halides<sup>226</sup> led to the formation of the iodido **37** (or the bromido **36**) while the chlorido was not detected.

The compounds were characterized by  $^1H$  and  $^{13}C$ , mono and bidimensional NMR, as well as by elemental analysis. The formation of the carbene complexes was clear by comparing the NMR spectra of the pro-carbene **L-im-Me** with those of **35-37** (Figure 7.5).

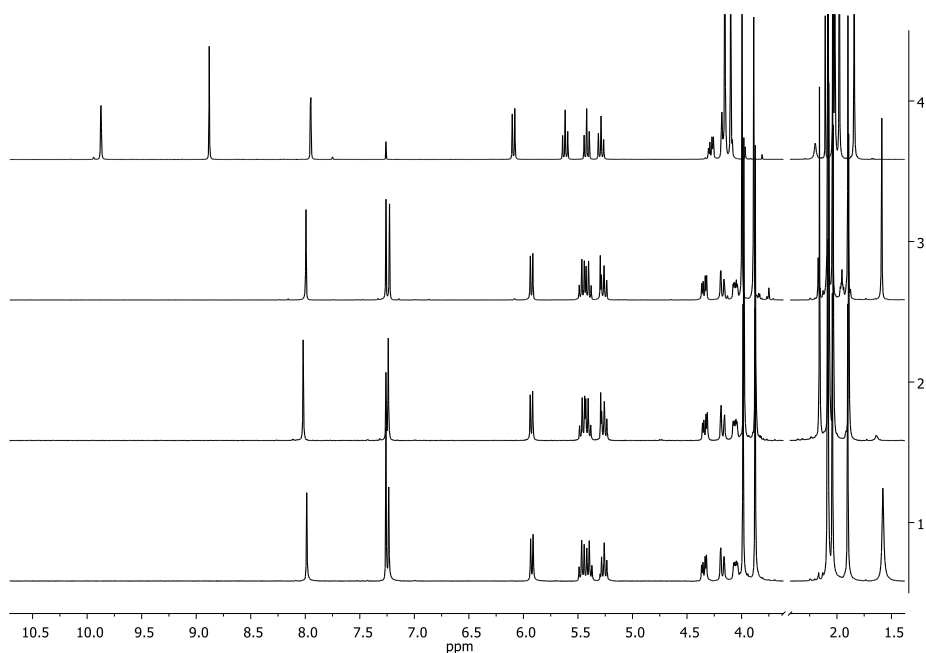


**Figure 7.5.**  $^1\text{H}$  NMR spectra of **35** (trace 1), **36** (trace 2), **37** (trace 3), and **L-im-Me** (trace 4) in  $\text{CDCl}_3$  at 400 MHz.

One evidence was the disappearance of the singlet at 9.87 ppm belonging to the  $\text{NCHN}$  proton. Moreover, the coordination to metal center resulted in a highfield shift of the imidazole proton at 7.23 ppm. The signals of sugar protons were found at the expected values of chemical shifts, with the coupling patterns for glucose in  $\beta$  configuration. However, the proton spectra of the complexes were perfectly overlapping, as the halide did not affect the signals of the protons on the carbene. Conversely, an effect of the X ligand was observable in the  $^{13}\text{C}$  NMR spectra, reported in **Figure 7.6**.

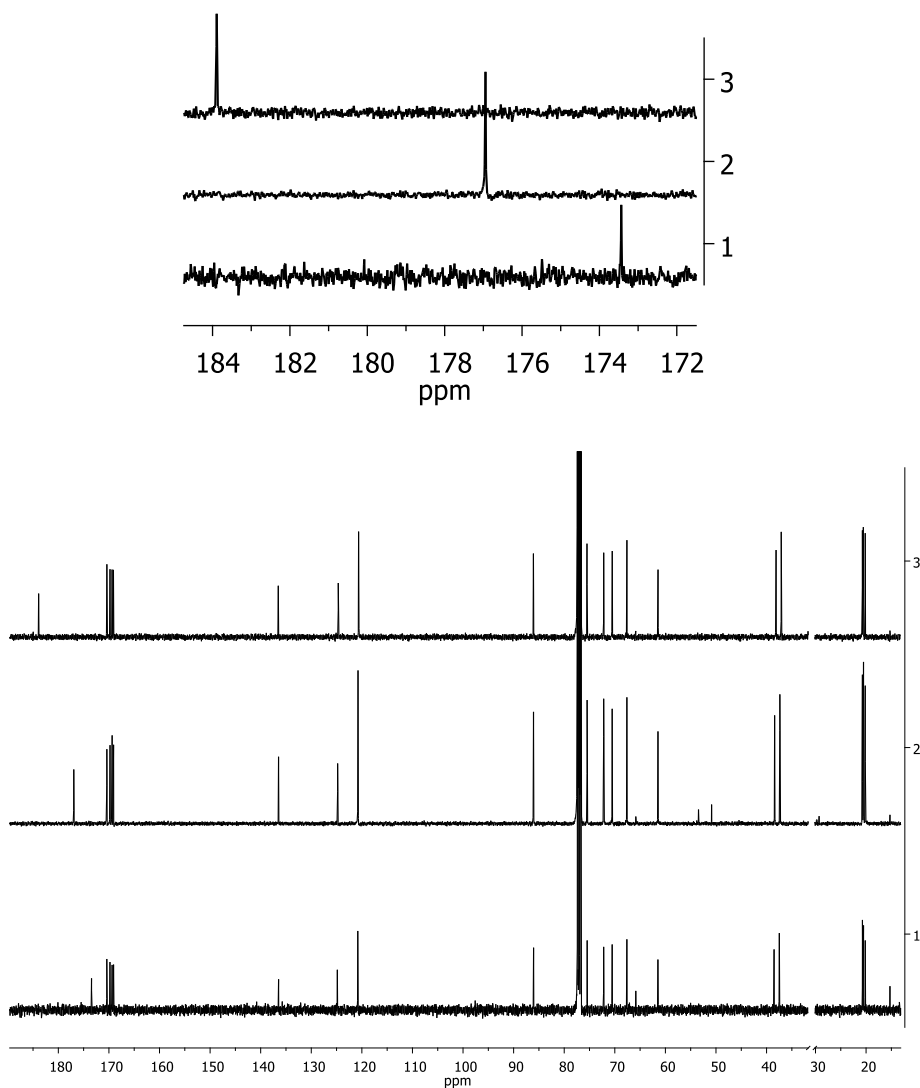


**Figure 7.6.**  $^{13}\text{C}$  NMR spectra of **35** (trace 1), **36** (trace 2), and **37** (trace 3) in  $\text{CDCl}_3$  at 400 MHz. .

The carbene atoms resonated progressively at higher frequencies going from the chlorido to the iodido derivative. Such deshielding trend was due to the *trans*

influence exerted by the halido co-ligand which follows the trend  $I > Br > Cl$ .<sup>227</sup> Such observation can be explained by considering the intrinsic electronic structure of N-Heterocyclic Carbenes. Indeed, in  $^{13}C$  NMR the carbene atom signal of non-coordinated NHCs ligands is generally highly downfield shifted, with values  $\delta > 200$  ppm. Such downfield shift is related to the singlet–triplet (S-T) transition which occurs in free-carbenes by promoting an electron from the  $\sigma$  (NHC lone-pair) to a vacant  $p_{\pi}$  orbital of the NHC.<sup>228</sup> This process strongly contributed to the paramagnetic shielding of the carbene atom resulting in a notable downfield shift. Stronger trans donor ligands weaken more the  $Au-C_{Carbene}$  bond, which acquire an increased “free NHC ligand” character resulting in the downfield shift observed in the  $^{13}C$  NMR spectra. Similar trend were observed in NHC metal complexes with different trans donor ligands.<sup>229,230</sup> Finally, the elemental analysis confirmed the identity as well as the purity of the compounds.

### 7.2.3 *In-solution stability*

The in-solution stability of **35-37** was first evaluated by recording  $^1\text{H}$  NMR spectra in acetone- $\text{d}_6$  and DMSO- $\text{d}_6$ . In both the solvents, the complexes gave rise to spectral profile that did not change over 24 h (**Figure 7.7- Figure 7.9**).

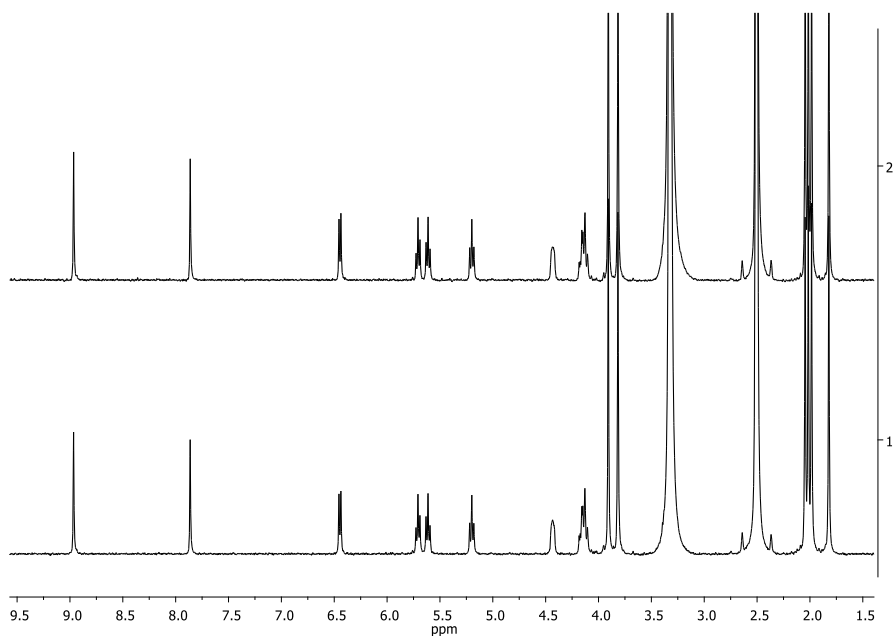


**Figure 7.7.**  $^1\text{H}$  NMR spectra of **35** in DMSO- $\text{d}_6$  following the dissolution (trace 1) and after 24 h (trace 2) at 500 MHz.

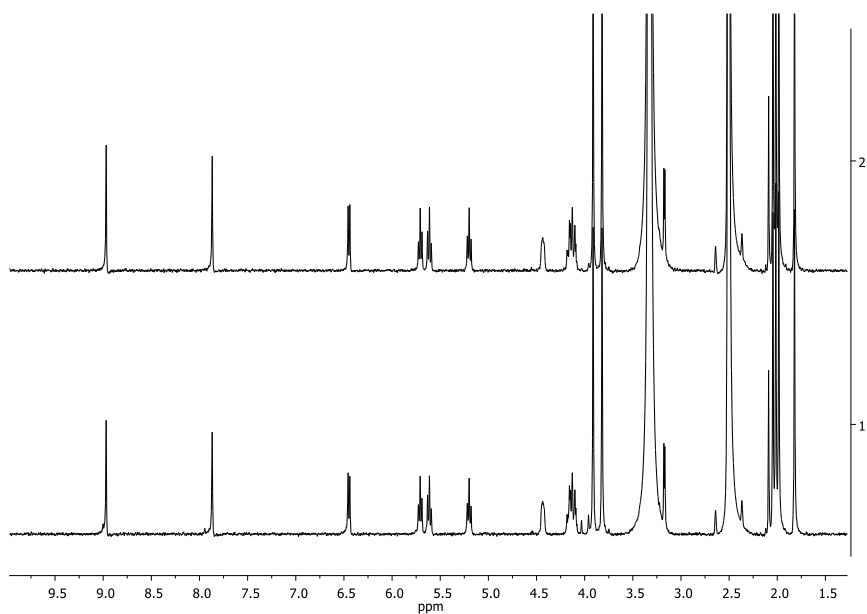


**Figure 7.8.**  $^1\text{H}$  NMR spectra of **36** in  $\text{DMSO-d}_6$  following the dissolution (trace 1) and after 24 h (trace 2) at 500 MHz.

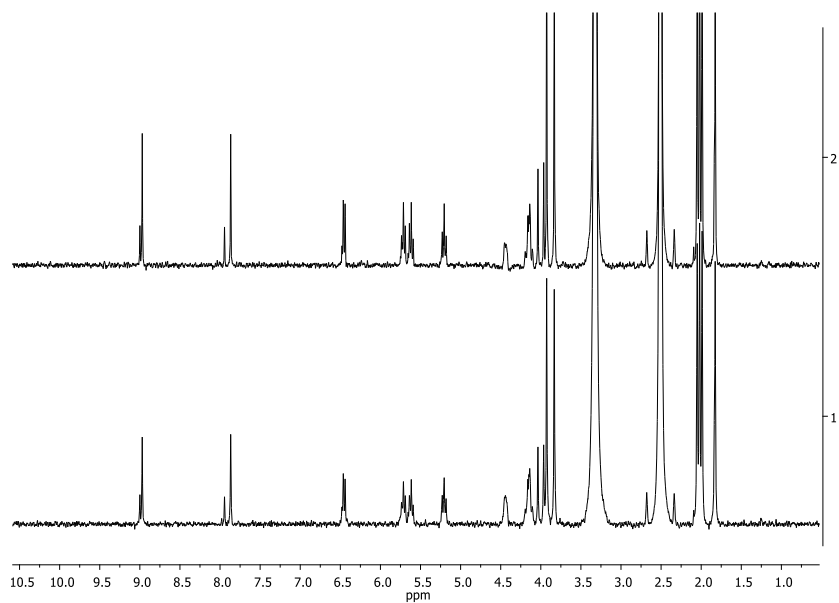
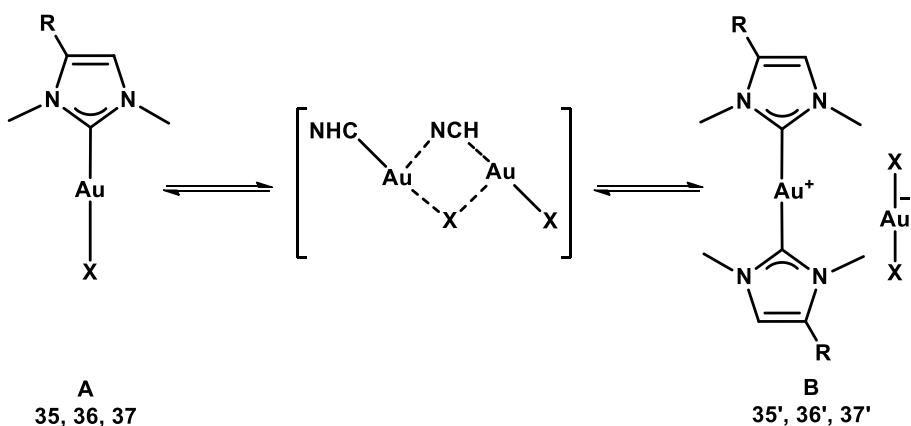


**Figure 7.9.**  $^1\text{H}$  NMR spectra of **37** in  $\text{DMSO-d}_6$  following the dissolution (trace 1) and after 24 h (trace 2) at 500 MHz.

Both in acetone and DMSO beyond the signals attributable to the NHC halide complex, the presence of another species was observable by a less intense set of signals for **36** and **37**. The less abundant species was hypothesized to be a bis carbene species of type  $[\text{Au}(\text{NHC})_2]^+[\text{AuX}_2]^-$ . Indeed,  $[\text{Au}(\text{NHC})\text{X}]$  ( $\text{X} = \text{Cl}, \text{Br}, \text{I}$ ) complexes are known to perform ligand scrambling in solution,<sup>231,232</sup> as reported in **Scheme 7.4**.



**Scheme 7.4.** Ligand scrambling as observed in  $[\text{Au}(\text{NHC})\text{X}]$  complexes.

According to this reactivity, the neutral NHC complex A is in equilibrium with a cationic di-carbene form (B) and the anionic  $[\text{AuX}_2]^-$ .

$^{13}\text{C}$  NMR spectrum of complex **37** in  $\text{DMSO-d}_6$  confirmed such hypothesis, as observable in **Figure 7.10**.



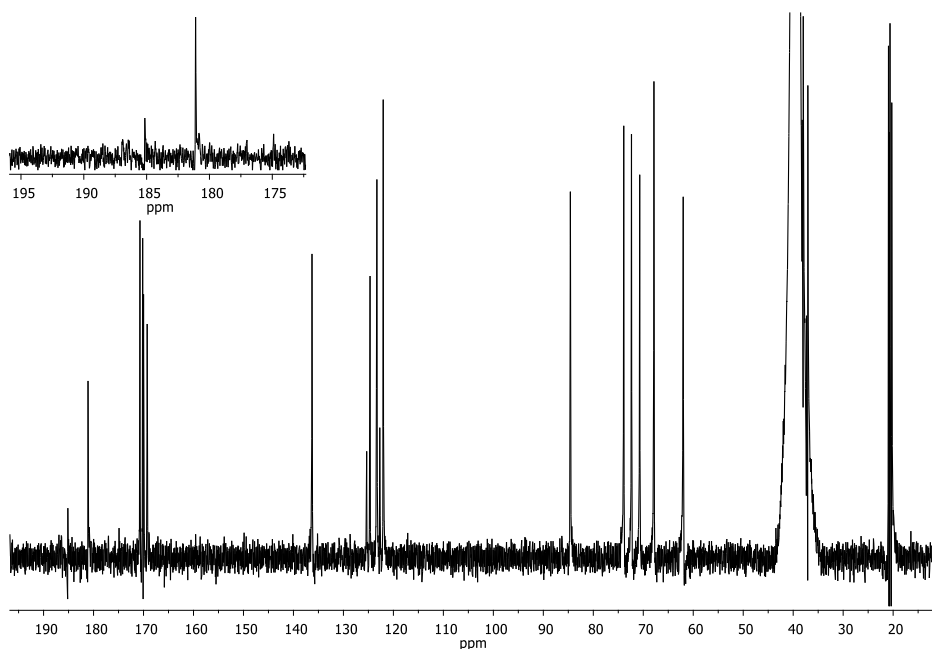


**Figure 7.10.**  $^{13}\text{C}$  NMR spectrum of complex **37** in  $\text{DMSO-d}_6$  at 500 MHz.

Indeed, the NHC ligand is a stronger trans donor than the halide. According to previously reported data,<sup>233</sup> the  $\text{C}_{\text{Carbene}}$  atom of the di-carbene species **37'** would resonate at higher frequencies than the iodo derivative **37**. Indeed, the spectrum revealed the presence of two species with the carbene atom of the less abundant downfield shifted (185 ppm) with respect the one belonging to the iodo complex (181 ppm).

Interestingly, the relative abundances of the second species were not the same for all the compounds. Indeed, by the integration of suitable signals, the di-carbene species was quantified ~3% and ~12% **36** and **37** respectively.

The different amount observed in the three complexes was in line with what reported by Huynh et al.<sup>233</sup> Indeed, they observed that in a series of halide  $\text{Au(I)}$

NHC complexes, the iodido derivative was present exclusively in the di-carbene form in the solid state, while the chlorido and bromido analogues were found in neutral form  $[\text{Au}(\text{NHC})\text{X}]$ .

To investigate the stability in aqueous systems, mixed  $\text{D}_2\text{O}$ -Acetone and  $\text{D}_2\text{O}$ -DMSO mixture were studied. No more than 50%-50% ratio of solvents could be reached, due to the precipitation of the compounds in presence of more water.

In aqueous solvents similar spectral profiles to what observed in pure organic solvents were observed, although the relative abundances between the mono- and the di-carbene changed over time. For instance, in **Figure 7.11** the spectra recorded for the bromido derivative **36** in 50%-50%  $\text{DMSO-d}_6$ - $\text{D}_2\text{O}$  are reported.

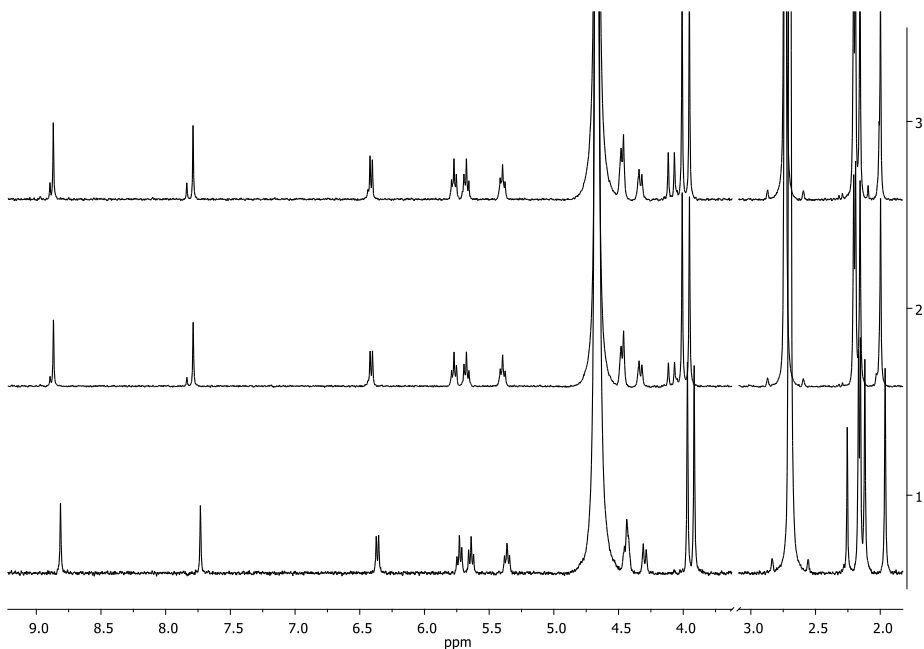


**Figure 7.10.**  $^1\text{H}$  NMR spectra of **36** in 50%-50%  $\text{D}_2\text{O}$ - $\text{DMSO-d}_6$  following the dissolution (trace 1), after 4 h (trace 2), and after 24 h (trace 3) at 500 MHz..

After 24 h the abundance of **36'** reached almost the 10% of the starting complex with respect the 5% reached in pure DMSO. Similar trend was observed for **35** (5% of **35'** after 24 h) and for **37** (almost 25% of **37'** after 24 h). Such behaviour was dependent on the polarity of the solvent mixture, increased by the presence of water.<sup>234</sup>

The reactivity observed in aqueous solvent mixtures was perfectly in line with the results obtained in water with other studied NHC halide gold(I) complexes.<sup>235–237</sup>

In summary, compounds **35–37** showed to be stable in aqueous solvent mixtures, with the retention of the Au-NHC fragment. The equilibrium between the neutral halide and the cationic di-carbene form, was found to be dependent on the halide (**37'** > **36'** > **35'**) and enhanced in presence of water. This observation could play a crucial role in the biological activity of the compounds. Indeed, cationic bis carbene species are usually more active than their neutral counterparts, then the speciation of complexes **35–37** in biological conditions would probably govern the cytotoxic effect as well as the propensity to react with biomolecules.<sup>238–240</sup> These considerations encouraged to test the *in vitro* biological activity of the compounds **35–37**.

#### 7.2.4 Cytotoxic activity of **31–37**

The biological activity of the NHC gold(I) **31–37** was assessed on two couples of cell lines, with each couple constituted by a cancerous line and a biologically related non-cancerous counterpart. Tumor cell line A431 (epidermoid carcinoma cells) and related non-tumor HaCaT (human keratinocyte cells), SVT2 cells (murine fibroblasts BALB/c-3T3 transformed with SV40 virus) and BALB/c3T3 were selected. The cytotoxicity was evaluated by determining the IC<sub>50</sub> values (the concentration of complex able to reduce to 50% the cell viability) through MTT

assay after 48 h incubation. The selectivity of the compounds was evaluated by relating the IC<sub>50</sub> of the cancer line with its healthy counterpart. Cells were incubated with increasing concentrations of the complex and then cell survival was evaluated. The IC<sub>50</sub> values are reported in **Table 7.1** and **Table 7.2**.

**Table 7.1.** IC<sub>50</sub> values (μM) obtained for **31-34** after 48 h incubation. Selectivity Index (SI), indicated by the ratio between the IC<sub>50</sub> of immortalized cells and cancer cells. (Tested concentrations 0.1 – 250 μM)<sup>225</sup>

Complex	IC <sub>50</sub> (μM)				SI HaCat/A431	SI BALB /c3T3/ SVT2
	HaCaT	A431	BALB/c3T3	SVT2		
<b>31</b>	181 ± 8	162 ± 34	148 ± 15	139 ± 12	1.1	1.1
<b>32</b>	N.D.	137 ± 5	108 ± 17	118 ± 6	N.D.	13
<b>33</b>	N.D.	N.D.	N.D.	72 ± 15	N.D.	N.D.
<b>34</b>	240 ± 15	241 ± 15	235 ± 16	207 ± 15	1	1.1

**Table 7.2.** IC<sub>50</sub> values (μM) obtained for **35-37** after 48 h incubation. Selectivity Index (SI), indicated by the ratio between the IC<sub>50</sub> of immortalized cells and cancer cells. (Tested concentrations 0.1 – 100 μM)

Complex	IC <sub>50</sub> (μM)				SI HaCat/A431	SI BALB /c3T3/ SVT2
	HaCaT	A431	BALB/c3T3	SVT2		
<b>35</b>	N.D.	91 ± 2	76 ± 1	84 ± 6	N.D.	0.90
<b>36</b>	N.D.	N.D.	82 ± 4	92 ± 4	N.D.	0.87
<b>37</b>	92.0 ± 0.1	83 ± 5	83 ± 8	35 ± 6	1.1	2.4

Carbene complexes **35-37** displayed  $IC_{50}$  values in the high micromolar range, lower than those obtained for dinuclear Au(I) complexes **31-34**, then demonstrating an increased cytotoxicity. No evident differences were observed by changing the halide ligand, although some distinction could be observed. The chlorido derivative **35** was active on A431 cell while no cell mortality was observed in the non-cancer counterpart HaCaT, stating for some selectivity of this complex. Similarly, the iodido complex **37** was almost 2- times more toxic on SVT2 with respect to BALB/c3T. Such outcome in the cytotoxicity could be affected by what emerged in the in-solution stability studies. Indeed, in the aqueous cell medium the equilibrium between the two forms of the carbene complexes could probably play an important role in the biological activity of **35-37**. The cytotoxicity of the synthesized di-carbene species will be tested to evidence more details on the biological mechanism of action of these gold NHC complexes. Noteworthy, di-nuclear species (**31-34**) showed reduced activity and lack of selectivity compared to the mono-gold NHC complexes.

## 7.3 Experimental Part

### 7.3.1 General

Reagents and solvents were purchased from Sigma-Aldrich and were used without further purification. Human A431 epidermoid carcinoma, murine BALB/c-3T3 and SVT2 fibroblasts were from ATCC. Human HaCaT keratinocyte cells were from Innoprot. Cells were cultured in Dulbecco's modified Eagle's medium (DMEM) (Sigma-Aldrich, St Louis, MO, USA), supplemented with 10% foetal bovine serum (HyClone), 2 mM L-glutamine and antibiotics, all from Sigma-Aldrich, under a 5% CO<sub>2</sub> humidified atmosphere at 37 °C. NMR spectra were acquired on 400 MHz Bruker AVANCE-IIIHD-400 located at the Institute of Chemical Sciences and Engineering of the École Polytechnique Fédérale de Lausanne (Switzerland), on a 400 Bruker Avance Ultrashield™ 400 and on a 500 Varian Inova, located at the Dipartimento di Scienze Chimiche, Università di Napoli Federico II, Napoli (Italy). The solvents were CDCl<sub>3</sub> (CHCl<sub>3</sub>,  $\delta$  7.26, and <sup>13</sup>CDCl<sub>3</sub>,  $\delta$  77.0, as internal standards), (CD<sub>3</sub>)<sub>2</sub>CO ((CD<sub>2</sub>H)<sub>2</sub>CO),  $\delta$  2.09, as internal standard), D<sub>2</sub>O (HDO,  $\delta$  4.80 as internal standard), and (CD<sub>3</sub>)<sub>2</sub>SO ((CD<sub>2</sub>H)<sub>2</sub>SO),  $\delta$  2.49, as internal standard). The following abbreviations were used for describing NMR multiplicities: s, singlet; d, doublet; dd, double doublet; triplet; app, apparent; m, multiplet; ABq, AB quartet. Au(tht)Cl was prepared according to literature starting from H[AuCl<sub>4</sub>].<sup>241</sup> The imidazole precursor **L-im** was prepared as reported in *Chapter 2*.

### 7.3.2 Synthesis and Characterization

#### 7.3.2.1 Synthesis of the pro-carbene ligand **L-im-Me**

**L-im** (0.60 g, 1.2 mmol) was dissolved in 10 mL of  $\text{CHCl}_3$  and iodomethane (2 mL, 35 mmol) was added. The solution was stirred at RT for 24 h and then the solvent was removed under vacuum. The product was isolated as brown oil which was treated with diethyl ether resulting in a white powder. Yield: 97% (0.73 g).

$^1\text{H}$  NMR (400 MHz,  $\text{CDCl}_3$ )  $\delta$  9.91 (br, 1H, H2-Im), 8.88 (s, 1H, H-Triazole), 7.95 (d,  $J = 1.6$  Hz, 1H, H4-Im), 6.09 (d,  $J_{\text{H1-H2}} = 9.3$  Hz, 1H, H1-glu), 5.62 (t,  $J_{\text{H2-H3}} = 9.4$  Hz, 1H, H2-glu), 5.42 (t,  $J_{\text{H3-H4}} = 9.5$  Hz, 1H, H3-glu), 5.29 (t, 1H,  $J_{\text{H4-H5}} = 9.6$  Hz, H4-glu), 4.28 (dd,  $J = 13.0, 5.3$  Hz, 1H, H6-glu), 4.21 – 4.02 (m, 2H, H5-glu and H6-glu), 4.15 (s, 3H, Me-Im), 4.15 (s, 3H, Me-Im), 2.03 (s, 3H, OAc), 2.02 (s, 3H, OAc), 1.98 (s, 3H, OAc), 1.84 (s, 3H, OAc). Anal. Calcd. (found) for  $\text{C}_{21}\text{H}_{28}\text{IN}_5\text{CO}_9$ : C, 40.59 (40.12), H, 4.54 (4.71), N, 11.27 (11.54).

#### 7.3.2.2 Synthesis of complex **35**

**L-im-Me** (0.30 g, 0.49 mmol) was dissolved in 5 mL of acetone and  $\text{Ag}_2\text{O}$  (0.062 g, 0.26 mmol) was added. The mixture was stirred at RT for 3 h and then  $[\text{Au}(\text{tht})\text{Cl}]$  (0.33 g, 0.45 mmol) was added. After stirring for 1.5 h the mixture was filtered through Celite and the solvent was removed. The crude material was dissolved in DCM and crystallized by adding diethyl ether. Yield: 78% (0.26 g).

$^1\text{H}$  NMR (400 MHz,  $\text{CDCl}_3$ )  $\delta$  7.92 (s, 1H, H-Triazole), 7.17 (s, 1H, H-Im), 5.86 (d,  $J_{\text{H1-H2}} = 9.0$  Hz, 1H, H1-glu), 5.40 (t,  $J_{\text{H2-H3}} = J_{\text{H3-H4}} = 9.4$  Hz, 1H, H3-glu), 5.33 (t, 1H, H2-glu), 5.20 (t,  $J_{\text{H4-H5}} = 9.6$  Hz, 1H, H4-glu), 4.28 (dd,  $J_{\text{H6-H6'}} = 12.7, J_{\text{H6-H5}} = 5.0$  Hz, 1H, H6-glu), 4.11 (d,  $J_{\text{H6'-H5}} = 1.4$  Hz, 1H, H6'-glu), 3.99 (ddd, 1H, H5-glu), 3.92 (s, 1H, Me-Im), 3.81 (s, 3H, Me-Im), 2.02 (s, 3H, OAc), 2.02 (s,

3H, OAc), 1.98 (s, 3H, OAc), 1.84 (s, 3H, OAc).  $^{13}\text{C}$  NMR (101 MHz,  $\text{CDCl}_3$ )  $\delta$  173.44, 170.42, 169.79, 169.37, 169.08, 136.46, 124.85, 120.81, 120.77, 86.06, 75.46, 72.20, 70.52, 67.62, 61.47, 38.52, 37.48, 20.72, 20.54, 20.51, 20.16. Anal. Calcd. (found) for  $\text{C}_{21}\text{H}_{27}\text{AuIN}_5\text{CO}_9$ : C, 34.75 (34.39), H, 3.75 (3.82), N, 9.65 (9.47).

### 7.3.2.3 Synthesis of complex **36**

Complex **35** (0.13 g, 0.17 mmol) was dissolved in acetone (4 mL) and LiBr (0.175 g, 2.0 mmol) was added. The mixture was stirred at RT for 12 h, and then the solvent was removed. The crude was dissolved in DCM (2 mL) and filtered through a pad of Silica, washed with DCM. The solvent was reduced in volume and the addition of diethyl ether resulted in crystallization of the product. Yield: 85% (0.11 g).

$^1\text{H}$  NMR (400 MHz,  $\text{CDCl}_3$ )  $\delta$  8.02 (s, 1H, H-Im), 7.24 (s, 1H, H-Triazole), 5.93 (d,  $J_{\text{H1-H2}} = 8.9$  Hz, 1H), 5.43 (m, 2H, H2-glu and H3-glu), 5.27 (t,  $J_{\text{H3-H4}} = J_{\text{H4-H5}} = 9.3$ , 1H, H4-glu), 4.34 (dd,  $J_{\text{H6-H6'}} = 12.7$ ,  $J_{\text{H6-H5}} = 5.0$  Hz, 1H, H6-glu), 4.17 (dd,  $J_{\text{H6'-H5}} = 2.0$  Hz, 1H, H6'-glu), 4.06 (ddd, 1H, H5-glu), 3.98 (s, 3H, Me-Im), 3.87 (s, 3H, Me-Im), 2.16 (s, 3H, OAc), 2.08 (s, 3H, OAc), 2.07 (s, 3H, OAc), 2.03 (s, 3H, OAc).  $^{13}\text{C}$  NMR (101 MHz,  $\text{CDCl}_3$ )  $\delta$  176.94, 170.41, 169.78, 169.36, 169.08, 136.47, 124.79, 120.76, 120.73, 86.07, 75.47, 72.20, 70.51, 67.61, 61.47, 38.41, 37.37, 20.72, 20.54, 20.51, 20.17. Anal. Calcd. (found) for  $\text{C}_{21}\text{H}_{27}\text{AuBrN}_5\text{CO}_9$ : C, 32.74 (31.63), H, 3.53 (3.67), N, 9.09 (8.59).

### 7.3.2.4 Synthesis of complex **37**

**L-im-Me** (0.28 g, 0.48 mmol) and  $[\text{Au}(\text{tht})\text{Cl}]$  (0.15 g, 0.45 mmol) were dissolved in 4 mL of acetone and then  $\text{K}_2\text{CO}_3$  (0.065 g, 0.47 mmol) was added.



The mixture was refluxed for 3h and then the solvent was removed in vacuo. The crude mixture was dissolved in DCM (2 mL) and filtered through a pad of silica, washed with DCM (3 x 1 mL). The eluted solvent was concentrated, and diethyl ether was added, to crystallize the product as a white solid that was washed with diethyl ether and dried under vacuum. Yield: 60% (0.22 g).

$^1\text{H}$  NMR (400 MHz,  $\text{CDCl}_3$ )  $\delta$  7.99 (s, 1H, H-Im), 7.23 (s, 1H, H-Triazole), 5.92 (d,  $J = 9.0$  Hz, 1H, H1-glu), 5.43 (m, 2H, H2-glu and H3-glu), 5.26 (t,  $J_{\text{H4-H3}} = 9.6$  Hz, 1H, H4-glu), 4.34 (dd,  $J_{\text{H6-H6'}} = 12.6$ ,  $J_{\text{H6-H5}} = 5.0$  Hz, 1H, H6-glu), 4.16 (dd,  $J_{\text{H6'-H5}} = 1.6$  Hz, 1H, H6'-glu), 4.06 (ddd, 1H, H5-glu), 4.00 (s, 3H, Me-Im), 3.87 (s, 3H, Me-Im), 2.09 (s, 3H, OAc), 2.08 (s, 3H, OAc), 2.04 (s, 3H, OAc), 1.90 (s, 3H, OAc).  $^{13}\text{C}$  NMR (101 MHz,  $\text{CDCl}_3$ )  $\delta$  183.89, 170.40, 169.78, 169.37, 169.11, 136.52, 124.66, 120.65, 120.59, 86.09, 75.50, 72.19, 70.50, 67.61, 61.46, 38.12, 37.10, 20.72, 20.54, 20.51, 20.17. Anal. Calcd. (found) for  $\text{C}_{21}\text{H}_{27}\text{AuIN}_5\text{CO}_9$ : C, 30.86 (29.94), H, 3.35 (3.67), N, 8.15 (8.59).

### 7.3.3 *In-solution experiments*

Stock solutions of every complex were prepared for each set of experiments. The appropriate complex (10 mM) was dissolved in 0.5 mL of DMSO- $d_6$  or Acetone- $d_6$ . The calculated volumes of solution were diluted to 600  $\mu\text{L}$  with the appropriate volumes  $\text{D}_2\text{O}$  or DMSO- $d_6$  / Acetone- $d_6$ . to provide a final concentration of 3 mM of gold complex with the appropriate v/v ratio of solvents.

### 7.3.4 *Evaluation of the biological activity*

Cell culture and cytotoxicity assays were performed in collaboration with Prof. Daria M. Monti research group at University of Naples Federico II.

To test the cytotoxicity of **35-37**, cells were seeded at a density of  $2.5 \times 10^3$  cells per well in 96-well plates. After 24 h, increasing concentrations of compound dissolved in DMSO, were added to the cells (0.1-250  $\mu$ M for **31-34**, 0.1–100  $\mu$ M **35-37**). After 48 h incubation, cell viability was assessed by the MTT (3-(4,5-dimethylthiazol-2-yl)-2,5-diphenyltetrazolium bromide) as previously described.<sup>158</sup> Cell survival was expressed as the percentage of viable cells in the presence of **35-37** compared to the controls, represented by untreated cells and cells supplemented with identical volumes of DMSO. Each sample was tested in three independent analyses, each carried out in triplicate.

## 8 Concluding Remarks and Future Perspectives

The work described in this PhD thesis was focused on the design, the synthesis, the study of the chemical properties, and the evaluation of the cytotoxic activity of novel organometallic glycoconjugate complexes. The main goal was to perform a systematic study to evidence structural key features that influence the reactivity in similar physiological conditions, as well as the biological activity of the studied compounds.

The conjugation of a sugar fragment in the coordination sphere of a metal complex provides several beneficial features as increased water solubility, enhanced biocompatibility and can finally enhance the selectivity of the resulting drug, due to the increased uptake of carbohydrates required to the proliferation of fast-growing cancer cells. In this frame, several panels of organometallic complexes with different glycosyl-derived motifs were compared.

In *Chapter 2* the effect of the molecular geometry was studied, by studying two classes of Pt(II) compounds with neutral *N*-based glucoconjugate ligands. Square-planar (*sp*) and trigonal bipyramidal (*tbp*) coordination environments were compared revealing different chemical reactivities and biological properties. Indeed, the square-planar species displayed higher robustness with respect to the substitution of the sugar-containing ligand than the *tbp* analogues. This aspect was reflected in the increased selectivity for cancer cells of *sp* complexes, although the non-selective *tbp* analogues displayed more competitive IC<sub>50</sub> values in the sub-micromolar range.

In *Chapter 3* a Pt(0) olefin complex with a glucose derived 2-iminopyridine ligand was synthesized and its stereochemistry of coordination was studied by NMR

techniques. The complex was soluble and stable for some days in water, thanks to the simultaneous presence of the chelate 2-iminopyridine and of the electron-withdrawing alkene dimethyl fumarate. Such compound was cytotoxic on different cancer cell lines and it represents one of the few examples of Pt(0) molecular complexes tested as anticancer drug.

In *Chapter 4* a family of neutral Pt(II) *tbp* complexes with glucosyl fragments directly bond to a Pt-centre was studied. The unexpected stereochemical outcome observed in the synthesis was studied combining experimental and theoretical approaches, to shed light on the mechanism of reaction.

Biological experiments confirmed a high level of cytotoxicity of *tbp* Pt(II) complexes (IC<sub>50</sub> in the low micromolar range) with the C1-linked galactosyl derivatives that displayed selectivity for cancer cells.

The study of coordinatively saturated Pt-complexes continued in *Chapter 5*, where two subclasses of Pt(II) and Pt(IV) complexes with glycosylated *N*-Heterocyclic Carbene (NHC) ligands were studied. The two types of compounds present close structural analogies, sharing an overlapping coordination environment in two formally different oxidations states. An extensive spectroscopic characterization allowed to disclose the structural analogies, while a comparative study involving their in-solution stability, their reactivity with model biomolecules and their biological activity revealed substantial differences in both chemical and biological features. Pt(II) compounds showed excellent activity while the changes in the oxidations state dramatically reduced the biological performances of the Pt(IV) analogues.

In this class of compounds, complex **12** (**Figure 8.1**) emerged as the best candidate considering all the panels studied during this PhD work.

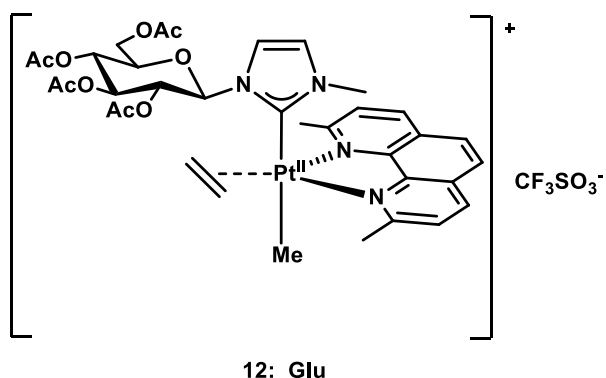


**Figure 8.1.** Complex **12** is the best candidate emerged in this PhD work

**12** is by far more active and selective than cisplatin on cancer cells ( $IC_{50}$  in the submicromolar range) and it probably acts through a different mechanism of action when compared to cisplatin and analogues. Results obtained with complex **12** are certainly worth of further investigations, although the next steps involving the test in *in vivo* systems, the elucidation of the uptake mechanism, and the identification of its biological targets were distant from the goal of this PhD work. Data collected for the studied platinum complexes evidenced that most of the proposed structures have an anticancer activity at least comparable to cisplatin. Five-coordinate *tbp* Pt(II) complexes showed encouraging performances in both cytotoxicity and selectivity, and represent a valid alternative to common square-planar Pt(II) species, considering the numerous synthetic opportunities that can result in several further functionalization and variations on the theme.

In the second part, glycoconjugation was extend to Ru(II) and Au(I) organometallic scaffolds, widely explored as alternative to Pt-drugs.

Such studies were carried out at the EPFL in Lausanne, under the supervision of Prof. P. Dyson.

In *Chapter 6* structure-activity relationships on a panel of Ru(II) arene complexes were collected by evaluating their reactivity in hydrolytic conditions and in presence of model biomolecules. Data evidence that different arene and ancillary ligands can tune the reactivity with biomolecules.

Finally, in *Chapter 7* the effect of the halide co-ligand was evaluated on a class of Au(I) NHC complexes. Au(I) NHC complexes display a different mechanism of action and alternatives biological targets when compared to platinum compounds. The in-solution study related to these complexes revealed the retention of the NHC fragment and encouraged to investigate their cytotoxicity, determined in micromolar values of IC<sub>50</sub>. Further studies involving their reactivity toward biomolecules will be performed to evidence differences due to the ancillary halide ligand.

In conclusion, glycoconjugation resulted to be a viable strategy to enhance the selectivity and the general pharmacological properties of anticancer metallodrugs. The experimental evidences suggested an active role of the sugar portion in the biological activity of the compounds, since small variation in the nature of the carbohydrate residues (as replacing galactose for glucose) resulted in great differences. Interestingly, generally the protected-sugar complexes displayed better performances than deprotected ones, which are more likely recognized by carbohydrate receptors.

The results collected over this PhD work are a useful part for reconstructing the colorful mosaic related to the biological activity of organometallic Pt, Ru and Au complexes, and represent a solid base for further developments in finding new drugs for treating cancer.

## Appendix

**Table A1.** Crystallographic data of complex **8<sup>a</sup>-I**

Compound	1 <sup>a</sup> -glu-I
Empirical formula	C <sub>30</sub> H <sub>35</sub> I N <sub>2</sub> O <sub>9</sub> Pt
Formula weight	889.59
Temperature (K)	173(2)
Wavelength (Å)	0.71073
Crystal system, space group	Monoclinic, P 21
Unit cell dimensions (Å, °)	a = 7.956(4), α = 90 b = 20.192(2), β = 109.670(6) c = 10.692(2), γ = 90°
Volume (Å <sup>3</sup> )	1617.4(9)
Z, Calculated density (Mg/m <sup>3</sup> )	2, 1.827
Absorption coefficient (mm <sup>-1</sup> )	5.345
F(000)	864
Θ range for data collection (°)	2.719 to 27.495
Reflections collected / unique	16713 / 6634 [R(int) = 0.0278]
Data / restraints / parameters	16713 / 6634 [R(int) = 0.0278]
Goodness-of-fit on F <sup>2</sup>	0.771
Final R indices [I>2σ(I)]	R <sub>I</sub> = 0.0233, wR <sub>2</sub> = 0.0607
R indices (all data)	R <sub>I</sub> = 0.0288, wR <sub>2</sub> = 0.0657
Absolute structural parameter	0.024(7)
Largest diff. peak / hole (e <sup>-</sup> Å <sup>-3</sup> )	1.251 / -0.952

**Table A2.** Crystallographic data of complex **8<sup>B</sup>-I**

Compound	<b>8<sup>B</sup>-I</b>
Empirical formula	C <sub>30</sub> H <sub>35</sub> I N <sub>2</sub> O <sub>9</sub> Pt
Formula weight	889.59
Temperature (K)	173(2)
Wavelength (Å)	0.71073
Crystal system, space group	Orthorhombic, P 21 21 21
Unit cell dimensions (Å, °)	a = 9.354(4), α = 90° b = 13.195(6), β = 90° c = 26.669(9), γ = 90
Volume (Å <sup>3</sup> )	3292(2)
Z, Calculated density (Mg/m <sup>3</sup> )	4, 1.795
Absorption coefficient (mm <sup>-1</sup> )	5.253
F(000)	1728
Θ range for data collection (°)	2.171 to 25.000
Reflections collected / unique	16939 / 5562 [R(int) = 0.1799]
Data / restraints / parameters	5562 / 262 / 395
Goodness-of-fit on F <sup>2</sup>	1.051
Final R indices [I>2sigma(I)]	R <sub>I</sub> = 0.1158, wR <sub>2</sub> = 0.2624
R indices (all data)	R <sub>I</sub> = 0.2184, wR <sub>2</sub> = 0.3453
Absolute structural parameter	0.17(4)
Largest diff. peak / hole (e <sup>-</sup> Å <sup>-3</sup> )	2.314 / -3.485

**Table A3.** Crystallographic data of complex **12**



Compound	12
Empirical formula	C <sub>35</sub> H <sub>43</sub> N <sub>4</sub> O <sub>9</sub> Pt · C F <sub>3</sub> S
Formula weight	1007.89
Temperature	298(2)K
Wavelength	0.71073 Å
Crystal system, space group	Orthorhombic, P 2 <sub>1</sub> 2 <sub>1</sub> 2 <sub>1</sub>
Unit cell dimensions	a = 13.170(2) Å, α = 90° b = 17.362(5) Å, β = 90° c = 17.639(6) Å, γ = 90°
Volume	4033.3(19) Å <sup>3</sup>
Z, Calculated density	4, 1.660 Mg/m <sup>3</sup>
Absorption coefficient	3.610 mm <sup>-1</sup>
F(000)	2016
Crystal size	0.50 x 0.40 x 0.08 mm
Theta range for data collection	2.590 to 27.656 °
Reflections collected / unique	23099 / 8502 [R(int) = 0.0391]
Data / restraints / parameters	8502 / 0 / 523
Goodness-of-fit on F <sup>2</sup>	1.093
Final R indices [I>2sigma(I)]	R <sub>I</sub> = 0.0374, wR <sub>2</sub> = 0.0811
R indices (all data)	R <sub>I</sub> = 0.0503, wR <sub>2</sub> = 0.0879
Absolute structural parameter	0.046(11)
Largest diff. peak and hole	1.371 and -0.787 e <sup>-</sup> Å <sup>-3</sup>

**Table A4.** Crystallographic data of complex **18**

Compound	18
Empirical formula	C <sub>33</sub> H <sub>41</sub> N <sub>4</sub> O <sub>9</sub> Pt · C F <sub>3</sub> O <sub>3</sub> S
Formula weight	981.86
Temperature	298(2)K
Wavelength	0.71073 Å
Crystal system, space group	Triclinic, P 1
Unit cell dimensions	a = 13.8920(14)Å, $\alpha$ = 74.640(11)° b = 18.426(2)Å, $\beta$ = 73.436(8)° c = 19.187(2)Å, $\gamma$ = 68.649(9)°
Volume	4312.5(9)Å <sup>3</sup>
Z, Calculated density	4, 1.512 Mg/m <sup>3</sup>
Absorption coefficient	3.374 mm <sup>-1</sup>
F(000)	1960
Crystal size	0.40 x 0.30 x 0.15 mm
Theta range for data collection	2.150 to 27.500 °
Reflections collected / unique	47334 / 27957 [R(int) = 0.0418]
Data / restraints / parameters	27957 / 217 / 2012
Goodness-of-fit on F <sup>2</sup>	1.072
Final R indices [I>2sigma(I)]	R1 = 0.0533, wR2 = 0.1316
R indices (all data)	R1 = 0.0876, wR2 = 0.1555
Absolute structural parameter	0.096(11)
Largest diff. peak and hole	1.262 and -1.307 e <sup>-</sup> Å <sup>-3</sup>

**Table A5.** Crystallographic data of complex **23**

Compound	23
Formula	C <sub>28</sub> H <sub>38</sub> Cl <sub>2</sub> N <sub>2</sub> O <sub>9</sub> Ru
$D_{calc}/\text{g cm}^{-3}$	1.282
$\mu/\text{mm}^{-1}$	5.114
Formula Weight	718.57
Colour	clear dark brown
Shape	prism
Size/mm <sup>3</sup>	0.45×0.23×0.18
$T/\text{K}$	140.00(10)
Crystal System	triclinic
Flack Parameter	0.03(2)
Hooft Parameter	-0.010(5)
Space Group	<i>P</i> 1
$a/\text{\AA}$	11.5724(3)
$b/\text{\AA}$	13.1667(6)
$c/\text{\AA}$	13.8386(4)
$\alpha/^\circ$	95.115(3)
$\beta/^\circ$	99.174(3)
$\gamma/^\circ$	114.745(4)
$V/\text{\AA}^3$	1861.69(13)
$Z$	2
$Z'$	2
Wavelength/ $\text{\AA}$	1.54184
Radiation type	Cu K $\alpha$
$\theta_{min}/^\circ$	3.285
$\theta_{max}/^\circ$	73.145
Measured Refl's.	32427
Indep't Refl's	13718
Refl's $I \geq 2 \sigma(I)$	12466
$R_{int}$	0.0460
Parameters	774
Restraints	27
Largest Peak	2.859
Deepest Hole	-1.674
GooF	1.382
$wR_2$ (all data)	0.3137
$wR_2$	0.3068
$R_1$ (all data)	0.1151
$R_1$	0.1106

**Table A6.** Crystallographic data of complex **25**

<b>Compound</b>	<b>25</b>
Formula	C <sub>25</sub> H <sub>32</sub> Cl <sub>2</sub> N <sub>2</sub> O <sub>9</sub> Ru
$D_{calc.}/\text{g cm}^{-3}$	1.599
$\mu/\text{mm}^{-1}$	6.738
Formula Weight	676.49
Colour	clear intense orange
Shape	needle
Size/mm <sup>3</sup>	0.49×0.05×0.03
$T/\text{K}$	140.00(10)
Crystal System	orthorhombic
Flack Parameter	-0.001(3)
Space Group	$P2_12_12_1$
$a/\text{\AA}$	11.93958(7)
$b/\text{\AA}$	14.52441(9)
$c/\text{\AA}$	32.40464(19)
$\alpha/^\circ$	90
$\beta/^\circ$	90
$\gamma/^\circ$	90
$V/\text{\AA}^3$	5619.46(6)
$Z$	8
$Z'$	2
Wavelength/ $\text{\AA}$	1.54184
Radiation type	CuK $\alpha$
$\theta_{min}/^\circ$	3.335
$\theta_{max}/^\circ$	72.556
Measured Refl's.	48267
Indep't Refl's	11047
Refl's $I \geq 2\sigma(I)$	10790
$R_{int}$	0.0320
Parameters	744
Restraints	226
Largest Peak/ $\text{e \AA}^{-3}$	0.869
Deepest Hole/ $\text{e \AA}^{-3}$	-0.637
GooF	1.040
$wR_2$ (all data)	0.0676
$wR_2$	0.0670
$R_1$ (all data)	0.0260
$R_1$	0.0251

**Table A7.** Crystallographic data of complex **28**

<b>Compound</b>	<b>28</b>
Formula	C <sub>31.5</sub> H <sub>40.25</sub> N <sub>2.75</sub> O <sub>13</sub> Ru
$D_{calc.}/\text{g cm}^{-3}$	1.406
$\mu/\text{mm}^{-1}$	4.064
Formula Weight	766.48
Colour	clear pale yellow
Shape	plate
Size/mm <sup>3</sup>	0.21×0.13×0.04
$T/\text{K}$	140.00(10)
Crystal System	monoclinic
Flack Parameter	-0.002(2)
Space Group	$P2_1$
$a/\text{\AA}$	13.19883(13)
$b/\text{\AA}$	17.38059(17)
$c/\text{\AA}$	15.89248(15)
$\alpha/^\circ$	90
$\beta/^\circ$	96.7072(9)
$\gamma/^\circ$	90
$V/\text{\AA}^3$	3620.84(6)
$Z$	4
$Z'$	2
Wavelength/ $\text{\AA}$	1.54184
Radiation type	CuK $\alpha$
$\theta_{min}/^\circ$	3.372
$\theta_{max}/^\circ$	72.573
Measured Refl's.	67489
Indep't Refl's	14118
Refl's $I \geq 2\sigma(I)$	13874
$R_{int}$	0.0363
Parameters	1014
Restraints	457
Largest Peak/ $\text{e \AA}^{-3}$	1.361
Deepest Hole/ $\text{e \AA}^{-3}$	-1.214
GooF	1.061
$wR_2$ (all data)	0.0927
$wR_2$	0.0922
$R_1$ (all data)	0.0369
$R_1$	0.0362

## List of publications related to this work

- A. Annunziata, M.E. Cucciolito, R. Esposito, P. Imbimbo, G. Petruk, G. Ferraro, V. Pinto, A. Tuzi, D.M. Monti, A. Merlino and F. Ruffo, "A highly efficient and selective antitumor agent based on a glucoconjugated carbene platinum(II) complex" *Dalton Trans.*, **2019**, 48, 7794-7800. <https://doi.org/10.1039/C9DT01614G>
- A. Annunziata, M.E. Cucciolito, R. Esposito, G. Ferraro, D.M. Monti, A. Merlino and F. Ruffo, "Five-Coordinate Platinum(II) Compounds as Potential Anticancer Agents", *Eur. J. Inorg. Chem.*, **2019**. DOI: 10.1002/ejic.201900771.
- A. Annunziata, A. Amoresano, M.E. Cucciolito, R. Esposito, G. Ferraro, I. Iacobucci, P. Imbimbo, R. Lucignano, M. Melchiorre, M. Monti, C. Scognamiglio, A. Tuzi, D. M. Monti, A. Merlino, and F. Ruffo, "Pt(II) versus Pt(IV) in Carbene Glycoconjugate Antitumor Agents: Minimal Structural Variations and Great Performance Changes" *Inorg. Chem.*, **2020**, 59, 4002-4014. doi.org/10.1021/acs.inorgchem.9b03683.
- F. Tresin, V. Stroppa, M. Baron, A. Biffis, A. Annunziata, L. D'Elia, D.M. Monti, F. Ruffo, M. Roverso, P. Sgarbossa, S. Bogialli and C. Tubaro, "Synthesis and Biological Studies on Dinuclear Gold(I) Complexes with Di-(N-Heterocyclic Carbene) Ligands Functionalized with Carbohydrates" *Molecules*, **2020**, 25, 3850. doi:10.3390/molecules25173850
- A. Annunziata, M.E. Cucciolito, P. Imbimbo, A. Silipo and F. Ruffo, "A hydrophilic olefin Pt(0) complex containing a glucoconjugated 2-iminopyridine ligand: Synthesis, characterization, stereochemistry and biological activity" *Inorganica Chimica Acta*, 516 (**2021**), 120092 <https://doi.org/10.1016/j.ica.2020.120092>.
- A. Annunziata, M. E. Cucciolito, R. Esposito, S. Traboni, A. Tuzi, P. H. M. Budzelaar and F. Ruffo, "Oxidative Addition of  $\alpha$ -Glycosyl Halides to a Platinum(0) Olefin Complex: Stereochemistry of Pt-C Bond Formation" *Eur. J. Inorg. Chem.*, **2021**, 543-549. doi.org/10.1002/ejic.202001088

- A. Annunziata, D. Liberti , E. Bedini, M. E. Cucciolito, D. Loreto , D. M. Monti , A. Merlino and F. Ruffo, “Square-Planar vs. Trigonal Bipyramidal Geometry in Pt(II) Complexes Containing Triazole-Based Glucose Ligands as Potential Anticancer Agents”, *Int. J. Mol. Sci.* **2021**, 22, 8704. <https://doi.org/10.3390/ijms22168704>

## Bibliography

- (1) Boros, E.; Dyson, P. J.; Gasser, G. Classification of Metal-Based Drugs According to Their Mechanisms of Action. *Chem* **2020**, 6 (1), 41–60. <https://doi.org/10.1016/j.chempr.2019.10.013>.
- (2) Noffke, A. L.; Habtemariam, A.; Pizarro, A. M.; Sadler, P. J. Designing Organometallic Compounds for Catalysis and Therapy. *Chem. Commun.* **2012**, 48 (43), 5219–5246. <https://doi.org/10.1039/C2CC30678F>.
- (3) Romero-Canelón, I.; Sadler, P. J. Next-Generation Metal Anticancer Complexes: Multitargeting via Redox Modulation. *Inorg. Chem.* **2013**, 52 (21), 12276–12291. <https://doi.org/10.1021/ic400835n>.
- (4) Siegel, R. L.; Miller, K. D.; Jemal, A. Cancer Statistics, 2018: Cancer Statistics, 2018. *CA: A Cancer Journal for Clinicians* **2018**, 68 (1), 7–30. <https://doi.org/10.3322/caac.21442>.
- (5) Hoeschele, J. D. Dr Barnett Rosenberg – a Personal Perspective. *Dalton Trans.* **2016**, 45 (33), 12966–12969. <https://doi.org/10.1039/C6DT02152B>.
- (6) Ghosh, S. Cisplatin: The First Metal Based Anticancer Drug. *Bioorganic Chemistry* **2019**, 88, 102925. <https://doi.org/10.1016/j.bioorg.2019.102925>.
- (7) Rixe, O.; Ortuzar, W.; Alvarez, M.; Parker, R.; Reed, E.; Paull, K.; Fojo, T. Oxaliplatin, Tetraplatin, Cisplatin, and Carboplatin: Spectrum of Activity in Drug-Resistant Cell Lines and in the Cell Lines of the National Cancer Institute's Anticancer Drug Screen Panel. *Biochemical Pharmacology* **1996**, 52 (12), 1855–1865. [https://doi.org/10.1016/S0006-2952\(97\)81490-6](https://doi.org/10.1016/S0006-2952(97)81490-6).
- (8) Heudi, O.; Mercier-Jobard, S.; Cailleux, A.; Allain, P. Mechanisms of Reaction Of L-Methionine with Carboplatin and Oxaliplatin in Different Media: A Comparison with Cisplatin. *Biopharm. Drug Dispos.* **1999**, 20 (2), 107–116. [https://doi.org/10.1002/\(SICI\)1099-081X\(199903\)20:2<107::AID-BDD161>3.0.CO;2-0](https://doi.org/10.1002/(SICI)1099-081X(199903)20:2<107::AID-BDD161>3.0.CO;2-0).
- (9) Peleg-Shulman, T.; Gibson, D. Cisplatin–Protein Adducts Are Efficiently Removed by Glutathione but Not by 5'-Guanosine Monophosphate. *J. Am. Chem. Soc.* **2001**, 123 (13), 3171–3172. <https://doi.org/10.1021/ja005854y>.
- (10) Siddik, Z. H. Cisplatin: Mode of Cytotoxic Action and Molecular Basis of Resistance. *Oncogene* **2003**, 22 (47), 7265–7279. <https://doi.org/10.1038/sj.onc.1206933>.



- (11) Gibson, D. The Mechanism of Action of Platinum Anticancer Agents—What Do We Really Know about It? *Dalton Trans.* **2009**, No. 48, 10681. <https://doi.org/10.1039/b918871c>.
- (12) Dasari, S.; Bernard Tchounwou, P. Cisplatin in Cancer Therapy: Molecular Mechanisms of Action. *European Journal of Pharmacology* **2014**, *740*, 364–378. <https://doi.org/10.1016/j.ejphar.2014.07.025>.
- (13) Dilruba, S.; Kalayda, G. V. Platinum-Based Drugs: Past, Present and Future. *Cancer Chemother Pharmacol* **2016**, *77* (6), 1103–1124. <https://doi.org/10.1007/s00280-016-2976-z>.
- (14) Johnstone, T. C.; Suntharalingam, K.; Lippard, S. J. The Next Generation of Platinum Drugs: Targeted Pt(II) Agents, Nanoparticle Delivery, and Pt(IV) Prodrugs. *Chem. Rev.* **2016**, *116* (5), 3436–3486. <https://doi.org/10.1021/acs.chemrev.5b00597>.
- (15) Binks, S. P.; Dobrota, M. Kinetics and Mechanism of Uptake of Platinum-Based Pharmaceuticals by the Rat Small Intestine. *Biochemical Pharmacology* **1990**, *40* (6), 1329–1336. [https://doi.org/10.1016/0006-2952\(90\)90400-F](https://doi.org/10.1016/0006-2952(90)90400-F).
- (16) Gately, D.; Howell, S. Cellular Accumulation of the Anticancer Agent Cisplatin: A Review. *Br J Cancer* **1993**, *67* (6), 1171–1176. <https://doi.org/10.1038/bjc.1993.221>.
- (17) Abada, P.; Howell, S. B. Regulation of Cisplatin Cytotoxicity by Cu Influx Transporters. *Metal-Based Drugs* **2010**, *2010*, 1–9. <https://doi.org/10.1155/2010/317581>.
- (18) Howell, S. B.; Safaei, R.; Larson, C. A.; Sailor, M. J. Copper Transporters and the Cellular Pharmacology of the Platinum-Containing Cancer Drugs. *Molecular Pharmacology* **2010**, *77* (6), 887–894. <https://doi.org/10.1124/mol.109.063172>.
- (19) Lau, J. K.-C.; Ensing, B. Hydrolysis of Cisplatin—a First-Principles Metadynamics Study. *Phys. Chem. Chem. Phys.* **2010**, *12* (35), 10348–10355. <https://doi.org/10.1039/B918301A>.
- (20) Reishus, J. W.; Martin, D. S. Cis-Dichlorodiammineplatinum(II). Acid Hydrolysis and Isotopic Exchange of the Chloride Ligands1. *J. Am. Chem. Soc.* **1961**, *83* (11), 2457–2462. <https://doi.org/10.1021/ja01472a009>.
- (21) Bancroft, D. P.; Lepre, C. A.; Lippard, S. J. Platinum-195 NMR Kinetic and Mechanistic Studies of Cis- and Trans-Diamminedichloroplatinum(II) Binding to DNA. *J. Am. Chem. Soc.* **1990**, *112* (19), 6860–6871. <https://doi.org/10.1021/ja00175a020>.
- (22) van Boom, S. S. G. E.; Chen, B. W.; Teuben, J. M.; Reedijk, J. Platinum–Thioether Bonds Can Be Reverted by Guanine–N7 Bonds in

- Pt(Dien)<sub>2</sub><sup>+</sup> Model Adducts. *Inorg. Chem.* **1999**, *38* (7), 1450–1455. <https://doi.org/10.1021/ic981086o>.
- (23) Fichtinger-Schepman, A. M. J.; Van der Veer, J. L.; Den Hartog, J. H. J.; Lohman, P. H. M.; Reedijk, J. Adducts of the Antitumor Drug Cis-Diamminedichloroplatinum(II) with DNA: Formation, Identification, and Quantitation. *Biochemistry* **1985**, *24* (3), 707–713. <https://doi.org/10.1021/bi00324a025>.
  - (24) Todd, R. C.; Lippard, S. J. Inhibition of Transcription by Platinum Antitumor Compounds. *Metallomics* **2009**, *1* (4), 280–291. <https://doi.org/10.1039/B907567D>.
  - (25) Wang, D.; Lippard, S. J. Cellular Processing of Platinum Anticancer Drugs. *Nat Rev Drug Discov* **2005**, *4* (4), 307–320. <https://doi.org/10.1038/nrd1691>.
  - (26) Rabik, C. A.; Dolan, M. E. Molecular Mechanisms of Resistance and Toxicity Associated with Platinating Agents. *Cancer Treatment Reviews* **2007**, *33* (1), 9–23. <https://doi.org/10.1016/j.ctrv.2006.09.006>.
  - (27) Graf, N.; Ang, W. H.; Zhu, G.; Myint, M.; Lippard, S. J. Role of Endonucleases XPF and XPG in Nucleotide Excision Repair of Platinated DNA and Cisplatin/Oxaliplatin Cytotoxicity. *ChemBioChem* **2011**, *12* (7), 1115–1123. <https://doi.org/10.1002/cbic.201000724>.
  - (28) Bergamo, A.; Dyson, P. J.; Sava, G. The Mechanism of Tumour Cell Death by Metal-Based Anticancer Drugs Is Not Only a Matter of DNA Interactions. *Coordination Chemistry Reviews* **2018**, *360*, 17–33. <https://doi.org/10.1016/j.ccr.2018.01.009>.
  - (29) Hato, S. V.; Khong, A.; de Vries, I. J. M.; Lesterhuis, W. J. Molecular Pathways: The Immunogenic Effects of Platinum-Based Chemotherapeutics. *Clin Cancer Res* **2014**, *20* (11), 2831. <https://doi.org/10.1158/1078-0432.CCR-13-3141>.
  - (30) Espósito, B. P.; Najjar, R. Interactions of Antitumoral Platinum-Group Metallodrugs with Albumin. *Coordination Chemistry Reviews* **2002**, *232* (1), 137–149. [https://doi.org/10.1016/S0010-8545\(02\)00049-8](https://doi.org/10.1016/S0010-8545(02)00049-8).
  - (31) Ivanov, A. I.; Christodoulou, J.; Parkinson, J. A.; Barnham, K. J.; Tucker, A.; Woodrow, J.; Sadler, P. J. Cisplatin Binding Sites on Human Albumin. *Journal of Biological Chemistry* **1998**, *273* (24), 14721–14730. <https://doi.org/10.1074/jbc.273.24.14721>.
  - (32) Di Pasqua, A. J.; Kerwood, D. J.; Shi, Y.; Goodisman, J.; Dabrowiak, J. C. Stability of Carboplatin and Oxaliplatin in Their Infusion Solutions Is Due to Self-Association. *Dalton Trans.* **2011**, *40* (18), 4821–4825. <https://doi.org/10.1039/C0DT01758B>.

- (33) Di Pasqua, A. J.; Goodisman, J.; Kerwood, D. J.; Toms, B. B.; Dubowy, R. L.; Dabrowiak, J. C. Activation of Carboplatin by Carbonate. *Chem. Res. Toxicol.* **2006**, *19* (1), 139–149. <https://doi.org/10.1021/tx050261s>.
- (34) Welink, J.; Boven, E.; Vermorken, J. B.; Gall, H. E.; van der Vijgh, W. J. F. Pharmacokinetics and Pharmacodynamics of Lobaplatin (D-19466) in Patients with Advanced Solid Tumors, Including Patients with Impaired Renal or Liver Function. *Clin Cancer Res* **1999**, *5* (9), 2349.
- (35) Graham, J.; Muhsin, M.; Kirkpatrick, P. Oxaliplatin. *Nature Reviews Drug Discovery* **2004**, *3* (1), 11–12. <https://doi.org/10.1038/nrd1287>.
- (36) Kidani, Y.; Inagaki, K.; Iigo, M.; Hoshi, A.; Kuretani, K. Antitumor Activity of 1,2-Diaminocyclohexaneplatinum Complexes against Sarcoma-180 Ascites Form. *J. Med. Chem.* **1978**, *21* (12), 1315–1318. <https://doi.org/10.1021/jm00210a029>.
- (37) Spingler, B.; Whittington, D. A.; Lippard, S. J. 2.4 Å Crystal Structure of an Oxaliplatin 1,2-d(GpG) Intrastrand Cross-Link in a DNA Dodecamer Duplex. *Inorg. Chem.* **2001**, *40* (22), 5596–5602. <https://doi.org/10.1021/ic010790t>.
- (38) Oun, R.; Moussa, Y. E.; Wheate, N. J. The Side Effects of Platinum-Based Chemotherapy Drugs: A Review for Chemists. *Dalton Trans.* **2018**, *47* (19), 6645–6653. <https://doi.org/10.1039/C8DT00838H>.
- (39) Anderson, G. K. Organometallic and Homogeneous Catalytic Chemistry of Palladium and Platinum. In *Chemistry of the Platinum Group Metals - Recent Developments*; Elsevier, 1991; pp 338–406. <https://doi.org/10.1016/b978-0-444-88189-2.50017-1>.
- (40) Cutillas, N.; Yellol, G. S.; de Haro, C.; Vicente, C.; Rodríguez, V.; Ruiz, J. Anticancer Cyclometalated Complexes of Platinum Group Metals and Gold. *Coordination Chemistry Reviews* **2013**, *257* (19), 2784–2797. <https://doi.org/10.1016/j.ccr.2013.03.024>.
- (41) Omae, I. Applications of Five-Membered Ring Products of Cyclometalation Reactions as Anticancer Agents. *Coordination Chemistry Reviews* **2014**, *280*, 84–95. <https://doi.org/10.1016/j.ccr.2014.07.019>.
- (42) Gao, P.; Pan, W.; Li, N.; Tang, B. Fluorescent Probes for Organelle-Targeted Bioactive Species Imaging. *Chem. Sci.* **2019**, *10* (24), 6035–6071. <https://doi.org/10.1039/C9SC01652J>.
- (43) Zhang, Q.; Wang, S.; Zhu, Y.; Zhang, C.; Cao, H.; Ma, W.; Tian, X.; Wu, J.; Zhou, H.; Tian, Y. Functional Platinum(II) Complexes with Four-Photon Absorption Activity, Lysosome Specificity, and Precise Cancer Therapy. *Inorg. Chem.* **2021**, *60* (4), 2362–2371. <https://doi.org/10.1021/acs.inorgchem.0c03245>.

- (44) Zamora, A.; Wachter, E.; Vera, M.; Heidary, D. K.; Rodríguez, V.; Ortega, E.; Fernández-Espín, V.; Janiak, C.; Glazer, E. C.; Barone, G.; Ruiz, J. Organoplatinum(II) Complexes Self-Assemble and Recognize AT-Rich Duplex DNA Sequences. *Inorg. Chem.* **2021**, *60* (4), 2178–2187. <https://doi.org/10.1021/acs.inorgchem.0c02648>.
- (45) Cucciolito, M. E.; De Felice, V.; Roviello, G.; Ruffo, F. Three-Coordinate [Pt(N,N'-Chelate)(H<sub>2</sub>-Olefin)] Complexes: Synthesis, Properties and Reactions with Electrophiles. *European Journal of Inorganic Chemistry* **2011**, *2011* (4), 457–469. <https://doi.org/10.1002/ejic.201001021>.
- (46) Fanizzi, F. P.; Maresca, L.; Natile, G.; Lanfranchi, M.; Tiripicchio, A.; Pacchioni, G. Five-Coordination in Platinum(II) Species: When and Why. *J. Chem. Soc., Chem. Commun.* **1992**, No. 4, 333–335. <https://doi.org/10.1039/C39920000333>.
- (47) Albano, V. G.; Natile, G.; Panunzi, A. Five-Coordinate Alkene Complexes of Palladium(II) and Platinum(II). *Coordination Chemistry Reviews* **1994**, *133*, 67–114. [https://doi.org/10.1016/0010-8545\(94\)80057-X](https://doi.org/10.1016/0010-8545(94)80057-X).
- (48) Cucciolito, M. E.; De Felice, V.; Panunzi, A.; Vitagliano, A. Five-Coordinate Olefin Complexes of Platinum(II) Containing .Sigma.-Bonded Carbon Ligands. Coordination Environment and Stability. *Organometallics* **1989**, *8* (5), 1180–1187. <https://doi.org/10.1021/om00107a009>.
- (49) Albano, V. G.; Monari, M.; Orabona, I.; Panunzi, A.; Roviello, G.; Ruffo, F. Synthesis and Characterization of Trigonal-Bipyramidal Platinum(II) Olefin Complexes with Chalcogenide Ligands in Axial Positions. X-Ray Molecular Structures of [Pt(SMe)<sub>2</sub>(Dmphen)(Diphenyl Fumarate)], Its Cationic Dipositive Derivative [Pt(SMe<sub>2</sub>)<sub>2</sub>(Dmphen)(Diphenyl Fumarate)][BF<sub>4</sub>]<sub>2</sub>, and Free Diphenyl Fumarate. *Organometallics* **2003**, *22* (6), 1223–1230. <https://doi.org/10.1021/om020807v>.
- (50) De Felice, V.; De Renzi, A.; Tesauero, D.; Vitagliano, A. Carbon-Carbon Bond Formation in Cationic Aryl-Olefin-Platinum(II) Complexes. *Organometallics* **1992**, *11* (11), 3669–3676. <https://doi.org/10.1021/om00059a033>.
- (51) Fanizzi, F. P.; Intini, F. P.; Maresca, L.; Natile, G.; Lanfranchi, M.; Tiripicchio, A. Four-versus Five-Coordination in Palladium(II) and Platinum(II) Complexes Containing 2,9-Dimethyl-1,10-Phenanthroline (Dmphen). Crystal Structures of [PtCl<sub>2</sub>(Dmphen)] and [Pt(H<sub>2</sub>-C<sub>2</sub>H<sub>4</sub>)Cl<sub>2</sub>(Dmphen)]. *J. Chem. Soc., Dalton Trans.* **1991**, No. 4, 1007–1015. <https://doi.org/10.1039/DT9910001007>.
- (52) Albano, V. G.; De Felice, V.; Monari, M.; Roviello, G.; Ruffo, F. Oxidative Addition of Phenylselenyl Halides to Platinum(0) Complexes:

- Characterisation and Reactivity of the Products [PtX(SePh) (N,N-Chelate)(Olefin)] (X = Cl, Br, I). *European Journal of Inorganic Chemistry* **2005**, 2005 (2), 416–422. <https://doi.org/10.1002/ejic.200400536>.
- (53) Albano, V. G.; Monari, M.; Orabona, I.; Panunzi, A.; Ruffo, F. Oxidative Additions of E–E Bonds (E = Chalcogen) to Group 10 Metals: “Tunable” Cleavage of Se–Se Bonds by Pt(0) Complexes. *J. Am. Chem. Soc.* **2001**, 123 (18), 4352–4353. <https://doi.org/10.1021/ja005870v>.
- (54) Albano, V. G.; Castellari, C.; L. Ferrara, M.; Panunzi, A.; Ruffo, F. Five-Coordinate Hydrido-Complexes [PtX(H)(N,N-Chelate)(Olefin)] (X □ Cl, Br or I). Crystal Structure of [PtCl(H)(2,9-Me<sub>2</sub>-1,10-Phenanthroline)(Dimethyl Maleate)]. *Journal of Organometallic Chemistry* **1994**, 469 (2), 237–244. [https://doi.org/10.1016/0022-328X\(94\)88078-6](https://doi.org/10.1016/0022-328X(94)88078-6).
- (55) Albano, V. G.; Castellari, C.; Monari, M.; De Felice, V.; Panunzi, A.; Ruffo, F. Synthesis and Characterization of Five-Coordinate Platinum [PtCl(L)(N-N)(Olefin)]<sup>+</sup> Complexes. Molecular Structure of [PtCl(Pyridine)(2,9-Dimethyl-1,10-Phenanthroline)(Ethylene)] (CF<sub>3</sub>SO<sub>3</sub>). *Organometallics* **1992**, 11 (11), 3665–3669. <https://doi.org/10.1021/om00059a032>.
- (56) Calvanese, L.; Cucciolito, M. E.; D’Amora, A.; D’Auria, G.; Esposito, A.; Esposito, R.; Falcigno, L.; Ruffo, F. Recognition of Prochiral Sulfides in Five-Coordinate Pt<sup>II</sup> Complexes. *Eur. J. Inorg. Chem.* **2015**, 2015 (24), 4068–4075. <https://doi.org/10.1002/ejic.201500523>.
- (57) Cucciolito, M. E.; Giordano, F.; Panunzi, A.; Ruffo, F.; De Felice, V. Trigonal-Bipyramidal Co-Ordinatively Saturated Platinum(II) Olefin Complexes Bearing an Organomercury Fragment in Axial Position. *J. Chem. Soc., Dalton Trans.* **1993**, No. 22, 3421–3426. <https://doi.org/10.1039/DT9930003421>.
- (58) Albano, V. G.; Castellari, C.; Monari, M.; De Felice, V.; Ferrara, M. L.; Ruffo, F. Organolead Derivatives of Coordinatively Saturated Platinum(II) Olefin Complexes. Molecular Structure of [PtCl(PbPh<sub>2</sub>Cl)(2,9-Dimethyl-1,10-Phenanthroline)(Dimethyl Maleate)] and Its Deplumbation Product [PtCl(Ph)(2,9-Dimethyl-1,10-Phenanthroline)(Dimethyl Maleate)]. *Organometallics* **1995**, 14 (9), 4213–4221. <https://doi.org/10.1021/om00009a025>.
- (59) Bartolucci, S.; Rossi, M.; Estenoz, M.; Panunzi, A.; Vitagliano, A. The Cytostatic Activity of a Five-Coordinate Pt(II) Complex: Preliminary Results. *Inorganica Chimica Acta* **1987**, 137 (1), 53–55. [https://doi.org/10.1016/S0020-1693\(00\)87115-7](https://doi.org/10.1016/S0020-1693(00)87115-7).

- (60) Ferraro, G.; Marzo, T.; Cucciolito, M. E.; Ruffo, F.; Messori, L.; Merlino, A. Reaction with Proteins of a Five-Coordinate Platinum(II) Compound. *International Journal of Molecular Sciences* **2019**, *20* (3). <https://doi.org/10.3390/ijms20030520>.
- (61) Bigioni, M.; Ganis, P.; Panunzi, A.; Ruffo, F.; Salvatore, C.; Vito, A. Electrophilic Attack of  $[I(Py)_2]^+(NO_3^-)$  on Three-Coordinate Pt(0) Precursors: Synthesis and In Vitro Antitumor Activity of Water-Soluble, Five-Coordinate Pt(II) Complexes. *European Journal of Inorganic Chemistry* **2000**, *2000* (8), 1717–1721. [https://doi.org/10.1002/1099-0682\(200008\)2000:8<1717::AID-EJIC1717>3.0.CO;2-1](https://doi.org/10.1002/1099-0682(200008)2000:8<1717::AID-EJIC1717>3.0.CO;2-1).
- (62) De Pascali, S. A.; Migoni, D.; Papadia, P.; Muscella, A.; Marsigliante, S.; Ciccarese, A.; Fanizzi, F. P. New Water-Soluble Platinum(I) Phenanthroline Complexes Tested as Cisplatin Analogues: First-Time Comparison of Cytotoxic Activity between Analogous Four- and Five-Coordinate Species. *Dalton Trans.* **2006**, No. 42, 5077. <https://doi.org/10.1039/b610945d>.
- (63) Kenny, R. G.; Chuah, S. W.; Crawford, A.; Marmion, C. J. Platinum(IV) Prodrugs - A Step Closer to Ehrlich's Vision?: Platinum(IV) Prodrugs - A Step Closer to Ehrlich's Vision? *Eur. J. Inorg. Chem.* **2017**, *2017* (12), 1596–1612. <https://doi.org/10.1002/ejic.201601278>.
- (64) Dolman, R. C.; Deacon, G. B.; Hambley, T. W. Studies of the Binding of a Series of Platinum(IV) Complexes to Plasma Proteins. *Journal of Inorganic Biochemistry* **2002**, *88* (3), 260–267. [https://doi.org/10.1016/S0162-0134\(01\)00360-9](https://doi.org/10.1016/S0162-0134(01)00360-9).
- (65) Crespo, M. Cyclometallated Platinum(IV) Compounds as Promising Antitumour Agents. *Journal of Organometallic Chemistry* **2019**, *879*, 15–26. <https://doi.org/10.1016/j.jorganchem.2018.10.008>.
- (66) Rendina, L. M.; Puddephatt, R. J. Oxidative Addition Reactions of Organoplatinum(II) Complexes with Nitrogen-Donor Ligands. *Chem. Rev.* **1997**, *97* (6), 1735–1754. <https://doi.org/10.1021/cr9704671>.
- (67) Wilson, J. J.; Lippard, S. J. Synthetic Methods for the Preparation of Platinum Anticancer Complexes. *Chem. Rev.* **2014**, *114* (8), 4470–4495. <https://doi.org/10.1021/cr4004314>.
- (68) Crespo, M.; Font-Bardia, M.; Solans, X. Compound  $[PtPh_2(SMe_2)_2]$  as a Versatile Metalating Agent in the Preparation of New Types of  $[C,N,N']$  Cyclometallated Platinum Compounds. *Organometallics* **2004**, *23* (8), 1708–1713. <https://doi.org/10.1021/om030674t>.
- (69) Dunham, S. O.; Larsen, R. D.; Abbott, E. H. Nuclear Magnetic Resonance Investigation of the Hydrogen Peroxide Oxidation of Platinum(II) Complexes. Crystal and Molecular Structures of Sodium Trans-

- Dihydroxobis(Malonato)Platinate(IV) Hexahydrate and Sodium Trans-Dihydroxobis(Oxalato)Platinate(IV) Hexahydrate. *Inorg. Chem.* **1993**, 32 (10), 2049–2055. <https://doi.org/10.1021/ic00062a029>.
- (70) Xu, Z.; Wang, Z.; Deng, Z.; Zhu, G. Recent Advances in the Synthesis, Stability, and Activation of Platinum(IV) Anticancer Prodrugs. *Coordination Chemistry Reviews* **2021**, 442, 213991. <https://doi.org/10.1016/j.ccr.2021.213991>.
- (71) Wilson, J. J.; Lippard, S. J. Synthesis, Characterization, and Cytotoxicity of Platinum(IV) Carbamate Complexes. *Inorg. Chem.* **2011**, 50 (7), 3103–3115. <https://doi.org/10.1021/ic2000816>.
- (72) Zheng, Y.-R.; Suntharalingam, K.; Johnstone, T. C.; Yoo, H.; Lin, W.; Brooks, J. G.; Lippard, S. J. Pt(IV) Prodrugs Designed to Bind Non-Covalently to Human Serum Albumin for Drug Delivery. *J. Am. Chem. Soc.* **2014**, 136 (24), 8790–8798. <https://doi.org/10.1021/ja5038269>.
- (73) Babu, T.; Sarkar, A.; Karmakar, S.; Schmidt, C.; Gibson, D. Multiaction Pt(IV) Carbamate Complexes Can Codeliver Pt(II) Drugs and Amine Containing Bioactive Molecules. *Inorg. Chem.* **2020**, 59 (7), 5182–5193. <https://doi.org/10.1021/acs.inorgchem.0c00445>.
- (74) Nemirovski, A.; Kasherman, Y.; Tzaraf, Y.; Gibson, D. Reduction of Cis,Trans,Cis-[PtCl<sub>2</sub>(OCOCH<sub>3</sub>)<sub>2</sub>(NH<sub>3</sub>)<sub>2</sub>] by Aqueous Extracts of Cancer Cells. *J. Med. Chem.* **2007**, 50 (23), 5554–5556. <https://doi.org/10.1021/jm070740j>.
- (75) Wexselblatt, E.; Gibson, D. What Do We Know about the Reduction of Pt(IV) pro-Drugs? *Journal of Inorganic Biochemistry* **2012**, 117, 220–229. <https://doi.org/10.1016/j.jinorgbio.2012.06.013>.
- (76) Dong, J.; Ren, Y.; Huo, S.; Shen, S.; Xu, J.; Tian, H.; Shi, T. Reduction of Ormaplatin and Cis-Diamminetetrachloroplatinum(IV) by Ascorbic Acid and Dominant Thiols in Human Plasma: Kinetic and Mechanistic Analyses. *Dalton Trans.* **2016**, 45 (28), 11326–11337. <https://doi.org/10.1039/C6DT01804A>.
- (77) Lasorsa, A.; Stuchlíková, O.; Brabec, V.; Natile, G.; Arnesano, F. Activation of Platinum(IV) Prodrugs by Cytochrome c and Characterization of the Protein Binding Sites. *Mol. Pharmaceutics* **2016**, 13 (9), 3216–3223. <https://doi.org/10.1021/acs.molpharmaceut.6b00438>.
- (78) Jin, S.; Muhammad, N.; Sun, Y.; Tan, Y.; Yuan, H.; Song, D.; Guo, Z.; Wang, X. Multispecific Platinum(IV) Complex Deters Breast Cancer via Interposing Inflammation and Immunosuppression as an Inhibitor of COX-2 and PD-L1. *Angew. Chem. Int. Ed.* **2020**, 59 (51), 23313–23321. <https://doi.org/10.1002/anie.202011273>.

- (79) Cao, Q.; Zhou, D.; Pan, Z.; Yang, G.; Zhang, H.; Ji, L.; Mao, Z. CAIXplatins: Highly Potent Platinum(IV) Prodrugs Selective Against Carbonic Anhydrase IX for the Treatment of Hypoxic Tumors. *Angew. Chem. Int. Ed.* **2020**, *59* (42), 18556–18562. <https://doi.org/10.1002/anie.202005362>.
- (80) Zajac, J.; Novohradsky, V.; Markova, L.; Brabec, V.; Kasparikova, J. Platinum (IV) Derivatives with Cinnamate Axial Ligands as Potent Agents Against Both Differentiated and Tumorigenic Cancer Stem Rhabdomyosarcoma Cells. *Angew. Chem. Int. Ed.* **2020**, *59* (8), 3329–3335. <https://doi.org/10.1002/anie.201913996>.
- (81) Wexselblatt, E.; Yavin, E.; Gibson, D. Platinum(IV) Prodrugs with Haloacetato Ligands in the Axial Positions Can Undergo Hydrolysis under Biologically Relevant Conditions. *Angewandte Chemie International Edition* **2013**, *52* (23), 6059–6062. <https://doi.org/10.1002/anie.201300640>.
- (82) Kastner, A.; Poetsch, I.; Mayr, J.; Burda, J. V.; Roller, A.; Heffeter, P.; Keppler, B. K.; Kowol, C. R. A Dogma in Doubt: Hydrolysis of Equatorial Ligands of Pt<sup>IV</sup> Complexes under Physiological Conditions. *Angew. Chem. Int. Ed.* **2019**, *58* (22), 7464–7469. <https://doi.org/10.1002/anie.201900682>.
- (83) Lemma, K.; Sargeson, A. M.; Elding, L. I. Kinetics and Mechanism for Reduction of Oral Anticancer Platinum(IV) Dicarboxylate Compounds by L-Ascorbate Ions. *J. Chem. Soc., Dalton Trans.* **2000**, No. 7, 1167–1172. <https://doi.org/10.1039/A909484I>.
- (84) Shi, H.; Imberti, C.; Sadler, P. J. Diazido Platinum( IV ) Complexes for Photoactivated Anticancer Chemotherapy. *Inorg. Chem. Front.* **2019**, *6* (7), 1623–1638. <https://doi.org/10.1039/C9QI00288J>.
- (85) Keppler, B. K.; Henn, M.; Juhl, U. M.; Berger, M. R.; Niebl, R.; Wagner, F. E. New Ruthenium Complexes for the Treatment of Cancer. In *Ruthenium and Other Non-Platinum Metal Complexes in Cancer Chemotherapy*; Baulieu, E., Forman, D. T., Ingelman-Sundberg, M., Jaenicke, L., Kellen, J. A., Nagai, Y., Springer, G. F., Träger, L., Will-Shahab, L., Wittliff, J. L., Eds.; Springer Berlin Heidelberg: Berlin, Heidelberg, 1989; pp 41–69.
- (86) Rademaker-Lakhai, J. M.; van den Bongard, D.; Pluim, D.; Beijnen, J. H.; Schellens, J. H. M. A Phase I and Pharmacological Study with Imidazolium-*trans*-DMSO-Imidazole-Tetrachlororuthenate, a Novel Ruthenium Anticancer Agent. *Clin Cancer Res* **2004**, *10* (11), 3717. <https://doi.org/10.1158/1078-0432.CCR-03-0746>.



- (87) Antonarakis, E. S.; Emadi, A. Ruthenium-Based Chemotherapeutics: Are They Ready for Prime Time? *Cancer Chemother Pharmacol* **2010**, *66* (1), 1–9. <https://doi.org/10.1007/s00280-010-1293-1>.
- (88) Allardyce, C. S.; Dyson, P. J.; Ellis, D. J.; Heath, S. L. [Ru( $\eta$ -Cymene)Cl(Pta)] (Pta = 1,3,5-Triaza-7-Phosphatricyclo-[3.3.1.1]Decane): A Water Soluble Compound That Exhibits PH Dependent DNA Binding Providing Selectivity for Diseased Cells. *Chem. Commun.* **2001**, No. 15, 1396–1397. <https://doi.org/10.1039/B104021A>.
- (89) Morris, R. E.; Aird, R. E.; del Socorro Murdoch, P.; Chen, H.; Cummings, J.; Hughes, N. D.; Parsons, S.; Parkin, A.; Boyd, G.; Jodrell, D. I.; Sadler, P. J. Inhibition of Cancer Cell Growth by Ruthenium(II) Arene Complexes. *J. Med. Chem.* **2001**, *44* (22), 3616–3621. <https://doi.org/10.1021/jm010051m>.
- (90) Yan, Y. K.; Melchart, M.; Habtemariam, A.; Sadler, P. J. Organometallic Chemistry, Biology and Medicine: Ruthenium Arene Anticancer Complexes. *Chem. Commun.* **2005**, No. 38, 4764–4776. <https://doi.org/10.1039/B508531B>.
- (91) Habtemariam, A.; Melchart, M.; Fernández, R.; Parsons, S.; Oswald, I. D. H.; Parkin, A.; Fabbiani, F. P. A.; Davidson, J. E.; Dawson, A.; Aird, R. E.; Jodrell, D. I.; Sadler, P. J. Structure–Activity Relationships for Cytotoxic Ruthenium(II) Arene Complexes Containing N,N-, N,O-, and O,O-Chelating Ligands. *J. Med. Chem.* **2006**, *49* (23), 6858–6868. <https://doi.org/10.1021/jm060596m>.
- (92) Chen, H.; Parkinson, J. A.; Parsons, S.; Coxall, R. A.; Gould, R. O.; Sadler, P. J. Organometallic Ruthenium(II) Diamine Anticancer Complexes: Arene-Nucleobase Stacking and Stereospecific Hydrogen-Bonding in Guanine Adducts. *J. Am. Chem. Soc.* **2002**, *124* (12), 3064–3082. <https://doi.org/10.1021/ja017482e>.
- (93) Baik, M.-H.; Friesner, R. A.; Lippard, S. J. Theoretical Study of Cisplatin Binding to Purine Bases: Why Does Cisplatin Prefer Guanine over Adenine? *J. Am. Chem. Soc.* **2003**, *125* (46), 14082–14092. <https://doi.org/10.1021/ja036960d>.
- (94) Scolaro, C.; Hartinger, C. G.; Allardyce, C. S.; Keppler, B. K.; Dyson, P. J. Hydrolysis Study of the Bifunctional Antitumour Compound RAPTA-C, [Ru(H6-p-Cymene)Cl<sub>2</sub>(Pta)]. *Journal of Inorganic Biochemistry* **2008**, *102* (9), 1743–1748. <https://doi.org/10.1016/j.jinorgbio.2008.05.004>.
- (95) Gossens, C.; Dorcier, A.; Dyson, P. J.; Rothlisberger, U. PKa Estimation of Ruthenium(II)–Arene PTA Complexes and Their Hydrolysis Products via a DFT/Continuum Electrostatics Approach. *Organometallics* **2007**, *26* (16), 3969–3975. <https://doi.org/10.1021/om700364s>.

- (96) Scolaro, C.; Bergamo, A.; Brescacin, L.; Delfino, R.; Cocchietto, M.; Laurenczy, G.; Geldbach, T. J.; Sava, G.; Dyson, P. J. In Vitro and in Vivo Evaluation of Ruthenium(II)–Arene PTA Complexes. *J. Med. Chem.* **2005**, *48* (12), 4161–4171. <https://doi.org/10.1021/jm050015d>.
- (97) Wu, B.; Ong, M. S.; Groessl, M.; Adhireksan, Z.; Hartinger, C. G.; Dyson, P. J.; Davey, C. A. A Ruthenium Antimetastasis Agent Forms Specific Histone Protein Adducts in the Nucleosome Core. *Chemistry – A European Journal* **2011**, *17* (13), 3562–3566. <https://doi.org/10.1002/chem.201100298>.
- (98) Nowak-Sliwinska, P.; van Beijnum, J. R.; Casini, A.; Nazarov, A. A.; Wagnières, G.; van den Bergh, H.; Dyson, P. J.; Griffioen, A. W. Organometallic Ruthenium(II) Arene Compounds with Antiangiogenic Activity. *J. Med. Chem.* **2011**, *54* (11), 3895–3902. <https://doi.org/10.1021/jm2002074>.
- (99) Rausch, M.; Dyson, P. J.; Nowak-Sliwinska, P. Recent Considerations in the Application of RAPTA-C for Cancer Treatment and Perspectives for Its Combination with Immunotherapies. *Adv. Therap.* **2019**, *2* (9), 1900042. <https://doi.org/10.1002/adtp.201900042>.
- (100) Dyson, P. J. Systematic Design of a Targeted Organometallic Antitumour Drug in Pre-Clinical Development. *CHIMIA* **2007**, *61* (11), 698–703. <https://doi.org/10.2533/chimia.2007.698>.
- (101) Ang, W. H.; Daldini, E.; Scolaro, C.; Scopelliti, R.; Juillerat-Jeannerat, L.; Dyson, P. J. Development of Organometallic Ruthenium–Arene Anticancer Drugs That Resist Hydrolysis. *Inorg. Chem.* **2006**, *45* (22), 9006–9013. <https://doi.org/10.1021/ic061008y>.
- (102) Steel, T. R.; Walsh, F.; Wieczorek-Błauż, A.; Hanif, M.; Hartinger, C. G. Monodentately-Coordinated Bioactive Moieties in Multimodal Half-Sandwich Organoruthenium Anticancer Agents. *Coordination Chemistry Reviews* **2021**, *439*, 213890. <https://doi.org/10.1016/j.ccr.2021.213890>.
- (103) Masaryk, L.; Nemec, I.; Kašpárková, J.; Brabec, V.; Štarha, P. Unexpected Solution Behaviour of Ester-Functionalized Half-Sandwich Ru(II) and Ir(III) Complexes. *Dalton Trans.* **2021**, *50* (23), 8017–8028. <https://doi.org/10.1039/D1DT00466B>.
- (104) Biancalana, L.; Kostrhunova, H.; Batchelor, L. K.; Hadiji, M.; Degano, I.; Pampaloni, G.; Zacchini, S.; Dyson, P. J.; Brabec, V.; Marchetti, F. Hetero-Bis-Conjugation of Bioactive Molecules to Half-Sandwich Ruthenium(II) and Iridium(III) Complexes Provides Synergic Effects in Cancer Cell Cytotoxicity. *Inorg. Chem.* **2021**, *60* (13), 9529–9541. <https://doi.org/10.1021/acs.inorgchem.1c00641>.

- (105) Swaminathan, S.; Haribabu, J.; Mohamed Subarkhan, M. K.; Gayathri, D.; Balakrishnan, N.; Bhuvanesh, N.; Echeverria, C.; Karvembu, R. Impact of Aliphatic Acyl and Aromatic Thioamide Substituents on the Anticancer Activity of Ru( II )- *p* -Cymene Complexes with Acylthiourea Ligands—*in Vitro* and *in Vivo* Studies. *Dalton Trans.* **2021**, 50 (44), 16311–16325. <https://doi.org/10.1039/D1DT02611A>.
- (106) Lee, B. Y. T.; Sullivan, M. P.; Yano, E.; Tong, K. K. H.; Hanif, M.; Kawakubo-Yasukochi, T.; Jamieson, S. M. F.; Soehnel, T.; Goldstone, D. C.; Hartinger, C. G. Anthracenyl Functionalization of Half-Sandwich Carbene Complexes: *In Vitro* Anticancer Activity and Reactions with Biomolecules. *Inorg. Chem.* **2021**, 60 (19), 14636–14644. <https://doi.org/10.1021/acs.inorgchem.1c01675>.
- (107) Chen, C.; Xu, C.; Li, T.; Lu, S.; Luo, F.; Wang, H. Novel NHC-Coordinated Ruthenium(II) Arene Complexes Achieve Synergistic Efficacy as Safe and Effective Anticancer Therapeutics. *European Journal of Medicinal Chemistry* **2020**, 203, 112605. <https://doi.org/10.1016/j.ejmech.2020.112605>.
- (108) Bonfili, L.; Pettinari, R.; Cuccioloni, M.; Cecarini, V.; Mozzicafreddo, M.; Angeletti, M.; Lupidi, G.; Marchetti, F.; Pettinari, C.; Eleuteri, A. M. Arene–RuII Complexes of Curcumin Exert Antitumor Activity via Proteasome Inhibition and Apoptosis Induction. *ChemMedChem* **2012**, 7 (11), 2010–2020. <https://doi.org/10.1002/cmdc.201200341>.
- (109) Pettinari, R.; Marchetti, F.; Pettinari, C.; Petrini, A.; Scopelliti, R.; Clavel, C. M.; Dyson, P. J. Synthesis, Structure, and Antiproliferative Activity of Ruthenium(II) Arene Complexes with N,O-Chelating Pyrazolone-Based  $\beta$ -Ketoamine Ligands. *Inorg. Chem.* **2014**, 53 (24), 13105–13111. <https://doi.org/10.1021/ic502274b>.
- (110) Pettinari, R.; Marchetti, F.; Pettinari, C.; Petrini, A.; Skelton, B. W.; White, A. H.; Bonfili, L.; Cuccioloni, M.; Eleuteri, A. M. Dinuclear (H6-Arene) Ruthenium(II) Acylpyrazolone Complexes: Synthesis, Characterization and Cytotoxicity. *Journal of Organometallic Chemistry* **2015**, 791, 1–5. <https://doi.org/10.1016/j.jorganchem.2015.04.049>.
- (111) Pettinari, R.; Condello, F.; Marchetti, F.; Pettinari, C.; Smoleński, P.; Riedel, T.; Scopelliti, R.; Dyson, P. J. Dicationic Ruthenium(II)–Arene–Curcumin Complexes Containing Methylated 1,3,5-Triaza-7-Phosphaadamantane: Synthesis, Structure, and Cytotoxicity. *European Journal of Inorganic Chemistry* **2017**, 2017 (22), 2905–2910. <https://doi.org/10.1002/ejic.201700183>.
- (112) Pettinari, R.; Marchetti, F.; Di Nicola, C.; Pettinari, C.; Galindo, A.; Petrelli, R.; Cappellacci, L.; Cuccioloni, M.; Bonfili, L.; Eleuteri, A. M.;

- Guedes da Silva, M. F. C.; Pombeiro, A. J. L. Ligand Design for N,O- or N,N-Pyrazolone-Based Hydrazones Ruthenium(II)-Arene Complexes and Investigation of Their Anticancer Activity. *Inorg. Chem.* **2018**, *57* (22), 14123–14133. <https://doi.org/10.1021/acs.inorgchem.8b01935>.
- (113) Sadler, P. J.; Sue, R. E. The Chemistry of Gold Drugs. *Metal-Based Drugs* **1994**, *1* (2–3), 107–144. <https://doi.org/10.1155/MBD.1994.107>.
- (114) Bertrand, B.; Casini, A. A Golden Future in Medicinal Inorganic Chemistry: The Promise of Anticancer Gold Organometallic Compounds. *Dalton Trans.* **2014**, *43* (11), 4209–4219. <https://doi.org/10.1039/C3DT52524D>.
- (115) Bertrand, B.; Williams, M. R. M.; Bochmann, M. Gold(III) Complexes for Antitumor Applications: An Overview. *Chem. Eur. J.* **2018**, *24* (46), 11840–11851. <https://doi.org/10.1002/chem.201800981>.
- (116) Bertrand, B.; Stefan, L.; Pirrotta, M.; Monchaud, D.; Bodio, E.; Richard, P.; Le Gendre, P.; Warmerdam, E.; de Jager, M. H.; Groothuis, G. M. M.; Picquet, M.; Casini, A. Caffeine-Based Gold(I) N-Heterocyclic Carbenes as Possible Anticancer Agents: Synthesis and Biological Properties. *Inorg. Chem.* **2014**, *53* (4), 2296–2303. <https://doi.org/10.1021/ic403011h>.
- (117) Barnard, P. J.; Baker, M. V.; Berners-Price, S. J.; Day, D. A. Mitochondrial Permeability Transition Induced by Dinuclear Gold(I)–Carbene Complexes: Potential New Antimitochondrial Antitumour Agents. *Journal of Inorganic Biochemistry* **2004**, *98* (10), 1642–1647. <https://doi.org/10.1016/j.jinorgbio.2004.05.011>.
- (118) Baker, M. V.; Barnard, P. J.; Berners-Price, S. J.; Brayshaw, S. K.; Hickey, J. L.; Skelton, B. W.; White, A. H. Cationic, Linear Au(i) N-Heterocyclic Carbene Complexes: Synthesis, Structure and Anti-Mitochondrial Activity. *Dalton Trans.* **2006**, No. 30, 3708–3715. <https://doi.org/10.1039/B602560A>.
- (119) Hickey, J. L.; Ruhayel, R. A.; Barnard, P. J.; Baker, M. V.; Berners-Price, S. J.; Filipovska, A. Mitochondria-Targeted Chemotherapeutics: The Rational Design of Gold(I) N-Heterocyclic Carbene Complexes That Are Selectively Toxic to Cancer Cells and Target Protein Selenols in Preference to Thiols. *J. Am. Chem. Soc.* **2008**, *130* (38), 12570–12571. <https://doi.org/10.1021/ja804027j>.
- (120) Bindoli, A.; Rigobello, M. P.; Scutari, G.; Gabbiani, C.; Casini, A.; Messori, L. Thioredoxin Reductase: A Target for Gold Compounds Acting as Potential Anticancer Drugs. *Coordination Chemistry Reviews* **2009**, *253* (11), 1692–1707. <https://doi.org/10.1016/j.ccr.2009.02.026>.
- (121) Rubbiani, R.; Kitanovic, I.; Alborzinia, H.; Can, S.; Kitanovic, A.; Onambele, L. A.; Stefanopoulou, M.; Geldmacher, Y.; Sheldrick, W. S.;

- Wolber, G.; Prokop, A.; Wölfl, S.; Ott, I. Benzimidazol-2-Ylidene Gold(I) Complexes Are Thioredoxin Reductase Inhibitors with Multiple Antitumor Properties. *J. Med. Chem.* **2010**, *53* (24), 8608–8618. <https://doi.org/10.1021/jm100801e>.
- (122) Rubbiani, R.; Can, S.; Kitanovic, I.; Alborzinia, H.; Stefanopoulou, M.; Kokoschka, M.; Mönchgesang, S.; Sheldrick, W. S.; Wölfl, S.; Ott, I. Comparative in Vitro Evaluation of N-Heterocyclic Carbene Gold(I) Complexes of the Benzimidazolylidene Type. *J. Med. Chem.* **2011**, *54* (24), 8646–8657. <https://doi.org/10.1021/jm201220n>.
- (123) Pratesi, A.; Gabbiani, C.; Michelucci, E.; Ginanneschi, M.; Papini, A. M.; Rubbiani, R.; Ott, I.; Messori, L. Insights on the Mechanism of Thioredoxin Reductase Inhibition by Gold N-Heterocyclic Carbene Compounds Using the Synthetic Linear Selenocysteine Containing C-Terminal Peptide HTrxR(488-499): An ESI-MS Investigation. *Journal of Inorganic Biochemistry* **2014**, *136*, 161–169. <https://doi.org/10.1016/j.jinorgbio.2014.01.009>.
- (124) Meier-Menches, S. M.; Neuditschko, B.; Zappe, K.; Schaier, M.; Gerner, M. C.; Schmetterer, K. G.; Del Favero, G.; Bonsignore, R.; Cichna-Markl, M.; Koellensperger, G.; Casini, A.; Gerner, C. An Organometallic Gold(I) Bis-N-Heterocyclic Carbene Complex with Multimodal Activity in Ovarian Cancer Cells. *Chemistry – A European Journal* **2020**, *26* (67), 15528–15537. <https://doi.org/10.1002/chem.202003495>.
- (125) Schmidt, C.; Casini, A. “Organometallic Chemistry of Gold-Based Drugs.” In *Reference Module in Chemistry, Molecular Sciences and Chemical Engineering*; Elsevier, 2021. <https://doi.org/10.1016/B978-0-12-820206-7.00032-9>.
- (126) Zutphen, S. van; Reedijk, J. Targeting Platinum Anti-Tumour Drugs: Overview of Strategies Employed to Reduce Systemic Toxicity. *Coordination Chemistry Reviews* **2005**, *249* (24), 2845–2853. <https://doi.org/10.1016/j.ccr.2005.03.005>.
- (127) Trauner, M.; Boyer, J. L. Bile Salt Transporters: Molecular Characterization, Function, and Regulation. *Physiological Reviews* **2003**, *83* (2), 633–671. <https://doi.org/10.1152/physrev.00027.2002>.
- (128) Chow, C. S. Amino Acid-Linked Platinum(II) Compounds: Non-Canonical Nucleoside Preferences and Influence on Glycosidic Bond Stabilities. *Journal of Biological Inorganic Chemistry*. <https://doi.org/10.1007/s00775-019-01693-y>.
- (129) Robillard, M. S.; Valentijn, A. R. P. M.; Meeuwenoord, N. J.; van der Marel, G. A.; van Boom, J. H.; Reedijk, J. The First Solid-Phase Synthesis of a Peptide-Tethered Platinum(II) Complex. *Angewandte Chemie*

- International Edition* **2000**, 39 (17), 3096–3099. [https://doi.org/10.1002/1521-3773\(20000901\)39:17<3096::AID-ANIE3096>3.0.CO;2-D](https://doi.org/10.1002/1521-3773(20000901)39:17<3096::AID-ANIE3096>3.0.CO;2-D).
- (130) Robillard, M. S.; Bacac, M.; van den Elst, H.; Flamigni, A.; van der Marel, G. A.; van Boom, J. H.; Reedijk, J. Automated Parallel Solid-Phase Synthesis and Anticancer Screening of a Library of Peptide-Tethered Platinum(II) Complexes. *J. Comb. Chem.* **2003**, 5 (6), 821–825. <https://doi.org/10.1021/cc030011z>.
  - (131) Pettenuzzo, A.; Pigot, R.; Ronconi, L. Metal-Based Glycoconjugates and Their Potential in Targeted Anticancer Chemotherapy. *Metallodrugs* **2016**, 1 (1). <https://doi.org/10.1515/medr-2015-0002>.
  - (132) Wilson, W. R.; Hay, M. P. Targeting Hypoxia in Cancer Therapy. *Nature Reviews Cancer* **2011**, 11 (6), 393–410. <https://doi.org/10.1038/nrc3064>.
  - (133) Otto, A. M. Warburg Effect(s)—a Biographical Sketch of Otto Warburg and His Impacts on Tumor Metabolism. *Cancer & Metabolism* **2016**, 4 (1), 5. <https://doi.org/10.1186/s40170-016-0145-9>.
  - (134) Patra, M.; Johnstone, T. C.; Suntharalingam, K.; Lippard, S. J. A Potent Glucose-Platinum Conjugate Exploits Glucose Transporters and Preferentially Accumulates in Cancer Cells. *Angew. Chem. Int. Ed.* **2016**, 55 (7), 2550–2554. <https://doi.org/10.1002/anie.201510551>.
  - (135) Patra, M.; Awuah, S. G.; Lippard, S. J. Chemical Approach to Positional Isomers of Glucose–Platinum Conjugates Reveals Specific Cancer Targeting through Glucose-Transporter-Mediated Uptake in Vitro and in Vivo. *J. Am. Chem. Soc.* **2016**, 138 (38), 12541–12551. <https://doi.org/10.1021/jacs.6b06937>.
  - (136) Han, J.; Gao, X.; Liu, R.; Yang, J.; Zhang, M.; Mi, Y.; Shi, Y.; Gao, Q. Design, Synthesis of Novel Platinum(II) Glycoconjugates, and Evaluation of Their Antitumor Effects. *Chem Biol Drug Des* **2016**, 87 (6), 867–877. <https://doi.org/10.1111/cbdd.12718>.
  - (137) Li, T.; Gao, X.; Yang, L.; Shi, Y.; Gao, Q. Methyl 6-Amino-6-Deoxy-d-Pyranoside-Conjugated Platinum(II) Complexes for Glucose Transporter (GLUT)-Mediated Tumor Targeting: Synthesis, Cytotoxicity, and Cellular Uptake Mechanism. *ChemMedChem* **2016**, 11 (10), 1069–1077. <https://doi.org/10.1002/cmdc.201600079>.
  - (138) Ma, J.; Liu, H.; Xi, Z.; Hou, J.; Li, Y.; Niu, J.; Liu, T.; Bi, S.; Wang, X.; Wang, C.; Wang, J.; Xie, S.; Wang, P. G. Protected and De-Protected Platinum(IV) Glycoconjugates With GLUT1 and OCT2-Mediated Selective Cancer Targeting: Demonstrated Enhanced Transporter-Mediated Cytotoxic Properties in Vitro and in Vivo. *Frontiers in Chemistry* **2018**, 6, 386. <https://doi.org/10.3389/fchem.2018.00386>.

- (139) Berger, I.; Hanif, M.; Nazarov, A. A.; Hartinger, C. G.; John, R. O.; Kuznetsov, M. L.; Groessl, M.; Schmitt, F.; Zava, O.; Biba, F.; Arion, V. B.; Galanski, M.; Jakupec, M. A.; Juillerat-Jeanneret, L.; Dyson, P. J.; Keppler, B. K. In Vitro Anticancer Activity and Biologically Relevant Metabolization of Organometallic Ruthenium Complexes with Carbohydrate-Based Ligands. *Chem. Eur. J.* **2008**, *14* (29), 9046–9057. <https://doi.org/10.1002/chem.200801032>.
- (140) Liu, J.; Liao, X.; Xiong, K.; Kuang, S.; Jin, C.; Ji, L.; Chao, H. Boosting Two-Photon Photodynamic Therapy with Mitochondria-Targeting Ruthenium–Glucose Conjugates. *Chem. Commun.* **2020**, *56* (43), 5839–5842. <https://doi.org/10.1039/D0CC01148G>.
- (141) Safir Filho, M.; Scattolin, T.; Dao, P.; Tzouras, N. V.; Benhida, R.; Saab, M.; Van Hecke, K.; Lippmann, P.; Martin, A. R.; Ott, I.; Nolan, S. P. Straightforward Synthetic Route to Gold(i)-Thiolato Glycoconjugate Complexes Bearing NHC Ligands (NHC = N-Heterocyclic Carbene) and Their Promising Anticancer Activity. *New J. Chem.* **2021**, *45* (22), 9995–10001. <https://doi.org/10.1039/D1NJ02117F>.
- (142) Cucciolito, M. E.; D’Amora, A.; De Feo, G.; Ferraro, G.; Giorgio, A.; Petruk, G.; Monti, D. M.; Merlino, A.; Ruffo, F. Five-Coordinate Platinum(II) Compounds Containing Sugar Ligands: Synthesis, Characterization, Cytotoxic Activity, and Interaction with Biological Macromolecules. *Inorg. Chem.* **2018**, *57* (6), 3133–3143. <https://doi.org/10.1021/acs.inorgchem.7b03118>.
- (143) Wang, F.-Y.; Liu, R.; Huang, K.-B.; Feng, H.-W.; Liu, Y.-N.; Liang, H. New Platinum(II)-Based DNA Intercalator: Synthesis, Characterization and Anticancer Activity. *Inorganic Chemistry Communications* **2019**, *105*, 182–187. <https://doi.org/10.1016/j.inoche.2019.04.039>.
- (144) Pages, B. J.; Garbutcheon-Singh, K. B.; Aldrich-Wright, J. R. Platinum Intercalators of DNA as Anticancer Agents: Platinum Intercalators of DNA as Anticancer Agents. *Eur. J. Inorg. Chem.* **2017**, *2017* (12), 1613–1624. <https://doi.org/10.1002/ejic.201601204>.
- (145) Zhang, S.; Yao, X.; Watkins, N. H.; Rose, P. K.; Caruso, S. R.; Day, C. S.; Bierbach, U. Discovery of a Chiral DNA-Targeted Platinum–Acridine Agent with Potent Enantioselective Anticancer Activity. *Angew. Chem. Int. Ed.* **2020**, *59* (49), 21965–21970. <https://doi.org/10.1002/anie.202009983>.
- (146) Vera, J. C.; Reyes, A. M.; Velásquez, F. V.; Rivas, C. I.; Zhang, R. H.; Strobel, P.; Slebe, J. C.; Núñez-Alarcón, J.; Golde, D. W. Direct Inhibition of the Hexose Transporter GLUT1 by Tyrosine Kinase Inhibitors. *Biochemistry* **2001**, *40* (3), 777–790. <https://doi.org/10.1021/bi001660j>.

- (147) Wu, M.; Li, H.; Liu, R.; Gao, X.; Zhang, M.; Liu, P.; Fu, Z.; Yang, J.; Zhang-Negrerie, D.; Gao, Q. Galactose Conjugated Platinum(II) Complex Targeting the Warburg Effect for Treatment of Non-Small Cell Lung Cancer and Colon Cancer. *European Journal of Medicinal Chemistry* **2016**, *110*, 32–42. <https://doi.org/10.1016/j.ejmech.2016.01.016>.
- (148) Guo, Y.; He, Y.; Wu, S.; Zhang, S.; Song, D.; Zhu, Z.; Guo, Z.; Wang, X. Enhancing Cytotoxicity of a Monofunctional Platinum Complex via a Dual-DNA-Damage Approach. *Inorg. Chem.* **2019**, *58* (19), 13150–13160. <https://doi.org/10.1021/acs.inorgchem.9b02033>.
- (149) Dabbish, E.; Russo, N.; Sicilia, E. Rationalization of the Superior Anticancer Activity of Phenanthriplatin: An In-Depth Computational Exploration. *Chem. Eur. J.* **2020**, *26* (1), 259–268. <https://doi.org/10.1002/chem.201903831>.
- (150) Liu, F.; Suryadi, J.; Bierbach, U. Cellular Recognition and Repair of Monofunctional–Intercalative Platinum–DNA Adducts. *Chem. Res. Toxicol.* **2015**, *28* (11), 2170–2178. <https://doi.org/10.1021/acs.chemrestox.5b00327>.
- (151) Li, C.; Xu, F.; Zhao, Y.; Zheng, W.; Zeng, W.; Luo, Q.; Wang, Z.; Wu, K.; Du, J.; Wang, F. Platinum(II) Terpyridine Anticancer Complexes Possessing Multiple Mode of DNA Interaction and EGFR Inhibiting Activity. *Front. Chem.* **2020**, *8*, 210. <https://doi.org/10.3389/fchem.2020.00210>.
- (152) Lozada, I. B.; Huang, B.; Stilgenbauer, M.; Beach, T.; Qiu, Z.; Zheng, Y.; Herbert, D. E. Monofunctional Platinum( II ) Anticancer Complexes Based on Multidentate Phenanthridine-Containing Ligand Frameworks. *Dalton Trans.* **2020**, *49* (20), 6557–6560. <https://doi.org/10.1039/D0DT01275K>.
- (153) Kemp, S.; Wheate, N. J.; Pisani, M. J.; Aldrich-Wright, J. R. Degradation of Bidentate-Coordinated Platinum(II)-Based DNA Intercalators by Reduced L -Glutathione. *J. Med. Chem.* **2008**, *51* (9), 2787–2794. <https://doi.org/10.1021/jm7016072>.
- (154) Aseman, M. D.; Aryamanesh, S.; Shojaeifard, Z.; Hemmateenejad, B.; Nabavizadeh, S. M. Cycloplatinated(II) Derivatives of Mercaptopurine Capable of Binding Interactions with HSA/DNA. *Inorg. Chem.* **2019**, *58* (23), 16154–16170. <https://doi.org/10.1021/acs.inorgchem.9b02696>.
- (155) Ortiz, D.; Gasilova, N.; Sepulveda, F.; Patiny, L.; Dyson, P. J.; Menin, L. Aom <sup>2</sup> S: A New Web-based Application for DNA/RNA Tandem Mass Spectrometry Data Interpretation. *Rapid Commun Mass Spectrom* **2020**, *34* (23). <https://doi.org/10.1002/rcm.8927>.
- (156) Giangrande, C.; Auberger, N.; Rentier, C.; Papini, A. M.; Mallet, J.-M.; Lavielle, S.; Vinh, J. Multi-Stage Mass Spectrometry Analysis of Sugar-



- Conjugated  $\beta$ -Turn Structures to Be Used as Probes in Autoimmune Diseases. *J. Am. Soc. Mass Spectrom.* **2016**, 27 (4), 735–747. <https://doi.org/10.1007/s13361-015-1321-9>.
- (157) Scott, J. D.; Puddephatt, R. J. Ligand Dissociation as a Preliminary Step in Methyl-for-Halogen Exchange Reactions of Platinum(II) Complexes. *Organometallics* **1983**, 2 (11), 1643–1648. <https://doi.org/10.1021/om50005a028>.
- (158) Rigano, M. M.; Raiola, A.; Tenore, G. C.; Monti, D. M.; Del Giudice, R.; Frusciante, L.; Barone, A. Quantitative Trait Loci Pyramiding Can Improve the Nutritional Potential of Tomato (*Solanum Lycopersicum*) Fruits. *J. Agric. Food Chem.* **2014**, 62 (47), 11519–11527. <https://doi.org/10.1021/jf502573n>.
- (159) Sucha, L.; Hroch, M.; Rezacova, M.; Rudolf, E.; Havelek, R.; Sispera, L.; Cmielova, J.; Kohlerova, R.; Bezrouk, A.; Tomsik, P. The Cytotoxic Effect of  $\alpha$ -Tomatine in MCF-7 Human Adenocarcinoma Breast Cancer Cells Depends on Its Interaction with Cholesterol in Incubation Media and Does Not Involve Apoptosis Induction. *Oncol Rep* **2013**, 30 (6), 2593–2602. <https://doi.org/10.3892/or.2013.2778>.
- (160) Holland, D.; Laidler, D. E.; Milner, D. J. Synthesis of Novel Copper(II) Complexes of Optically Active Schiff Bases. *Inorganica Chimica Acta* **1981**, 54, L21–L23. [https://doi.org/10.1016/S0020-1693\(00\)95372-6](https://doi.org/10.1016/S0020-1693(00)95372-6).
- (161) Kuduk-Jaworska, J. New Platinum(II) Complexes with Schiff Base Ligands. *Transition Met Chem* **1994**, 19 (3), 296–298. <https://doi.org/10.1007/BF00139096>.
- (162) Ou, S.; Lin, Z.; Duan, C.; Zhang, H.; Bai, Z. A Sugar-Quinoline Fluorescent Chemosensor for Selective Detection of  $Hg^{2+}$  Ion in Natural Water. *Chem. Commun.* **2006**, No. 42, 4392–4394. <https://doi.org/10.1039/B607287A>.
- (163) Makhubela, B. C. E.; Jardine, A.; Smith, G. S. Pd Nanosized Particles Supported on Chitosan and 6-Deoxy-6-Amino Chitosan as Recyclable Catalysts for Suzuki–Miyaura and Heck Cross-Coupling Reactions. *Applied Catalysis A: General* **2011**, 393 (1), 231–241. <https://doi.org/10.1016/j.apcata.2010.12.002>.
- (164) Tanaka, M.; Kataoka, H.; Yano, S.; Ohi, H.; Kawamoto, K.; Shibahara, T.; Mizoshita, T.; Mori, Y.; Tanida, S.; Kamiya, T.; Joh, T. Anti-Cancer Effects of Newly Developed Chemotherapeutic Agent, Glycoconjugated Palladium (II) Complex, against Cisplatin-Resistant Gastric Cancer Cells. *BMC Cancer* **2013**, 13 (1), 237. <https://doi.org/10.1186/1471-2407-13-237>.

- (165) Tarantino, G.; Curcio, M.; Pica, A.; Carpentieri, A.; Cucciolito, M. E.; Ruffo, F.; Vitagliano, A.; Lega, M. Hydrophilic Pd0 Complexes Based on Sugars for Efficient Suzuki–Miyaura Coupling in Aqueous Systems. *European Journal of Inorganic Chemistry* **2014**, 2014 (25), 4199–4208. <https://doi.org/10.1002/ejic.201402456>.
- (166) Baquero, E. A.; Flores, J. C.; Perles, J.; Gómez-Sal, P.; de Jesús, E. Water-Soluble Mono- and Dimethyl N-Heterocyclic Carbene Platinum(II) Complexes: Synthesis and Reactivity. *Organometallics* **2014**, 33 (19), 5470–5482. <https://doi.org/10.1021/om500753v>.
- (167) Hayashi, N.; Kataoka, H.; Yano, S.; Kikuchi, J.-I.; Tanaka, M.; Nishie, H.; Kinoshita, Y.; Hatano, M.; Nomoto, A.; Ogawa, A.; Inoue, M.; Mizoshita, T.; Shimura, T.; Mori, Y.; Kubota, E.; Tanida, S.; Joh, T. Anticancer Effects of a New Aminosugar-Conjugated Platinum Complex Agent Against Cisplatin-Resistant Gastric Cancer. *AR* **2016**, 36 (11), 6005–6010. <https://doi.org/10.21873/anticancer.11189>.
- (168) Lu, C. C.; Weyhermüller, T.; Bill, E.; Wieghardt, K. Accessing the Different Redox States of  $\alpha$ -Iminopyridines within Cobalt Complexes. *Inorg. Chem.* **2009**, 48 (13), 6055–6064. <https://doi.org/10.1021/ic9004328>.
- (169) Cucciolito, M. E.; Litto, R. D.; Fanizzi, F. P.; Migoni, D.; Roviello, G.; Ruffo, F. Hydrophilic Ligands Derived from Glucose: Synthesis, Characterization and in Vitro Cytotoxic Activity on Cancer Cells of Pt(II) Complexes. *Inorganica Chimica Acta* **2010**, 363 (4), 741–747. <https://doi.org/10.1016/j.ica.2009.11.031>.
- (170) Billing, J. F.; Nilsson, U. J. Cyclic Peptides Containing a  $\delta$ -Sugar Amino Acid—Synthesis and Evaluation as Artificial Receptors. *Tetrahedron* **2005**, 61 (4), 863–874. <https://doi.org/10.1016/j.tet.2004.11.024>.
- (171) Crascall, L. E.; Spencer, J. L.; Doyle, R. A.; Angelici, R. J. Olefin Complexes of Platinum. In *Inorganic Syntheses*; John Wiley & Sons, Ltd, 1990; pp 126–132. <https://doi.org/10.1002/9780470132593.ch34>.
- (172) Cucciolito, M. E.; De Luca Bossa, F.; Esposito, R.; Ferraro, G.; Iadonisi, A.; Petruk, G.; D’Elia, L.; Romanetti, C.; Traboni, S.; Tuzi, A.; Monti, D. M.; Merlino, A.; Ruffo, F. C -Glycosylation in Platinum-Based Agents: A Viable Strategy to Improve Cytotoxicity and Selectivity. *Inorg. Chem. Front.* **2018**, 5 (11), 2921–2933. <https://doi.org/10.1039/C8QI00664D>.
- (173) Valerio, S.; Iadonisi, A.; Adinolfi, M.; Ravidà, A. Novel Approaches for the Synthesis and Activation of Thio- and Selenoglycoside Donors. *J. Org. Chem.* **2007**, 72 (16), 6097–6106. <https://doi.org/10.1021/jo070670o>.
- (174) DeShong, P.; Slough, G. A.; Elango, V.; Trainor, G. L. An Organotransition Metal Based Approach to the Synthesis of C-Glycosides.

- J. Am. Chem. Soc.* **1985**, *107* (25), 7788–7790. <https://doi.org/10.1021/ja00311a109>.
- (175) Jones, G. S.; Scott, W. J. Oxidative Addition of Palladium(0) to the Anomeric Center of Carbohydrate Electrophiles. *J. Am. Chem. Soc.* **1992**, *114* (4), 1491–1492. <https://doi.org/10.1021/ja00030a060>.
- (176) Pelczar, E. M.; Munro-Leighton, C.; Gagné, M. R. Oxidative Addition of Glycosylbromides to *Trans*- Ir(PMe<sub>3</sub>)<sub>2</sub>(CO)Cl. *Organometallics* **2009**, *28* (3), 663–665. <https://doi.org/10.1021/om8011135>.
- (177) Munro-Leighton, C.; Adduci, L. L.; Becker, J. J.; Gagné, M. R. Oxidative Addition of Secondary C–X Bonds to Palladium(0): A Beneficial Anomeric Acceleration. *Organometallics* **2011**, *30* (10), 2646–2649. <https://doi.org/10.1021/om200221r>.
- (178) Marianski, M.; Mucha, E.; Greis, K.; Moon, S.; Pardo, A.; Kirschbaum, C.; Thomas, D. A.; Meijer, G.; von Helden, G.; Gilmore, K.; Seeberger, P. H.; Pagel, K. Remote Participation during Glycosylation Reactions of Galactose Building Blocks: Direct Evidence from Cryogenic Vibrational Spectroscopy. *Angewandte Chemie International Edition* **2020**, *59* (15), 6166–6171. <https://doi.org/10.1002/anie.201916245>.
- (179) Adinolfi, M.; Iadonisi, A.; Ravidà, A.; Schiattarella, M. Efficient and Direct Synthesis of Saccharidic 1,2-Ethylidenes, Orthoesters, and Glycals from Peracetylated Sugars via the in Situ Generation of Glycosyl Iodides with I<sub>2</sub>/Et<sub>3</sub>SiH. *Tetrahedron Letters* **2003**, *44* (43), 7863–7866. <https://doi.org/10.1016/j.tetlet.2003.09.022>.
- (180) Giordano, M.; Iadonisi, A. A Practical Approach to Regioselective O-Benzoylation of Primary Positions of Polyols. *Tetrahedron Letters* **2013**, *54* (12), 1550–1552. <https://doi.org/10.1016/j.tetlet.2013.01.023>.
- (181) Traboni, S.; Bedini, E.; Iadonisi, A. Solvent-Free Conversion of Alcohols to Alkyl Iodides and One-Pot Elaborations Thereof. *ChemistrySelect* **2018**, *3* (6), 1616–1622. <https://doi.org/10.1002/slct.201800130>.
- (182) Bruker-Nonius, SADABS, Delft, The Netherlands. 2002.
- (183) Altomare, A.; Burla, M. C.; Camalli, M.; Cascarano, G. L.; Giacovazzo, C.; Guagliardi, A.; Moliterni, A. G. G.; Polidori, G.; Spagna, R. SIR 97: A New Tool for Crystal Structure Determination and Refinement. *J Appl Crystallogr* **1999**, *32* (1), 115–119. <https://doi.org/10.1107/S0021889898007717>.
- (184) Farrugia, L. J. WinGX and ORTEP for Windows : An Update. *J Appl Crystallogr* **2012**, *45* (4), 849–854. <https://doi.org/10.1107/S0021889812029111>.
- (185) Murshudov, G. N.; Skubák, P.; Lebedev, A. A.; Pannu, N. S.; Steiner, R. A.; Nicholls, R. A.; Winn, M. D.; Long, F.; Vagin, A. A. REFMAC 5 for

- the Refinement of Macromolecular Crystal Structures. *Acta Crystallogr D Biol Crystallogr* **2011**, *67* (4), 355–367. <https://doi.org/10.1107/S0907444911001314>.
- (186) Macrae, C. F.; Bruno, I. J.; Chisholm, J. A.; Edgington, P. R.; McCabe, P.; Pidcock, E.; Rodriguez-Monge, L.; Taylor, R.; van de Streek, J.; Wood, P. A. *Mercury CSD 2.0 – New Features for the Visualization and Investigation of Crystal Structures*. *J Appl Crystallogr* **2008**, *41* (2), 466–470. <https://doi.org/10.1107/S0021889807067908>.
- (187) Fantasia, S.; Petersen, J. L.; Jacobsen, H.; Cavallo, L.; Nolan, S. P. Electronic Properties of N-Heterocyclic Carbene (NHC) Ligands: Synthetic, Structural, and Spectroscopic Studies of (NHC)Platinum(II) Complexes. *Organometallics* **2007**, *26* (24), 5880–5889. <https://doi.org/10.1021/om700857j>.
- (188) Liu, W.; Gust, R. Update on Metal N-Heterocyclic Carbene Complexes as Potential Anti-Tumor Metallodrugs. *Coordination Chemistry Reviews* **2016**, *329*, 191–213. <https://doi.org/10.1016/j.ccr.2016.09.004>.
- (189) Fang, T.; Ye, Z.; Wu, J.; Wang, H. Reprogramming Axial Ligands Facilitates the Self-Assembly of a Platinum( IV ) Prodrug: Overcoming Drug Resistance and Safer *in Vivo* Delivery of Cisplatin. *Chem. Commun.* **2018**, *54* (66), 9167–9170. <https://doi.org/10.1039/C8CC03763A>.
- (190) Lo Re, D.; Montagner, D.; Tolan, D.; Di Sanza, C.; Iglesias, M.; Calon, A.; Giralt, E. Increased Immune Cell Infiltration in Patient-Derived Tumor Explants Treated with Traniplatin: An Original Pt( IV ) pro-Drug Based on Cisplatin and Tranilast. *Chem. Commun.* **2018**, *54* (60), 8324–8327. <https://doi.org/10.1039/C8CC02071J>.
- (191) Rehm, T.; Rothmund, M.; Dietel, T.; Kempe, R.; Schobert, R. Synthesis, Structures and Cytotoxic Effects *in Vitro* of *Cis* - and *Trans* -[Pt<sup>IV</sup> Cl<sub>4</sub> (NHC)<sub>2</sub>] Complexes and Their Pt<sup>II</sup> Precursors. *Dalton Trans.* **2019**, *48* (43), 16358–16365. <https://doi.org/10.1039/C9DT02438G>.
- (192) Tan, M.-X.; Wang, Z.-F.; Qin, Q.-P.; Huang, X.-L.; Zou, B.-Q.; Liang, H. Complexes of Platinum(II/IV) with 2-Phenylpyridine Derivatives as a New Class of Promising Anti-Cancer Agents. *Inorganic Chemistry Communication*. <https://doi.org/10.1016/j.inoche.2019.107510>.
- (193) Nishioka, T.; Shibata, T.; Kinoshita, I. Sugar-Incorporated N-Heterocyclic Carbene Complexes. *Organometallics* **2007**, *26* (5), 1126–1128. <https://doi.org/10.1021/om061128d>.
- (194) Astakhov, A. V.; Khazipov, O. V.; Degtyareva, E. S.; Khrustalev, V. N.; Chernyshev, V. M.; Ananikov, V. P. Facile Hydrolysis of Nickel(II) Complexes with N-Heterocyclic Carbene Ligands. *Organometallics* **2015**, *34* (24), 5759–5766. <https://doi.org/10.1021/acs.organomet.5b00856>.

- (195) Li, D.; Ollevier, T. Mechanism Studies of Oxidation and Hydrolysis of Cu(I)–NHC and Ag–NHC in Solution under Air. *Journal of Organometallic Chemistry* **2020**, *906*, 121025. <https://doi.org/10.1016/j.jorgchem.2019.121025>.
- (196) Hux, J. E.; Puddephatt, R. J. Reactivity of Tetramethylplatinum(IV) Complexes: Thermal Reactions with Electrophiles and Unsaturated Reagents. *Inorganica Chimica Acta* **1985**, *100* (1), 1–5. [https://doi.org/10.1016/S0020-1693\(00\)88287-0](https://doi.org/10.1016/S0020-1693(00)88287-0).
- (197) Crumpton-Bregel, D. M.; Goldberg, K. I. Mechanisms of C–C and C–H Alkane Reductive Eliminations from Octahedral Pt(IV): Reaction via Five-Coordinate Intermediates or Direct Elimination? *J. Am. Chem. Soc.* **2003**, *125* (31), 9442–9456. <https://doi.org/10.1021/ja029140u>.
- (198) Lindner, R.; Wagner, C.; Steinborn, D. Synthesis of Trimethylplatinum(IV) Complexes with *N,N*- and *N,O*-Heterocyclic Carbene Ligands and Their Reductive C–C Elimination Reactions. *J. Am. Chem. Soc.* **2009**, *131* (25), 8861–8874. <https://doi.org/10.1021/ja901264t>.
- (199) Denisova, E. A.; Eremin, D. B.; Gordeev, E. G.; Tsedilin, A. M.; Ananikov, V. P. Addressing Reversibility of R–NHC Coupling on Palladium: Is Nano-to-Molecular Transition Possible for the Pd/NHC System? *Inorg. Chem.* **2019**, *58* (18), 12218–12227. <https://doi.org/10.1021/acs.inorgchem.9b01630>.
- (200) Zhang, J. Z.; Wexselblatt, E.; Hambley, T. W.; Gibson, D. Pt(IV) Analogs of Oxaliplatin That Do Not Follow the Expected Correlation between Electrochemical Reduction Potential and Rate of Reduction by Ascorbate. *Chem. Commun.* **2012**, *48* (6), 847–849. <https://doi.org/10.1039/C1CC16647F>.
- (201) Escolà, A.; Crespo, M.; López, C.; Quirante, J.; Jayaraman, A.; Polat, I. H.; Badía, J.; Baldomà, L.; Cascante, M. On the Stability and Biological Behavior of Cyclometallated Pt(IV) Complexes with Halido and Aryl Ligands in the Axial Positions. *Bioorganic & Medicinal Chemistry* **2016**, *24* (22), 5804–5815. <https://doi.org/10.1016/j.bmc.2016.09.037>.
- (202) Monaghan, P. K.; Puddephatt, R. J. Reactivity and Mechanism in the Oxidative Addition of Iodoalkanes and Di-Iodoalkanes to a Dimethylplatinum(II) Complex. *J. Chem. Soc., Dalton Trans.* **1988**, No. 3, 595–599. <https://doi.org/10.1039/DT9880000595>.
- (203) Pontillo, N.; Pane, F.; Messori, L.; Amoresano, A.; Merlino, A. Cisplatin Encapsulation within a Ferritin Nanocage: A High-Resolution Crystallographic Study. *Chem. Commun.* **2016**, *52* (22), 4136–4139. <https://doi.org/10.1039/C5CC10365G>.

- (204) Streciwilk, W.; Terenzi, A.; Misgeld, R.; Frias, C.; Jones, P. G.; Prokop, A.; Keppler, B. K.; Ott, I. Metal NHC Complexes with Naphthalimide Ligands as DNA-Interacting Antiproliferative Agents. *ChemMedChem* **2017**, *12* (3), 214–225. <https://doi.org/10.1002/cmdc.201600557>.
- (205) Ott, I. Metal N-Heterocyclic Carbene Complexes in Medicinal Chemistry. In *Advances in Inorganic Chemistry*; Elsevier, 2020; Vol. 75, pp 121–148. <https://doi.org/10.1016/bs.adioch.2019.10.008>.
- (206) Lam, N. Y. S.; Truong, D.; Burmeister, H.; Babak, M. V.; Holtkamp, H. U.; Movassaghi, S.; Ayine-Tora, D. M.; Zafar, A.; Kubanik, M.; Oehninger, L.; Söhnle, T.; Reynisson, J.; Jamieson, S. M. F.; Gaiddon, C.; Ott, I.; Hartinger, C. G. From Catalysis to Cancer: Toward Structure–Activity Relationships for Benzimidazol-2-Ylidene-Derived *N* -Heterocyclic-Carbene Complexes as Anticancer Agents. *Inorg. Chem.* **2018**, *57* (22), 14427–14434. <https://doi.org/10.1021/acs.inorgchem.8b02634>.
- (207) Truong, D.; Sullivan, M. P.; Tong, K. K. H.; Steel, T. R.; Prause, A.; Lovett, J. H.; Andersen, J. W.; Jamieson, S. M. F.; Harris, H. H.; Ott, I.; Weekley, C. M.; Hummitzsch, K.; Söhnle, T.; Hanif, M.; Metzler-Nolte, N.; Goldstone, D. C.; Hartinger, C. G. Potent Inhibition of Thioredoxin Reductase by the Rh Derivatives of Anticancer M(Arene/Cp\*)(NHC)Cl<sub>2</sub> Complexes. *Inorg. Chem.* **2020**, *59* (5), 3281–3289. <https://doi.org/10.1021/acs.inorgchem.9b03640>.
- (208) Patil, S. A.; Patil, S. A.; Patil, R.; Keri, R. S.; Budagumpi, S.; Balakrishna, G. R.; Tacke, M. *N* -Heterocyclic Carbene Metal Complexes as Bio-Organometallic Antimicrobial and Anticancer Drugs. *Future Medicinal Chemistry* **2015**, *7* (10), 1305–1333. <https://doi.org/10.4155/fmc.15.61>.
- (209) Monney, A.; Venkatachalam, G.; Albrecht, M. Synthesis and Catalytic Activity of Histidine-Based NHC Ruthenium Complexes. *Dalton Trans.* **2011**, *40* (12), 2716. <https://doi.org/10.1039/c0dt01768j>.
- (210) Monney, A.; Albrecht, M. A Chelating Tetrapeptide Rhodium Complex Comprised of a Histidylidene Residue: Biochemical Tailoring of an NHC-Rh Hydrosilylation Catalyst. *Chem. Commun.* **2012**, *48* (89), 10960. <https://doi.org/10.1039/c2cc35491h>.
- (211) Monney, A.; Natri, F.; Albrecht, M. Peptide-Tethered Monodentate and Chelating Histidylidene Metal Complexes: Synthesis and Application in Catalytic Hydrosilylation. *Dalton Trans.* **2013**, *42* (16), 5655. <https://doi.org/10.1039/c3dt50424g>.
- (212) Marozsán, N.; Horváth, H.; Kováts, É.; Udvardy, A.; Erdei, A.; Purgel, M.; Joó, F. Catalytic Racemization of Secondary Alcohols with New (Arene)Ru(II)-NHC and (Arene)Ru(II)-NHC-Tertiary Phosphine

- Complexes. *Molecular Catalysis* **2018**, *445*, 248–256. <https://doi.org/10.1016/j.mcat.2017.11.040>.
- (213) Jantke, D.; Cokoja, M.; Pöthig, A.; Herrmann, W. A.; Kühn, F. E. Synthesis and Characterization of Highly Water Soluble Ruthenium(II) and Osmium(II) Complexes Bearing Chelating Sulfonated N-Heterocyclic Carbene Ligands. *Organometallics* **2013**, *32* (3), 741–744. <https://doi.org/10.1021/om301218k>.
- (214) Hackenberg, F.; Müller-Bunz, H.; Smith, R.; Streciwilk, W.; Zhu, X.; Tacke, M. Novel Ruthenium(II) and Gold(I) NHC Complexes: Synthesis, Characterization, and Evaluation of Their Anticancer Properties. *Organometallics* **2013**, *32* (19), 5551–5560. <https://doi.org/10.1021/om400819p>.
- (215) Dorcier, A.; Dyson, P. J.; Gossens, C.; Rothlisberger, U.; Scopelliti, R.; Tavernelli, I. Binding of Organometallic Ruthenium(II) and Osmium(II) Complexes to an Oligonucleotide: A Combined Mass Spectrometric and Theoretical Study. *Organometallics* **2005**, *24* (9), 2114–2123. <https://doi.org/10.1021/om049022a>.
- (216) Renfrew, A. K.; Phillips, A. D.; Egger, A. E.; Hartinger, C. G.; Bosquain, S. S.; Nazarov, A. A.; Keppler, B. K.; Gonsalvi, L.; Peruzzini, M.; Dyson, P. J. Influence of Structural Variation on the Anticancer Activity of RAPTA-Type Complexes: Ptn versus Pta. *Organometallics* **2009**, *28* (4), 1165–1172. <https://doi.org/10.1021/om800899e>.
- (217) Bergamo. Modulation of the Metastatic Progression of Breast Cancer with an Organometallic Ruthenium Compound. *Int J Oncol* **1992**. [https://doi.org/10.3892/ijo\\_00000119](https://doi.org/10.3892/ijo_00000119).
- (218) Howard, R. A.; Sherwood, E.; Erck, A.; Kimball, A. P.; Bear, J. L. Hydrophobicity of Several Rhodium(II) Carboxylates Correlated with Their Biologic Activity. *J. Med. Chem.* **1977**, *20* (7), 943–946. <https://doi.org/10.1021/jm00217a016>.
- (219) Schäfer, S.; Ott, I.; Gust, R.; Sheldrick, W. S. Influence of the Polypyridyl (Pp) Ligand Size on the DNA Binding Properties, Cytotoxicity and Cellular Uptake of Organoruthenium(II) Complexes of the Type [(H6-C6Me6)Ru(L)(Pp)]N<sup>+</sup> [L = Cl, n = 1; L = (NH<sub>2</sub>)<sub>2</sub>CS, n = 2]. *Eur. J. Inorg. Chem.* **2007**, *2007* (19), 3034–3046. <https://doi.org/10.1002/ejic.200700206>.
- (220) Aguirre, J. D.; Angeles-Boza, A. M.; Chouai, A.; Turro, C.; Pellois, J.-P.; Dunbar, K. R. Anticancer Activity of Heteroleptic Diimine Complexes of Dirhodium: A Study of Intercalating Properties, Hydrophobicity and in Cellulo Activity. *Dalton Trans.* **2009**, No. 48, 10806–10812. <https://doi.org/10.1039/B915357H>.

- (221) Aguirre, J. D.; Angeles-Boza, A. M.; Chouai, A.; Pellois, J.-P.; Turro, C.; Dunbar, K. R. Live Cell Cytotoxicity Studies: Documentation of the Interactions of Antitumor Active Dirhodium Compounds with Nuclear DNA. *J. Am. Chem. Soc.* **2009**, *131* (32), 11353–11360. <https://doi.org/10.1021/ja9021717>.
- (222) Bennett, M. A.; Huang, T.-N.; Matheson, T. W.; Smith, A. K.; Ittel, S.; Nickerson, W. 16. ( $\eta^6$ -Hexamethylbenzene)Ruthenium Complexes. In *Inorganic Syntheses*; Fackler, J. P., Ed.; John Wiley & Sons, Inc.: Hoboken, NJ, USA, 2007; pp 74–78. <https://doi.org/10.1002/9780470132524.ch16>.
- (223) Chao, H. S. I.; Berchtold, G. A. Aromatization of Arene 1,2-Oxides. 1,2-Oxides of Methyl Phenylacetate and Methyl Trans-Cinnamate. *J. Org. Chem.* **1981**, *46* (6), 1191–1194. <https://doi.org/10.1021/jo00319a029>.
- (224) Cucciolito, M. E.; Trinchillo, M.; Iannitti, R.; Palumbo, R.; Tesauro, D.; Tuzi, A.; Ruffo, F.; D'Amora, A. Sugar-Incorporated N-Heterocyclic-Carbene-Containing Gold(I) Complexes: Synthesis, Characterization, and Cytotoxic Evaluation: Sugar-Incorporated N-Heterocyclic-Carbene-Containing Gold(I) Complexes: Synthesis, Characterization, and Cytotoxic Evaluation. *Eur. J. Inorg. Chem.* **2017**, *2017* (42), 4955–4961. <https://doi.org/10.1002/ejic.201700768>.
- (225) Tresin, F.; Stoppa, V.; Baron, M.; Biffis, A.; Annunziata, A.; D'Elia, L.; Monti, D. M.; Ruffo, F.; Roverso, M.; Sgarbossa, P.; Bogialli, S.; Tubaro, C. Synthesis and Biological Studies on Dinuclear Gold(I) Complexes with Di-(N-Heterocyclic Carbene) Ligands Functionalized with Carbohydrates. *Molecules* **2020**, *25* (17), 3850. <https://doi.org/10.3390/molecules25173850>.
- (226) Xu, H.; Xu, D. C.; Wang, Y. Natural Indices for the Chemical Hardness/Softness of Metal Cations and Ligands. *ACS Omega* **2017**, *2* (10), 7185–7193. <https://doi.org/10.1021/acsomega.7b01039>.
- (227) Huynh, H. V. Electronic Properties of N-Heterocyclic Carbenes and Their Experimental Determination. *Chem. Rev.* **2018**, *118* (19), 9457–9492. <https://doi.org/10.1021/acs.chemrev.8b00067>.
- (228) Tapu, D.; Dixon, D. A.; Roe, C.  $^{13}\text{C}$  NMR Spectroscopy of “Arduengo-Type” Carbenes and Their Derivatives. *Chem. Rev.* **2009**, *109* (8), 3385–3407. <https://doi.org/10.1021/cr800521g>.
- (229) Huynh, H. V.; Han, Y.; Jothibas, R.; Yang, J. A.  $^{13}\text{C}$  NMR Spectroscopic Determination of Ligand Donor Strengths Using N-Heterocyclic Carbene Complexes of Palladium(II). *Organometallics* **2009**, *28* (18), 5395–5404. <https://doi.org/10.1021/om900667d>.



- (230) Guo, S.; Sivaram, H.; Yuan, D.; Huynh, H. V. Gold and Palladium Hetero-Bis-NHC Complexes: Characterizations, Correlations, and Ligand Redistributions. *Organometallics* **2013**, *32* (13), 3685–3696. <https://doi.org/10.1021/om400313r>.
- (231) Sivaram, H.; Jothibas, R.; Huynh, H. V. Gold Complexes of an Alicyclic Indazole-Derived N-Heterocyclic Carbene: Syntheses, Characterizations, and Ligand Disproportionation. *Organometallics* **2012**, *31* (3), 1195–1203. <https://doi.org/10.1021/om201268m>.
- (232) Glodek, M.; Makal, A.; Paluch, P.; Kadziolka-Gawel, M.; Kobayashi, Y.; Zakrzewski, J.; Plazuk, D. (Ar-CO-C $\equiv$ C)(PET<sub>3</sub>)Au and (Ar-C $\equiv$ C)(PET<sub>3</sub>)Au Complexes Bearing Pyrenyl and Ferrocenyl Groups: Synthesis, Structure, and Luminescence Properties. *Dalton Trans.* **2018**, *47* (19), 6702–6712. <https://doi.org/10.1039/C8DT01061G>.
- (233) Guo, S.; Bernhammer, J. C.; Huynh, H. V. 1,2,4-Triazole-Derived Carbene Complexes of Gold: Characterization, Solid-State Aggregation and Ligand Disproportionation. *Dalton Trans.* **2015**, *44* (34), 15157–15165. <https://doi.org/10.1039/C4DT03201B>.
- (234) Hormann-Arendt, A. L.; Shaw, C. F. Ligand-Scrambling Reactions of Cyano(Trialkyl/Triarylphosphine)Gold(I) Complexes: Examination of Factors Influencing the Equilibrium Constant. *Inorg. Chem.* **1990**, *29* (23), 4683–4687. <https://doi.org/10.1021/ic00348a019>.
- (235) Karaca, Ö.; Scalcon, V.; Meier-Menches, S. M.; Bonsignore, R.; Brouwer, J. M. J. L.; Tonolo, F.; Folda, A.; Rigobello, M. P.; Kühn, F. E.; Casini, A. Characterization of Hydrophilic Gold(I) N-Heterocyclic Carbene (NHC) Complexes as Potent TrxR Inhibitors Using Biochemical and Mass Spectrometric Approaches. *Inorg. Chem.* **2017**, *56* (22), 14237–14250. <https://doi.org/10.1021/acs.inorgchem.7b02345>.
- (236) Schmidt, C.; Albrecht, L.; Balasubramanian, S.; Misgeld, R.; Karge, B.; Brönstrup, M.; Prokop, A.; Baumann, K.; Reichl, S.; Ott, I. A Gold(I) Biscarbene Complex with Improved Activity as a TrxR Inhibitor and Cytotoxic Drug: Comparative Studies with Different Gold Metallodrugs. *Metallomics* **2019**, *11* (3), 533–545. <https://doi.org/10.1039/C8MT00306H>.
- (237) Goetzfried, S. K.; Gallati, C. M.; Cziferszky, M.; Talmazan, R. A.; Wurst, K.; Liedl, K. R.; Podewitz, M.; Gust, R. N-Heterocyclic Carbene Gold(I) Complexes: Mechanism of the Ligand Scrambling Reaction and Their Oxidation to Gold(III) in Aqueous Solutions. *Inorg. Chem.* **2020**, *59* (20), 15312–15323. <https://doi.org/10.1021/acs.inorgchem.0c02298>.
- (238) Kaps, L.; Biersack, B.; Müller-Bunz, H.; Mahal, K.; Münzner, J.; Tacke, M.; Mueller, T.; Schobert, R. Gold(I)–NHC Complexes of Antitumoral

- Diarylimidazoles: Structures, Cellular Uptake Routes and Anticancer Activities. *Journal of Inorganic Biochemistry* **2012**, *106* (1), 52–58. <https://doi.org/10.1016/j.jinorgbio.2011.08.026>.
- (239) Muenzner, J. K.; Biersack, B.; Kalie, H.; Andronache, I. C.; Kaps, L.; Schuppan, D.; Sasse, F.; Schobert, R. Gold(I) Biscarbene Complexes Derived from Vascular-Disrupting Combretastatin A-4 Address Different Targets and Show Antimetastatic Potential. *ChemMedChem* **2014**, *9* (6), 1195–1204. <https://doi.org/10.1002/cmdc.201400049>.
- (240) Schmidt, C.; Karge, B.; Misgeld, R.; Prokop, A.; Franke, R.; Brönstrup, M.; Ott, I. Gold(I) NHC Complexes: Antiproliferative Activity, Cellular Uptake, Inhibition of Mammalian and Bacterial Thioredoxin Reductases, and Gram-Positive Directed Antibacterial Effects. *Chem. Eur. J.* **2017**, *23* (8), 1869–1880. <https://doi.org/10.1002/chem.201604512>.
- (241) Uson, R.; Laguna, A.; Laguna, M.; Briggs, D. A.; Murray, H. H.; Fackler Jr., J. P. (Tetrahydrothiophene)Gold(I) or Gold(III) Complexes. In *Inorganic Syntheses*; John Wiley & Sons, Ltd, 1989; pp 85–91. <https://doi.org/10.1002/9780470132579.ch17>.